Exploiting replication stress induced by IGF blockade in cancer therapy

Xiaoning Wu

Linacre College

Department of Oncology

University of Oxford

Thesis submitted for the degree of Doctor of Philosophy in Oncology

Trinity Term 2020

Abstract

In recent work from our group, we found that genetic or pharmacological inhibition of type 1 insulin-like growth factor receptor (IGF-1R) promotes accumulation of cells in S phase and causes endogenous DNA damage by inducing replication stress. Blocking IGF signalling reduces expression of the regulatory subunit M2 of ribonucleotide reductase (RRM2) and disturbs deoxynucleotide triphosphate (dNTP) supply. The aim of my project is to develop approaches to exploit this effect in therapy. Therefore, with the objective of enhancing replication stress induced by IGF blockade to intolerable levels, a compound screen was conducted in combination with an IGF neutralising antibody drug that is currently being evaluated in clinical trials. Five breast cancer cell lines were screened; top hits include inhibitors of EGFR/HER2, ATM, PARP, RAD51, and CHK1. Low throughput validation focused on inhibition of checkpoint kinase CHK1, which has been reported to induce replication stress through downregulating RRM2. Co-inhibition of IGF and CHK1 significantly suppressed cell viability and cell survival in both 2D cell culture and 3D spheroid culture models. In IGF-1R depleted or inhibited cells, inhibition of CHK1 further downregulated RRM2, reduced dNTP supplies and delayed replication fork progression. Combining IGF blockade with CHK1 inhibition led to accumulation of DNA damage and single-stranded DNA (ssDNA), a replication stress marker, and significant increase in cell death, suggesting replication catastrophe. Exogenous RRM2 expression rescued these replication stress phenotypes, indicating a mechanism in which RRM2 regulation is a critical target of the interaction between IGF blockade and CHK1. Final experiments confirmed that the replication stress was also exacerbated by co-inhibiting IGFs and WEE1, which was a screen hit in one of the five cell lines and had also been reported to regulate RRM2 expression. Combining WEE1 inhibition and IGF-1R depletion induced RRM2 downregulation, delayed replication fork progression, and caused accumulation of DNA damage and ssDNA, resulting in cell death. These results may help to identify novel therapeutic vulnerabilities and provide guidance for future clinical trials of IGF inhibitory drugs.

Acknowledgment

First of all, I would like to express my sincere gratitude to my supervisor Dr Valentine Macaulay for all the opportunities she has given me throughout my 4 years' DPhil study. I am extremely grateful for all her persistent support, thoughtful guidance, valuable advice, and enormous help on not only my study but also my life and career. I feel deeply blessed to have Val as my mentor during this incredible and life-changing journey in Oxford.

Next, I would like to thank my second supervisor Dr Guillaume Rieunier for always being incredibly supportive, caring, and helpful throughout my study. I have learned so much from our discussion of experiments and science. I truly appreciate all his help and support that make this thesis happen.

I would also like to thank all the people who offered great help with this project, especially Elena Seraia and Daniel Ebner from Target Discovery Institute (TDI) for the help with the compound screen, Xiao Wan and Stephanie Hatch for helping me establish 3D spheroid culture model and perform experiments on Incucyte Live-Cell Analysis System at TDI, Carol Walker for helping me establish the method for dNTP measurement, Yanyan Jiang, and Karla Watson, Magdalena Hutchins from BMS for the help with the animal experiment. I would also thank Dr Ulrike Weyer-Czernilofsky and Dr Thomas Bogenrieder from Boehringer Ingelheim for providing IGF ligand-neutralising antibody BI-836845 (xentuzumab), Professor Anderson Ryan, Professor Ester Hammond, Professor Tim Humphrey, Dr Andrew Blackford, and Dr David Clynes for the advice and comments on this project.

A special thank you to all the team members of our lab: Lina Guo, Nick Coupe, Tamara Aleksic, Frances Willenbrock, Christopher Towers, Victoria Ma, Jenetta Soo, Eliot Osher, Jack Mills, Ashwin Nandakumar, Matthew Ellis, Jinseon Kim, Avigail

Taylor, Monica Mantri, and Zhi Wong. I was lucky to meet all of them who are friendly and supportive all the time.

Finally, I would like to express my deepest appreciation to my parents and all my family members for all their unconditional support and continuous encouragement. I would like to say a heartfelt thank you to all of them for always believing in me.

I declare that this thesis describes my own research work except the following experiments, which were performed with the help of others:

- The cell proliferation assay shown in Figure 4.1 A: cell seeding and drug treatment processes were performed by Dr Guillaume Rieunier and myself; cell imaging and analysis on Incucyte system were performed by Elena Seraia at High Throughput Screening Facility, Target Discovery Institute (TDI) Oxford.
- The compound screen shown in Figure 4.1 B and C: the preparation of cells and drug plates was done by Dr Guillaume Rieunier and myself; cell seeding and drug treatment on Janus liquid handling workstations and cell viability experiments on Envison multilabel plate reader were performed by Elena Seraia at TDI; data analysis was done by myself.
- The 3D cell proliferation assay shown in Figure 4.15 B and 5.13 E: spheroid culture was done by myself; cell imaging and analysis on Incucyte system were performed by Xiao Wan and Stephanie Hatch at TDI.

Table of Contents

List of Figures

List of Tables

List of Abbreviations

2D	two-dimensional
3AP	triapine
3D	three-dimensional
53BP1	p53-binding protein 1
9-1-1	RAD9-RAD1-HUS1 complex
ANOVA	analysis of variance
APC	Anaphase-promoting complex
ATCC	American Type Culture Collection
ATM	Ataxia Telangiectasia Mutated
ATP	adenosine triphosphate
ATR	Ataxia Telangiectasia and Rad3-related protein kinase
ATRIP	ATR-interacting protein
BCL-2	B-cell lymphoma 2
BLM	Bloom syndrome helicase
bp	base-pair(s)
BRCA	Breast Cancer susceptibility gene
BrdU	5-bromo-2'-deoxyuridine
BSA	bovine serum albumin
CDC	Cell Division Cycle protein
CDK	Cyclin-dependent kinase
CDH1	Cadherin 1
CDT1	Chromatin licensing and DNA replication factor 1
cGAMP	cyclic guanosine monophosphate–adenosine monophosphate
cGAS	cGAMP synthase
CHK1	Checkpoint kinase 1
CHK2	Checkpoint kinase 2
CldU	5-chloro-2'-deoxyuridine
CO_2	carbon dioxide
dADP	deoxyadenosine diphosphate
DAPI	4',6-diamidino-2-phenylindole
dATP	deoxyadenosine triphosphate
dCDP	deoxycytidine diphosphate

dCTP	deoxycytidine triphosphate
DDR	DNA damage response
dGDP	deoxyguanosine diphosphate
dGTP	deoxyguanosine triphosphate
DMEM	Dulbecco's Modified Eagle's Medium
DMSO	dimethyl sulfoxide
DNA	deoxyribonucleic acid
DNA-PK	DNA-dependent protein kinase
dNDP	deoxynucleotide diphosphate
dNTP	deoxynucleotide triphosphate
DSB	double-strand break
dsDNA	double-stranded DNA
dTDP	deoxythymidine diphosphate
dTTP	deoxythymidine triphosphate
EGFR	Epidermal Growth Factor Receptor
ELK-1	E26 transformation-specific Like protein-1
ER	Estrogen Receptor
ERK	Extracellular signal-regulated kinase
EXO1	Exonuclease 1
FACS	fluorescence activity sorting assay
FBS	foetal bovine serum
GDP	guanosine diphosphate
GI50	50% cell growth inhibition concentration
Grb2	growth factor receptor-bound protein 2
GSK-3β	Glycogen synthase kinase-3β
GTP	guanosine triphosphate
HCl	hydrochloric acid
HDAC	Histone deacetylase
HER2	Human epidermal growth factor receptor 2
HGPS	Hutchinson-Gilford progeria syndrome
HPLC	high-performance liquid chromatography
HR	homologous recombination
HU	hydroxyurea

IdU	5-Iodo-2'-deoxyuridine
IF	immunofluorescence
IFN	interferon
IGF-1	Insulin-like growth factor 1
IGF-1R	Insulin-like growth factor 1 receptor
IGF-2	Insulin-like growth factor 2
IGF-2R	Insulin-like growth factor 2 receptor
IGFALS	IGF acid labile subunit
IGFBP	Insulin-like growth factor-binding protein
INSR	Insulin receptor
IR	ionising radiation
IRF3	Interferon response factor 3
IRS	Insulin receptor substrate
MAPK	Mitogen-activated protein kinase
MCM	Minichromosome maintenance
MDC1	Mediator of DNA damage checkpoint 1
MDM2	Mouse double minute 2 homolog
MEK	MAPK/ERK kinase
MRE11	Meiotic recombination 11 homolog A
MRN	MRE11/RAD50/NBS1
mTORC	Mammalian target of rapamycin complex
MYPT1	Myosin phosphatase targeting subunit 1
NaCl	sodium chloride
NaOH	sodium hydroxide
NDP	ribonucleoside diphosphate
NDPK	nucleoside diphosphate kinase
NF-κB	Nuclear factor-kappa B
NHEJ	non-homologous end-joining
NSCLC	non-small cell lung cancer
NTP	Ribonucleotide triphophate
ORC	Origin recognition complex
PAPP-A	Pregnancy-associated plasma protein A
PARP	Poly (ADP-ribose) polymerase

PBS	phosphate-buffered saline
PBST	phosphate-buffered saline with 0.1% Tween-20
PCNA	Proliferating cell nuclear antigen
PDGFR	Platelet-derived growth factor receptor
PDK-1	Phosphoinositide-dependent kinase 1
PI	propidium iodide
PI3K	Phosphatidylinositide-3-kinase
PIP2	phosphatidylinositol 4,5-bisphosphate
PIP3	phosphatidylinositol 3,4,5-trisphosphate
PLK	Polo-like kinase
PP1	Protein phosphatase 1
PP2A	Protein phosphatase 2A
pre-RC	pre-replicative complex
PTEN	Protein phosphatase and tensin homologue
RAF	Rapidly accelerated fibrosarcoma
RAS	Rat sarcoma
RB	Retinoblastoma protein
RIF1	Replication timing regulatory factor 1
RIPA	radioimmunoprecipitation assay
RNA	ribonucleic acid
RNR	Ribonucleotide reductase
RPA	Replication protein A
RRM1	Ribonucleotide reductase regulatory subunit M1
RRM2	Ribonucleotide reductase regulatory subunit M2
RRM2B	Ribonucleotide reductase regulatory TP53 inducible subunit M2B
RTK	Receptor tyrosine kinase
SAMHD1	Sterile alpha motif and HD domain-containing protein 1
SEM	standard error of the mean
SD	standard deviation
SH2	Src homology 2
siRNA	small interfering RNA

SMARCAL1	SWI/SNF-related, matrix-associated, actin-dependent regulator of chromatin, subfamily A-like1
SOS	Son of sevenless
SSB	single strand break
ssDNA	single-stranded DNA
STING	Stimulator of interferon genes
TCGA	The Cancer Genome Atlas
TKI	tyrosine kinase inhibitor
TMPK	Thymidylate phosphate kinase
TOPBP1	DNA topoisomerase II-binding protein 1
UTB	urea-tris-bicine buffer
UV	ultraviolet

Chapter 1

Introduction

1.1 Insulin-like growth factor (IGF) axis

1.1.1 IGF-1 and IGF-2 ligands

Insulin-like growth factor 1 (IGF-1) and IGF-2 are circulating ligands that play a fundamental role in normal growth, development and differentiation. IGF-1 and IGF-2 are members from insulin protein super family that exhibit a significant sequence and structural homology with insulin (Rinderknecht and Humbel, 1978), but have evolved to have different biological functions. Insulin is an important mediator of glucose metabolism (Saltiel and Kahn, 2001), whereas IGF-1 and IGF-2 are more involved in regulating growth and development (Constancia et al., 2002; Duan et al., 2010; Rowzee et al., 2008). The synthesis, processing and secretion of IGF-1 and IGF-2 are distinct from Insulin. Unlike insulin that is produced, stored and secreted by β cells of the pancreatic islets (Suckale and Solimena, 2008), IGF-1 and IGF-2 are mainly produced in liver, in the case of IGF-1 stimulated by pituitary growth hormone (GH), and then secreted without prior storage into circulation as an endocrine hormone (Zapf and Froesch, 1986). Other tissues are also involved in IGF production, such as cartilage and bone cells, acting locally in an autocrine/paracrine fashion (Nilsson et al., 1986; Xian et al., 2012). Most of the

circulating IGFs remain inactive in complexes with their binding proteins (IGFBPs), which consist of 6 protein family members encoded by *IGFBP1-6* (Baxter, 2000). IGFBPs bind circulating IGFs with high-affinity as transport proteins to modulate the tissue distribution and access to IGF receptors (Baxter, 2000). Among the 6 IGFBPs in human, IGFBP-3 is a major carrier of circulating IGFs and also interacts with IGF acid labile subunit (IGFALS) to form a ternary complex, which significantly prolongs the circulating half-life of IGFs (Baxter, 1990). To release free IGFs from the IGF-IGFBPs complex, pregnancy-associated plasma protein A (PAPP-A) promotes the proteolysis of IGFBPs, particularly IGFBP-3 and IGFBP-5, leading to the reduced binding affinity of IGFBPs with IGFs (Overgaard et al., 2001).

Aberrant IGF production has been implicated in several human syndromes. In 1950s, Dr Zvi Laron described a human condition of GH insensitivity caused by inherited mutation of GH receptor, named as Laron Syndrome (Laron, 2015). People with Laron Syndrome therefore are unable to respond to GH or produce IGF-1 in liver, resulting in a type of dwarfism named Laron-type dwarfism (Laron, 2015). In human, partial deletion of *IGF-1* gene has been showed to cause pre- and postnatal growth retardation (Woods et al., 1996). The inactivation of *IGFALS* gene that encodes ALS results in the reduction of circulating IGF-1 and mild short stature (Domene et al., 2004). Patients with loss of function mutations in *PAPP-A2* gene have high levels of IGFBP-bound IGFs in circulation, but low levels of free and activated IGFs, leading to a phenotype of growth retardation (Dauber et al., 2016). In parallel with these clinical reports, previous studies in mouse models revealed a growth deficiency phenotype in mice carrying disrupted *IGF* and *IGF1R* genes (Baker et al., 1993; Liu et al., 1993).

1.1.2 IGF receptors and IGF signalling

Insulin activates insulin receptor (INSR) on cell surface to transduce the cellular signalling to mediate its metabolic functions (Saltiel and Kahn, 2001). Similarly, the physiological effects of IGF-1 and IGF-2 ligands are mediated by the interaction with their own transmembrane receptors: insulin-like growth factor 1 receptor (IGF-1R) and insulin-like growth factor 2 receptor (IGF-2R). IGF-1R is a transmembrane receptor tyrosine kinase (RTK) that shares 84% sequence homology with INSR in cytoplasmic kinase domain and 100% in ATP bind cleft (Ullrich et al., 1986). IGF-1R has a high affinity for IGF-1, a lower affinity (4~5 fold) with IGF-2 and a much lower affinity (>100 fold) for insulin (Forbes et al., 2002; Gustafson and Rutter, 1990). IGF-1R is a heterotetramer formed by 2 extracellular α subunits with IGF binding site and 2 transmembrane β subunits that contain the intracellular tyrosine kinase domains (Xu et al., 2018). IGF-2R is distinct from either IGF-1R or INSR in that it has no tyrosine kinase activity (Morgan et al., 1987). IGF-2R is preferred to be bound with IGF-2 than IGF-1, mediating the internalisation and degradation of IGF-2 (Kornfeld, 1992). IGF-2R has been considered as growth-suppressive due to this salvaging role of circulating IGF-2 (Kornfeld, 1992). IGF-1 and IGF-2 are not only able to bind IGF-1R and IGF-2R but also interact with INSRs, which consist of 2 isoforms INSR-A and the classical metabolic isoform INSR-B due to the alternative splicing of exon 11 (Moller et al., 1989). INSR-B has very low affinity for IGFs, but IGF-2 binds to INSR-A with an equal affinity to IGF-1R, and this interaction is implicated in the growth of fetal and cancer cells (Frasca et al., 1999).

IGF signalling pathway has been investigated intensively in many studies and is now relatively well characterised (Baserga et al., 1997; Chitnis et al., 2008; Hakuno and Takahashi, 2018). Structural studies indicated that IGF-1R remains in an

autoinhibited state until the binding of IGF ligands, inducing a conformational change (Li et al., 2019; Xu et al., 2018). The relaxation of conformational restraints enables autophosphorylation of specific tyrosine residues at 1131, 1135, and 1136 on β subunits of IGF-1R, leading to the recruitment and phosphorylation of the docking proteins insulin receptor substrates (IRS-1/2) and SHC (Sasaoka et al., 1994; Valverde et al., 1998). These recruited proteins further transmit the signal and activate two independent pathways: phosphoinositide 3-kinase - protein kinase B (PI3K-AKT) pathway and mitogen-activated protein kinase (MAPK) pathway (Figure 1.1).

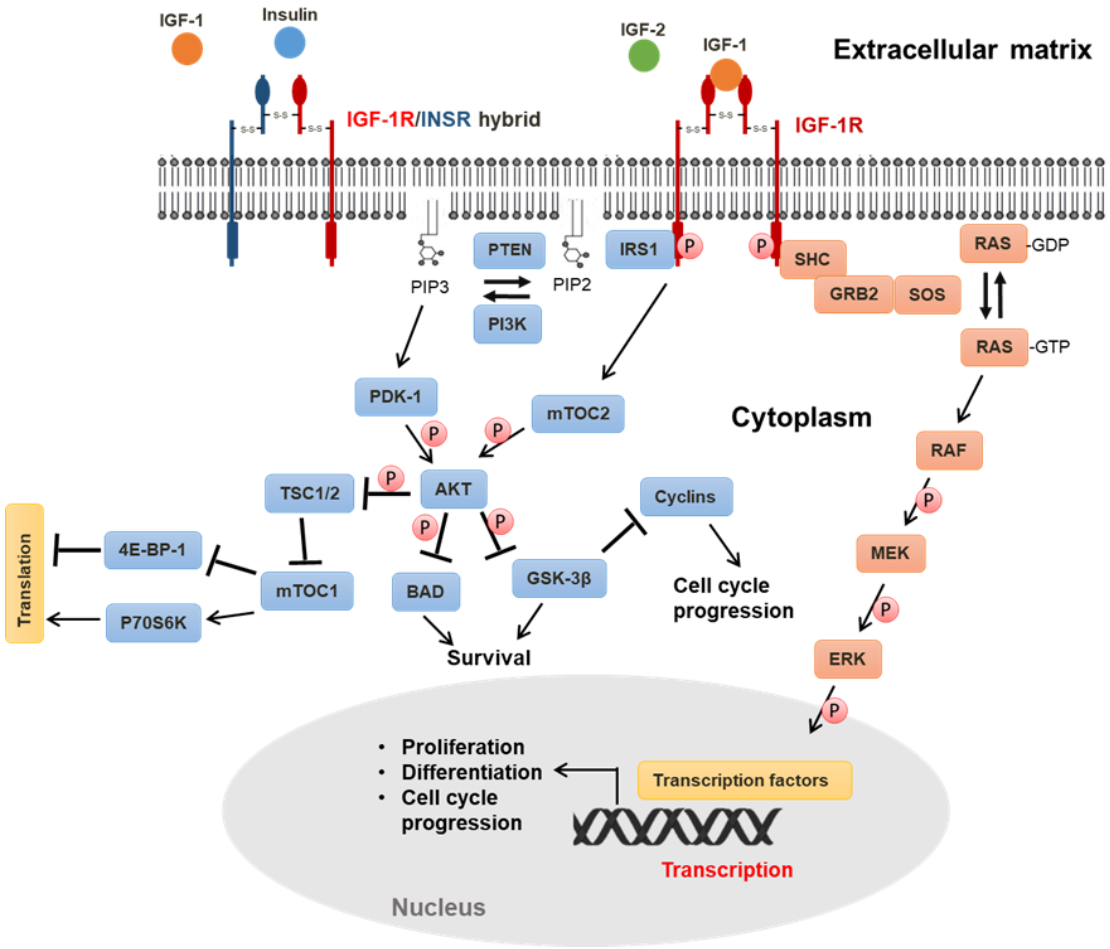

Figure 1.1 IGF signalling pathways
Schematic representation of IGF-1/IGF-2-activated PI3K-AKT pathway and MAPK pathway. Arrow indicates activation. T-symbol indicates inhibition. P in red circle indicates phosphorylation.

PI3K/AKT pathway is a major effector of IGF-1 signalling to mediate cell growth, survival, protein synthesis and metabolism (Manning and Cantley, 2007). Once IRS-1 is recruited to phosphorylated IGF-1R, the phosphotyrosine residues on IRS-1 and IGF-1R itself interact with p85 regulatory subunit of PI3K and consequently activate p110 α catalytic subunit (Myers et al., 1992; Yu et al., 1998). PI3K is recruited to the inner surface of cell membrane and phosphorylates phosphatidylinositol 4,5-bisphosphate (PIP2) to phosphatidylinositol 3,4,5-trisphosphate (PIP3) (Czech, 2000). PIP3 can be dephosphorylated by phosphatase and tensin homolog deleted on chromosome 10 (PTEN), which acts as a negative regulator of PI3K/AKT pathway (Maehama and Dixon, 1998). PIP3 recruits and interacts with a number of PH-domain-containing proteins, including AKT, one of the most characterised downstream targets of PI3K (Burgering and Coffer, 1995). Recruited ATK is further phosphorylated by phosphoinositide-dependent kinase 1 (PDK-1) at Threonine 308 and the mammalian target of rapamycin complex 2 (mTORC2) at Serine 473 to achieve full activation (Alessi et al., 1996). Activated AKT phosphorylates numerous downstream substrates that mediate many different biological functions (Manning and Cantley, 2007). AKT mediates cell growth mainly through phosphorylating mTOC1, which enables p70 S6 kinase activation and 4E-BP1 inhibition for protein translation (Zoncu et al., 2011). AKT is directly involved in cell survival through inhibitory phosphorylation of pro-apoptotic BAD protein and caspase-9 protease (Cardone et al., 1998; Datta et al., 1997). PI3K-AKT signalling cascade also regulates cell cycle via mediating the expression and interaction of cyclins and cyclin-dependent kinases (CDKs) (Liang and Slingerland, 2003). AKT signalling also phosphorylates and inhibits glycogen synthase kinase-3β (GSK-3β), which is a key

regulator in mediating glycogen metabolism, cell proliferation, cell cycle control, microtubule dynamics and apoptosis (Frame and Cohen, 2001).

MAPK pathway is the second major effector of IGF-1R signalling that governs cell proliferation and differentiation (Zhang and Liu, 2002). Upon the recruitment of SHC, growth factor receptor-bound protein 2 (GRB2) binds to the phosphotyrosine residues on SHC and interacts with a guanine nucleotide exchange factor, son of sevenless (SOS) (Ravichandran et al., 1995). Once SOS is recruited to the inner surface of cell membrane, SOS catalyses guanosine triphosphate (GTP) / guanosine diphosphate (GDP) exchange, leading to the activation of RAS protein from GDP- bound to GTP-bound state (Egan et al., 1993). Activated GTP-bound RAS recruits and activates several downstream effectors, including serine/threonine kinase RAF (Vojtek et al., 1993). Activated RAF phosphorylates its major substrates MEK1/2, which subsequently phosphorylates and activates ERK1/2 (Kyriakis et al., 1992). Activated ERK undergoes nuclear translocation and phosphorylates a large number of substrates including E26 transformation-specific Like protein-1 (ELK-1), c-JUN, c-FOS, and MYC, which are important for proliferation, differentiation and cell cycle progression (Yoon and Seger, 2006).

Of note, both PI3K/AKT pathway and MAPK pathway can also be activated by other RTKs, including INSR, epidermal growth factor receptor (EGFR), fibroblast growth factor receptor (FGFR) and platelet-derived growth factor receptor (PDGFR) (Lemmon and Schlessinger, 2010). The cross-talk between these pathways in both physiological and pathological conditions has been intensively studied (Lemmon and Schlessinger, 2010). Due to the high degree of homology between IGF-1R and INSR, high concentration of IGF and insulin ligands can bind to each other's specific receptor, triggering their downstream signalling pathways to regulate glucose

homeostasis and cell growth (Nakae et al., 2001). IGF-1R, INSR-A and INSR-B can form hybrid receptors with one α-β heterodimeric receptor from each and these hybrid receptors can be activated by both IGF and insulin ligands (Soos et al., 1990).

Although IGF-1R and INSR signal through common downstream effectors, they mediate distinct cellular functions in glucose metabolism or cell growth. A previous study by Professor Carl Ronald Kahn's group demonstrated that the different intracellular domains in IGF-1R and INSR contribute to their distinct patterns of signalling (Cai et al., 2017). They generated chimeric receptors that contain intracellular domains of INSR and extracellular domains of IGF-1R or conversely contain intracellular domains of IGF-1R and extracellular domains of INSR. They found that upon the stimulation of either insulin or IGF-1, receptors with intracellular domain of IGF-1R showed more recruitment of SHC and GAB, activating downstream targets involved in cell proliferation. In contrast, receptors with the intracellular domain of INSR had higher IRS-1 phosphorylation and stronger activation of components of metabolic pathways (Cai et al., 2017).

Previous studies in our group and Dr Olle Larsson's group suggest a non-canonical IGF-1/IGF-1R pathway: activated IGF-1R can be internalised and translocated into the cell nucleus (Aleksic et al., 2010; Aleksic et al., 2018; Sehat et al., 2010). Larsson's group further reported that IGF-1R internalisation and translocation require sumoylation of IGF-1Rβ to interact with p150 (Glued) and importin-β/RanBP2 (Packham et al., 2015).

1.1.3 IGF axis and cancer

Given the important role of IGF signalling in mediating numerous biological functions, IGF axis has been intensively studied in endocrine disorders, skin diseases, cardiovascular diseases, aging and cancer (Osher and Macaulay, 2019; Puche and Castilla-Cortázar, 2012). Through both PI3K/AKT and MAPK pathways, IGF-1R activation by IGFs enables cancer cells to promote tumour growth and transformation, to protect cells from apoptosis, and to drive tumour invasion and metastasis (Baserga et al., 1997; Kim et al., 2007; Lopez and Hanahan, 2002; Resnicoff et al., 1995).

A previous survey by Dr Zvi Laron showed that people with Laron syndrome, also known as Laron-type dwarfs, are almost free from cancers (Shevah and Laron, 2007). Similar protective effects of IGF-1 deficiency against cancers was reported in the Ecuadorian population who carry GH receptor gene mutations (Guevara-Aguirre et al., 2011). Studies in the general population also highlight the association between circulating IGF-1 levels and the risk of cancer, in that people with high serum IGF-1 are at increased risk of common cancers including breast, prostate and colorectal cancers (Ahlgren et al., 2004; Chan et al., 1998; Kaaks et al., 2014; Ma et al., 1999; Renehan et al., 2004; Travis et al., 2016). In addition to IGF-1, loss of *IGF-2* gene imprinting leads to the overexpression of IGF-2, which has been identified as a potential marker of increased risk of colorectal cancer (Cui et al., 2003). IGF-2 overexpression or epigenetic alteration has also been found in hepatocellular carcinoma and Ewing sarcoma, which is associated with cancer progression and poor prognosis (Couvert et al., 2008; Steigen et al., 2009). Circulating IGF-2 has been reported not only to activate IGF-1R, but also INSR-A (Frasca et al., 1999). INSR-A is commonly overexpressed in human cancers and its

interaction between IGF-2 has been demonstrated in breast, lung, and colon cancer tissues (Frasca et al., 1999).

Solid tumours frequently show elevated expression of IGF-1R in prostate, breast, colorectal and head and neck cancers (Farabaugh et al., 2015; Hellawell et al., 2002; Rochester et al., 2007; Weber et al., 2002). Previous work from our group showed that high level of IGF-1R expression in prostate tumour tissues associates with increased risk of post-radiotherapy recurrence (Aleksic et al., 2017). IGF-1R overexpression in head and neck tumours was found in association with negativity for human papillomavirus and poor prognosis (Dale et al., 2015). Recent work of brain cancers from our group showed that IGF-1R mediates radioresistance and IGF-1R overexpression associates with worse survival in paediatric high-grade glioma patients but not in adult high-grade glioma patients (Simpson et al., 2020). It has also been shown that IGF-1R overexpression promotes radioresistance in breast cancers and IGF-1R expression in primary breast tumours highly associates with recurrence following lumpectomy and radiation (Turner et al., 1997). Notably, different breast cancer subtypes display the distinct correlations between IGF-1R signalling and prognosis (Farabaugh et al., 2015). Previous tissue analysis of tumours from patients with different subtypes of breast cancers showed that IGF-1R expression has no association with the survival of patients with luminal A breast cancers, but associates with better prognosis in luminal B cancers, whereas IGF-1R correlates with worse survival in Human epidermal growth factor receptor 2 (HER2)-enriched breast cancer (Yerushalmi et al., 2012). Patients with triple-negative breast cancers whose tumours have high levels of IGF-1R expression have lower survival rates (Hartog et al., 2011). Due to the growth inhibition effect of IGF-2R, the role of IGF-2R in cancers has been considered as tumour-suppressive

(Martin-Kleiner and Gall Troselj, 2010). Indeed, loss of IGF-2R function has been associated with the development of breast, prostate and liver cancers (De Souza et al., 1995; Hankins et al., 1996; Hu et al., 2006).

Our group previously reported the association between nuclear IGF-1R and tumour stage in prostate cancer that IGF-1R is predominantly detected on cell membrane in patient benign tissues, whereas tumour tissues contain more internalised nuclear IGF-1R (Aleksic et al., 2010). We further demonstrated that nuclear IGF-1R plays an important role in mediating tumour cell survival and migration through interacting with chromatin at the transcription start sites of genes including *JUN* and *FAM21* (Aleksic et al., 2018).

Although *IGFBP* genes are not frequently mutated in cancers, epigenetic silencing of *IGFBP* gene expression is associated with some types of cancers (Baxter, 2014). For example, patients with hepatocellular carcinoma have reduced IGFBP-3 expression due to the hypermethylation on its promoter (Hanafusa et al., 2002). High circulating IGFBP-3 is associated with a lower risk of colorectal cancer in a prospective case-control study (Ma et al., 1999). However, the opposite correlation has been reported in breast cancer that high level of circulating IGFBP-3 is associated with the increased risk (Renehan et al., 2004). In a previous report, high levels of IGFBP-3 were also observed in primary tumour tissues in breast cancer patients, which was correlated with poor prognosis (Rocha et al., 1996). Therefore, the role of IGFBP-3 in cancers can be oncogenic or tumour-suppressive in different cancer types or cancer stages. A previous tissue microarray analysis of over 400 ovarian cancer patient tissues showed that IGFBP-2 and IGFBP-5 were overexpressed in high grade serous carcinomas compared to normal surface

epithelium, benign tissues and low-grade serous carcinoma, suggesting a potential role of IGFBP-2 and 5 in cancer development (Wang et al., 2006).

1.1.4 IGF-targeted cancer therapy

Targeting IGF signalling has been long recognised as a promising strategy to treat various types of cancer (Gualberto and Pollak, 2009; Osher and Macaulay, 2019). A large number of IGF-targeted therapies have been evaluated or are currently under evaluation in clinical trials (Table 1.1), which are mainly categorised into 3 classes: monoclonal anti-IGF-1R antibodies, small molecule tyrosine kinase inhibitors (TKIs), and IGF ligand antibodies.

Table 1.1 Examples of IGF-targeted therapies in clinical trials (https://clinicaltrials.gov/)

Drug name	Mechanism of action	Clinical stage
Figitumumab (CP-751,871)	anti-IGF-1R antibody	Phase III (NCT00673049), Phase III (NCT00596830), Phase Ib/2 (NCT00560573), Phase I (NCT00147537) in Lung cancer; Phase II (NCT00560560) in Colorectal cancer; Phase I (NCT00474760) in Ewing sarcoma
Ganitumab (AMG 479)	anti-IGF-1R antibody	Phase III (NCT02306161, ongoing), Phase II (NCT04129151) in Ewing sarcoma; Phase I/II (NCT03041701, ongoing) in Rhabdomyosarcoma; Phase Ib/II (NCT00807612), Phase I (NCT01061788) in lung cancer; Phase Ib/II (NCT00788957) in Colorectal cancer; Phase II (NCT00719212), Phase II (NCT00718523) in Ovarian cancer; Phase III (NCT01231347), Phase II (NCT01318642), Phase I (NCT01298401), Phase Ib/II (NCT00630552) in Pancreatic cancer; Phase II (NCT00563680), Phase II (NCT01327612), Phase Ib/II (NCT01708161), Phase Ib/II (NCT00819169) Phase I (NCT01122199) in multiple cancer types
Cixutumumab (IMC-A12)	anti-IGF-1R antibody	Phase II (NCT00955305), Phase II (NCT01232452), Phase II (NCT00870870), Phase II (NCT00986674), Phase II (NCT01263782), Phase II (NCT00887159), Phase I/II (NCT00778167) in Lung cancer; Phase II (NCT00684983), Phase II (NCT00728949), Phase Ib/II (NCT00699491), Phase I (NCT00699491) in Breast cancer Phase II (NCT01120236), Phase II (NCT00520481) in Prostate cancer;

		Phase II (NCT00503685) in Colorectal cancer; Phase I/II (NCT00617708) in Pancreatic Cancer; Phase II (NCT00906373), Phase I (NCT01008566) in Liver cancer; Phase II (NCT00617734) in Head and neck cancer; Phase I (NCT01204476) in Neuroendocrine tumours Phase II (NCT01142388) in Esophageal Adenocarcinoma; Phase II (NCT01055314) in Rhabdomyosarcoma; Phase II (NCT01614795), Phase II (NCT01016015), Phase II (NCT00831844), Phase I (NCT01007032) in multiple cancer types
Dalotuzumab (MK-0646, h7C10)	anti-IGF-1R antibody	Phase II (NCT00654420), Phase II (NCT00799240), Phase I/II (NCT00869752) in Lung cancer; Phase II (NCT01605396), Phase II (NCT01234857), Phase I (NCT00759785) in Breast cancer; Phase II (NCT00614393), Phase I (NCT00925015) in Colorectal cancer; Phase II (NCT00769483) in Pancreatic cancer Phase II (NCT00610129) in Neuroendocrine tumours Phase I (NCT00635778), Phase I (NCT00701103), Phase I (NCT00694356), Phase I (NCT01431547), Phase I (NCT01243762) in multiple cancer types
Robatumumab (SCH 717454, 19D12)	anti-IGF-1R antibody	Phase II (NCT00617890) in Ewing sarcoma; Phase II (NCT00551213) in Colorectal cancer;
Istiratumab (MM-141)	anti-IGF-1R antibody	Phase II (NCT02399137) in Pancreatic Cancer Phase I (NCT01733004) in multiple cancer types
R1507	anti-IGF-1R antibody	Phase II (NCT00760929), Phase II (NCT00773383) in Lung cancer Phase II (NCT00796107), Phase I (NCT00882674) in Breast cancer Phase II (NCT00642941), Phase I (NCT00400361), Phase I (NCT00560144) in multiple cancer types
BIIB022	anti-IGF-1R antibody	Phase I (NCT00970580) in Lung cancer; Phase I (NCT00956436) in Liver cancer; Phase I (NCT00555724) in multiple cancer types
AVE1642	anti-IGF-1R antibody	Phase I (NCT01233895) in multiple cancer types
Linsitinib (OSI-906)	IGF-1R TKI	Phase III (NCT00924989) in Adrenocortical carcinoma; Phase II (NCT02546544) in Ewing Sarcoma; Phase II (NCT01186861), Phase II (NCT01221077), Phase II (NCT01533181) in Lung cancer; Phase II (NCT01533246) in Prostate cancer; Phase II (NCT01205685) in Breast cancer; Phase I/II (NCT00889382) in Ovarian cancer; Phase I (NCT01154335) in Colorectal cancer; Phase I (NCT00514306), Phase I (NCT00514007), Phase I (NCT00739453) in multiple cancer types

BMS-754807	IGF-1R TKI	Phase I/II (NCT00788333), Phase II (NCT01225172) in Breast cancer Phase I/II (NCT00908024), Phase I (NCT00898716), Phase I (NCT00569036), Phase I (NCT00793897) in multiple cancer types
XL-228	IGF-1R TKI	Phase I (NCT00464113) in Leukaemia; Phase I (NCT00526838) in multiple cancer types
Picropodophyllin (AXL1717)	IGF-1R TKI	Phase II (NCT01561456), Phase I (NCT01466647) in Lung cancer; Phase I (NCT01725555), Phase I (NCT01062620) in multiple cancer types
Masoprocol (NDGA)	IGF-1R TKI	Phase II (NCT00678015) in Prostate cancer
Dusigitumab (MEDI-573)	IGF neutralising antibody	Phase II (NCT01446159) in Breast cancer; Phase I (NCT01498952) in Liver cancer; Phase I (NCT01340040), Phase I (NCT00816361) in multiple cancer types
Xentuzumab (BI-836845)	IGF neutralising antibody	Phase II (NCT03659136, ongoing), Phase I (NCT03099174, ongoing), Phase II (NCT02123823, ongoing) in Breast cancer; Phase Ib/II (NCT02204072, ongoing) in Prostate cancer; Phase I (NCT02191891) in Lung cancer; Phase I (NCT01403974), Phase I (NCT02145741), Phase I (NCT01317420) in multiple cancer types

Monoclonal anti-IGF-1R antibodies are designed to bind IGF-1R α subunit and induce receptor internalisation and degradation, thus preventing the binding of IGF-1 and IGF-2. Preclinical studies of anti-IGF-1R antibodies, such as figitumumab, cixutumumab and ganitumab, showed the blockade of IGF signalling and preliminary anti-tumour activities in gastrointestinal carcinomas, prostate and ovarian cancer cell lines (Beltran et al., 2014; Ii et al., 2011; Wu et al., 2006). Several of these anti-IGF-1R antibodies have been tested in clinical trials and reached to Phase II or Phase III (Table 1.1). Some of them showed clinical benefits, particularly in patients with Ewing sarcoma (Tolcher et al., 2009; van Maldegem et al., 2016), but many trials reported insufficient activity in unselected patients (Fuchs et al., 2015; Konecny et al., 2014; Kundranda et al., 2020; Scagliotti et al., 2015). This might be due to the activation of compensating pathways, such as INSR, EGFR, C-MET, thereby restoring IGF-1R downstream signalling (Liu et al., 2018; van der Veeken

et al., 2009; Zhang et al., 2007). Although anti-IGF-1R antibodies are highly specific to IGF-1R with no affinity for INSR, some anti-IGF-1R antibodies still interact with and downregulate IGF1R-INSR hybrid receptor, causing dose-limiting hyperglycemia (Malempati et al., 2012). There is still one monoclonal anti-IGF-1R antibody drug ganitumab, currently in evaluation in two clinical trials. In an ongoing phase I/II trial, ganitumab is tested in combination with Src Family Kinase (SFK) inhibitor in patients with embryonal and alveolar rhabdomyosarcoma (NCT03041701). Another phase III trial is studying the combination treatment of ganitumab and chemotherapy in patients with metastatic Ewing sarcoma (NCT02306161).

IGF-1R TKIs are small molecules that inhibit IGF-1R tyrosine kinase domain, leading to the blockade of downstream signalling. A number of IGF-1R TKIs have been developed, and many of them showed promising anti-tumour activities in preclinical studies (Carboni et al., 2009; Garcia-Echeverria et al., 2004; Litzenburger et al., 2009; Mulvihill et al., 2009; Sanderson et al., 2015). However, only a few of them were used in clinical studies (Table 1.1), and their clinical evaluation turned out to be disappointing (Fassnacht et al., 2015; Friedlander et al., 2012). This is largely because that most IGF-1R TKIs also inhibit INSR as IGF-1R and INSR have 100% conserved ATP binding cleft on their kinase domains (Ullrich et al., 1986). Therefore, some patients treated with IGF-1R TKIs experienced dose-limiting hyperglycemia (Fassnacht et al., 2015; Schwartz et al., 2016). The limited clinical activities of IGF-1R TKIs might also be the results of the rebound effect, which can be caused by the high levels of IGF and insulin induced by IGF-1R TKI that stimulate IGF-1R or INSR signalling if IGF-1R TKI withdrawal (Macaulay et al., 2016).

IGF neutralising antibodies directly target IGF-1 and IGF-2 ligands with high affinity to prevent IGF ligand binding to IGF-1R, INSR and INSR/IGF-1R hybrid receptor. Two IGF neutralising antibodies, dusigitumab (MEDI-573) and xentuzumab (BI-836845), have been developed (Table 1.1). Dusigitumab and xentuzumab have high binding affinity for both IGF-1 and IGF-2, but dusigitumab is more selective to IGF-2, whereas xentuzumab is more selective to IGF-1 (Friedbichler et al., 2014; Gao et al., 2011). Both antibodies have no impact on circulating insulin, thus not likely to induce hyperglycemia (Friedbichler et al., 2014; Gao et al., 2011). Dusigitumab and xentuzumab showed very effective IGF signalling blockade and promising anti-tumour activities *in vitro* and *in vivo* in Ewing sarcoma, breast and colorectal cancers (Friedbichler et al., 2014; Gao et al., 2011) and have also been tested in clinical studies (Table 1.1). In two phase I clinical trials in patients with advanced solid tumours (NCT00816361, NCT01340040), dusigitumab showed favourable tolerability and some preliminary activities (Haluska et al., 2014; Iguchi et al., 2015). Dusigitumab has also been tested in a phase Ib/II trial (NCT01446159) to combine aromatase inhibitor in patients with hormone receptor (HR) + and HER2- metastatic breast cancer, but the addition of dusigitumab had no impact on overall survival rate (https://clinicaltrials.gov). Xentuzumab is currently being evaluated in several clinical trials. In a phase I trial in advanced solid tumours (NCT01403974), xentuzumab was well-tolerated and had preliminary anti-tumour activity (de Bono et al., 2020). Another phase I trial (NCT02191891) investigated the combination of xentuzumab and EGFR inhibitor afatinib in patients with EGFR-mutant non-small cell lung cancer (NSCLC), but no results are published to date. The ongoing phase Ib/II clinical trials include testing xentuzumab in combination with enzalutamide in prostate cancer patients (NCT02204072), and in combination with everolimus and exemestane in

patients with HR+/HER2- breast cancer (NCT02123823). In the phase II trial (NCT02123823) in breast cancer, xentuzumab did not improve progression-free survival, but showed the evidence of benefit in patients with non-visceral disease (Crown et al., 2019). This prompted a phase II trial (NCT03659136) of investigating xentuzumab in patients with HR+/HER2- breast cancer and non-visceral disease.

Together, current IGF-targeted drugs showed some clinical benefit in some cancer patients, such as in patients with Ewing Sarcoma, but most of these drugs had insufficient activity in unselected patients, suggesting the necessity to characterise sensitive tumours and design rational drug combinations to improve IGF-targeted therapy.

1.2 Cell cycle

IGFs are well-known to promote cell proliferation by regulating passage through the cell cycle (Chakravarthy et al., 2000; Dupont and Holzenberger, 2003; Muise-Helmericks et al., 1998; Tang et al., 2017).

1.2.1 Cell cycle phases

Cell cycle is a fundamental biological process that has been intensively studied over many decades (Hunt et al., 2011). In human, quiescent and terminally differentiated cells are arrested in a state, which is described as G0 phase of cell cycle (Terzi et al., 2016). The terminally differentiated cells are permanently arrested, but quiescent cells can be stimulated by mitogenic signalling to enter into cell cycle for proliferation (O'Farrell, 2011). Proliferating cells sequentially progress through four distinct cell cycle phases: G1, S, G2, M. In G1 phase, cells actively start to accumulate the proteins, building blocks and energy reserves for DNA replicating (Bertoli et al.,

2013). DNA replication takes place in S phase, resulting in the formation of two identical sister chromatids. During S phase, cells also duplicate the centrosome, which is the organelle that is required in mitosis (Ganem et al., 2009). In G2 phase, cells prepare the proteins, enzymes, and energy reserves for M phase, known as Mitosis. Mitosis is divided into four phases: prophase, metaphase, anaphase, and telophase (Walczak et al., 2010), resulting in cell division into two daughter cells. In prophase, nuclear envelope breaks down, chromosomes condense and mitotic spindle microtubules are formed from the two centrosomes (Inoué, 1981). In metaphase, mitotic spindles attach to chromosomes at their kinetochores on the centromeric regions (Rieder and Salmon, 1994). Two centrosomes move to two opposing poles and chromosomes are lined up at the metaphase plate (Wood et al., 1997). In anaphase, cohesin proteins that bind two sister chromatids together break down, and each sister chromatid is pulled toward one centrosome on one of the opposing poles (Uhlmann et al., 2000). In telophase, chromosomes start to decondense, nuclear envelopes begin to form and mitotic spindles break down (Inoué, 1981). The cell undergoes cytokinesis and forms two daughter cells. Newly formed cells either exit cell cycle to stay in G0 phase (quiescence) or progress to G1 phase for another cell cycle.

1.2.2 Cell cycle regulation

1.2.2.1 Cyclin-dependent kinases

The cell cycle includes numerous biological events that require timely and carefully organisation during each cell cycle phase to ensure correct genome duplication and cell division (Hunt et al., 2011). Therefore, the cell cycle is tightly regulated by a complex network, involving a large number of cell cycle proteins (Figure 1.2).

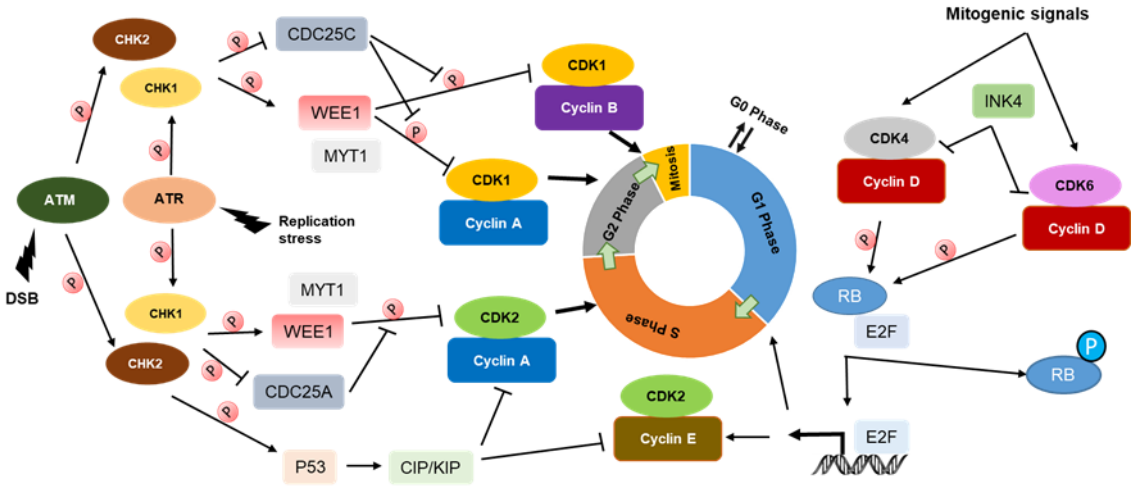

Figure 1.2 Cell cycle progression and the key regulators
Schematic representation of cell cycle progression mediated by cyclin-dependent kinases (CDKs), CDK inhibitory proteins and checkpoint kinases. Arrow indicates activation. T-symbol indicates inhibition. P in red circle indicates phosphorylation. DSB: double-strand breaks. Adapted from (Otto and Sicinski, 2017)

The major proteins in regulating cell cycle progression are cyclin-dependent kinases (CDKs). CDKs are serine/threonine kinases and their catalytic activity requires the binding with their regulatory subunits, known as Cyclins (Malumbres and Barbacid, 2005). The human genome contains 21 genes encoding CDKs that share the sequence and functional similarity (Malumbres et al., 2009). However, only 4 human CDKs are closely relevant to cell cycle control, which are CDK1, CDK2, CDK4 and CDK6, and they can form active complexes with 4 types of Cyclins, which are Cyclin A, Cyclin B, Cyclin D and Cyclin E (Hochegger et al., 2008). The expression and degradation of Cyclins are timely regulated at specific cell cycle phases, thus controlling CDK kinase activity for proper cell cycle progression (Glotzer et al., 1991). Once cells receive a mitogenic stimulus, such as is provided by IGFs, cells enter into G1 phase. Activated PI3K/AKT and MEK/ERK pathways increase the expression of Cyclin D (Diehl et al., 1998; Lavoie et al., 1996; Muise-Helmericks et al., 1998; Tang et al., 2017). Cyclin D has high binding affinity with both CDK4 and

CDK6, which exhibit high sequence and structural homology and share a large number of overlapping phosphorylation substrates (Wood and Endicott, 2018). One of the most characterised substrates of CDK4/6-Cyclin D complex is retinoblastoma protein (RB) (Lundberg and Weinberg, 1998). CDK4/6-Cyclin D also phosphorylates RB related proteins p107 (RBL1) and p130 (RBL2) (Graña et al., 1998). RB, RBL1 and RBL2 bind and inhibit the transactivation domain of E2F transcription factors (Chellappan et al., 1991). Phosphorylation of RB, RBL1 and RBL2 releases and activates E2F, promoting the expression of numerous proteins that drive G1/S transition, including Cyclin E (Weinberg, 1995). CDK2 preferably interacts with Cyclin E, and CDK2-Cyclin E complex further phosphorylates RB and releases E2F, forming a positive feedback loop (Akiyama et al., 1992). After cells enter into S phase, CDK2-Cyclin E complex phosphorylates various proteins that mediate DNA replication and centrosome duplication (Coverley et al., 2002; Okuda et al., 2000). Of note, during S phase, Cyclin E protein level gradually decreases, which is mainly due to SCF-Fbw7-mediated ubiquitination and degradation (Koepp et al., 2001). However, Cyclin A protein level increases and CDK2 switches to form complexes with Cyclin A (Coverley et al., 2002). Cyclin E and Cyclin A have distinct roles when binding with CDK2, in that CDK2-Cyclin E stimulates replication machinery assembly, whereas CDK2-Cyclin A activates replication machinery that is already assembled and prevents replication re-initiation (Coverley et al., 2002). Cyclin A protein level maintains until cells enter into mitosis when Cyclin A is recognised by APC/C ubiquitin ligase for degradation (Geley et al., 2001). During G2 phase and mitosis, CDK1 is the predominant CDK that can bind to either Cyclin A or Cyclin B, phosphorylating many substrates, including proteins that mediate G2/M transition, chromosome condensation, mitotic spindle assembly, and cytokinesis (Enserink

and Kolodner, 2010). Cyclin B protein is also degraded by APC-CDC20-mediated proteolysis, but at a later stage of mitosis (Hershko, 1999). Cyclin A and Cyclin B are degraded at different time, which might be due to fact that the active spindle checkpoint during early mitosis appears to delay the degradation of cyclin B, while Cyclin A is not affected (Tin Su, 2001).

1.2.2.2 CDK inhibitory proteins

Given the important role of CDK-Cyclin complexes in promoting cell cycle progression, the interactions between CDKs and their partner Cyclins are tightly regulated. There are two important families of proteins, INK4 family and Cip/Kip family that negatively regulate CDK-Cyclin complexes, known as CDK inhibitors (CKIs) (Otto and Sicinski, 2017). The INK4 family consists of p15, p16, p18 and p19 proteins, which specifically interact with CDK4/6, preventing their binding to Cyclin D (Jeffrey et al., 2000). The Cip/Kip family contains p21, p27 and p57 proteins that interfere with the formation of CDK2-Cyclin E, CDK2-Cyclin A, CDK4/6-Cyclin D (Denicourt and Dowdy, 2004). Of note, the p21 gene is a transcriptional target of p53 tumour suppressor (el-Deiry et al., 1993). In addition to the function of p21 in cell cycle control, p21 protein also mediates DNA replication by directly interacting with PCNA (Waga et al., 1994; Xiong et al., 1993).

1.2.2.3 Cell cycle checkpoints

In response to replication stress or DNA damage, cells can activate cell cycle checkpoints to arrest cell cycle, providing sufficient time for replication fork recovery and DNA repair (Kastan and Bartek, 2004). Cell cycle checkpoints play a critical role in safeguarding genome integrity. There are 4 checkpoint kinases that have been characterised, including Checkpoint kinase 1 (CHK1), CHK2, WEE1 and MYT1 kinases. CHK1 and CHK2 are mainly activated by two master regulators of DNA

damage ataxia-telangiectasia mutated (ATM) and ATM and RAD3-related (ATR) protein kinases (Figure 1.3).

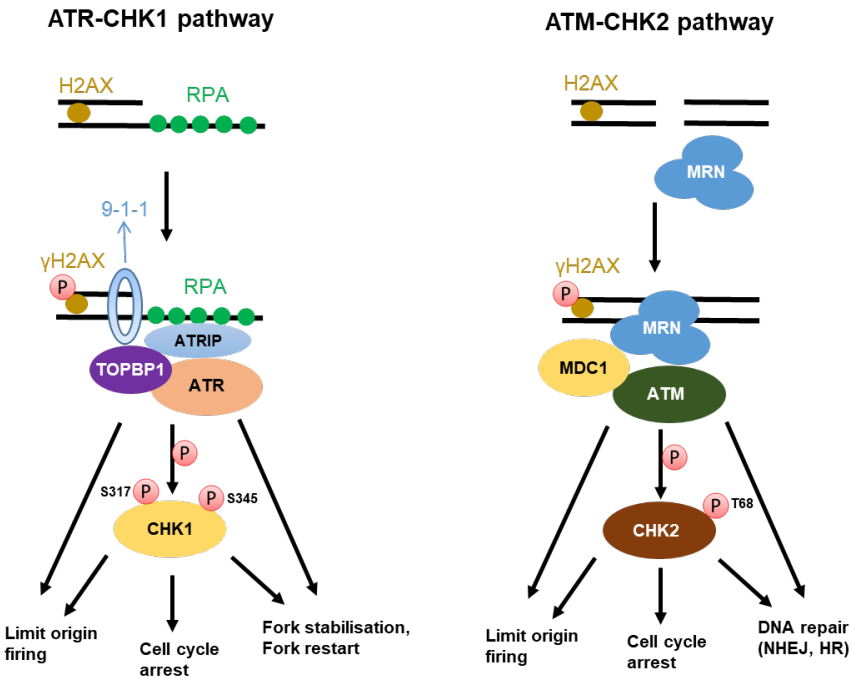

Figure 1.3 ATR and ATM signalling pathways
Schematic representation of ATR-CHK1 signalling pathway in response to replication stress (left) and ATM-CHK2 signalling pathway in response to DSB (right). Adapted from (Cimprich and Cortez, 2008)

In response to DNA single stranded breaks (SSB) induced by ultraviolet (UV) exposure or replication stress, the exposed single-stranded DNAs (ssDNA) are coated with replication protein A (RPA), which is essential to stabilise the stalled replication fork and activate ATR signalling cascade(Iftode et al., 1999). The recruitment and activation of ATR requires RPA-coated ssDNA to first recruit a protein complex including ATR-interacting protein (ATRIP), DNA clamp protein Rad9-Rad1-Hus1 (9-1-1) and Topoisomerase II-binding protein 1 (TOPBP1) (Cimprich and Cortez, 2008). Activated ATR phosphorylates its major downstream effector CHK1 at Serine 317 and Serine 345 to transduce the signalling cascade (Zhao and Piwnica-Worms, 2001). Activated CHK1 phosphorylates numerous

substrates, including CDC25s (Figure 1.2), a family of phosphatases that remove the inhibitory phosphorylation of CDK1 and CDK2 at tyrosine 15 and threonine 14 (Bartek and Lukas, 2003). CHK1 phosphorylates CDC25s and promotes their degradation (Xiao et al., 2003), resulting in the accumulation of inhibitory phosphorylation of CDK1 and CDK2. Therefore, CDK1 and CDK2 cannot form active complexes with Cyclin A or Cyclin B, leading to cell cycle arrest in S phase or at G2/M transition. The inhibitory phosphorylation of CDK1 and CDK2 at tyrosine 15 is directly induced by protein kinase WEE1 (Parker and Piwnica-Worms, 1992) and the inhibitory phosphorylation at threonine 14 is performed by MYT1 kinase (Booher et al., 1997). WEE1 and MYT1 act as checkpoint kinases to restrain CDK1 or CDK2 activity, but WEE1 is indispensable for cell cycle arrest, whereas MYT1 is considered to be not important for normal cell cycle checkpoint activation, but contribute checkpoint recovery when CHK1 or WEE1 is inhibited (Chow and Poon, 2013).

ATM is the major regulator to orchestrate responses to DSB (Shiloh, 2003). At DSB sites, ATM is recruited and activated in cooperation with Mre11-Rad50-Nbs1 (MRN) complex and the adaptors 53BP1 and DNA damage checkpoint 1 (MDC1) (Figure 1.3) (Lee et al., 2010; Lou et al., 2006; Uziel et al., 2003). Activated ATM phosphorylates CHK2 at threonine 68 (Matsuoka et al., 2000). Similar to CHK1, activated CHK2 actives cell cycle checkpoints though CDC25s phosphorylation and CDKs inhibition (Bartek and Lukas, 2003). In addition, ATM is involved in two major DSB repair pathways, non-homologous end joining (NHEJ), which efficiently repairs most DSBs in mammalian cells and is mostly accurate, and homologous recombination (HR), which occurs only in S and G2 phases as sister chromatids are required (Beucher et al., 2009; Riballo et al., 2004; Scully et al., 2019). HR is

typically considered error-free, but it has also been shown that HR can be error-prone, which is mainly caused by the intermediates of HR including gene conversion and crossing over, generating genetic instability (Guirouilh-Barbat et al., 2014). Of note, previous work from our lab and others showed that IGF-1R depletion or inhibition impairs both NHEJ and HR pathways and delays repair of ionising radiation (IR)-induced DSBs (Chitnis et al., 2014; Turney et al., 2012; Wang et al., 2013).

Both CHK1 and CHK2 can phosphorylate p53 at Serine 20, enhancing the expression of p21 for further inhibition of CDKs (Shieh et al., 2000). In addition, ATM/CHK2 and ATR/CHK1 pathways not only regulate cell cycle progression, but also play an important role in mediating apoptosis via regulating p53 (Figure 1.4) (Adam et al., 2018; Bartek and Lukas, 2003; Nai et al., 2019).

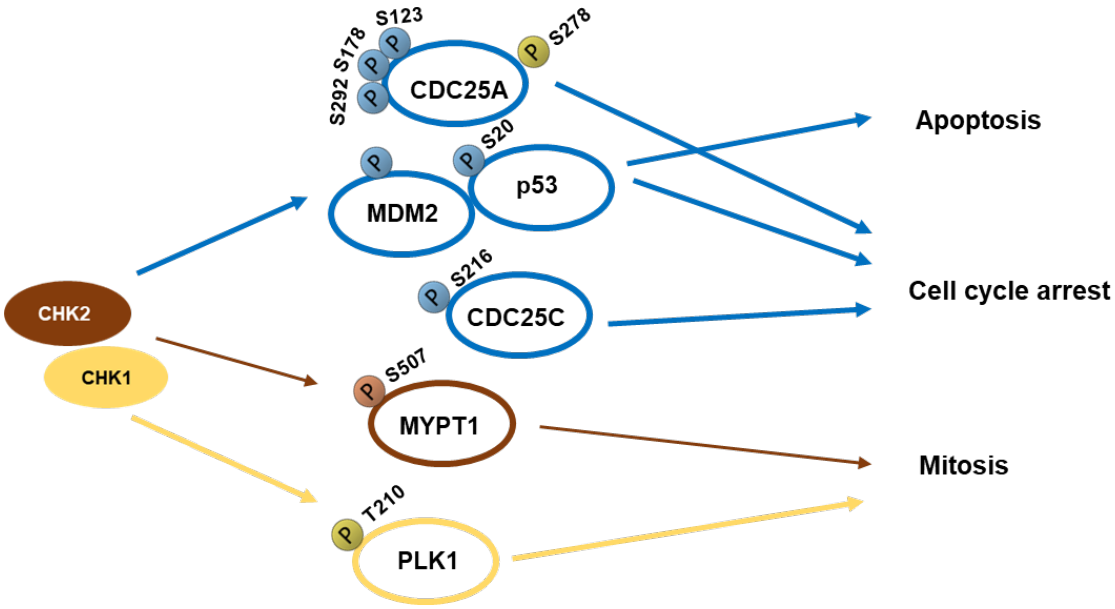

Figure 1.4 Downstream effectors of CHK1 and CHK2
Schematic representation of substrates that can be phosphorylated by CHK1 and/or CHK1. Yellow: phosphorylated by CHK1 alone. Brown: phosphorylated by CHK2 alone. Blue: phosphorylated by both CHK1 and CHK2.

1.2.3 Cell cycle and cancer

Tumour cells usually acquire mutations that lead to aberrant cell cycle controls to maintain not only the sustained cell proliferation but also genome instability (Malumbres and Barbacid, 2009). For example, *CCND1* gene that encodes Cyclin D1 is the second most frequently amplified locus in all human cancers (Beroukhim et al., 2010). The analysis of TCGA data showed that *CCNE1* and *CCNE2* genes that encode Cyclin E1 and Cyclin E2 are frequently amplified in ovarian, breast and bladder cancers (Otto and Sicinski, 2017). In human melanoma, an INK4-insensitive mutation (R24C) of CDK4 has been observed, which can constitutively activate CDK4 (Wolfel et al., 1995). RB is a tumour suppressor that is commonly depleted in many types of cancers, resulting in the loss of cell cycle control by CDKs (Otto and Sicinski, 2017). The genetic alterations of CKIs are also frequently detected in cancers. For example, *CDKN2A* that encodes INK4 p16 and p14 proteins is the most frequently deleted locus in human malignancies (Beroukhim et al., 2010). Tumour suppressor p53 is mutated in many types of cancers (Olivier et al., 2010). P53 inactivation leads to the reduction of p21 to abrogate cell cycle arrest upon DNA damage, which might contribute to p53 loss-induced tumorigenesis (Engeland, 2018).

Cell cycle checkpoint kinases were initially considered tumour suppressive because loss of cell cycle checkpoints may favour the rapid proliferation of cancer cells. Although homozygous mutations of CHK1 haven't been reported so far (Zhang and Hunter, 2014), heterozygous loss of function mutations of CHK1 are detected in breast and gastric cancer (Menoyo et al., 2001; Mu et al., 2011). However, CHK1 overexpression is also commonly observed in various types of cancers, including triple-negative breast cancer, cervical cancer and hepatocellular carcinoma

(Verlinden et al., 2007; Xie et al., 2014b; Xu et al., 2013). WEE1 overexpression is observed in many cancers, including glioblastoma, melanoma and hepatocellular carcinoma (Magnussen et al., 2012; Masaki et al., 2003; Mir et al., 2010). The elevated expression of CHK1 and WEE1 in cancer cells might reflect their important roles in cell cycle control and DNA replication upon DNA damage and replication stress. Both CHK1 and WEE1 play an important role in maintaining sufficient and balanced dNTP pools, required to avoid replication stress (Buisson et al., 2015; Koppenhafer et al., 2020; Pfister et al., 2015). Cell cycle checkpoint abrogation upon DNA damage leads to the premature transition of cell cycle phases, resulting in mitotic catastrophe or replication catastrophe (Aarts et al., 2012; Toledo et al., 2013). It has also been recently reported that CHK1 inhibition synergises with cyclin F loss in cancer cells to aberrantly accumulate E2F1 transcription factor, causing catastrophic DNA damage in S phase (Burdova et al., 2019). Therefore, targeting CHK1 and WEE1 might be a promising therapeutic strategy for cancer treatment.

1.2.4 Targeting cell cycle checkpoints and CDKs in cancer treatment

Several CHK1 inhibitors have been developed and evaluated in clinical studies (Table 1.2). Highly selective CHK1 inhibitor MK-8776 (also known as SCH-900776) has been tested in combination with gemcitabine in a Phase I clinical trial in patients with advanced solid tumours (NCT00779584), showing acceptable tolerability and early evidence of clinical efficacy (Daud et al., 2015). MK-8776 has also been evaluated in combination with cytarabine in a Phase I clinical trial in patients with acute myelogenous leukemia (AML) (NCT00907517), showing that the combination of MK-8776 and cytarabine were tolerable and showed some preliminary anti-leukemia activity (Karp et al., 2012). However, the combination of cytarabine and MK-8776 did not show a better response rate than cytarabine alone in the Phase II

trial in patients with relapsed AML (NCT01870596) (Webster et al., 2017). LY2606368, also known as Preasertib, is a CHK1/2 inhibitor that is being tested as monotherapy in an ongoing Phase II trial in patients with breast, ovarian or prostate cancers (NCT02203513). Another Phase I clinical trial in patients with advanced solid tumours is studying LY2606368 in combination with PD-L1 inhibitor LY3300054 (NCT03495323). SRA737, a potent and orally bioavailable CHK1 inhibitor, is currently in a phase I/II trial in patients with advanced solid tumours (NCT02797964). MK-1775 (also known as AZD 1775 or Adavosertib) is the only WEE1 inhibitor currently in clinical application. The completed clinical trials of MK-1775 have shown preliminary clinical benefits either alone or in combination with other cancer therapies (Fu et al., 2018). To date, there are over 20 ongoing clinical trials in various types of cancers, including a Phase II trial of testing MK-1775 as monotherapy in patients with SETD2 mutated cancers (NCT03284385) based on the data from Pfister *et al.* 2015, and a Phase II trial testing MK-1775 in combination with cisplatin in patients with triple-negative breast cancer (NCT03012477).

A large number of preclinical studies support the concept that targeting CDK activity to suppress cell cycle progression and cell proliferation is a potential strategy to treat cancers (Cook Sangar et al., 2017; McClue et al., 2002; O'Brien et al., 2018; Smith et al., 2008). Pharmaceutical companies have developed a large number of either specific or pan CDK small molecule inhibitors. Early generation of pan CDK inhibitors, including flavopiridol and roscovitine did not show sufficient clinical benefit due to their limited efficacy and dose-limiting toxicities (Otto and Sicinski, 2017). Abemaciclib is a specific and potent CDK4/6 inhibitor that has been used in breast cancer treatment in several clinical trials, such as MONARCH 1, 2, and 3 trials, which showed promising response rates in patients with advanced breast cancers

(Palumbo et al., 2019). Abemaciclib is currently being evaluated in several ongoing clinical trials, including a Phase Ib/II trial that is investigating abemaciclib in combination with xentuzumab and hormonal therapy in patients with lung or breast cancers (NCT03099174). This clinical trial of abemaciclib and xentuzumab was encouraged by the observation of a synergistic interaction between these two drugs in a preclinical study (Weyer-Czernilofsky et al., 2018). A most recently developed pan CDK inhibitor, Roniciclib (also known as BAY 1000394), has been investigated in combination with platinum-based chemotherapy in patients with small cell lung cancer in a Phase II trial (NCT02161419), but this study was prematurely terminated due to severe toxicities observed in patients (Reck et al., 2019).

1.3 Replication stress

1.3.1 Basic biology of DNA replication

DNA replication is one of the most fundamental biological processes, which is crucial for cell proliferation and genome stability (Bell and Dutta, 2002). DNA replication is tightly regulated in coordination with cell cycle progression and DNA damage responses (Bell and Dutta, 2002). To initiate DNA replication, origin recognition complexes (ORCs) first bind to DNA at replication origins. During G1 phase, ORCs recruit replication factors, including cell division control protein 6 (CDC6) and chromatin licensing and DNA replication factor 1 (CDT1) (Cocker et al., 1996; Nishitani et al., 2000). In coordination with these replication factors, minichromosome maintenance replicative helicases (MCM2-7) are loaded to form pre-replicative complexes (pre-RCs) (Tye, 1999). This process is described as DNA replication licensing. In humans, there are 30,000 ~ 50,000 replication origins, however only 10% origins are activated in S-phase for replication, and most of them

remained inactivated called dormant origins (McIntosh and Blow, 2012). When cells pass through G1/S transition, MCM helicases are activated through the phosphorylation by CDC7 and CDKs and also the interaction with other factors, including CDC45 and a protein complex of Sld5–Psf1–Psf2–Psf3, called GINS (Gambus et al., 2006; Roberts et al., 1999). Activated MCM helicases unwind double-strand DNA and establish the replication fork (Labib et al., 2000). At replication fork, DNA polymerases, proliferating cell nuclear antigen (PCNA) clamp protein and other replication factors are recruited as a protein-DNA complex, termed replisome (Branzei and Foiani, 2010). Replication forks progress bi-directionally from replication origin sites while replisome is responsible for the incorporation of nucleotides into newly synthesised DNA (Bell and Dutta, 2002).

1.3.2 Causes of replication stress

DNA replication machinery is tightly regulated to ensure the timely and accurate duplication of genetic information (Bell and Dutta, 2002). However, during DNA replication, cells are usually in face of numerous obstacles that slow, stall or terminate DNA replication, termed replication stress (Zeman and Cimprich, 2014). Replication stress can be caused by a large number of either endogenous or exogenous sources (Zeman and Cimprich, 2014). There are several major causes of replication stress and 3 are discussed here: (1) Limiting nucleotides; (2) Unrepaired DNA lesions; (3) Replication and transcription collisions.

The first common recognised cause of replication stress is the lack of replication factors and nucleotide availability (Branzei and Foiani, 2010). A sufficient and balanced dNTP pool is crucial for providing the building blocks for faithful DNA replication, while dNTP reduction results in slow replication fork progression and increased origin firing (Anglana et al., 2003). Excessive origin firing and replication

initiation triggered by aberrant cell cycle control consumes dNTP pools and slows DNA replication, causing replication stress (Beck et al., 2012). On the contrary, excess dNTP pool seems also able to induce replication stress. This is demonstrated by a previous study showing that up-regulation of ribonucleotide reductase (RNR), which mediates dNTP de novo synthesis, induces the expansion of dNTP pools, resulting in replication stress and a hypermutation phenotype (Davidson et al., 2012).

Secondly, unrepaired DNA lesions are considered a major source of replication stress because they inhibit replication fork progression as physical barriers (Zeman and Cimprich, 2014). These DNA lesions can be induced exogenously by UV light, IR and DNA damaging agents. For example, platinum anti-cancer drugs induce the accumulation of DNA inter-strand crosslinks, resulting in the arrest of DNA replication and cell cycle progression (Wang and Lippard, 2005). DNA lesions can also arise from endogenous sources including reactive oxygen species and metabolic by-products, such as reactive aldehyde from alcohol metabolism (Brooks and Theruvathu, 2005). Ribonucleotides (rNTP) can be misincorporated instead of dNTP during replication, and failure to resolve rNTP misincorporation leads to replication stress (Dalgaard, 2012). Moreover, cells intrinsically contain some types of DNA sequences and structures that are difficult to replicate. For example, trinucleotide repeats can form hairpins and triplex DNA structures, and G-quadruplexes exist in GC-rich regions (Mirkin and Mirkin, 2007). When replication forks progress to the regions of these complicated secondary DNA structures, replicative helicases cannot efficiently unwind the DNA and cells need to repair or bypass of these impediments, leading to stalled replication forks and replication stress (Mirkin and Mirkin, 2007).

A third major source of endogenous replication stress is the collisions between replication and transcription machineries (Bermejo et al., 2012). As replication and transcription use the same DNA template, failure to coordinate these two processes results in the formation of RNA/DNA hybrids, such as R-loops, which hinder the passage of replication forks through transcription regions (Bermejo et al., 2012). Therefore, highly transcribed regions are also known as early replication fragile sites because these regions are prone to the collisions between replication and transcription (Barlow et al., 2013). In addition, replication machinery is more likely to encounter transcription complexes in long genes, thus these regions are sensitive to replication stress, known as common fragile sites (Helmrich et al., 2011). The collisions between replication and transcription can be caused by many processes. For example, inactivation of alternative splicing factor/splicing factor 2 (ASF/SF2) results in replication and transcription collisions, inducing R Loop formation and genomic instability, while Ribonuclease H (RNase H) cleaves RNA/DNA hybrids and suppress genomic instability (Li and Manley, 2005). Another study showed that deficiencies in Sen1/Senataxin, a DNA/RNA helicase, impairs DNA replication across the RNA-Polymerase-II-transcribed genes, causing the accumulation of RNA/DNA hybrids (Alzu et al., 2012). Both replication and transcription generate topological perturbations that need to be efficiently resolved by DNA topoisomerases (Wang, 2002). Topoisomerase II has been reported to orchestrate replication and transcription encounter in S phase, and topoisomerase II inhibition causes accumulation of DNA entangling, resulting in DNA breaks during chromosome segregation (Bermejo et al., 2009).

1.3.3 Replication stress responses

Replication stress responses are activated at slowed or stalled replication forks in coordination with DNA damage responses and cell cycle controls to resolve replication stress and safeguard genome integrity (Zeman and Cimprich, 2014). At slowed or stalled replication forks, replicative helicases continue to unwind the parental double-stranded DNA, leading to the formation of stretches of ssDNA, which has been recognised as marker of replication stress (Buisson et al., 2015). These ssDNA are coated with RPA and activate ATR-CHK1 signalling cascade to stabilise replication forks, arrest cell cycle and efficiently remove the impediments at the forks (Figure 1.3). ATR phosphorylates and inhibits SWI/SNF-related, matrix-associated, actin-dependent regulator of chromatin, subfamily A-like1 (SMARCAL1), preventing replication stress-induced replication fork collapse (Couch et al., 2013). Activating ATR/CHK1 also inhibits CDK activity and prevents BRCA2 phosphorylation in the C-terminal to stabilise RAD51 filaments, suppressing the degradation of nascent DNA strands by MRE11 nuclease (Schlacher et al., 2011). If cells fail to rescue the stalled replication fork as some DNA lesions cannot be repaired, replication machinery can bypass the DNA lesions and restart DNA replication, which is mediated by translesion DNA synthesis (Mailand et al., 2013). High levels of replication stress may eventually lead to fork collapse, resulting in DSB formation either passively or through endonuclease-mediated cleavage (Hanada et al., 2006). ATM is recruited at DSB sites and activates ATM/CHK2 signalling pathway to arrest cell cycle and regulate p53 and apoptosis (Bartek and Lukas, 2003; Hirao et al., 2002). Through activating ATR/CHK1 and ATM/CHK2 signalling pathways, cells can also limit CDKs-mediated original firing (Shechter et al., 2004), preventing dNTP pool exhaustion. Severe replication stress leads to

excess ssDNA formation, replication fork collapse, deleterious DSBs accumulation and cell death in S phase, described as replication catastrophe (Buisson et al., 2015; Toledo et al., 2017; Toledo et al., 2013). Hereditary mutations in genes involved in DNA replication or replication stress responses cause various human syndromes. For example, Seckel syndrome characterised by growth retardation, microcephaly, mental retardation and dysmorphic features, is an inherited disorder caused by mutations in ATR or ATRIP (Faivre et al., 2002; Verloes et al., 1993). Mutations in components of pre-replication complexes including ORC1, ORC4, ORC6, CDT1 and CDC6 cause Meier-Gorlin syndrome, characterised by microtia, patellar applasia/hypoplasia, and short stature (de Munnik et al., 2015). The autosomal recessive disease Rothmund-Thomson syndrome characterised by facial rash, sparse hair, eyelashes and/or eyebrows, short stature, skeletal and dental abnormalities, juvenile cataracts, and an increased risk of osteosarcoma, is caused by mutations in *RECQL4* gene, which encodes ATP-dependent DNA helicase Q4 (Wang and Plon, 1993). Loss-of-function mutations in BLM helicase cause Bloom Syndrome associated with growth deficiency, immune abnormalities, sensitivity to sunlight, insulin resistance and increased risk of cancers (Flanagan and Cunniff, 1993). Patients with these syndromes commonly have growth abnormities and short stature, which are also the major symptoms in patients with partial deletion of *IGF-1* gene (Woods et al., 1996) and Laron-type dwarfism due to GH receptor mutation (Laron, 2015). Cockayne syndrome is caused by nucleotide excision repair defect, associated with growth retardation, abnormal sensitivity to light and progeria (Laugel, 2013). It has been shown that the growth retardation in Cockayne syndrome is potentially due to the suppression of GH-IGF axis by unrepaired DNA damage (Garinis et al., 2009; Monnat, 2007; van der Pluijm et al., 2007).

1.3.4 Replication stress and cancer

Replication stress is implicated in genomic instability, which is a hallmark of cancer (Hanahan and Weinberg, 2000, 2011). In cancer cells, constitutive activation of oncogenes, such as *cyclin E* and *MYC*, promote CDC45-mediated replication initiation and decrease dNTP pools, leading to replication stress and genomic instability (Bester et al., 2011; Srinivasan et al., 2013). Overexpression of oncogene *MYC* has also been reported to elevate global transcription activities in cancer cells (Lin et al., 2012), which might increase the possibility of replication and transcription collisions, leading to replication stress. Moreover, tumour suppressors BRCA1 and BRCA2 are directly involved in replication fork protection (Schlacher et al., 2012); it is plausible that loss of BRCA1/2 may induce replication stress, which contributes to tumorigenesis in BRCA deficient cancers. Although replication stress markers have been detected in various types of tumour, including NSCLC, colon cancer and melanoma, replication stress is hardly seen in normal tissues (Gorgoulis et al., 2005). This selective nature of intrinsic replication stress in cancers might represent a therapeutic vulnerability. Several approaches have been developed and used in clinical studies to exacerbate replication stress and induce cell death in tumour cells (Table 1.2). These include using (1) nucleoside analogues to directly inhibit DNA replication, (2) DNA damaging reagents to directly modify DNA structure, (3) RNR inhibitors to deplete dNTP availability, (4) Inhibitors targeting ATR-CHK1 and WEE1 signalling to impair replication stress responses, (5) PARP inhibitors to impede SSB repair, (7) topoisomerase inhibitors to induce replication and transcription collisions.

Table 1.2 Examples of clinical therapies that potentially induce replication stress. Adapted from (Aye et al., 2015)

Class of agents or target	Mechanism of action	Compounds	Clinical stage
Nucleoside analogues	Inhibit DNA replication; Inhibit RNR	Azacitidine	All approved for use
		Cytarabine	
		Decitabine	
		Gemcitabine	
		5-Fluorouracil	
Alkylating agents and platinum compounds	Direct modification of DNA	Carboplatin Cisplatin	All approved for use
		Cyclophosphamide	
		Dacarbazine	
		Methotrexate	
		Mitomycin C	
		Oxaliplatin	
		Procarbazine	
		Temozolomide	
RNR inhibitors	Inhibit RNR for suppressing dNTP biosynthesis	Hydroxyurea	Approved
		Triapine	Phase III
Topoisomerase I and II inhibitors	Impair the relaxation of DNA supercoiling that occurs during DNA replication and transcription	Belotecan	Approved
		CRLX101	Phase II
		Doxorubicin	Approved
		Epirubicin	Approved
		Etoposide	Approved
		Idarubicin	Approved
		Irinotecan	Approved
		LMP400	Phase I

		LMP776	Phase I
		Mitoxantrone	Approved
		NKTR-102	Phase III
		Teniposide	Approved
		Topotecan	Approved
PARP inhibitors	Impede single-strand DNA break repair	Olaparib	Approved
		Niraparib	Approved
		Rucaparib	Approved
		Talazoparib	Approved
		Veliparib	Phase III
ATR inhibitors	Inhibit central replication stress response kinase	AZD6738	Phase I/II
		BAY1895344	Phase I/II
		M6620	Phase II
CHK1 inhibitors	Inhibit main effector of ATR in replication stress responses	GDC-0575	Phase I
		MK-8776 (SCH 900776)	Phase I
		SRA737	Phase I
		Prexasertib (LY2606368)	Phase I/II
WEE1 inhibitor	Abrogate G2/M checkpoint	MK-1775 (A7D1775)	Phase I/II

1.4 Ribonucleotide reductase

1.4.1 RNR and dNTP biosynthesis

Maintaining dNTP homeostasis is crucial for DNA replication, and as already discussed, dNTP imbalance leads to replication stress and genomic instability. Cellular dNTP levels are tightly regulated by de novo biosynthesis and the rate-limiting step of dNTP synthesis is reduction of ribonucleoside diphosphate (NDP) to

produce deoxyribonucleoside diphosphate (dNDP), which is catalysed by RNR (Figure 1.5) (Mathews, 2015). Nucleoside diphosphate kinase (NDPK) then phosphorylates dNDP to produce dNTP (Mathews, 2015). Among four dNTPs, the synthesis of deoxythymidine triphosphate (dTTP) is more complicated than deoxyadenosine triphosphate (dATP), deoxycytidine triphosphate (dCTP) and deoxyguanosine triphosphate (dGTP), because it requires more reactions catalysed by thymidylate phosphate kinase (TMPK) and thymidylate synthase (Mathews, 2015). RNR-catalysed reaction is essential for the synthesis of all four dNTPs and is highly conserved from prokaryotes to eukaryotes (Stubbe and van der Donk, 1995). RNR consists of two subunits: ribonucleotide reductase subunit M1 (RRM1) and M2 (RRM2), also named α and β subunits (Figure 1.5). Catalytically-active RNR is formed as α2β2 heterotetramer, in which RRM1 contains the catalytic site and RRM2 contains the oxygen-linked di-iron center to generate tyrosyl radicals for catalysis (Stubbe and van der Donk, 1995). Of note, β subunit can be formed by an isoform of RRM2, ribonucleotide reductase regulatory TP53 inducible subunit M2B (RRM2B), which is encoded by *p53R2* gene (Tanaka et al., 2000). RRM2B exhibits 80% sequence homology with RRM2 and is directly involved in p53-mediated DNA damage responses (Tanaka et al., 2000). It has been previously reported that cells in hypoxia rely on the RRM1/RRM2B version of RNR to maintain the basal dNTPs level (Foskolou et al., 2017).

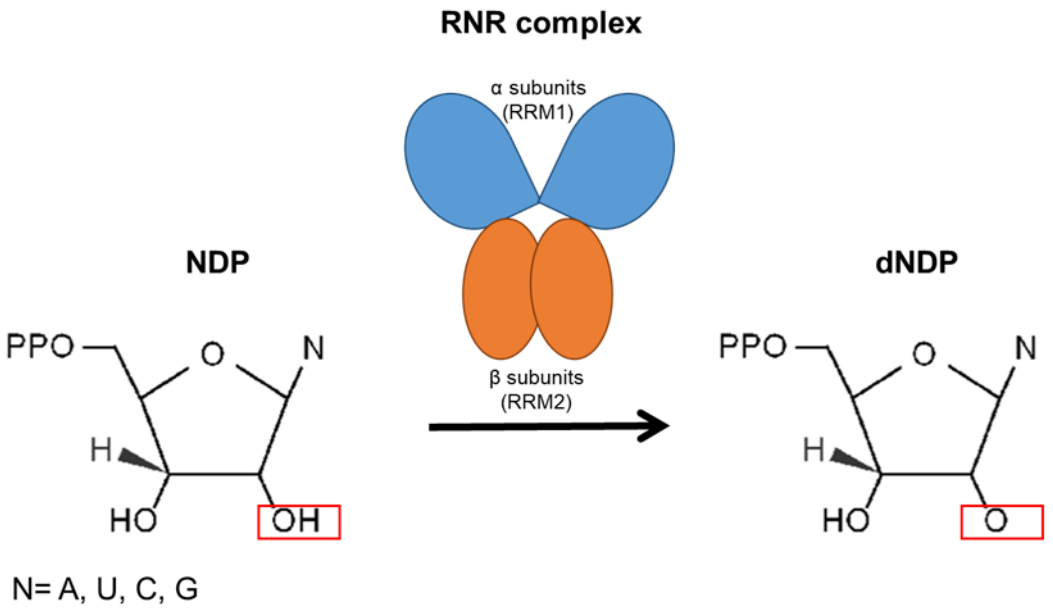

Figure 1.5 The basic catalytic reaction of RNR enzyme for dNDP formation
A: adenosine; U: uracil; C: cytidine and G: guanosine. Adapted from (Huang et al., 2014)

1.4.2 RNR activity regulation

Given the essential role of RNR in catalysing dNTP synthesis for DNA replication, both RRM1 and RRM2 are tightly regulated throughout cell cycle. The gene transcription and protein translation of RRM1 and RRM2 are regulated by mTOR signalling (He et al., 2017). RRM1 and RRM2 expression can be transcriptionally upregulated by E2F1 transcription factor during G1/S phase transition (DeGregori et al., 1995). Although both RRM1 and RRM2 protein levels peak at S phase, RRM1 protein level remains relatively constant and in excess throughout cell cycle due to its long half-life, whereas RRM2 protein level starts to decrease in G2 phase (Engstrom et al., 1985). This is because RRM2 protein is regulated by ubiquitin ligase for degradation when cells exit S phase. During the G2 phase, RRM2 is phosphorylated at Threonine 33 by CDK1/2, promoting the binding to Cyclin F, and is then degraded by Skip1/Cullin/F-box (SCF) complex ubiquitin ligase (D'Angiolella et al., 2012). During mitosis, RRM2 is further degraded via anaphase-promoting

complex (APC)-CDH1-mediated proteolysis (Chabes et al., 2003). Furthermore, upon DNA damage, both RRM1 and RRM2 can translocate to the cell nucleus and are recruited by histone acetyltransferase Tip60 to DSB sites to provide dNTPs for DNA repair (Niida et al., 2010).

1.4.3 RNR and cancer

The expression of RNR subunits RRM1, RRM2, and RRM2B are frequently elevated in many types of tumours (Aye et al., 2015), suggesting an important role of RNR in cancer. To maintain sustained proliferation, cancer cells require the sufficient supply of macromolecules, including dNTPs, mediated by RNR-catalysed de novo biosynthesis. Altered RNR activity (either increased or decreased) may induce dNTP imbalance and cause replication stress, contributing to genomic instability and tumorigenesis. Previous studies suggested that dNTP pool imbalance impairs the proofreading capacity of replicative DNA polymerases, promoting them to introduce mutations into DNA during replication (Mertz et al., 2015; Williams et al., 2015). It has also been reported that RNR recruitment in nucleus plays an important role in DNA repair by supplying dNTPs at DSB sites (Niida et al., 2010), which might be involved in mediating chemo/radiotherapy resistance. Indeed, a significant correlation between RRM1 expression and drug resistance to gemcitabine and platinum drugs has been reported in NSCLC (Bepler et al., 2006). The overexpression of RRM2 has been observed in breast, ovarian, bladder and colorectal cancers, and is correlated with poor clinical outcomes (Ferrandina et al., 2010; Liu et al., 2013; Morikawa et al., 2010; Zhang et al., 2014). Given the important role of RNR in cancer, targeting RNR subunits has been recognised as a potential strategy to treat cancers (Aye et al., 2015). Nucleoside analogue drugs, such as gemcitabine and cytarabine, have been considered as RRM1-targeting drugs

because their active substrates form covalent complexes with RRM1, resulting in RRM1 inhibition (Galmarini et al., 2001b). Hydroxyurea (HU) and triapian (3AP) are commonly used anti-cancer drugs that target RRM2, and have been used to treat patients with multiple types of cancers (Aye et al., 2015). Notably, previous studies showed that cell cycle checkpoint abrogation by inhibiting CHK1 or WEE1 is another approach to deplete RRM2 proteins through promoting CDK-mediated RRM2 degradation, suggesting a potential cancer treatment strategy (Buisson et al., 2015; Koppenhafer et al., 2020; Pfister et al., 2015).

1.5 IGF and replication stress

Previous studies in our group and others found that targeting IGF signalling sensitised human tumour cells to IR and cytotoxic drugs (Chitnis et al., 2014; Cosaceanu et al., 2007; Ferte et al., 2013; Riesterer et al., 2011; Rochester et al., 2005; Turney et al., 2012). IGF-1R depletion delayed the repair of IR-induced DNA double-strand breaks in prostate cancer cells (Turney et al., 2012). Our group further reported that DSB repair via both HR and NHEJ was attenuated in IGF-1R inhibited cells (Chitnis et al., 2014). Notably, IGF-1R depletion or inhibition was also found to lead to accumulation of endogenous DNA lesions in prostate cancer cells (Lodhia et al., 2015). However, the origins of these endogenous DNA damage induced by IGF blockade is yet to be elucidated.

Current unpublished work in our group done by post-doctoral scientist Dr Guillaume Rieunier revealed an unrecognised role of IGF-1 signalling in maintaining replication integrity even in the absence of exogenous damage. Dr Rieunier found that IGF-1R inhibited or depleted cells accumulated DNA damage marked by phosphorylation of histone H2AX at serine 139 (γH2AX). γH2AX foci accumulate at DSB sites and

stalled replication forks to recruit DNA repair machineries and signalling factors, serving as a sensitive indicator of DNA damage and replication stress (Gagou et al., 2010; Rogakou et al., 1998). Cells after IGF blockade also contained more under-replicated regions shielded by 53BP1 bodies, which are important to protect DNA against erosion during passage through mitosis (Harrigan et al., 2011; Lukas et al., 2011). The increased endogenous DNA lesions induced by IGF-1R inhibition or depletion were accompanied by slowed replication fork progression and ATR/CHK1 checkpoint activation, which are the key indicators of replication stress (Zeman and Cimprich, 2014). These are previously unreported effects of IGF axis blockade, although are consistent with a report that IGF-1 regulates the gene expression at the mRNA level of several components involved in DNA replication including RRM2, MCM7, replication factors C and GINS proteins PSF1/2 (Creighton et al., 2008). Dr Rieunier further demonstrated that IGF blockade reduced the expression of RRM2 via inhibiting both MEK/ERK and PI3K/AKT pathways. Consistent with the critical role of RNR activity as the rate-limiting step for dNTP production (Mathews, 2015), Dr Rieunier found IGF blockade reduced dATP supply and impaired the balance of dNTP pools, leading to slow replication fork progression and replication stress.

1.6 Research aim

Current unpublished work in our group done by Dr Rieunier demonstrate a replication stress phenotype in IGF-1R depleted or inhibited cells. This replication stress phenotype is striking, but we found that cells remain viable after IGF blockade, albeit growing at a slower growth rate, suggesting that the replication is tolerable. We hypothesised that the replication stress induced by IGF blockade might be clinically relevant, serving as an exploitable vulnerability for cancer treatment. IGF-

1R depleted or inhibited cells might be more sensitive to replication stress-inducing reagents, such as inhibitors targeting cell cycle controls, DNA replication and repair.

The research aims of this project were:

(1) To confirm replication stress phenotype in IGF-1R depleted or inhibited breast cancer cells;

(2) To perform a targeted compound screen to identify effective drug combinations that sensitise cells to IGF inhibitor and validate screen hits in 2D cell and 3D spheroid culture model;

(3) To identify approaches to exacerbate replication stress induced by IGF blockade to intolerable levels, leading to tumour cell death;

(4) To investigate the mechanism of the interactions between IGF blockade and the identified treatment partners.

Chapter 2

Methods and materials

2.1 Materials, chemicals and reagents

General laboratory chemicals, reagents and materials are listed in Table 2.1

Table 2.1 Chemicals, reagents and materials used in this study

Name	Application	Catalogue number	Supplier
Phosphate buffered saline (PBS)	General chemicals /reagents	P4417	Sigma-Aldrich
Trizma hydrochloride (Tris-HCl)	General chemicals /reagents	T3253	Sigma-Aldrich
Sodium dodecyl sulfate (SDS)	General chemicals /reagents	20-4002-01	Severn Biotech
Tween 20	General chemicals /reagents	10113103	Fisher Scientific
Triton X-100	General chemicals /reagents	30632410	BDH
IGEPAL CA-630 (NP-40)	General chemicals /reagents	I-3021	Sigma-Aldrich
EDTA	General chemicals /reagents	3690	Sigma-Aldrich
Sodium deoxycholate	General chemicals /reagents	D5670	Sigma-Aldrich
Urea	General chemicals /reagents	U6504	Sigma-Aldrich
Bromophenol blue	General chemicals /reagents	114391	Sigma-Aldrich
Glycerol	General chemicals /reagents	G/0650/08	Fisher Scientific
β-mercaptoethanol	General chemicals /reagents	M6250	Sigma-Aldrich

Dithiothreitol (DTT)	General chemicals /reagents	D9779	Sigma-Aldrich
Bovine serum albumin (BSA)	General chemicals /reagents	421501J	VWR
Sodium Chloride (NaCl)	General chemicals /reagents	S/3120/60	Fisher Scientific
Hydrochloric acid (HCl)	General chemicals /reagents	320331	Sigma-Aldrich
Sodium Hydroxide (NaOH)	General chemicals /reagents	71690	Sigma-Aldrich
Dimethyl sulfoxide (DMSO)	General chemicals /reagents	D2650	Sigma-Aldrich
Ethanol	General chemicals /reagents	E/6665DF/17	Fisher Scientific
Methanol	General chemicals /reagents	M/3950/17	Fisher Scientific
Acetic acid	General chemicals /reagents	A/0400/PB16	Fisher Scientific
Dulbecco's Modified Eagle Medium (DMEM)	Cell culture	41966-029	Gibco
Roswell Park Memorial Institute (RPMI) 1640	Cell culture	21875-034	Gibco
Fetal bovine serum (FBS)	Cell culture	10500-064	Gibco
Penicillin-Streptomycin	Cell culture	15140-122	Gibco
Trypsin/EDTA	Cell culture	BE02-007E	Lonza
MycoAlerta Mycoplamsa Detection Kit	Cell culture	LT07- 318	Lonza
Cryogenic vial 2 mL	Cell culture	430489	Corning
Trypan blue solution	Cell counting	T10282	Invitrogen
Cell counting chamber slide	Cell counting	C10283	Invitrogen
96-well white flat bottom microplate	Cell viability assay	655094	Greiner Bio-One
CellTiter-Blue Cell Viability Assay	Cell viability assay	G8081	Promega
96-well clear flat bottom microplate	Cell death assay	3596	Corning
Propidium iodide	Cell death assay	P4864	Sigma-Aldrich
Hoechst 33342	Cell death assay	B2261	Sigma-Aldrich
Brilliant Blue R	Cell survival assay	B7920	Sigma-Aldrich
Opti-MEM, Reduced Serum Medium	Cell transfection	31985-047	Gibco
Oligofectamine	Cell transfection	12252-011	Invitrogen
Lipofectamine 3000	Cell transfection	L3000-008	Invitrogen
cOmplete, EDTA-free Protease Inhibitor Cocktail	Western blot	11873580001	Roche
Phosphatase Inhibitor Cocktail 2	Western blot	P5726	Sigma-Aldrich
Phosphatase Inhibitor Cocktail 3	Western blot	P0044	Sigma-Aldrich

Pierce BCA Protein Assay Kit	Western blot	23225	Thermo Scientific
Spectra Multicolor Broad Range Protein Ladder	Western blot	26634	Thermo Scientific
x4 LDS sample buffer	Western blot	NP0007	Invitrogen
4–15% Criterion TGX Precast Midi Protein Gel	Western blot	5671084	Bio-Rad
Tris/Glycine/SDS running buffer	Western blot	1610772	Bio-Rad
Trans-Blot Turbo RTA Midi Nitrocellulose Transfer Kit	Western blot	1704271	Bio-Rad
Nitrocellulose membrane	Western blot	10600016	GE Healthcare
Odyssey Blocking Buffer	Western blot	927-40000	LI-COR Biosciences
IRDye 680RD Donkey anti-Goat IgG Secondary Antibody	Western blot	926-68074	LI-COR Biosciences
IRDye 680RD Goat anti-Rabbit IgG Secondary Antibody	Western blot	926-68071	LI-COR Biosciences
IRDye 800CW Goat anti-Mouse IgG Secondary Antibody	Western blot	926-32210	LI-COR Biosciences
Pepsin	Flow cytometry	P7000	Sigma-Aldrich
5-Bromo-2'-deoxyuridine (BrdU)	FACS/Immunofluorescence	19-160	Sigma-Aldrich
BrdU (B44) antibody	FACS/Immunofluorescence	347580	BD Biosciences
Paraformaldehyde (methanol free)	Immunofluorescence	43368	Alfa Aesar
Goat anti-Mouse IgG (H+L) Highly Cross-Adsorbed Secondary Antibody, Alexa Fluor 488	Immunofluorescence	A11029	Invitrogen
Goat anti-Rat IgG (H+L) Highly Cross-Adsorbed Secondary Antibody, Alexa Fluor 594	Immunofluorescence	A11007	Invitrogen
Goat anti-Rabbit IgG (H+L) Highly Cross-Adsorbed Secondary Antibody, Alexa Fluor 594	Immunofluorescence	A11037	Invitrogen
VECTASHIELD Antifade Mounting Medium with DAPI	Immunofluorescence	H-1200	VECTOR LABORATORIES
22 x 22 mm cover glasses	Immunofluorescence	631-0124	VWR
Microscope slides, Superfrost	Immunofluorescence	631-0912	VWR
5-chloro-2’-deoxyuridine (CIdU)	DNA fiber assay	105478	MP Biomedicals

5-Iodo-2'-deoxyuridine (IdU)	DNA fiber assay	100357	MP Biomedicals
VECTASHIELD Antifade Mounting Medium	DNA fiber assay	H-1000	VECTOR LABORATORIES
Adhesion slides, SuperFrost Plus	DNA fiber assay/H&E/IHC	631-0108	VWR
22 x 50 mm cover glasses	DNA fiber assay/H&E/IHC	12342118	Menzel Gläser
Deoxynucleotide (dNTP) Solution Set	dNTP assay	N0446S	New England Biolabs
Streptavidin coated 96-well plate	dNTP assay	15125	Thermo Scientific
Klenow polymerase	dNTP assay	EP0052	Thermo Scientific
[^{3}H]-dATP	dNTP assay	NET268250UC	PerkinElmer
[^{3}H]-dTTP	dNTP assay	NET520A250UC	PerkinElmer
OptiPhase supermix cocktail	dNTP assay	1200-439	PerkinElmer
96-well Clear Round Bottom Ultra-Low Attachment Microplate	3D spheroid assay	7007	Corning
CellTiter-Glo 3D cell viability assay	3D spheroid assay	G9681	Promega
(2-Hydroxypropyl)-beta-cyclodextrin	Animal experiment	H107	Sigma-Aldrich
Matrigel matrix	Animal experiment	356230	Corning
neutral buffered formalin (NBF)	Animal experiment	HT501128	Sigma-Aldrich
Citroclear	H&E/IHC	HC5005	TCS Biosciences
Harris's haematoxylin	H&E/IHC	351945S	VWR
Alcoholic Eosin	H&E/IHC	HT110132	Sigma-Aldrich
EnVisionTM + Dual Link System-HRP (DAB+)	H&E/IHC	K4065	Dako
DPX mountant	H&E/IHC	06522	Sigma-Aldrich

2.2 Cell culture

Cell lines used in this study are listed in Table 2.2, including the tissue type, provider and culture medium. Cells were tested for mycoplasma infection upon arrival and re-tested routinely by using MycoAlerta Mycoplasma Detection Kit (#LT07- 318, Lonza). Cell lines identify was verified by authentication of using PCR-based short tandem repeats (STR) locus detection by Eurofins Genomics.

Table 2.2 Cell lines used in this study

Cell line	Tissue type	Provider	Culture medium
MCF7	Breast cancer	[1]	DMEM
ZR-75-1	Breast cancer	[1]	DMEM
T47D	Breast cancer	[1]	DMEM
KPL-1	Breast cancer	[2]DSMZ #ACC317	DMEM
HCC1143	Breast cancer	[1]	DMEM
HeLa	Cervical cancer	[3]	DMEM
SK-CO-1	Colorectal cancer	[4]ATCC # HTB-39	DMEM
H1299	Non-small cell lung cancer	[5]	DMEM

1 Kindly provided by Dr Anthony Kong, University of Birmingham;
2 DSMZ-German Collection of Microorganisms and Cell Cultures GmbH;
3 Kindly provided by Professor Adrian Harris, University of Oxford;
4 ATCC= American Type Culture Collection (Manassas, USA);
5 Kindly provided by Professor Xin Lu, University of Oxford

All cell lines is this study were maintained and cultured in Dulbecco's Modified Eagle Medium (DMEM) (#41966-029, Gibco) supplemented with 10% fetal bovine serum (FBS, #10500-064, Gibco) and penicillin (100 units/mL) / streptomycin (100 µg/mL) (#10500-064, Gibco) at 37 °C with 5% CO_2. Cells were routinely passaged at sub-confluence (~80%) every 3 or 4 days. For cell passaging, cells were washed once with 1x sterile PBS after removing the culture medium, and then trypsinised with 2.5 g/L trypsin (50% v/v of Trypsin/EDTA solution in sterile 1x PBS) (#BE02-007E, Lonza) for 3 minutes. Cells were collected with fresh medium and cell count was determined. For cell number counting, cell suspension was mixed with an equal volume of 0.4 % trypan blue stain (#T10282, Invitrogen) and added into a cell counting chamber slide (#C10283, Invitrogen) that could be measured on the Countess Automated Cell Counter (Invitrogen) for viability determination. For cell

seeding, cells were diluted from the cell suspension in fresh medium based on the desired plating densities.

For cryostorage, cells were cultured to 80-90% confluency, trypsinised and collected as just described. Cells were pelleted after centrifugation at 300 g for 5 minutes at room temperature. Cell pellets were resuspended in cell freezing solution (10% DMSO in FBS), and then transferred to cryogenic vials (1 mL/vial, usually 3 vials for one T175 flask of cells at 80-90% confluency). Cryogenic vials were stored in Mr. Frosty Freezing Containers (Thermo Scientific) and frozen in -80 °C freezer for at least 24 hours before being transferred to liquid nitrogen storage tank in vapour phase. To recover cells from cryostorage, cryogenic vials were taken from liquid nitrogen storage tank or -80 °C freezer, and defrosted in 37 °C water bath until completely thawed. Cell suspensions were gently mixed and transferred to pre-warmed cell culture medium in a T75 cell culture flask. Cell culture medium was changed to fresh complete medium on the next day to remove the excess DMSO and dead cells in the medium.

2.3 Compounds

IGF ligand-neutralising antibody BI-836845 (xentuzumab) in the same formulation as for clinical use (10 mg/mL, stored at 4 °C), and IGF-1R tyrosine kinase inhibitor (TKI) BI-885578 (10mM in DMSO, stored at −20 °C) were obtained under Material Transfer Agreement from Dr Ulrike Weyer-Czernilofsky and Dr Thomas Bogenrieder from Boehringer Ingelheim. IGF-1R TKI BMS-754807 was purchased from Sigma-Aldrich (#BM0003) and dissolved in DMSO at 10 mM and stored at −20 °C. CHK1 inhibitors MK-8776 (#S2735, Selleck Chemicals), SRA737 (#S8253, Selleck Chemicals), UCN-01 (#18130, Cambridge Bioscience) and LY2603618 (#S2626,

Selleck Chemicals) and WEE1 inhibitor MK-1775 (#1494, Axon Medchem) were dissolved in DMSO at 10 mM and stored at −20 °C.

2.4 Cell viability, death and survival assay

For cell viability assay, cells were seeded in triplicate in white wall and clear bottom 96-well plates (#655094, Greiner Bio-One). Seeding densities for different cell lines were determined in a pilot test (MCF7: 1000 cells/well; ZR-75-1, HCC1143, SK-CO-1: 5000 cells/well; T47D: 8000 cells/well; KPL1: 10000 cells/well). The following day, different treatments were added into triplicate wells, usually 20 µL of x5 drug solution added to 80 µL or 10 µL of x10 drug solution added to 90 µL, or the equivalent volume of solvent as control. The treated cells were cultured for 5 days at 37 °C with 5% CO_2. For endpoint measurement, CellTiter-Blue reagent (#G8081, Promega) (1:5 v/v, usually 20 µL of reagent added to 100 µL) was added into the wells, followed by incubation at 37 °C with 5% CO_2 for 1~3 hours, the duration of incubation being optimised for each cell line. The assay is based on the detection of resorufin that reduced from resazurin by viable cells, which can be measured by fluorescence. The fluorescence intensity ($579_{Excitation}/584_{Emission}$) was determined by reading on a POLARstar Omega microplate reader (BMG Labtech), and then exported and analysed in Graphpad Prism 8 to generate dose-response curve and calculate the half maximal inhibitory concentration (IC50).

For cell death assay, cells were seeded in triplicate in clear and flat bottom 96-well plates (#3595, Corning). Cell seeding and treatment were the same as for cell viability assay. For endpoint measurement, 50 µL of a mixed solution of 4 µM Hoechst 33342 (#B2261, Sigma-Aldrich) and 4 µM propidium iodide (#P4864, Sigma-Aldrich) were added into the wells. The plate was incubated for 30 minutes

at 37 °C with 5% CO_2. The cell death percentage (% PI positive cells / Hoechst positive cells) was determined by Celigo Imaging Cytometer (Nexcelom) and the dose-response curve was generated in Graphpad Prism 8.

For clonogenic survival assay, cells were seeded in 6-well plates at a density of 1000 cells per well. On the following day, different treatments were added into each well, usually 0.5 mL of x4 drug added to 1.5 mL, or the equivalent volume of solvent as control. After culturing at 37 °C with 5% CO_2 for 7 days, cells were washed once with 1x PBS and fixed and stained with Brilliant Blue buffer (0.1% Brilliant Blue R, 7% acetic acid, 30% methanol) for 30 minutes. The plates were gently washed with deionized water and dried at room temperature for overnight. The plates were imaged and the colonies were counted on the GelCount automated counter (Oxford Optronix).

2.5 Compound screen

This compound screen was conducted with Dr Guillaume Rieunier in collaboration with Elena Seraia and Daniel Ebner from Target Discovery Institute, Oxford. The 60-compound custom library consisted of 59 drugs with different targets and 1 additional DMSO solvent control (listed in Table 4.1).

This compound screen was performed in 5 estrogen receptor (ER) positive breast cancer cell lines: MCF7, ZR-75-1, KPL1, HCC1143 and T47D. The 60 compounds were treated at 3 concentrations (0.1 μM, 1 μM, 10 μM) in combination with PBS solvent control or BI-836845 (1 μM, near to the steady-state circulating concentration of ~1.3 μM in patients in Phase 2 clinical trials; personal communication, Dr Thomas Bogenrieder, Boehringer Ingelheim) for 5 days. A resazurin-based cell viability assay was used to determine the effects of the

treatments in the screen. Cells were seeded in 96-well plates with the seeding densities described in section 2.4, and treated with compound library on the following day. The treatment layout was shown in Table 2.3 and duplicate plates were prepared. For each cell line, there were 6 plates for single treatment with compounds at 0.1 μM, 1 μM, 10 μM and 6 plates for combination treatment with BI-836845.

Table 2.3 Compound treatment layout for screen

	1	2	3	4	5	6	7	8	9	10	11	12
A	Empty	Empty	Empty	Empty	Empty	Empty	Empty	Empty	Empty	Empty	Empty	Empty
B	Aphidicolin 500nM	1 Veliparib	2 Deforolimus	3 Lapatinib	4 Tozasertib	5 BMS-599626	6 Obatoclax Mesylate	7 Olaparib	8 Nutlin 3	9 MK-2206	10 KU-55933	Aphidicolin 500nM
C	Aphidicolin 500nM	11 Rucaparib	12 BI 2536	13 Palbociclib	14 SNS-032	15 Gemcitabine	16 Roscovitine	17 JNJ 26854165	18 Fulvestrant	19 CUDC-101	20 Irinotecan	Aphidicolin 500nM
E	Aphidicolin 500nM	21 PIK-75	22 Adriamycin	23 Clofarabine	24 Etoposide	25 Flavopiridol	26 Camptothecin e	27 Rigosertib	28 Ispinesib	29 MC1568	30 DMSO	Aphidicolin 500nM
E	Aphidicolin 500nM	31 AT7519	32 Hesperadin	33 BIX 02189	34 AZD7762	35 PD318088	36 KU-60019	37 BS-181	38 LY500307	39 Cytarabine	40 Flucytosine	Aphidicolin 500nM
F	Aphidicolin 500nM	41 Tamoxifen Citrate	42 MLN2238	43 SB 743921	44 Indirubin	45 RITA	46 Talazoparib	47 Rociletinib	48 E3330	49 CRT0044876	50 VE-821	Aphidicolin 500nM
G	Aphidicolin 500nM	51 BO2	52 Mirin	53 Ro-3306	54 MK-8776	55 MK-1775	56 Abemaciclib	57 ML-216	58 AZD 5363	59 Celastrol	60 NSC 19630	Aphidicolin 500nM
H	Empty	Empty	Empty	Empty	Empty	Empty	Empty	Empty	Empty	Empty	Empty	Empty

The cell seeding and compound treatment processes on Janus liquid handling workstations (Perkin Elmer) were performed by Elena Seraia from Target Discovery Institute, Oxford. To determine the cell viability after 5 days treatment, cell culture medium was replaced by 100 μL phenol red-free DMEM (#21063029, Gibco) containing 10 μg/mL resazurin. After 2 hours incubation at 37 °C with 5% CO_2, the fluorescence intensities were measured on an Envison multilabel plate reader (Perkin Elmer). Data were collected and further analysed using Microsoft Excel and GraphPad Prism 8.

To assess the quality of the compound screen, Z-factor was calculated using Zhang and colleagues' method (Zhang et al., 1999):

$$Z = 1 - \frac{3(\sigma_P + \sigma_N)}{|\mu_P - \mu_N|}$$

μ_P is the mean value of positive control and μ_N is the mean value of negative control. σ_P is the standard deviation (SD) of positive control and σ_N is the SD of negative control.

For Z-factor calculation, the fluorescence intensity of DMSO solvent control well was used as negative control. The fluorescence intensity of PLK inhibitor (BI-2536) - treated well was used as positive control since PLK inhibition is toxic to many cell types (Plyte and Musacchio, 2007), and PLK depletion had been used as positive control in the siRNA screen previously published in our group (Gao et al., 2014). To interpret the Z-factor, guideline from Zhang and colleagues' publication (Zhang et al., 1999) was used (Table 2.4):

Table 2.4 Interpretation of Z-factor

Z-factor	Interpretation
1.0	Ideal, Z-factors can never exceed 1.
0.5-1.0	Excellent assay
0-0.5	Marginal
≤0	Not useful, too much overlap between positive and negative controls

To determine the efficacy of each compound as single treatment or in combination treatment with BI-836845, the fluorescence intensities measured in the duplicate plates were first averaged. The relative viability (compared with the DMSO solvent

control well) of the cells in single treatment plate or combination treatment plate was calculated:

$$Relative\ viability = \frac{Fluorescence\ intensity\ of\ test\ compound\ well\ (+/-BI836845)}{Fluorescence\ intensity\ of\ DMSO\ well\ (+/-BI836845)}$$

The relative viability of cells in DMSO solvent control-treated well in single treatment plate or combination treatment plate becomes 1.

To compare the efficacies of each compound in single treatment and combination treatment with BI-836845, the relative effectiveness was calculated with the formula:

$$E_{compound} = \log_{10} \frac{relative\ viability\ in\ single\ treatment\ plate}{relative\ viability\ in\ combination\ treatment\ plate}$$

$E_{compound}$ = 0 indicates no combination effect as the relative viability of the cells treated with the compound in single treatment plate is the same with the combination treatment plate (E= $Log_{10}(1) = 0$). $E_R > 0$ indicates the increase of efficacy when the compound is combined with BI-836845 (relative viability of the cells in single treatment is larger than in combination treatment), suggesting a combination effect. $E_R < 0$ indicates the decrease of efficacy when the compound is combined with BI-836845 (relative viability of the cells in single treatment is smaller than in combination treatment).

For each cell line, $E_{compound}$ values of all compounds at 0.1 μM, 1 μM, 10 μM were ranked. Z-score was calculated using a robust method based on median and median absolute deviation (MAD) as follows (Brideau et al., 2003):

$$Z_{compound} = \frac{E_{compound} - Median\ (all\ \ compounds)}{MAD}$$

$$MAD = 1.4826\ \times Median\ (|E_{compound} - Median\ (all\ \ compounds)|)$$

To identify the positive hits showing the combination effect with BI-836845 treatment, the cut-off of Z-score > 2 was used, suggested by the previous publication (Goktug et al., 2013). The positive hits in all cell lines were imported into (http://bioinformatics.psb.ugent.be/webtools/Venn/) to generate Venn diagram and identify the overlapping hits in different cell lines.

2.6 Gene silencing by siRNA

Cells were cultured to 30% confluency in 10 cm dishes. Transfection used IGF-1R siRNA #1 (S100017521, Qiagen) and #2 (designed in house (Bohula et al., 2003)), synthesised by Qiagen or AllStars Negative Control siRNA (1027281, Qiagen). The siRNAs (50nM) were mixed with Oligofectamine Transfection Reagent (#12252-011, Invitrogen) and Opti-MEM I Reduced-Serum Medium (#31985-047, Gibco) for 25 minutes at room temperature (shown in Table 2.5).

Table 2.5 siRNA transfection solution components

	Volume (μL)
Tube 1	
20 μM siRNA stock	6.8
Opti-MEM	1523.5
Tube 2	
Oligofectamine	12.3
Opti-MEM	410
In cell culture dish	
Opti-MEM	780

Cells were washed twice with Opti-MEM I Reduced-Serum Medium, and incubated with the siRNA mixtures at 37 °C with 5% CO_2 for 4 hours, followed by adding 11 mL fresh cell culture medium with 10% FBS. After 24 hours or 48 hours transfection, cells were collected for western blot analysis or reseeded for other experiments.

2.7 Generation of RRM2-overexpressing MCF7 cells

To generate RRM2-overexpressing cell lines, plasmid pcDNA3.1 RRM2 (Addgene, Plasmid #13796) (Duxbury and Whang, 2007) and pcDNA3.1 empty vector control (#V79520, Invitogen) were used. To amplify the plasmids in bacteria, DH5α Competent E. coli (#C2987I, New England Biolabs) were first transformed. Specifically, 50 μL of competent cells were thawed on ice and mixed with 70 ng DNA. The cell mixtures were incubated on ice for 30 minutes, followed by a heat shock at 42 °C for 30 seconds. Then 950 μL of SOC medium (#H8032, Sigma-Aldrich) was added, and then the cells were incubated at 37°C for 1 hour while shaking. Transformed cells were spread onto LB-agar plates supplemented with

ampicillin and incubated at 37 °C overnight. On the following day, a sterile tip was used to pick a single bacterial colony, which was placed in 3 mL of LB in a 15 mL tube and incubated at 37°C with shaking overnight. Bacterial culture was then expanded into a 2 L culture flask in 100 ml of LB with ampicillin at 37 °C overnight. The bacterial cells were harvested after centrifugation at 6000 x g for 15 minutes at 4 °C and stored as a glycerol stock (1:1 v/v) at - 80 °C. The plasmid DNA was extracted and purified by using Maxi preparation kit (Qiagen) following the manufacturer's instructions. DNA concentration was determined by NanoDrop Microvolume Spectrophotometer (Thermo Fisher Scientific). Purified plasmid was sent to Integrated DNA Technologies (IDT) for sequence validation using 5' sequencing primer T7 (5'-TAATACGACTCACTATAGGG-3') and 3' sequencing primer BGH reverse (5'-TAGAAGGCACAGTCGAGG-3').

To generate RRM2-overexpressing MCF7 cells, 2.5 μg plasmid DNA was transfected into MCF7 cells using Lipofectamine 3000 Reagent Kit (Thermo Fisher Scientific, #L3000001) following the manufacturer's instructions. Specifically, MCF7 cells were cultured to 70% confluency. Lipofectamine 3000 reagent and P3000 reagent in the kit were diluted with Opi-MEM medium and then mixed with 2.5 μg pcDNA 3.1 control plasmid or pcDNA3.1 RRM2 plasmid. The transfection mixtures were added into cell culture medium for 48 hours. The cells were then cultured with medium containing 800 μg/mL G418 (#G8186, Sigma-Aldrich) for 72 hours. The surviving colonies were picked and cultured with medium containing 800 μg/mL G418 for 30 days to obtain stably expressing cells. The expression level of RRM2 was determined by western blot analysis.

2.8 Protein extraction and western blot

Cells were harvested after the required treatment in 6 cm dishes. Cell pellets were washed with cold 1x PBS and lysed in 80 µL Radioimmunoprecipitation assay (RIPA) buffer (0.1% SDS, 1% NP-40, 1 mM EDTA, 50 mM Tris PH 7.5, 150 mM NaCl, 0.25% Deoxycholate) or Urea-Tris-Bicine (UTB) buffer (1 M Tris PH 7.5, 1 M Urea) containing protease inhibitor cocktail (#11873580001, Roche) and phosphatase inhibitor cocktail solutions (#P5726 and #P0044, Sigma-Aldrich) for 15 minutes on ice. Cell lysates were centrifuged at 13,000 x g for 15 minutes at 4 °C. The supernatants were collected as protein extracts. Protein concentrations were determined by Pierce BCA Protein Assay (#23225, Thermo Fisher Scientific). The protein extracts were mixed with x4 LDS sample buffer (#NP0007, Invitrogen) containing 0.1 M DTT and boiled at 4 °C for 5 minutes. Equal amounts of protein extracts (50~70 µg) were separated by electrophoresis on 4-15% Midi-PROTEAN TGX precast Gels (#5671084, Bio-Rad) and transferred to Nitrocellulose Blotting Membranes (#10600016, GE Healthcare) using Trans-Blot Turbo RTA Midi Nitrocellulose Transfer Kit (#1704271, Bio-Rad). Membranes were washed with 1x PBS containing 0.1% Tween 20 (PBST) and blocked in Odyssey Blocking Buffer (#927-40000, LI-COR Biosciences) for 45 minutes. Membranes were incubated with primary antibodies (shown in table 2.6, diluted in Odyssey Blocking Buffer) overnight at 4 °C.

Table 2.6 Antibodies used for western blot

Antibody name	Species	Dilution	Catalogue #	Supplier
IGF-1R β	Rabbit	1:1000	3027	Cell Signaling Technology
pIGF-1Rβ(Tyr1135/1136) /pINSR β (Tyr1150/1151)	Rabbit	1:500	3024	Cell Signaling Technology
AKT	Rabbit	1:1000	9272	Cell Signaling Technology
pATK (S473)	Rabbit	1:1000	4060	Cell Signaling Technology
ERK	Mouse	1:1000	4696	Cell Signaling Technology
pERK (T202/Y204)	Rabbit	1:1000	9101	Cell Signaling Technology
RRM2	Goat	1:2000	SC-10844	Santa Cruz Biotechnology
CHK1	Mouse	1:1000	SC-8408	Santa Cruz Biotechnology
pCHK1 (S296)	Rabbit	1:1000	90178	Cell Signaling Technology
pCHK1 (S345)	Rabbit	1:1000	2348	Cell Signaling Technology
CDK1	Rabbit	1:1000	77055	Cell Signaling Technology
pCDK1 (Y15)	Rabbit	1:1000	4539	Cell Signaling Technology
β-tubulin	Mouse	1:3000	86298	Cell Signaling Technology
β-actin	Mouse	1:3000	A1978	Sigma-Aldrich
γH2AX (S139)	Rabbit	1:1000	2577	Cell Signaling Technology

Membranes were washed 3 times with PBST (5 minutes each time), and then incubated with IRDye secondary antibodies (#926-68074, #926-68071, #926-32210, LI-COR Biosciences) for 1 hour at room temperature. After 3 times washes with PBST, the signals on membranes were detected by Odyssey Imaging System (LI-COR Biosciences). The quantification of western blot data was performed on ImageJ software (NIH).

2.9 Cell cycle analysis with flow cytometry

Cells were cultured to ~70% confluence on the day of cell cycle analysis. Cells were first incubated with 20 μM 5-Bromo-2'-deoxyuridine (BrdU, #19-160, Sigma-Aldrich) in cell culture medium for 30 minutes at 37 °C with 5% CO_2, and then trypsinised. After trypsinisation, cells were collected in fresh medium as previously described (section 2.2). Cells were pelleted by centrifugation at 300 g for 5 minutes and fixed with 1 mL cold 70% ethanol, added dropwise while gently vortexing. Cells were then incubated for 30 minutes or overnight at -20 °C. Cells were pelleted again by centrifugation at 300 g for 5 minutes and then denatured with 1mL 2 M HCl containing 0.1 mg/mL pepsin (#P7000, Sigma-Aldrich) for 20 minutes. Cells were pelleted, washed once with 1x PBS and once with 1x PBS containing 2% FBS, followed by overnight incubation with primary BrdU antibody (1:500 in 1x PBS containing 2% FBS, #347580 BD Biosciences) at 4 °C. Cells were washed once with 1x PBS containing 2% FBS and incubated with anti-mouse secondary antibody Alexa Fluor 488 (1:500, #A11029, Invitrogen) in 1x PBS containing 2% FBS for 90 minutes at room temperature (protected from light and vortexing every 30 minutes). Cells were washed once with 1x PBS and then re-suspended in PBS containing 0.1 mg/ml propidium iodide (#P4864, Sigma-Aldrich). Intensity of BrdU staining and PI staining of 10,000 cells per sample were acquired by FACS Calibur (BD Biosciences) using BD Cell Quest Pro software (BD Biosciences). The analysis of data was performed with FlowJo V10 Software (BD Biosciences).

2.10 DNA fiber assay

DNA fiber assay was performed with the method modified from (Manders et al., 1992; Merrick et al., 2004).

2.10.1 Pulse and chase labelling

Cells were cultured to ~70% confluence on the day of DNA fiber assay. Cells were first labelled with 25 μM 5-chloro-2'-deoxyuridine (CIdU, MP Biomedicals #105478, diluted in full DMEM) for 20 minutes at 37 °C with 5% CO_2, following by two quick washes with 1x PBS to remove the remaining CIdU. Cells were then incubated with 20 μM 5-Iodo-2'-deoxyuridine (IdU, #100357, MP Biomedicals, diluted in DMEM) for 20 minutes at 37 °C with 5% CO_2. Cells were washed twice with 1x PBS, trypsinised and collected in cold 1x PBS. Cell number was counted as previously described, and cell suspension was diluted to 5 x 10^5 cells/mL.

2.10.2 DNA spreading

Cell suspension (2 μL) was placed as one drop near to one end of a positively charged slide (#631-0108, VWR). After 6 minutes, cells were gently mixed with 7 μL spreading buffer (200 mM Tris-HCl, pH 7.4, 50 mM EDTA, 0.5% SDS in H_2O). Samples became relatively sticky after mixing with spreading buffer. DNA fibers were spread by tilting the slides slowly to an approximate angle of 15°~30°, allowing the samples to slowly spread to the end of the slides in about 3 minutes. All the slides were air-dried (less than 10 minutes at room temperature), followed by the fixation with methanol/acetic acid (3:1, v/v) for 10 minutes at room temperature. The slides were air-dried again at room temperature for 10 minutes and were ready for DNA fiber staining.

2.10.3 DNA fiber staining

The slides were first re-hydrated with 1x PBS for 5 minutes and then DNA were denatured in 2.5 M HCl for 1 hour at room temperature. After washing 3 times with 1x PBS, slides were blocked with blocking buffer (2% BSA and 0.2% Tween 20 in 1x PBS, filtered with 0.22 µm filter) for 40 minutes. Slides were incubated in primary antibodies (1:300 for CIdU, # ab6326, abcam and 1:100 for IdU, #347580, BD biosciences) in blocking buffer overnight at 4 °C. After gently washing with 1x PBS twice and blocking buffer once, slides were then incubated with anti-mouse secondary antibody Alexa Fluor 488 (#A11029, Invitrogen, 1:500) and anti-rat secondary antibody Alexa Fluor 594 (#A11007, Invitrogen, 1:500) for 1 hour at room temperature (protected from light). The slides were washed twice with 1 x PBS and mounted with coverslips with antifade mounting medium (#H-1000, Vector Laboratories). DNA fibers were visualised on ZEISS LSM710 confocal microscope (Carl Zeiss Microscopy) and analysed using ImageJ software (NIH), typically measuring 150-200 fibers per condition.

2.11 Immunofluorescence

Cells were seeded on 22 mm x 22 mm sterile coverslips in 6-well plates. To visualize ssDNA, BrdU was used to label DNA and detected under non-denaturing condition (Buisson et al., 2015). Specifically, 10 µM BrdU (#19-160, Sigma-Aldrich) was added in cell culturing medium 36 hours before fixation, which enabled BrdU incorporation into DNA. For immunostaining, cells were fixed with 4% Paraformaldehyde (#43368, Alfa Aesar, diluted in 1 x PBS) for 12 minutes, followed by washing twice with 1 x PBS for 5 minutes on a shaker. Cells were then permeabilized using TFT buffer (0.1% Triton X-100, 4% FBS in 1x PBS, stored at

4 °C) for 5 minutes. Cells were washed twice with 1x PBS, and blocked with 5% BSA in PBS for 1 hour. Primary BrdU antibody (#347580, BD biosciences) and γH2AX antibody (# 2577, Cell Signaling Technology) were diluted 1:500 in 1% BSA and incubated overnight at 4 °C. After 3 times washes with 1 x PBS, anti-mouse secondary antibody Alexa Fluor 488 (#A11029, Invitrogen) and anti-rabbit secondary antibody Alexa Fluor 594 (#A11037, Invitrogen) were diluted 1:500 in 1% BSA and incubated for 1 hour at room temperature (protected from light). After 3 times washes with 1x PBS, coverslips were mounted onto microscope slides (#631-0912, VWR) with antifade mounting medium containing DAPI (#H-1200, Vector Laboratories). The slides were imaged on ZEISS LSM 710 confocal microscope (Carl Zeiss Microscopy).

2.12 dNTP measurement

The method for dNTP measurement was a solid-phase polymerase assay using tritium (^{3}H)-labelled substrates, modified from (Landoni et al., 2018; Sherman and Fyfe, 1989).

2.12.1 dNTP extraction

At least 10^6 cells were cultured to similar confluency (~70%) for all samples. Cells were gently washed with 1 x PBS, trypsinised and collected in 1x PBS, followed by cell number counting as previously described. All samples were normalised with the same cell number and diluted in 1x PBS at 10^6 cells/mL. Same number of cells were pelleted by centrifugation at 250 g for 5 minutes at room temperature. To extract the dNTPs from the cell pellets, 1 mL cold (- 20 °C) 60% methanol was added while vortexing, and then incubated for 1 hour (or overnight) at – 80 °C. The samples were boiled at 95 °C for 3 minutes. After cooling down to room temperature for ~30

minutes, samples were centrifuged at 15,000 g for 10 minutes. The supernatants were collected and divided into two aliquots of 500 µL and dried in a speed vacuum concentrator for 1 hour at 60 °C. The solid dNTP extracts were assayed immediately or stored at – 80 °C until analysis.

2.12.2 Solid-phase polymerase assay using tritium (^{3}H) labelled substrates

The polymerase reactions were performed in a streptavidin-coated 96-well plate (#15125, Thermo Scientific). The streptavidin-coated 96-well plate was first prepared by affinity capture of biotinylated oligonucleotides as the templates for dNTP incorporation. The 4 oligonucleotides and the common primer for 4 dNTP incorporation reactions were designed and modified based on Sherman and Fyfe's protocol (Sherman and Fyfe, 1989) (shown in Table 2.7).

Table 2.7 Primer and 5'-biotinylated [B] oligonucleotides used for dNTP assay

	Sequence (5' – 3')	Length
Primer	CCCGCCTCCACCGCC	21 bp
Oligo for dATP	[B]AAATAAATAAATAAATAAATGGCGGTGGAGGCGGG	41 bp
Oligo for dTTP	[B]TTATTATTATTATTATTAGGCGGTGGAGGCGGG	39 bp
Oligo for dCTP	[B]TTTGTTTGTTTGTTTGTTTGGGCGGTGGAGGCGGG	41 bp
Oligo for dGTP	[B]TTTCTTTCTTTCTTTCTTTCGGCGGTGGAGGCGGG	41 bp

The 5'-biotinylated oligonucleotides were synthesised and HPLC-purified by IDT, diluted to 5 µM in sterile H_2O, aliquoted and stored at – 20 °C. The biotinylated oligonucleotides were added into the streptavidin-coated plate at the final concentration of 0.25 µM in 50 µL PBS-0.1 % TWEEN 20 (PBST). The plate was incubated while gently shaking at room temperature for 2 hours, allowing for biotin-

streptavidin binding. After washing 3 times with 50 µL TENT buffer (40 mM Tris-HCl, 1mM EDTA, 50mM NaCl, 0.1% TWEEN-20, pH 8.0), the primer was added into the plate at the concentration of 0.25 µM in 50 µL PBST. The plate was heated up to 95 °C for 4 minutes and cooled down to room temperature over 1 hour, allowing primer annealing to the oligonucleotide template. Commercial dNTPs (#N0446S, New England Biolabs), dATP, dTTP, dCTP and dGTP were individually diluted to series concentrations with sterile water as the standards (Landoni et al., 2018): 100 nM, 80 nM, 40 nM, 20 nM, 10 nM, and a sterile water blank. Through initial tests with these standards of each dNTP, we determined the optimal measurement range to be 10~100 nM because the radioactivity showed linear correlation with the concentration of each dNTP within the measurement range. To prepare the samples, solid dNTP extracts were diluted in sterile water (normally 500 µL for the extracts from 10^6 MCF7 cells gave the concentrations within optimal measurement range). The next step was preparing polymerase reaction solution, and all the procedures from this step onwards were performed in the supervised radiation suite after radiation safety training and registration as a radiation worker in accordance with University rules. The components of polymerase reaction mixtures (50 µL/sample) for each dNTP measurement are shown in Table 2.8.

Table 2.8 DNA polymerase reaction components for dNTP assay

	Volume (µL)	Final concentration
10x polymerase buffer	5	1x
Klenow polymerase (10 U/ µL)	0.125	1.25 U
DTT (500 mM)	0.5	5 mM
[^{3}H]-dATP/[^{3}H]-dTTP	2	[^{3}H]-dATP: 0.04 uCi/ µL [^{3}H]-dTTP: 0.1 uCi/ µL
Sample/standard	12.5	
Sterile water	29.875	
Total	**50**	

For dATP measurement, [3H]-dTTP (#NET520A250UC, PerkinElmer) was used. For dTTP, dCTP and dGTP measurement, [3H]-dATP (#NET268250UC, PerkinElmer) was used. The reaction mixtures were first prepared by mixing the components without samples or standards and then aliquoted (37.5 µL/well) into oligonucleotide template-coated 96-well plate. The samples (in triplicate) and the standards (in duplicate) were added into the plate (12.5 µL/well). The plate was incubated at room temperature for 1 hour, allowing dNTP incorporation. The contents of the wells were discarded and the wells were washed 4 times with 50 µL TENT buffer. All the TENT buffer was removed after the final wash. To release the newly synthesised labelled DNA strand, 60 µL of 50 mM NaOH was added into the wells and incubated for 3 minutes at room temperature. The eluted DNA was transferred to scintillation vials containing 3 mL scintillation cocktail (OptiPhase supermix cocktail, #1200-439, PerkinElmer). The radioactivity was determined on a Beckman LSC LS6500 scintillation counter (PerkinElmer) at 1 minute counting per sample. The counts-per-minute (CPM) data were imported into Microsoft Excel for further analysis. Data first were normalised to the blank controls, and the data from

assays where the standard curves gave concentration-dependent results were used and expressed as % controls.

2.13 3D spheroids culture

Tumour spheroids were generated in a round bottom ultra-low attachment 96-well plate (#7007, Corning), seeding 5000 cells (for HeLa, SKCO1, MCF7 cells) were seeded in 160 µL full culture medium in each well. Plates were centrifuged at 250 g at room temperature for 10 minutes and incubated for 72 hours at 37 °C with 5% CO_2, allowing for spheroid formation. After 72 hours, plates were imaged at 1200 dpi on the Gelcount (Oxford Optronix). Spheroids were treated by adding 40 µL x 5 drug or solvent control (or 20 µL x 10 drug #1 + 20 µL x10 drug #2 for drug combinations). At least 6 spheroids were used for each treatment condition. Plates were imaged daily on the Gelcount for 7~14 days. All images were exported and analysed by ImageJ for spheroid size quantification (set measurements to area limiting to threshold on ImageJ in order to quantify spheroid size above background). In addition to measuring size, spheroids were used for three endpoint experiments:

2.13.1 CellTiter Glo 3D cell viability assay

At least 3 spheroids per treatment condition were measured following the manufacturer's protocol. CellTiter-Glo 3D (#G9681, Promega) reagent was defrosted at room temperature. Plates were equilibrated to room temperature for approximately 30 minutes. CellTiter-Glo 3D reagent was gently mixed to obtain a homogeneous solution and 100 µL reagent/well was added into the plate. The solutions in the wells were vigorously mixed for 300 seconds to induce cell lysis using the shake function (orbital shaking 700 rpm) of POLARstar Omega Plate Reader (BMG LABTECH). The well content (spheroids with medium/assay solution)

were then transferred into a new clear bottom and white wall 96-well plate (#655094, Greiner Bio-one). The plate was incubated at room temperature for an additional 25 minutes to stabilize the luminescent signal. The luminescence intensity was determined on a POLARstar Omega Plate Reader. Data were exported and further analysed in GraphPad Prism 8.

2.13.2 Western blot

Multiple spheroids (3~12 spheroids per condition) were collected with wide bore pipette tips into 1.5 mL tubes. Once the spheroids settled on the bottom of the tubes, medium was removed and spheroids were washed once with ice-cold 1x PBS and then directly lysed in 3 x Laemmli sample buffer (150 mM Tris-HCl PH 6.8, 0.3 mg/mL Bromophenol blue, 30% Glycerol, 9% SDS, 15% β-mercaptoethanol). Samples were homogenized, denatured by boiling for 10 mins, and then loaded onto 4-15% Midi-PROTEAN TGX precast Gel (#5671084, Bio-Rad) for electrophoresis and western blot analysis as described in section 2.8.

2.13.3 dNTP measurement

Twelve spheroids were collected with wide bore pipette tips and washed once with 1 x PBS. The dNTPs were extracted by adding 1 mL cold (- 20 °C) 60% methanol. The solutions were vigorously vortexed to break down the spheroids or sonicated at 4 °C using the Bioruptor sonicator for 30 cycles of 15 seconds on/15 seconds off. The samples were incubated at – 80 °C overnight, followed by the same procedures as described in section 2.12. For sample normalization, CellTiter Glo 3D readings from assay described in 2.13.1, or BCA protein assay results were used to adjust the volume of each extract used for dNTP assay.

2.14 Statistics

Data were presented as mean ± standard error of the mean (SEM), n=3 independent experiments, unless stated otherwise. Using Graphpad Prism 8, one-way analysis of variance (ANOVA) was used for group comparisons (>2 groups), and unpaired and two-tailed t test was used if 2 groups were compared. Two-way ANOVA was used to compare the growth curves of 3D spheroids. P value of less than 0.05 was considered as statistically significant. Combination index was calculated in CalcuSyn Software (Chou, 2010).

Chapter 3

IGF blockade induces replication stress

3.1 Introduction

As described in section 1.1.3, high levels of circulating IGF ligands or overexpression of IGF-1R have been frequently detected in many types of cancers, including prostate, breast and colorectal cancers (Ahlgren et al., 2004; Chan et al., 1998; Farabaugh et al., 2015; Hellawell et al., 2002; Renehan et al., 2004; Weber et al., 2002). IGF signalling through MEK/ERK and PI3K/AKT pathways mediates cancer cell proliferation, cell cycle progression, DNA damage response, and protection from apoptosis (Borowiec et al., 2011; Chitnis et al., 2008; Hamelers et al., 2002). Current unpublished work in our group done by post-doctoral scientist Dr Guillaume Rieunier suggested that IGF signalling mediated the expression of RRM2, the essential regulatory subunit of RNR, through both MEK/ERK and PI3K/AKT pathways. Dr Rieunier found that IGF blockade induced accumulation of endogenous DNA lesions, accompanied by slowed replication fork progression and ATR/CHK1 checkpoint activation, which are the key markers of replication stress (Zeman and Cimprich, 2014). Dr Rieunier further demonstrated that replication stress induced by IGF blockade was through downregulating RRM2 and reducing

dATP supply, leading to the imbalanced dNTP pools, which is in line with the critical role of RNR activity as the rate-limiting step for dNTP production (Mathews, 2015),

In work described in this Chapter, multiple IGF-1R inhibitors and small interfering RNA (siRNA) targeting IGF-1R were used to examine the effects of IGF blockade on cell proliferation and replication fork progression to confirm the replication stress phenotype identified by Dr Rieunier in breast cancer cells. Through collaboration with Drs Ulrike Weyer-Czernilofsky and Thomas Bogenrieder from Boehringer Ingelheim, we have access to two IGF signalling-targeting drugs, BI-836845 (xentuzumab) and BI-885578. BI-836845 is an efficient and tolerable IGF ligand-neutralising antibody used in clinical trials (NCT02204072, NCT02123823, NCT03659136) that shows high selectivity for IGFs without interfering with insulin signalling (Friedbichler et al., 2014; Mireuta et al., 2014), compared to the IGF-1R tyrosine kinase inhibitors used in previous preclinical and clinical studies, such as BI-885578 and BMS-754807 that also inhibit INSR on its kinase domain (Carboni et al., 2009; Sanderson et al., 2015; Sanderson et al., 2017).

3.2 Results

3.2.1 IGF blockade suppresses cancer cell proliferation

We first used three IGF signalling-targeting inhibitors: BI-836845 (IGF ligand antibody), BI-885578 (IGF-1R TKI), and BMS-754807 (IGF-1R TKI) to investigate their effects on IGF signalling. Western blot analysis was performed with MCF7 cells after IGF stimulation with or without exposure to different concentrations of these inhibitors. All three inhibitors led to the inhibition of IGF-induced phosphorylation of IGF-1R (Y1135/1136) and its downstream effectors, pAKT (s473) and pERK (T202/Y204) in a dose-dependent manner (Figure 3.1 A). A resazurin-based viability assay was performed and the results showed that 5 days treatment of all three

inhibitors suppressed the proliferation of MCF7 cells in a dose-dependent manner (Figure 3.1 B), consistent with previous findings of tumour growth inhibition by these IGF inhibitors in other models (Carboni et al., 2009; Friedbichler et al., 2014; Sanderson et al., 2015). Notably, although high concentrations of IGF or IGF-1R inhibitors that almost abolished IGF-1R signalling significantly did suppress cell proliferation, the cells after the treatment still remained a cell viability of 50% ~ 60% of levels in solvent treated controls (Figure 3.1 B).

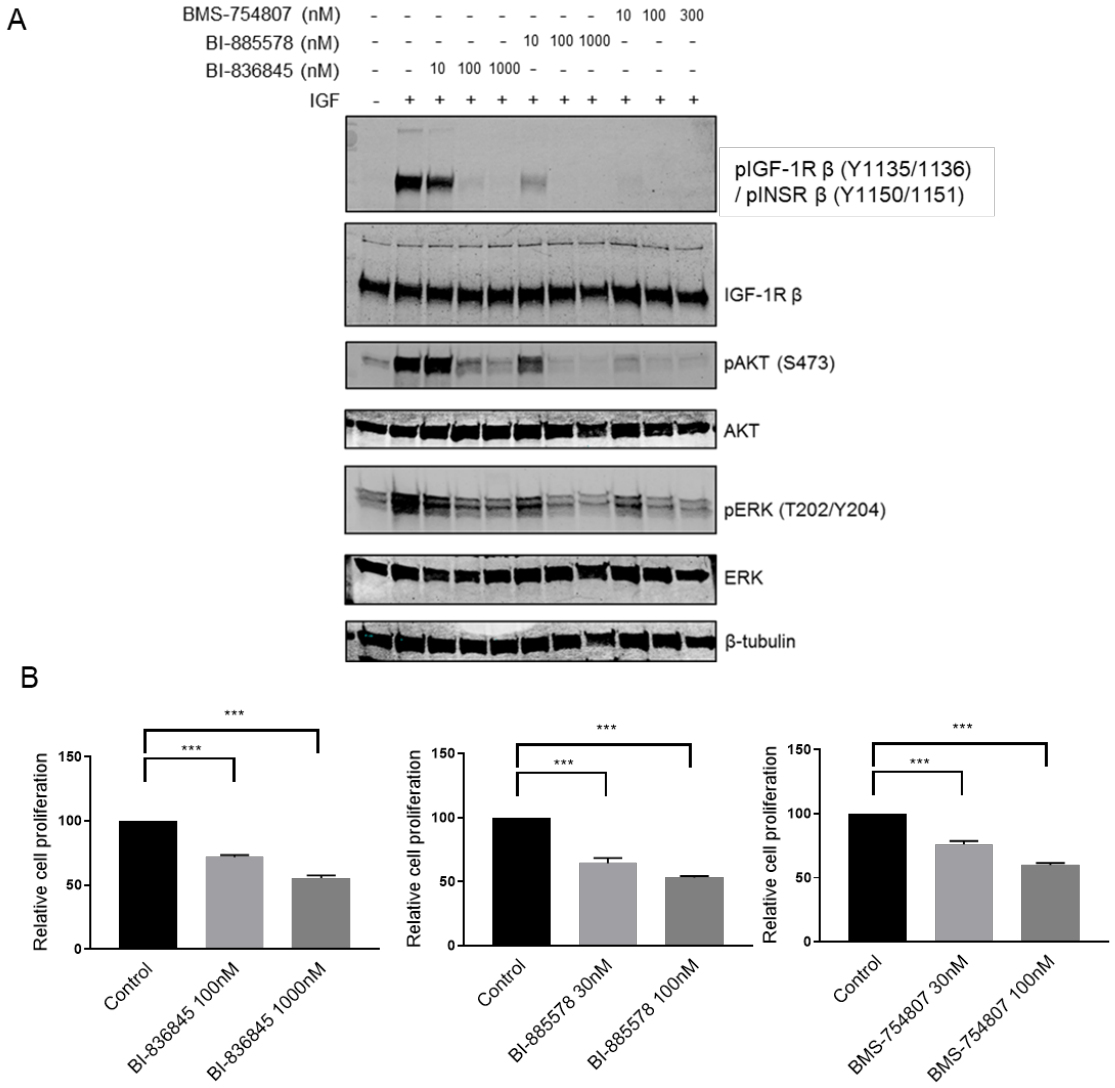

Figure 3.1 IGF signalling blockade inhibits breast cancer cell viability
(A) Western blot analysis of MCF7 cells exposed to BI-836845 (IGF ligand antibody), BI-885578 (IGF-1R TKI), and BMS-754807 (IGF-1R TKI) for 4 days, then serum starved for 24 hours in the presence of the same inhibitors and stimulated with 50 nM IGF-1 for 15 minutes.

Western blot analysis was performed twice. Similar results were seen in a repeat western blot using a second set of independently prepared lysates. (B) Cell viability tested 5 days after drug treatment (CellTiter Blue assay) expressed as % viability of solvent-treated control (left). Data are represented as mean ± SEM, pooled from 3 independent experiments. One-way ANOVA analysis was applied. ***P < 0.001.

We also genetically depleted IGF-1R by using two different siRNAs targeting IGF-1R (#1 purchased from Qiagen, #2 from the sequence designed in our group (Bohula et al., 2003)). The expression of IGF-1R markedly decreased 24 hours after siRNA transfection (Figure 3.2 A).

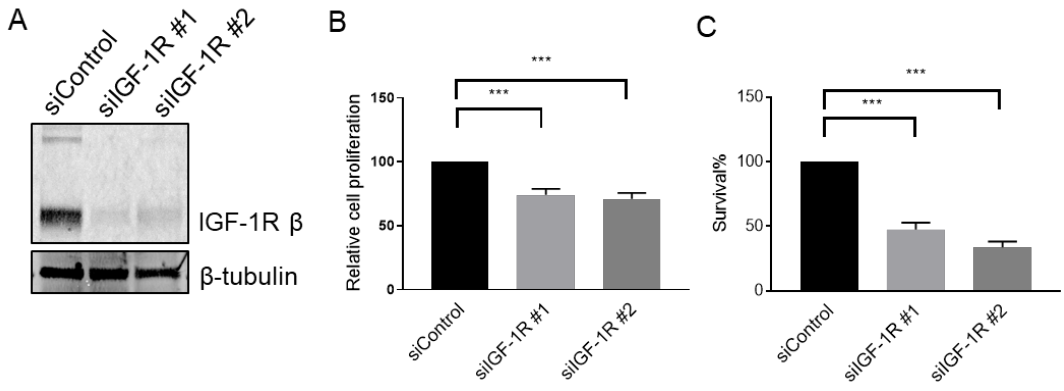

Figure 3.2 IGF-1R depletion inhibits breast cancer cell viability and survival
(A) Western blot analysis of MCF7 cells transfected with siControl or siIGF-1R and lysed after 24 hours. (B, C) Cells transfected as A were collected 24 hour later and reseeded for assay of B) cell viability (5 days after 24 hours transfection) and C) cell survival (7 days after 24 hours transfection). Results were expressed as % viability or % survival of siControl-transfected cells (left). Data are represented as mean ± SEM, pooled from 3 independent experiments. One-way ANOVA analysis was applied. ***P < 0.001.

After 24 hours of siRNA transfection, the IGF-1R-depleted and siControl cells were re-plated in 96-well plates for resazurin-based cell viability assay or in 6-well plates for clonogenic survival assay. After 5 days, cell viability of IGF-1R-depleted cells reduced to ~70% of siControl cells (Figure 3.2 B). Cell survival rate also reduced in IGF-1R depleted cells, compared to siControl cells (Figure 3.2 C). Thus, these data

showed that both pharmacological inhibition of IGF signalling and genetic depletion of IGF-1R slowed cell proliferation and survival, but cells still remained viable.

3.2.2 IGF-1R depletion or inhibition induces endogenous DNA damage

Previous study in our group found IGF-1R inhibitor AZ12254801 (IGF-1R TKI) delayed the repair of IR-induced DNA damage and also caused accumulation of the endogenous DNA damage in prostate cancer cells, assessed by foci formed by phosphorylated-H2AX at serine 139 (γH2AX) (Chitnis et al., 2014; Lodhia et al., 2015). Using the same method of immunofluorescence (IF) to assess the formation of γH2AX foci, we examined the induction of endogenous DNA damage after IGF-1R depletion by siRNA and IGF-1R inhibition by inhibitor treatment in breast cancer cells.

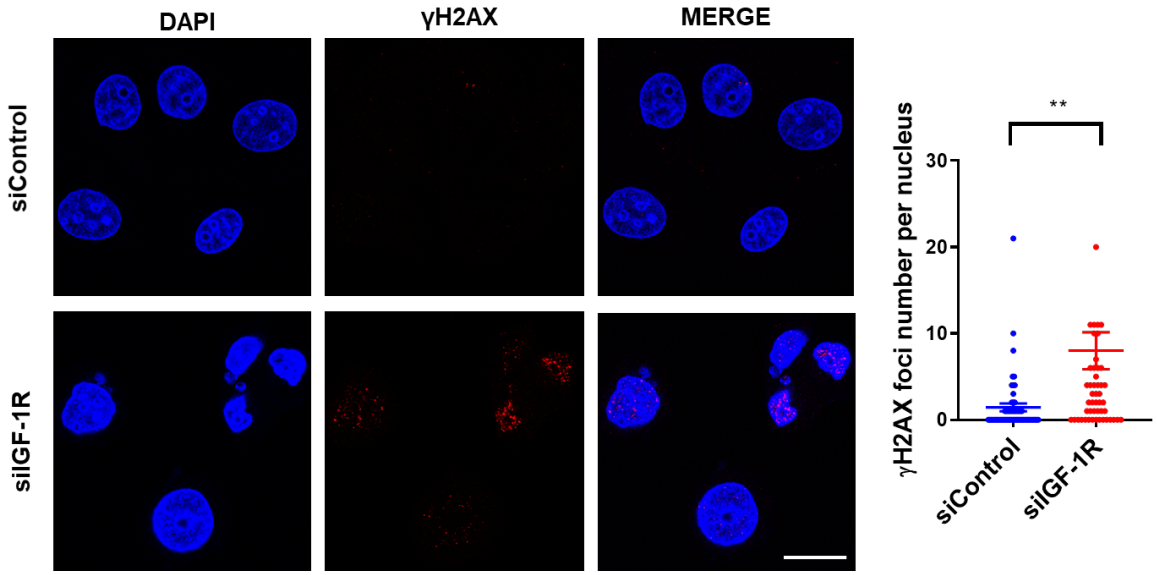

Figure 3.3 IGF-1R depletion induces endogenous DNA damage
Representative image of γH2AX immunostaining in MCF7 cells transfected with siControl or siIGF-1R for 48 hours. Cell nucleus was stained by DAPI. Scale bar: 20 μm. Quantification of γH2AX (>50 cells) shown on the right. Data are represented as mean ± SEM, pooled from 3 independent experiments. Unpaired and two-tailed t test was applied. **P < 0.01.

The IF analysis showed that 48 hours transfection of siRNA targeting IGF-1R significantly promoted the formation of γH2AX foci in MCF7 cells (Figure 3.3), consistent with the data in prostate cancer cells reported by our group (Lodhia et al., 2015). Furthermore, MCF7 cells treated with BI-836845 for 72 hours also represented significantly higher number of γH2AX foci, compared to the solvent control-treated cells (Figure 3.4 A). A similar increased level of γH2AX foci formation was observed in a second ER+ breast cancer cell line ZR-75-1 (Figure 3.4 B). Therefore, these results supported the concept that IGF-1R depletion or inhibition accumulated γH2AX foci that formed at endogenous DNA damage lesions. Together with the work by Dr Rieunier showing the accumulation of under-replicated DNA after IGF blockade, measured by 53BP1 bodies in G1 phase (unpublished data not shown), these results strongly suggested replication stress in cells after IGF blockade that might be responsible for the increased endogenous DNA damage.

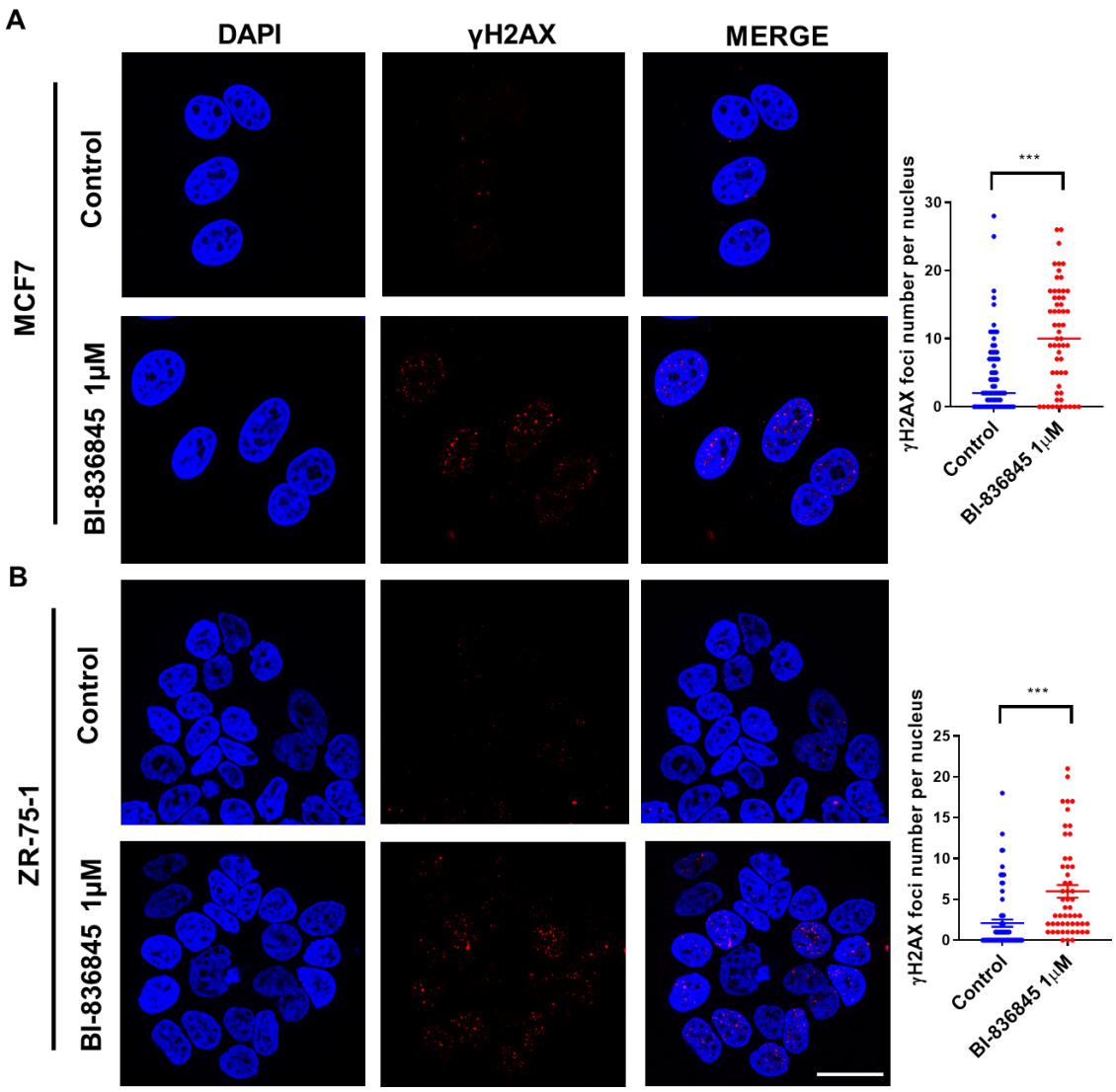

Figure 3.4 IGF-1R inhibition induces endogenous DNA damage
(A) Representative image of γH2AX immunostaining in MCF7 cells treated with 1 μM BI-836845 for 72 hours. Cell nucleus was stained by DAPI. Scale bar: 20 μm. Quantification of γH2AX (>50 cells) shown on the right. Data are represented as mean ± SEM, pooled from 3 independent experiments. (B) Same experiment performed in ZR-75-1 cells. Quantification of γH2AX (>50 cells) shown on the right. Data are presented as mean ± SEM, pooled from 2 independent experiments. Unpaired and two-tailed t test was applied. ***P < 0.001.

3.2.3 IGF-1R depletion or inhibition slows replication fork progression

To investigate replication stress, we next performed DNA fiber assay to directly assess replication fork dynamics. Using double DNA labelling scheme with two modified nucleotides CIdU and IdU, DNA fiber assay is able to measure the rate of

fork progression, fork stalling and origin firing (Merrick et al., 2004). DNA fiber tracts were analysed 48 hours after siRNA transfection in MCF7 cells, and the significantly shorter DNA fibers were observed in IGF-1R-depleted cells compared to siControl cells (Figure 3.5 A), suggesting DNA replication is slower after IGF-1R depletion.

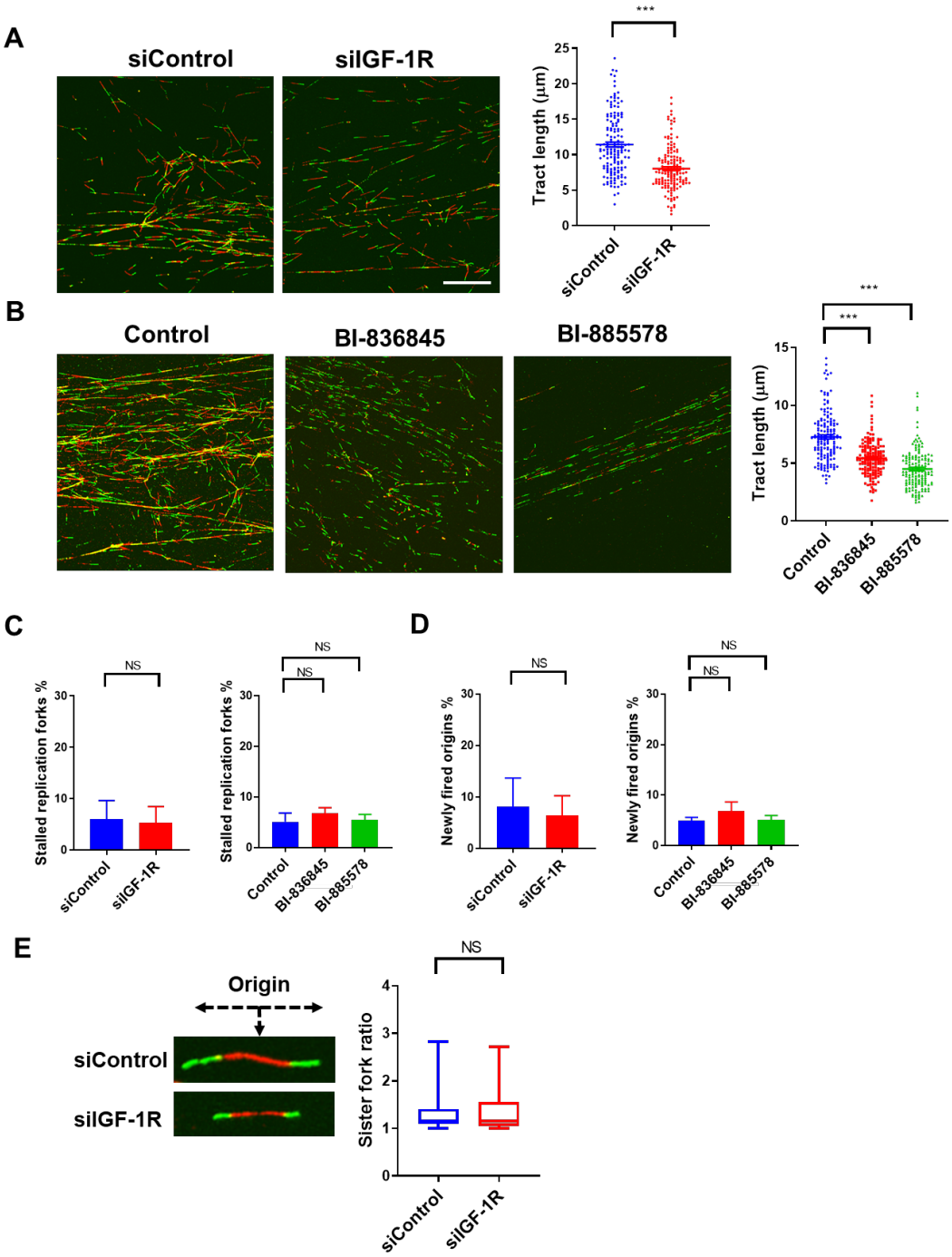

Figure 3.5 IGF-1R depletion or inhibition suppresses DNA replication fork progression

(A) Representative image of DNA fiber tract (CIdU (Red), IdU (Green)) in MCF7 cells transfected with siControl or siIGF-1R for 48 hours. Scale bar: 20 μm. Quantification of fiber tract length (>150 tracts) shown on the right. (B) Representative image of DNA fiber tract (CIdU (Red), IdU (Green)) in MCF7 treated with BI-836845 (1 μM) or BI-885578 (300nM) for 24 hours. Scale bar: 20 μm. Quantification of fiber tract length (>150 tracts) shown on the right. Data (mean ± SEM) are one representative experiment of 3 independent experiments with similar results. One-way ANOVA analysis was applied. ***P < 0.001. (C) Quantification of stalled replication forks (CIdU (red)-only tracts) as percentages of the total number of tracts (≥ 5 images in A and B). (D) Quantification of newly fired origins (IdU (green)-only tracts) as percentages of the total number of tracts (≥ 5 images in A and B). Unpaired and two-tailed t test (left) and one-way ANOVA (right) were applied. (E) Representative images of sister forks from MCF7 cells after 48 hours siRNA transfection. Quantification of ratios of sister forks (> 20 pairs of sister forks) shown on the right as median with 25th and 75th percentiles and the whiskers mark the smallest and largest values. Unpaired and two-tailed t test was applied. NS: P> 0.05 not significant.

Consistent with the results in IGF-1R depleted cells, a similar reduction of DNA fiber length was observed in cells treated with BI-836845 or BI-885578 for 24 hours (Figure 3.5 B). Notably, replication forks in IGF-1R depleted or inhibited cells were still able to progress, albeit at a slower rate. In response to replication fork slowing or stalling, cells can either fire more dormant origins nearby to compensate the replication or inhibit origin firing via activating CHK1 or WEE1-mediated checkpoint to prevent the global exhaustion of replication factors (Yekezare et al., 2013). We next analysed DNA fiber results to assess fork stalling (only CIdU labelling) and origin firing (only IdU labelling) (Merrick et al., 2004). We did not observe significant fork stalling or increased newly fired origins after IGF-1R depletion or inhibition (Figure 3.5 C, D), suggesting that IGF blockade slowed replication fork progression but not affected origin firing. In line with the unpublished results by Dr Rieunier, no significant sister fork asymmetry was observed after IGF-1R depletion or inhibition (Figure 3.5 E), suggesting that replication stress induced by IGF blockade was mainly caused by global reduction of DNA replication, not physical impediment by DNA lesions, which have been shown to affect sister fork symmetry (Conti et al.,

2007). Taken together, these data suggested a replication stress phenotype in IGF-1R depleted or inhibited cells.

3.3 Discussion

The results in this chapter confirmed that genetic and pharmacological inhibition of IGF signalling suppressed cell proliferation and led to accumulation of endogenous DNA damage, consistent with the previous study in our group (Lodhia et al., 2015). DNA fiber analysis shown in this chapter suggested that IGF blockade significantly slowed replication fork progression, confirming the replication stress phenotype in IGF-1R depleted or inhibited cells demonstrated by Dr Rieunier's unpublished work. Dr Rieunier's data further showed that slowed replication fork progression after IGF blockade was accompanied with the decrease of origin firing and the activation of replication stress responses, indicated by the increase of ATR-activated CHK1 phosphorylation at serine 345 and RPA phosphorylation at serine 33. As a consequence of replication stress, IGF-1R depleted or inhibited cells accumulated endogenous DNA lesions, marked by 53BP1 bodies and γH2AX foci. However, although replication rates were significant slower after IGF blockade, DNA replication still proceeded and cells were still viable, albeit at a slower growth rate (Figure 3.1), suggesting that this replication stress is tolerable.

The tolerable replication stress observed in IGF-1R depleted or inhibited cells prompted us to think whether this replication stress represents an exploitable therapeutic vulnerability to cancer treatments. From previous clinical trials of IGF-targeted therapies, some patients responded well, but many did not benefit (King et al., 2014). If we could find approaches to enhance this replication stress induced by IGF blockade from tolerable level to intolerable replication catastrophe, we might be

able to identify potential biomarkers or novel combination treatments to improve the response to IGF inhibitory drugs in cancer patients.

Chapter 4

Targeting CHK1 induces replication catastrophe after IGF blockade

4.1 Introduction

As described in section 1.3.2, the timely and accurate DNA replication requires cells to resolve numerous obstacles that slow or stall replication fork progression, termed replication stress (Zeman and Cimprich, 2014). Unpublished data generated in our group and the results in Chapter 3 demonstrated that IGF blockade induced replication stress, but only partially reduced DNA replication and cell proliferation. Previous studies suggested a tolerable threshold of intrinsic replication stress in cancer cells (Buisson et al., 2015; Toledo et al., 2017; Toledo et al., 2013). This basal level of replication stress is a consequence of the rapid cell proliferation and dysregulated DNA damage response, contributing to genome instability and tumorigenesis (Gorgoulis et al., 2005; Macheret and Halazonetis, 2015; Maya-Mendoza et al., 2018). However, this intrinsic replication stress is at the tolerable level because cancer cells activate replication stress responses and DNA damage repair machinery to protect slowed or stalled replication forks and resolve toxic DNA lesions (Branzei and Foiani, 2010; Buisson et al., 2015; Toledo et al., 2017; Toledo et al., 2013; Zeman and Cimprich, 2014). If the replication stress is elevated above

the tolerable threshold, excess single stranded DNA (ssDNA) would be accumulated in cells, leading to replication fork collapse and deleterious DSBs, described as replication catastrophe (Buisson et al., 2015; Toledo et al., 2017; Toledo et al., 2013). We hypothesise that IGF-1R inhibited or depleted cells show tolerable replication stress, but might be more dependent on replication stress responses and DNA repair to resolve toxic replication intermediates, serving as an exploitable vulnerability for cancer treatment. Previous studies discussed the rationales to exacerbate replication stress in cancer cells as a promising strategy for cancer treatment (Bian and Lin, 2019; Buisson et al., 2015; Pfister et al., 2015; Ubhi and Brown, 2019). In this chapter, we aimed to develop approaches to enhance the replication stress induced by IGF blockade to an intolerable level, triggering replication catastrophe and cell death. Therefore, we performed a compound screen to combine IGF blockade with replication stress-inducing reagents, such as inhibitors targeting DNA replication, cell cycle controls and DNA damage repair.

4.2 Results

4.2.1 Compound screen for identifying effective drug combinations with IGF inhibition

We first performed a compound screen to identify additive or synergistic drug combinations with BI-836845. We selected 5 ER+ luminal breast cancer cell lines: MCF7, ZR-75-1, KPL1, T47D, and HCC1143. These cell lines were first tested using IncuCyte live cell analysis imaging system with the help of Dr Rieunier and Elena Seraia from Target Discovery Institute, and the Incucyte results showed that BI-836845 had a minor effect on cell growth inhibition (Figure 4.1 A). We next designed a custom compound library that consisted of DMSO solvent control and 59 bioactive

small molecule drugs, which are mainly targeting cell signalling, cell cycle controls, DNA replication and DNA damage responses (Table 2.3, 4.1, Figure 4.1 B).

Table 4.1 Compound used in drug screen

	Compound name	Main compound target	Catalogue number	Supplier
1	ABT-888 (Veliparib)	PARP1/2	S1004	Selleck Chemicals
2	Deforolimus (MK-8669)	mTOR	S1022	Selleck Chemicals
3	Lapatinib Ditosylate	EGFR | HER2	S1028	Selleck Chemicals
4	VX-680 (Tozasertib)	Aurora kinase (pan A,B,C)	S1048	Selleck Chemicals
5	BMS-599626 (AC480)	EGFR | HER2	S1056	Selleck Chemicals
6	Obatoclax Mesylate	BCL-2	S1057	Selleck Chemicals
7	AZD2281(Olaparib)	PARP	S1060	Selleck Chemicals
8	Nutlin 3	Mdm2/p53	S1061	Selleck Chemicals
9	MK-2206	AKT	S1078	Selleck Chemicals
10	KU-55933	ATM	S1092	Selleck Chemicals
11	AG-014699 (Rucaparib)	PARP1	S1098	Selleck Chemicals
12	BI 2536	PLK1	S1109	Selleck Chemicals
13	PD0332991 (Palbociclib)	CDK4/6	S1116	Selleck Chemicals
14	SNS-032(BMS-387032)	CDK2, CDK7/9	S1145	Selleck Chemicals
15	Gemcitabine Hydrochloride	DNA synthesis	S1149	Selleck Chemicals
16	Roscovitine (CYC202)	CDK1/2, CDK5	S1153	Selleck Chemicals
17	JNJ 26854165 (Serdemetan)	p53	S1172	Selleck Chemicals
18	Fulvestrant	Estrogen receptor	S1191	Selleck Chemicals
19	CUDC-101	HDAC | EGFR | HER2	S1194	Selleck Chemicals
20	Irinotecan	Topoisomerase I	S1198	Selleck Chemicals
21	PIK-75 Hydrochloride	PI3K | DNA-PK	S1205	Selleck Chemicals
22	Adriamycin (Doxorubicin)	Topoisomerase II	S1208	Selleck Chemicals
23	Clofarabine	Ribonucleotide reductase	S1218	Selleck Chemicals
24	Etoposide	Topoisomerase II	S1225	Selleck Chemicals

25	Flavopiridol (Alvocidib)	CDK1/2, CDK4/6, CDK9	S1230	Selleck Chemicals
26	Camptothecin	Topoisomerase I	S1288	Selleck Chemicals
27	ON-01910 (Rigosertib)	PLK1	S1362	Selleck Chemicals
28	Ispinesib (SB-715992)	Kinesin spindle protein	S1452	Selleck Chemicals
29	MC1568	HDAC	S1484	Selleck Chemicals
30	DMSO	Solvent control	D2650	Sigma-Aldrich
31	AT7519	CDK1/2, CDK4/6, CDK9	S1524	Selleck Chemicals
32	Hesperadin	Aurora kinase B	S1529	Selleck Chemicals
33	BIX 02189	MEK	S1531	Selleck Chemicals
34	AZD7762	CHK1/2	S1532	Selleck Chemicals
35	PD318088	MEK	S1568	Selleck Chemicals
36	KU-60019	ATM	S1570	Selleck Chemicals
37	BS-181 hydrochloride	CDK7	S1572	Selleck Chemicals
38	LY500307 (Erteberel)	Estrogen receptor β	S1598	Selleck Chemicals
39	Cytarabine (Cytosar-U)	DNA synthesis	S1648	Selleck Chemicals
40	Flucytosine (Ancobon)	DNA/RNA synthesis	S1666	Selleck Chemicals
41	Tamoxifen Citrate	Estrogen receptor	S1972	Selleck Chemicals
42	MLN2238 (Ixazomib)	Proteasome inhibitor	S2180	Selleck Chemicals
43	SB 743921	Kinesin spindle protein	S2182	Selleck Chemicals
44	Indirubin	CDK pan| GSK-3β	S2386	Selleck Chemicals
45	RITA (NSC 652287)	p53 inhibitor	S2781	Selleck Chemicals
46	BMN673 (Talazoparib)	PARP1/2	S7048	Selleck Chemicals
47	CO-1686 (Rociletinib)	EGFR	S7284	Selleck Chemicals
48	E3330	APE1	S7445	Selleck Chemicals
49	CRT0044876	APE1	S7449	Selleck Chemicals
50	VE-821	ATR	S8007	Selleck Chemicals
51	B02	RAD51	SML0364	Sigma-Aldrich
52	Mirin	MRN complex	S8096	Selleck Chemicals
53	Ro-3306	CDK1	15149	Cayman Chemical
54	SCH-900776 (MK-8776)	CHK1	S2735	Selleck Chemicals

55	MK-1775 (Adavosertib)	WEE1	1494	Axon Medchem
56	Abemaciclib (LY2835219)	CDK4/6	S7158	Selleck Chemicals
57	ML216	BLM	SML0661	Sigma-Aldrich
58	AZD5363 (Capivasertib)	AKT	S8019	Selleck Chemicals
59	Celastrol	NF-κB	3203	Tocris Bioscience
60	NSC 19630	WRN Helicase	681647	Calbiochem

MCF7, ZR-75-1, KPL1, T47D, and HCC1143 cells were seeded in 96-well plates at the seeding densities which were optimised in the initiate Incucyte tests (Figure 4.1 C). Compounds were tested at the concentrations of 0.1 μM, 1 μM and 10 μM in the absence or presence of 1 μM BI-836845, which is near to the steady-state circulating concentration of ~1.3 μM in patients of Phase II clinical trials, and cell viability was determined by resazurin-based viability assay after 5 days (Figure 4.1 C).

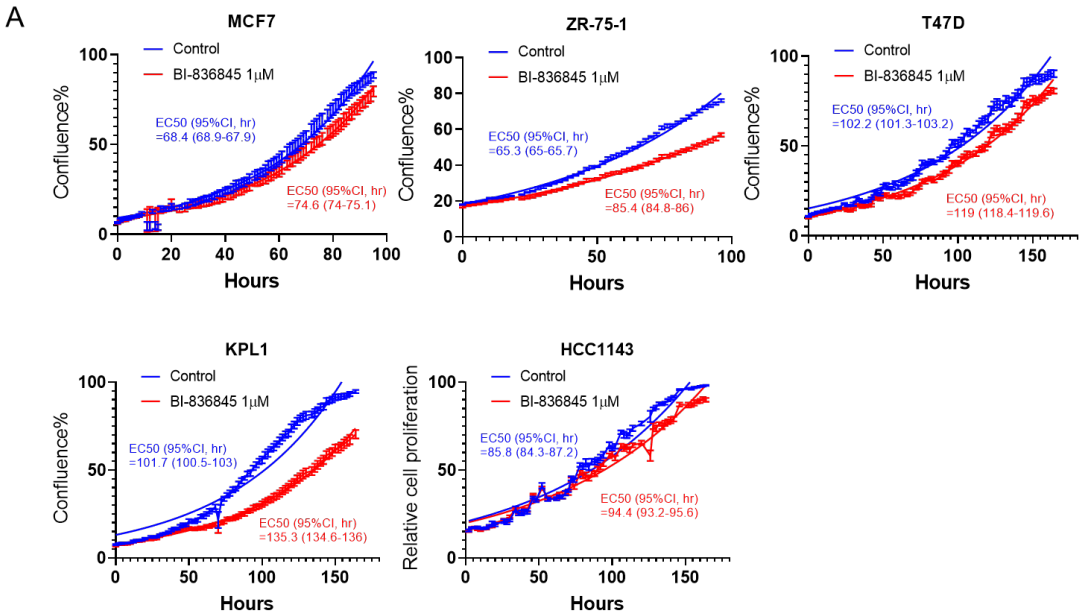

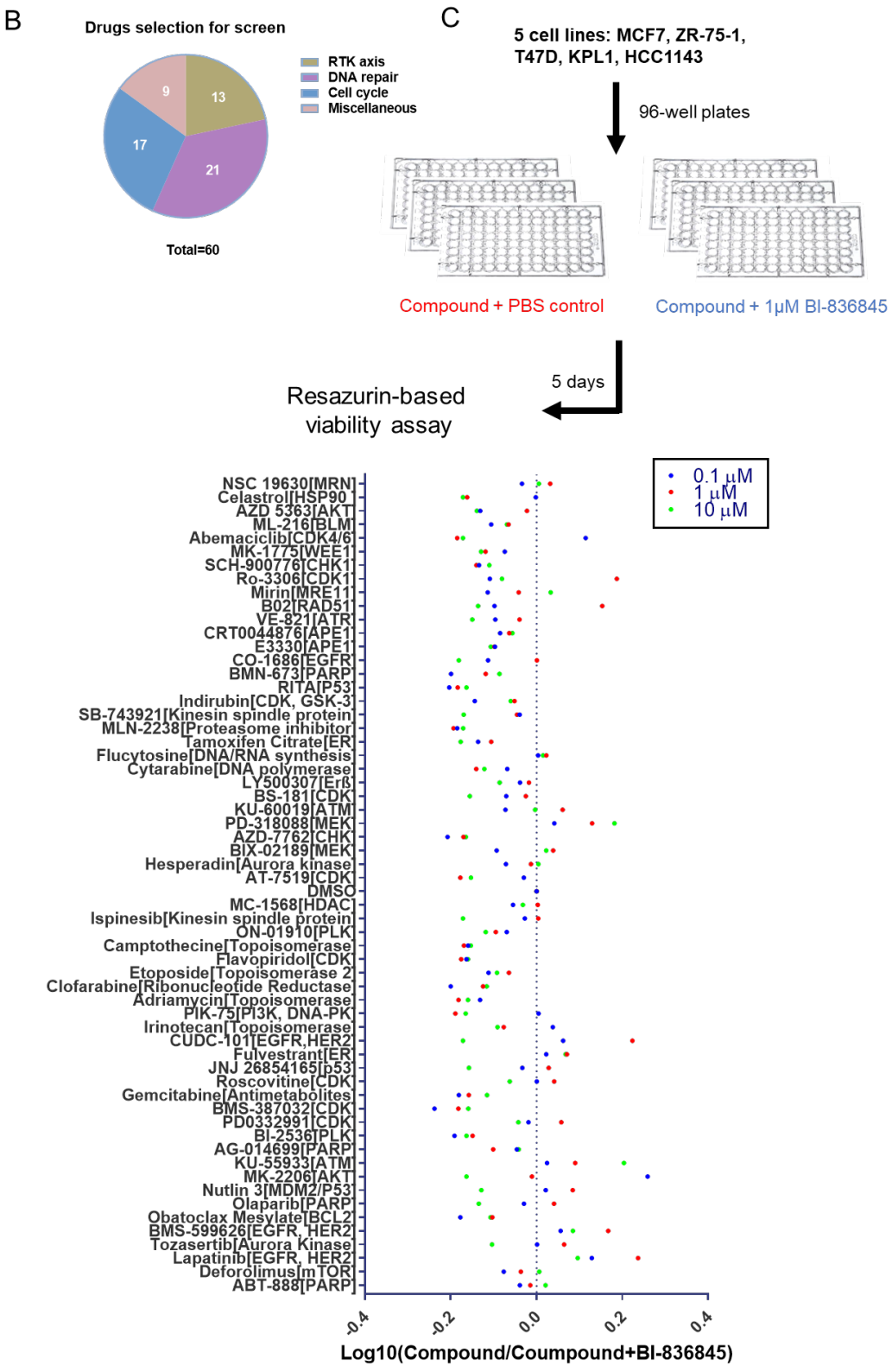

Figure 4.1 Compound screen to identify effective drug combinations with BI-836845

(A) Luminal breast cancer cell lines: MCF7, ZR-75-1, KPL1, T47D, HCC1143 were selected. Cells were exposure to 1 μM BI-836845 for 4-6 days and growth curves was obtained by using IncuCyte live cell analysis imaging system. Half maximal effective concentrations

(EC50) and the 95% confidence intervals were determined in Graphpad Prism 8. Experiment was performed once. (B) Total of 59 small molecule drugs and 1 DMSO solvent control were selected in the compound library. (C) Cells were seeded in 96-well plates and treated with the compound library drugs at 0.1 μM, 1 μM, 10 μM in combination of PBS solvent control or 1 μM BI-836845. Cell viability was determined after 5 days of treatment using resazurin-based cell viability assay. Data were exported and analysed in Microsoft Excel. The graph on the right showed the analysed results in MCF7 cells: each dot represents relative effectiveness of each compound reflecting the difference of efficacy between single treatment and in combination with 1 μM BI-836845. The line (relative effectiveness=0) indicates DMSO solvent control in compound library showing no combination effect.

The cell viability data were used to calculate the relative effectiveness (described in section 2.5) to compare the efficacies of each compound as single treatment and in combination with BI-836845. Relative effectiveness of DMSO solvent control was normalised to 0 (Figure 4.1 C). If the relative effectiveness of the compound was greater than 0, cells were more sensitive to this compound in combination with BI-836845, suggesting an additive or synergistic effect (Figure 4.1 C). If the relative effectiveness of the compound was less than 0, cells were more sensitive to this compound as single treatment, suggesting an antagonistic effect (Figure 4.1 C).

We ranked the relative effectiveness of all compounds at 0.1 μM, 1 μM and 10 μM in MCF7 cells (Figure 4.2 A). To assess the ability of the screen to differentiate the negative and positive controls, Z-factors were calculated using Zhang and colleagues' method (Zhang et al., 1999). As described in section 2.5, we used DMSO-treated well as negative control and PLK inhibitor (BI-2536)-treated well as positive control as PLK inhibition is toxic to many cell types (Plyte and Musacchio, 2007), and we have used PLK depletion as negative control in the siRNA screen previously published in our group (Gao et al., 2014). According Zhang and colleagues' method, Z-factor < 0.5 suggests excellent assay and Z-factor between 0 and 0.5 indicates acceptable assay, while Z-factor ≤ 0 means that there are too

much overlap between positive and negative controls, suggesting insufficient quality of the screen (Zhang et al., 1999). The Z-factors for the MCF7 screens were ≥ 0.64, suggesting excellent quality of these screens (Figure 4.2 A). The Z-factors were calculated and compounds were also ranked in ZR-75-1 (Figure 4.3 A), T47D (Figure 4.4 A), KPL1 (Figure 4.5 A), and HCC1143 (Figure 4.6 A) cells. The T47D and HCC1143 screens were also of excellent quality with the Z-factors ≥ 0.5 (Figure 4.4 A, 4.6 A). For ZR-75-1 screens, the Z-factors were 0.52 and 0.65 for 1 μM screen and 10 μM screen respectively, suggesting excellent quality, but 1 μM screen was only of acceptable quality with the Z-factor of 0.24 (Figure 4.3 A). For KPL1 cells, Z-factors for screens at 0.1 μM and 1 μM were < 0, indicating small screen windows as positive and negative controls overlapped, and these screens might not be thus useful for further screen analysis (Figure 4.5 A). However, the Z-factor for KPL1 screen at 10 μM was 0.48, showing acceptable quality (Figure 4.5 A). Therefore, we only analysed 10 μM screen for subsequent screen hit selection in KPL1 cells.

We next calculated Z-scores of all compounds in each cell line for hit selection. Notably, several strong outliers were observed in ZR-75-1 (Figure 4.3 A), T47D (Figure 4.4 A), and HCC1143 (Figure 4.6 A) cells. These strong outliers can markedly affect mean and SD of the screen results especially in screen with a relative low number of compounds (60 for this screen) (Chung et al., 2008). Therefore, we calculated Z-score using a robust method based on median and median absolute deviation (MAD) (Chapter 2.5). This median and MAD-based method was reported as improving hit selection strategy for high-throughput RNA interference screen as it is less affected by outliers than mean and SD-based method (Chung et al., 2008).

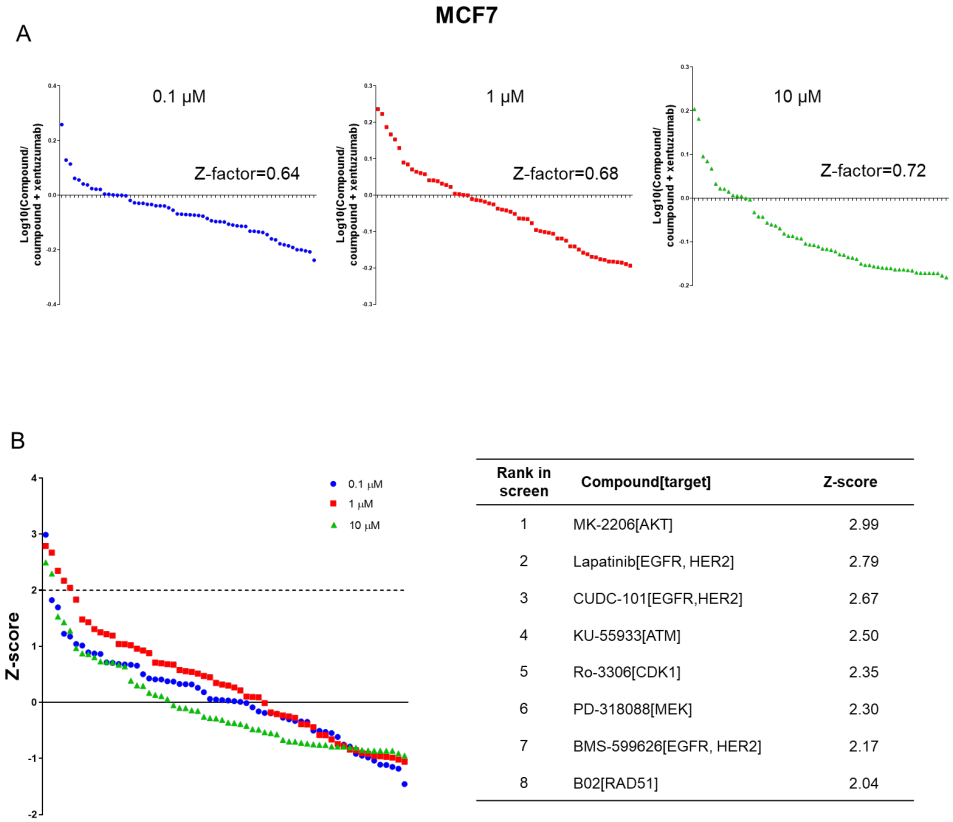

Rank in screen	Compound[target]	Z-score
1	MK-2206[AKT]	2.99
2	Lapatinib[EGFR, HER2]	2.79
3	CUDC-101[EGFR,HER2]	2.67
4	KU-55933[ATM]	2.50
5	Ro-3306[CDK1]	2.35
6	PD-318088[MEK]	2.30
7	BMS-599626[EGFR, HER2]	2.17
8	B02[RAD51]	2.04

Figure 4.2 Ranking of the compounds in MCF7 cells

(A) The ranking of 60 compounds at 0.1 μM, 1 μM, 10 μM based on the relative effectiveness reflecting difference of efficacies of each compound as single treatment and in combination with 1 μM BI-836845. Z-factor was calculated using DMSO solvent control reading as positive control and PLK inhibitor (BI-2536) reading as negative control. (B) Z-scores were calculated using the method in section 2.5 and ranked for all compounds. The dotted line indicates Z-score=2. The top hits with Z-score>2 were shown on the right.

All compounds at 3 concentrations were ranked based on their Z-scores, and the compounds with Z-score greater than 2 were identified as positive hits that sensitised cells to BI-836845. Total of 8 positive hits were identified in MCF7 cells, including 3 EGFR inhibitors, AKT inhibitor MK-2206, RAD51 inhibitor BO2, and CDK1 inhibitor RO-3306 (Figure 4.2 B). The combination effects of co-inhibiting IGF-1R with EGFR, AKT or HR machineries have been showed in previous studies published in our groups and others (Li et al., 2013; Lodhia et al., 2015; Ou et al., 2014; Suleymanova et al., 2017). Interestingly, ATM inhibitor KU-55933 was identified as a positive hit that sensitised cells to IGF inhibition, and this has not been shown in any published studies.

Using the same method for hit selection (Z-score > 2), we identified the positive hits in ZR-75-1, T47D, KPL1, and HCC1143 cells (Figure 4.3 B - 4.6 B). ATM inhibitors KU-55933 and/or KU-60019 were also identified as positive hits in ZR-75-1 and HCC1143 cells (Figure 4.3 B, 4.6 B). Previous study suggested a critical role of ATM in DNA replication to maintain genome stability by coordinating SSB repair and cell cycle progression (Khoronenkova and Dianov, 2015). Therefore, ATM could be a promising target to exacerbate replication stress phenotype in IGF inhibited cells. ATM has been investigated as a screen hit by Dr Rieunier in our group, and his unpublished data strongly support this concept.

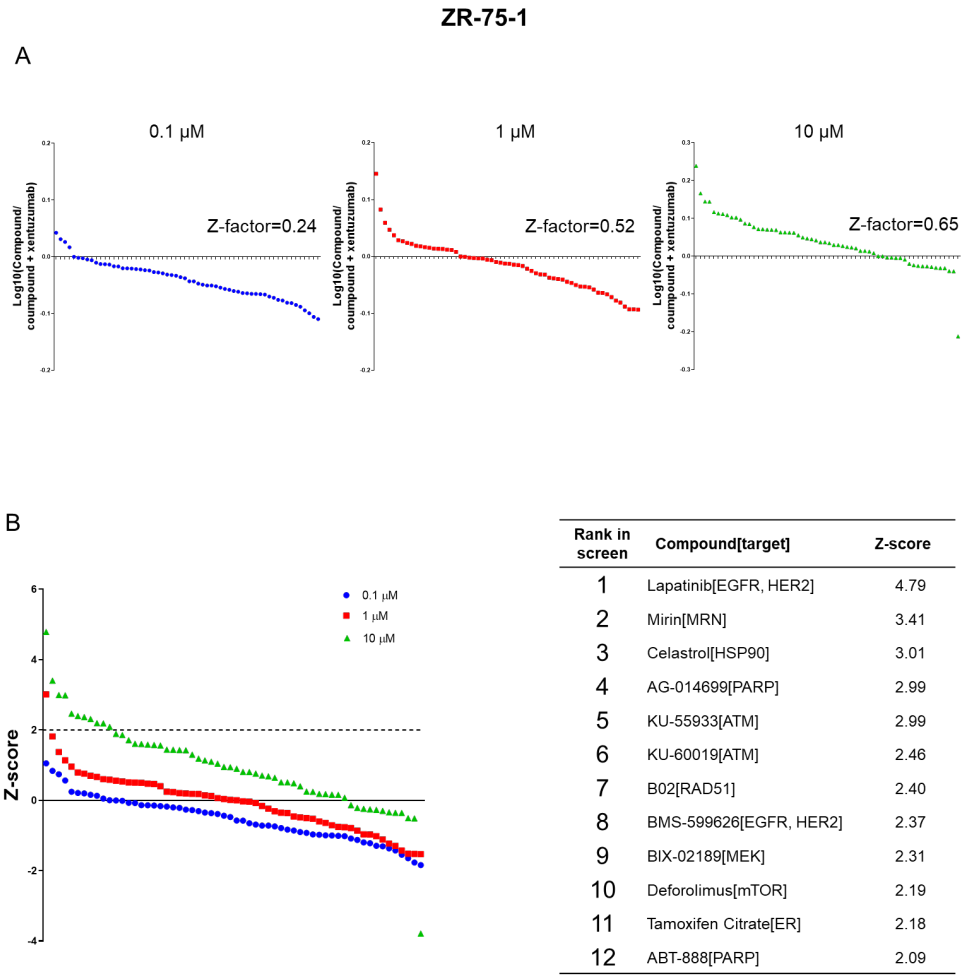

Rank in screen	Compound[target]	Z-score
1	Lapatinib[EGFR, HER2]	4.79
2	Mirin[MRN]	3.41
3	Celastrol[HSP90]	3.01
4	AG-014699[PARP]	2.99
5	KU-55933[ATM]	2.99
6	KU-60019[ATM]	2.46
7	B02[RAD51]	2.40
8	BMS-599626[EGFR, HER2]	2.37
9	BIX-02189[MEK]	2.31
10	Deforolimus[mTOR]	2.19
11	Tamoxifen Citrate[ER]	2.18
12	ABT-888[PARP]	2.09

Figure 4.3 Ranking of the compounds in ZR-75-1 cells
(A) The ranking of 60 compounds at 0.1 μM, 1 μM, 10 μM based on the relative effectiveness reflecting difference of efficacies of each compound as single treatment and in combination with 1 μM BI-836845. Z-factor was calculated as described in legend to Figure 4.2. (B) Z-scores were calculated using the method in section 2.5 and ranked for all compounds. The line dotted indicates Z-score=2. The top hits with Z-score>2 were shown on the right.

Of note, PARP is another key player in mediating the repair of SSBs, which was reported as a synergistic target in HR deficient tumours (Bryant et al., 2005; Farmer et al., 2005). Several PARP inhibitors Veleparib (ABT-888), Rucaparib (AG-014699) and/or Olaparib (AZD2281) were identified as positive hits in T47D, KPL1, and HCC1143 cells. (Figure 4.3 B – 4.6 B). These results were in line with a previous study showing that IGF-1R inhibition impaired HR function and sensitised cells to

PARP inhibitors (Amin et al., 2015). Results in T47D, KPL1 and HCC1143 suggested that targeting checkpoint kinases CHK1 or WEE1 also sensitised cells to BI-836845 treatment (Figure 4.4 B – 4.6 B). Although IGF-1R inhibition was shown to sensitise breast cancer cells to ATR inhibitor (O'Flanagan et al., 2016), targeting ATR downstream effector CHK1 has not been previously studied in combination with IGF blockade. Given the important role of activating cell cycle checkpoints in response to replication stress (Saldivar et al., 2017), we next aimed to investigate whether targeting checkpoint kinases could exacerbate IGF blockade-induced replication stress and selectively kill IGF-1R depleted or inhibited cells.

A

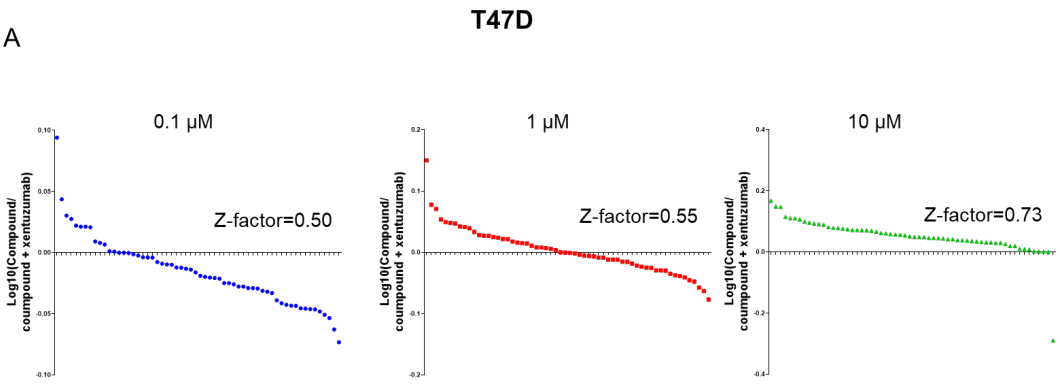

B

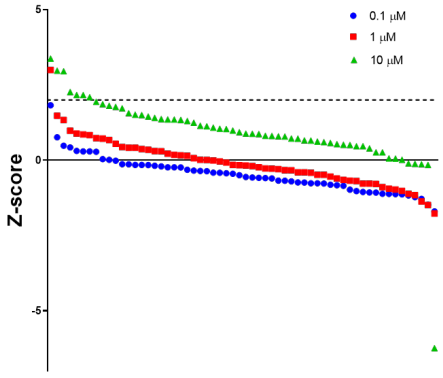

Rank in screen	Compound[target]	Z-score
1	MK-8776[CHK1]	3.38
2	CUDC-101[EGFR,HER2]	3.00
3	Lapatinib[EGFR, HER2]	2.97
4	BMS-599626[EGFR, HER2]	2.95
5	PD0332991[CDK]	2.26
6	AG-014699[PARP]	2.17
7	AZD-7762[CHK]	2.16
8	Deforolimus[mTOR]	2.09

Figure 4.4 Ranking of the compounds in T47D cells
(A) The ranking of 60 compounds at 0.1 μM, 1 μM, 10 μM based on the relative effectiveness reflecting difference of efficacies of each compound as single treatment and

in combination with 1 μM BI-836845. Z-factor was calculated as described in legend to Figure 4.2. (B) Z-scores were calculated using the method in section 2.5 and ranked for all compounds. The line dotted indicates Z-score=2. The top hits with Z-score>2 were shown on the right.

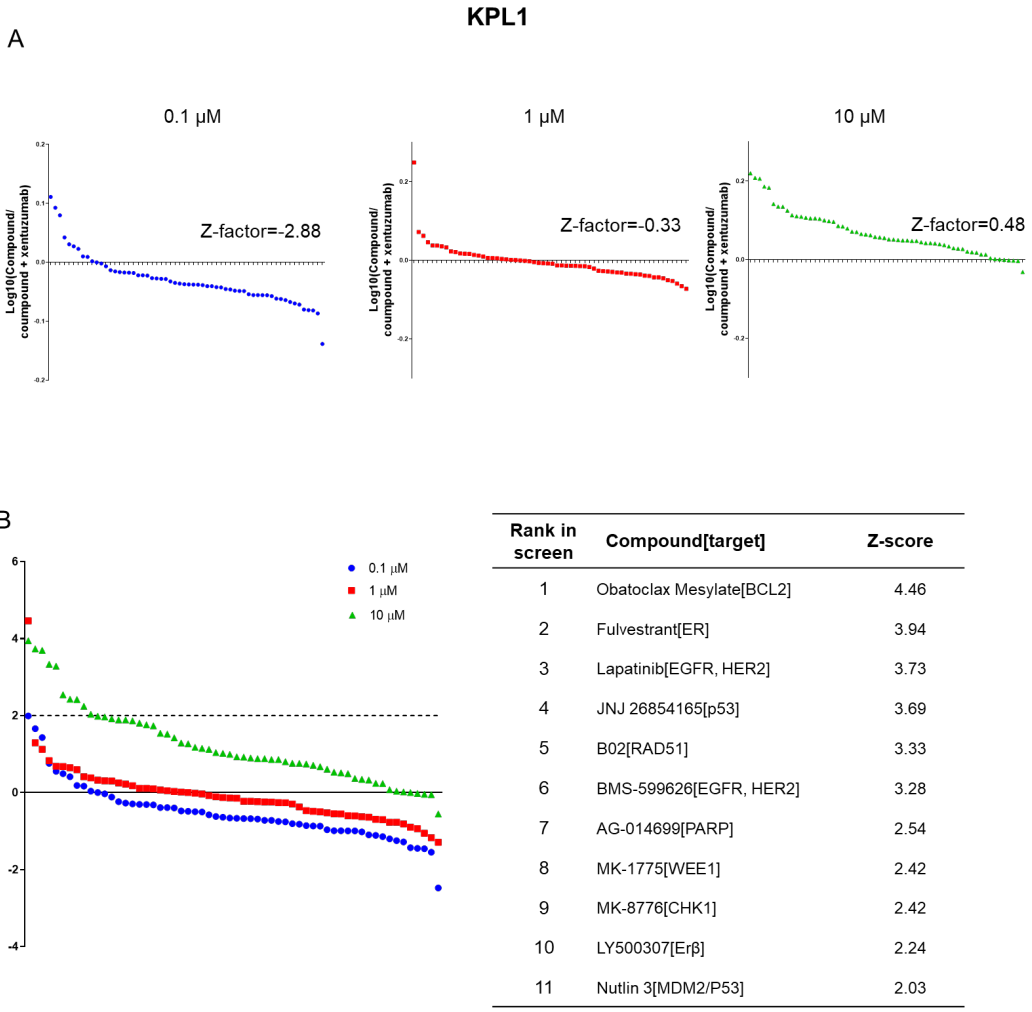

Rank in screen	Compound[target]	Z-score
1	Obatoclax Mesylate[BCL2]	4.46
2	Fulvestrant[ER]	3.94
3	Lapatinib[EGFR, HER2]	3.73
4	JNJ 26854165[p53]	3.69
5	B02[RAD51]	3.33
6	BMS-599626[EGFR, HER2]	3.28
7	AG-014699[PARP]	2.54
8	MK-1775[WEE1]	2.42
9	MK-8776[CHK1]	2.42
10	LY500307[Erβ]	2.24
11	Nutlin 3[MDM2/P53]	2.03

Figure 4.5 Ranking of the compounds in KPL1 cells

(A) The ranking of 60 compounds at 0.1 μM, 1 μM, 10 μM based on the relative effectiveness reflecting difference of efficacies of each compound as single treatment and in combination with 1 μM BI-836845. Z-factor was calculated as described in legend to Figure 4.2. (B) Z-scores were calculated using the method in section 2.5 and ranked for all compounds. The line dotted indicates Z-score=2. The top hits with Z-score>2 were shown on the right.

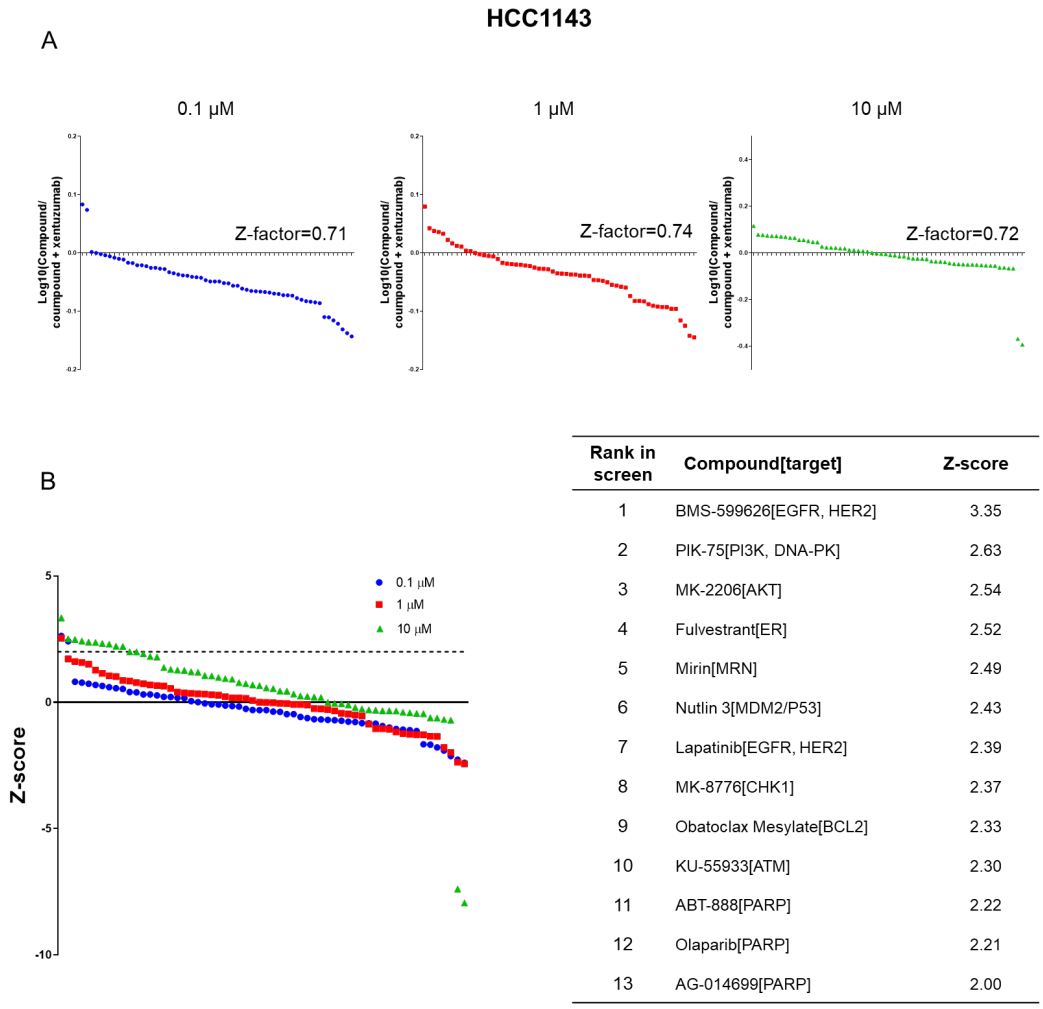

Rank in screen	Compound[target]	Z-score
1	BMS-599626[EGFR, HER2]	3.35
2	PIK-75[PI3K, DNA-PK]	2.63
3	MK-2206[AKT]	2.54
4	Fulvestrant[ER]	2.52
5	Mirin[MRN]	2.49
6	Nutlin 3[MDM2/P53]	2.43
7	Lapatinib[EGFR, HER2]	2.39
8	MK-8776[CHK1]	2.37
9	Obatoclax Mesylate[BCL2]	2.33
10	KU-55933[ATM]	2.30
11	ABT-888[PARP]	2.22
12	Olaparib[PARP]	2.21
13	AG-014699[PARP]	2.00

Figure 4.6 Ranking of the compounds in HCC1143 cells

(A) The ranking of 60 compounds at 0.1 μM, 1 μM, 10 μM based on the relative effectiveness reflecting difference of efficacies of each compound as single treatment and in combination with 1 μM BI-836845. Z-factor was calculated as described in legend to Figure 4.2. (B) Z-scores were calculated using the method in section 2.5 and ranked for all compounds. The line dotted indicates Z-score=2. The top hits with Z-score>2 were shown on the right.

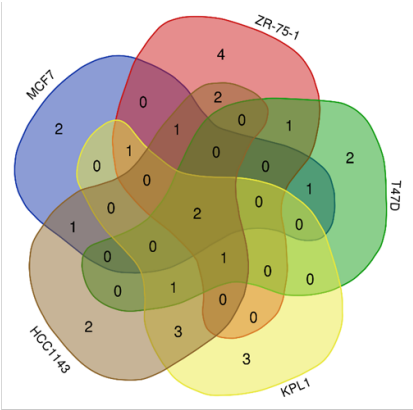

	Compound[target]
Hits in 5 cell lines	Lapatinib[EGFR, HER2]
	BMS-599626[EGFR, HER2]
Hits in 4 cell lines	AG-014699[PARP]
Hits in 3 cell lines	B02[RAD51]
	KU-55933[ATM]
	MK-8776[CHK1]
Hits in 2 cell lines	CUDC-101[EGFR,HER2]
	MK-2206[AKT]
	Deforolimus[mTOR]
	Mirin[MRN]
	Fulvestrant[ER]
	Nutlin 3[MDM2/P53]
	Obatoclax Mesylate[BCL2]
	ABT-888[PARP]

Figure 4.7 Positive hits identified in compound screen
Venn diagram showing the overlap of the identified compounds in 5 cell lines. The overlap compounds in at least 2 cell lines were listed in the table below. The compounds identified in at least 3 cell lines were considered as positive hits in this screen.

We compared the top-ranked compounds (Z-score > 2) in 5 cell lines in a Venn diagram (Figure 4.7). The overlapping compounds were identified shown in Figure 4.7. Among the positive hits shown in at least 3 cell lines, the only hits that have not been reported as at least additive with IGFs or IGF-1R targeting in previous published studies are ATM inhibitor KU-55933 and CHK1 inhibitor MK-8776. CHK1

inhibitor MK-8776 has been shown to be an effective compound to induce replication stress and sensitise leukaemia and pancreatic cancer cells to histone deacetylase (HDAC) inhibitor or gemcitabine (Buisson et al., 2015; Dai et al., 2013; Parsels et al., 2018). Therefore, CHK1 was selected for further study to investigate the potential protective role of CHK1 function in cells upon IGF blockade.

4.2.2 CHK1 inhibition sensitises cells to IGF blockade

We next validated the combination effect of MK-8776 and BI-836845 in low-throughput viability assay using different concentrations of MK-8776 in combination with PBS solvent control or 1 μM BI-836845. Although MK-8776 was not ranked as a positive hit in MCF7 and ZR-75-1 cells in the screen, the validation assays in MCF7 and ZR-75-1 after 5 days treatment showed that MK-8776 led to a significantly greater reduction of cell viability when in combination with 1 μM BI-836845 (Figure 4.8 A and B). An additive inhibition of cell proliferation was also observed when KPL1 cells were treated with MK-8776 in combination with 1 μM BI-836845 (Figure 4.8 C), consistent with identification of MK-8776 in the screen. A similar combination effect of MK-8776 and BI-836845 was observed in HeLa cervical cancer cells (Figure 4.8 D).

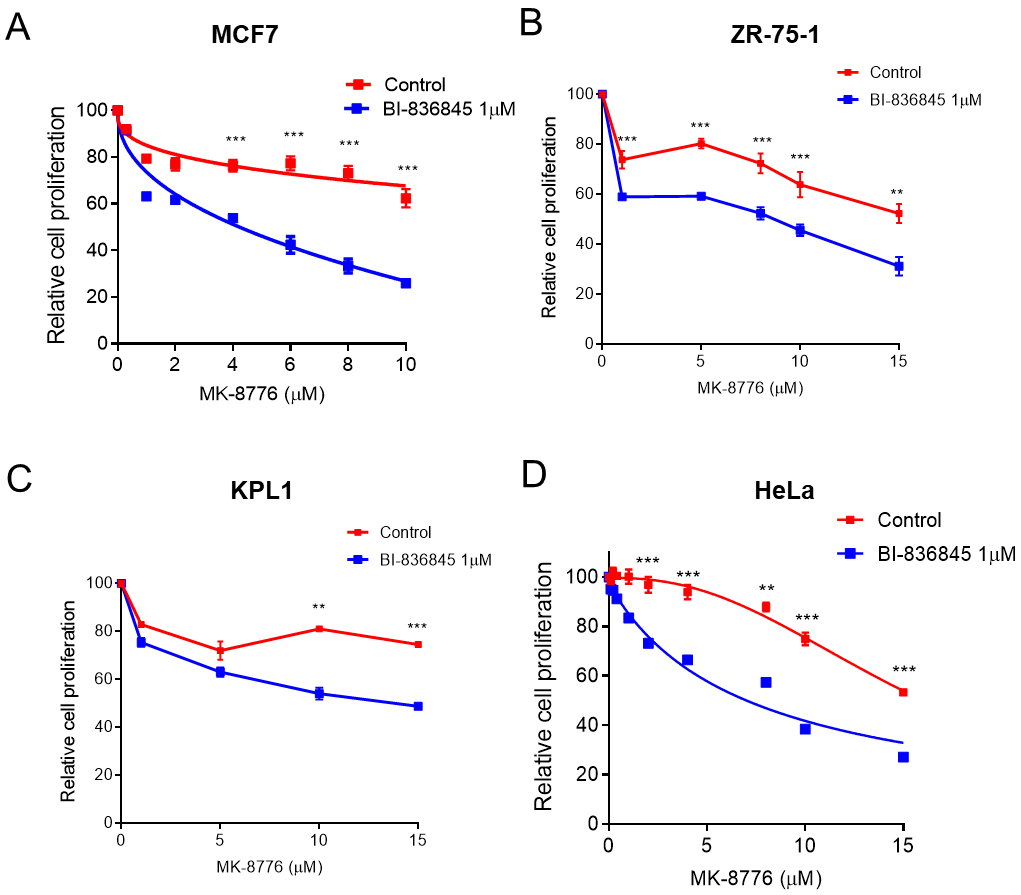

Figure 4.8 IGF inhibited cells are more sensitive to CHK1 inhibition
MCF7, ZR-75-1, KPL1, HeLa cells were exposed to BI-836845 and MK-8776 for 5 days, followed by cell viability assay. Data were expressed as % viability of solvent-treated control and represented as mean ± SEM, pooled from (A: n=3 independent experiments; B and D: 2 independent experiments, C: one experiment). Unpaired and two-tailed t test was applied. ***P < 0.001, **P < 0.01, *P < 0.05.

We next assessed whether cells were more sensitive to MK-8776 after IGF-1R depletion. MCF7 cells were transfected with siRNA control or siRNA targeting IGF-1R for 24 hours and then exposed to different concentrations of MK-8776 for 5 days. Compared to PBS-treated control cells (Figure 4.8 A), we noted that cells after siControl transfection were more sensitive to lower concentrations (< 3 μM) of MK-8776 (Figure 4.9 A). This might be due to the mild toxicity induced by transient siRNA transfection, increasing the drug sensitivity to MK-8776. Importantly, IGF-1R depleted cells were significantly more sensitive to MK-8776 treatment, compared

with the drug responses observed in siControl cells (Figure 4.9 A). IGF-1R TKI BI-885578 was also tested in combination with MK-8776 in MCF7 cells. Consistent with the results in BI-836835 treated cells, BI-885578 treated cells were also more sensitive to MK-8776 compared with DMSO solvent control-treated cells in cell viability assay (Figure 4.9 B).

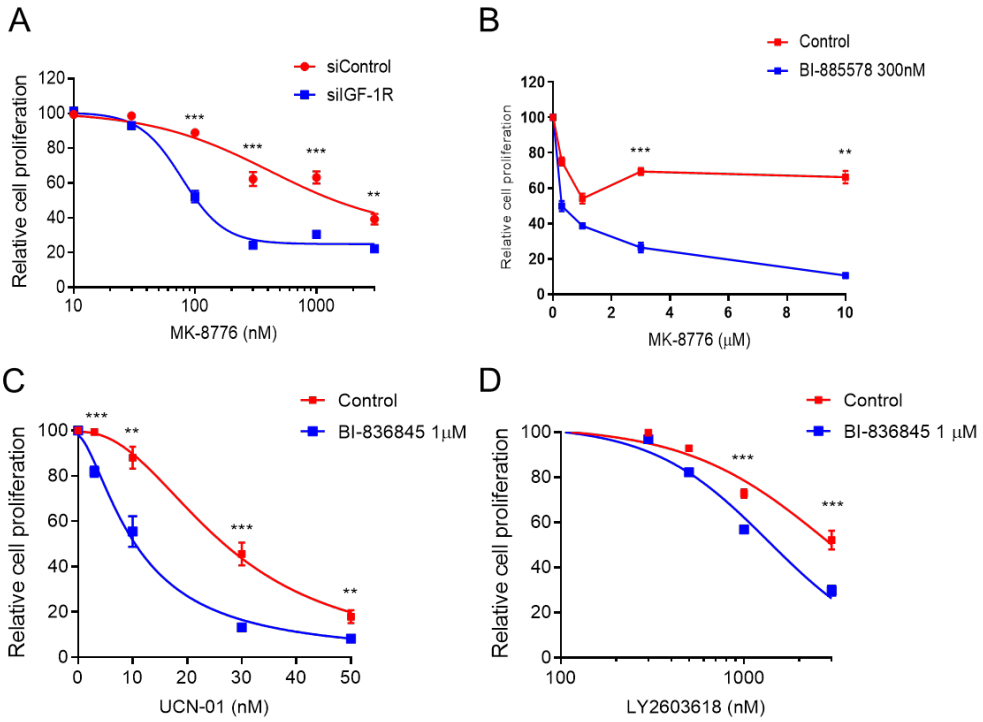

Figure 4.9 IGF-1R depleted or inhibited MCF7 cells are more sensitive to CHK1 inhibition

(A) MCF7 cells were transfected with siControl or siIGF-1R for 24 hours, and then exposed to solvent-treated control or MK-8776 for 5 days, followed by cell viability assay. Viability was expressed as % viability of siControl cells. (B-D) MCF7 cells were exposed to IGF inhibitors BI-836845, BI-885578 and CHK1 inhibitors MK-8776, UCN-01, LY2603618 for 5 days, followed by cell viability assay. Data were expressed as % viability of solvent-treated control and represented as mean ± SEM, pooled from (A, C, D: n=3 independent experiments; B: one experiment). Unpaired and two-tailed t test was applied. ***P < 0.001, **P < 0.01, *P < 0.05.

To further validate the combinational interaction between CHK1 inhibition and IGF blockade, two alternative CHK1 inhibitors LY2603618 and UCN-01 were tested in combination with BI-835845. The cell viability assay in MCF7 cells showed that UCN-01, one of the early-generation CHK1 inhibitors, was poorly tolerated as a

single treatment with a substantial reduction of viability at nM concentrations (Figure 4.9 C), whereas LY2603618 single treatment led to a mild inhibition of viability at μM concentrations, which was similar to MK-8776. The addition of BI-836845 shifted the drug-response curves to the left, suggesting the increased sensitivity to UCN-01 or LY2603618 (Figure 4.9 C, D). Taken together, the results from these cell viability assays suggested that CHK1 inhibition sensitised cells to IGF blockade.

4.2.3 CHK1 inhibition induces replication catastrophe after IGF blockade

ATR/CHK1 pathway plays a critical role in mediating replication stress responses during S phase (Buisson et al., 2015; Toledo et al., 2017; Toledo et al., 2013). This prompted us to hypothesise that targeting CHK1 might be able to worsen the replication stress induced by IGF blockade, contributing to the inhibition of cell proliferation. We next performed DNA fiber assay to assess the replication fork progression. MCF7 cells were transfected with siControl or siRNA targeting IGF-1R for 24 hours and then exposed to solvent-treated control or MK-8776 for 24 hours. Consistent with the results in Figure 3.5 A, IGF-1R depletion induced a reduction of DNA fiber length (Figure 4.10 A). Importantly, the addition of MK-8776 further shortened DNA fibers in IGF-1R depleted cells (Figure 4.10 A). We also tested SK-CO-1 colorectal cancer cells that were recently reported ATM-deficient (Wang et al., 2017). Given the important roles of ATM and ATR in mediating DNA damage responses, ATM loss has been reported to sensitise cancer cells to ATR/CHK1 inhibition (Rafiei et al., 2020). Therefore, we speculated that SK-CO-1 cells might be potentially sensitive to CHK1 inhibition. In our compound screen, ATM inhibitor KU-55933 was identified as a positive hit that sensitised cells to IGF inhibition in 3 cell lines (Figure 4.7). The lack of ATM expression in SK-CO-1 cells might confer the increased sensitivity to IGF inhibition. Indeed, the DNA fiber assay in SK-CO-1

cells showed that both MK-8776 alone and IGF-1R depletion alone led to a significantly reduction of DNA fiber length (Figure 4.10 B). Moreover, the combination of MK-8776 and IGF-1R depletion induced a more dramatic suppression of replication fork progression, consistent with the results in MCF7 cells (Figure 4.10 B). It has been reported that ATR-CHK1 inhibition induces unscheduled origin firing, which is mediated by CDC7 and GINS (Moiseeva et al., 2017). Our DNA fiber analysis in MCF7 and SK-CO-1 cells showed that MK-8776 significantly promoted origin firing (Figure 4.10 A, B). However, IGF-1R depletion had no effect on origin firing (Figure 4.10 A, B), which is consistent with the results in Figure 3.5 D.

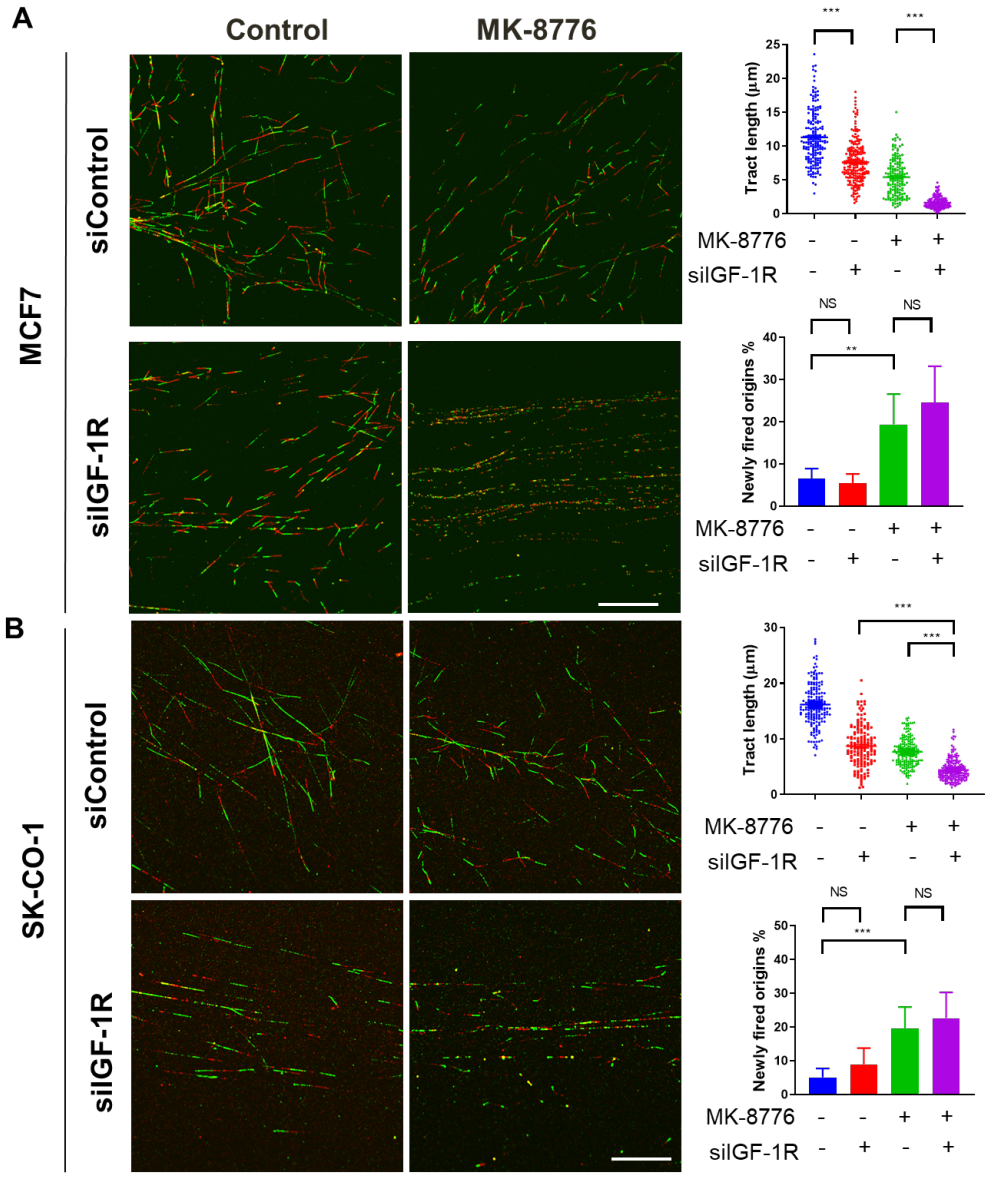

Figure 4.10 CHK1 inhibition suppresses replication fork progression in IGF-1R depleted cells

Representative images of DNA fiber tract (CIdU (Red), IdU (Green)) in MCF7 (A) and SK-CO-1 (B) cells transfected with siControl or siIGF-1R for 24 hours and then exposed to solvent control or MK-8776 at 300 nM (A) or 1 µM (B) for 24 hours. Scale bar: 20 µm. Quantification of fiber tract length (>150 tracts) and newly fired origins (IdU (green)-only tracts as percentages of the total number of tracts (⩾ 5 images in A and B)) was shown on the right. Data in A (mean ± SEM) are from one representative experiment of 3 independent experiments with similar results. Data in B (mean ± SEM) are from one representative experiment of 2 independent experiments with similar results. One-way ANOVA was applied. ***P < 0.001.

We also performed DNA fiber assay in MCF7 cells after exposure to MK-8776 in combination with BI-836845 or BI-885578 for 24 hours. A significant reduction of DNA fiber length was observed in cells treated with BI-836845 or BI-885578 alone for 24 hours (Figure 4.11), consistent with the results in Figure 3.5 B. Although MK-8776 alone also induced a moderate reduction of DNA fiber length, supporting the important role of CHK1 in DNA replication (Buisson et al., 2015), the addition of BI-836845 or BI-885578 resulted in the much shorter DNA fibers, compared with either treatment alone (Figure 4.11). Consistent with the results in Figure 4.10, the addition of MK-8776 increased newly fired origins but IGF blockade by BI-836845 or BI-885578 had no significant effect on origin firing (Figure 4.11). These DNA fiber assays suggested that CHK1 inhibition dramatically suppressed cell replication after IGF blockade, indicating a high level of replication stress.

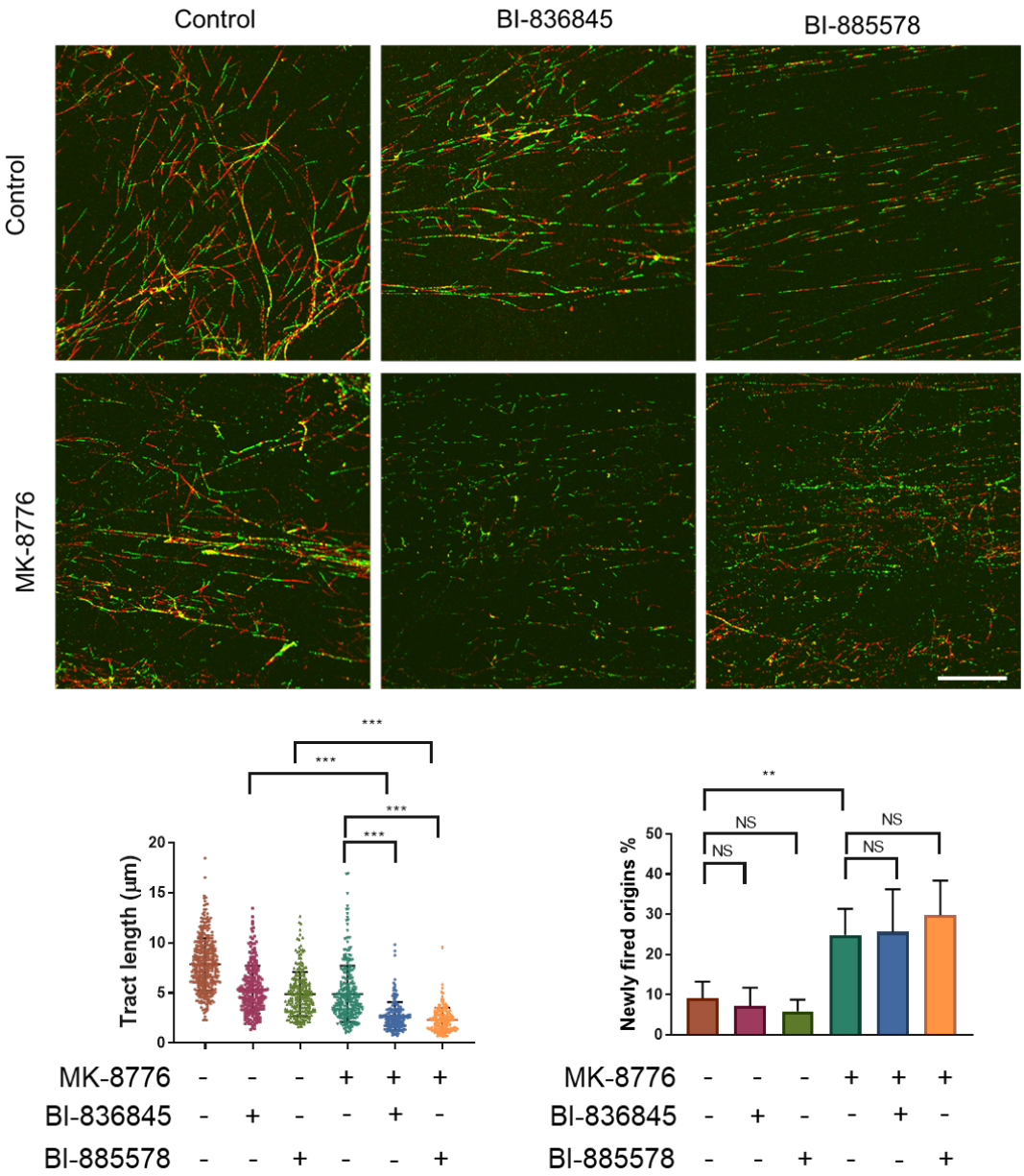

Figure 4.11 CHK1 inhibition suppresses replication fork progression in IGF inhibited cells

Representative images of DNA fiber tract (CIdU (Red), IdU (Green)) in MCF7 cells exposed to 1 µM BI-836845 or 300 nM BI-885578 in combination with solvent control or 3 µM MK-8776 for 24 hours. Scale bar: 20 µm. Quantification of fiber tract length (>150 tracts) and newly fired origins (IdU (green)-only tracts as percentages of the total number of tracts (⩾ 5 images)) was shown below. Data (mean ± SEM) are from one representative of 3 independent experiments with similar results. One-way ANOVA was applied. ***P < 0.001.

We next examined the cell cycle distribution using BrdU labelling method analysed by flow cytometry. MCF7 cells were transfected with siRNA control or siRNA

targeting IGF-1R for 24 hours and then exposed to solvent-treated control or MK-8776 for 24 hours. A clear disturbance in S-phase was observed in cells treated with MK-8776 and IGF-1R depletion (Figure 4.12 A). Particularly, MK-8776 caused 21.77 ± 6.62 % IGF-1R depleted cells to accumulate in non-replicating S phase, showing DNA content between 2N and 4N, but not incorporating BrdU, whereas MK-8776 had no significant effect in siControl cells (Figure 4.12 A-C). These results further suggested that CHK1 inhibition delayed DNA replication in S phase in IGF-1R depleted cells.

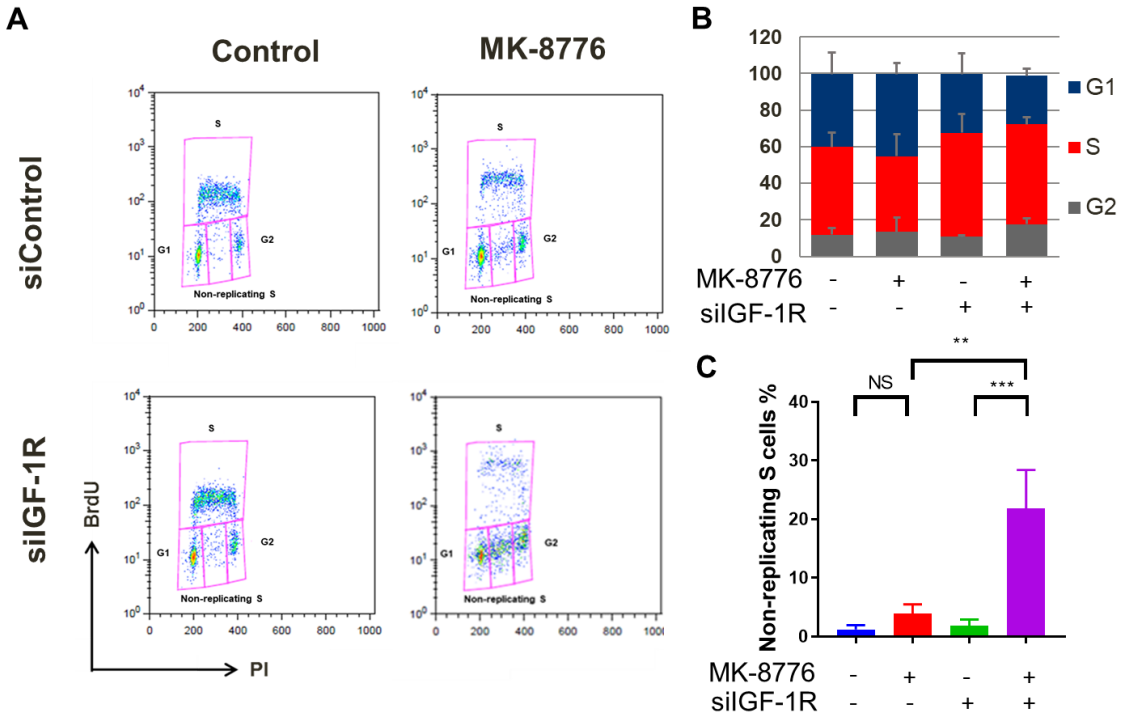

Figure 4.12 CHK1 inhibition induces the accumulation of non-replicating S phase cells in IGF-1R depleted cells

(A) BrdU FACS analysis of cell cycle distribution of MCF7 cells after siRNA transfection for 24 hours and then exposed to solvent control or 300 nM MK-8776 for 24 hours. (B) Quantification of cells in each cell cycle phase in A. (C) Quantification of non-replicating S phase cells in A. Data are represented as mean ± SD, pooled from 3 independent experiments. One-way ANOVA analysis was applied. ***P < 0.001, **P < 0.01.

To further investigate replication stress induced by CHK1 inhibition after IGF blockade, we performed a double immunostaining assay to examine two replication stress markers: γH2AX and ssDNA. To visualize ssDNA, BrdU was used to label DNA and detected by immunofluorescence under non-denaturing condition, in which BrdU antibody can only bind BrdU exposed on ssDNA (Buisson et al., 2015). MCF7 cells were transfected with siRNA control or siRNA targeting IGF-1R for 24 hours and then exposed to solvent-treated control or MK-8776 for 24 hours. MK-8776 significantly promoted γH2AX foci formation and induced the accumulation of cells with γH2AX pan-nuclear staining (Figure 4.13 A), consistent with the immunostaining results in UCN-01 treated cells reported in a previous study (Syljuasen et al., 2005). Both focal and pan-nuclear patterns of γH2AX are established markers of replication stress-induced strand breaks (Gagou et al., 2010; Moeglin et al., 2019) and pan-nuclear γH2AX formation is also associated with lethal DNA damage – induced apoptosis (Solier et al., 2009). Using the same quantification method in study by Gagou *et al.* (Gagou et al., 2010), we quantified the population of cells with >10 γH2AX foci and pan-nuclear staining as γH2AX positive cells to assess the levels of replication stress upon the treatments. The quantification revealed that MK-8776 induced the accumulation of γH2AX positive cells in siControl transfected cells, whereas a significantly higher percentage of γH2AX positive cells was detected in IGF-1R depleted cells (Figure 4.13 B). Similarly, we also quantified the BrdU staining in the same cells to examine their ssDNA levels. IGF-1R depletion did not induce a substantial increase of BrdU staining (Figure 4.13 B). Although a moderate increase of BrdU positive cells was observed in MK-8776-treated siControl cells, MK-8776 led to a significantly higher percentage of BrdU positive cells in IGF-1R depleted cells (Figure 4.13 B),

suggesting a higher level of ssDNA. The similar additive effects observed using γH2AX staining and ssDNA staining in cells upon treatment of IGF-1R depletion and CHK1 inhibition supported the concept that CHK1 inhibition exacerbates the replication stress induced by IGF blockade. In addition, native BrdU staining appeared to also be detected in cytoplasm after IGF-1R depletion and combining MK-8776 (Figure 4.13), might suggesting cytoplasmic ssDNA, and the possible implications would be discussed in Chapter 6.

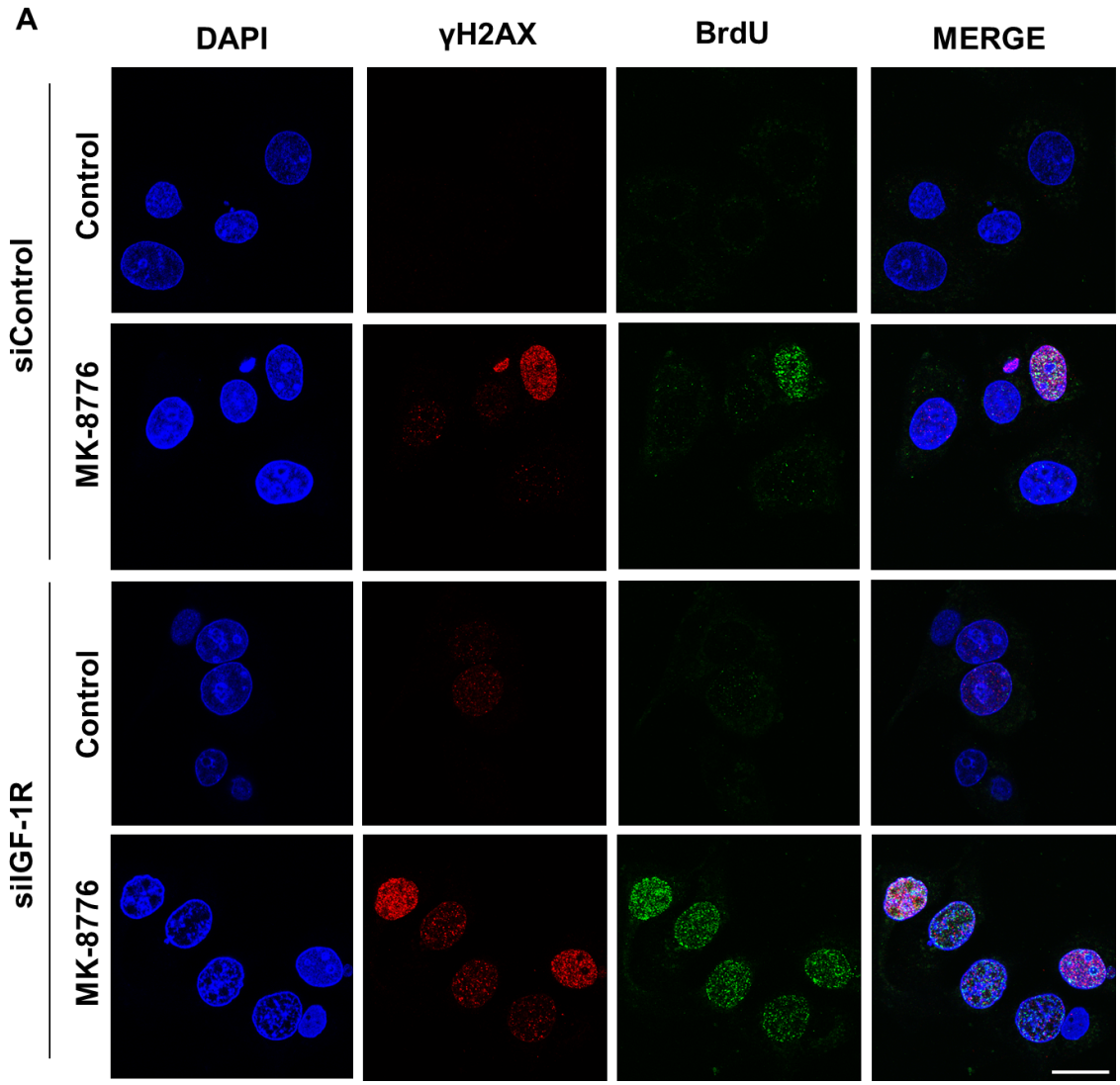

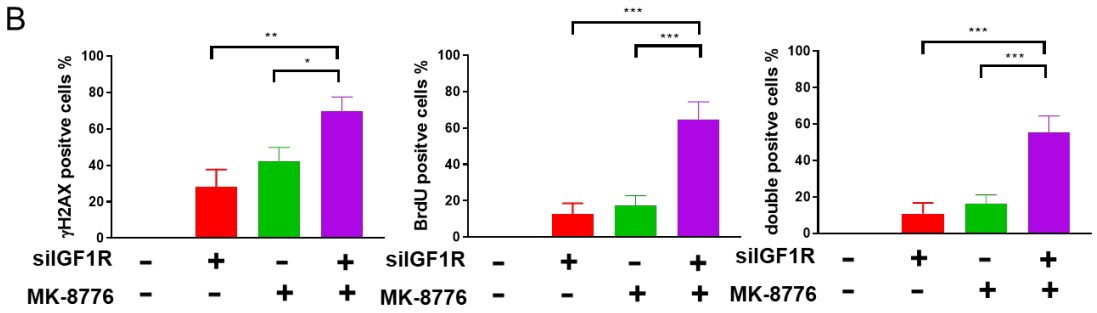

Figure 4.13 CHK1 inhibition induces the accumulation of ssDNA and DNA damage in IGF-1R depleted cells

(A) Representative images of BrdU and γH2AX immunostaining in MCF7 cells transfected with siControl or siIGF-1R for 24 hours and then exposed to solvent control or 300 nM MK-8776 for 24 hours. Cells were cultured with 10 μM BrdU for 36 hours before fixation and analysed in non-denaturing condition to detect ssDNA. Nucleus was stained by DAPI. Scale bar: 20 μm. (B) Quantification of γH2AX positive (>10 foci + pan-nuclear staining) and BrdU positive (>5 foci + pan-nuclear staining) cells (≥10 images) shown on the right. Data are represented as mean ± SEM, pooled from 3 independent experiments. One-way ANOVA analysis was applied. ***P < 0.001, **P < 0.01, *P < 0.05.

We also quantified the cells with double positive staining of both γH2AX and BrdU. The quantification showed that IGF-1R depletion caused accumulation of 10.76 ± 5.96 %, MK-8776 caused the accumulation of 16.07 ± 5.04 % double positive cells in siControl cells, whereas 55.29 ± 9.58 % double positive cells were detected after MK-8776 treatment in IGF-1R depleted cells (Figure 4.13 B). Again, this suggests an additive effect of combining IGF-1R depletion and CHK1 inhibition. Moreover, those double positive cells contained high levels of both ssDNA and deleterious strand breaks, suggesting high levels of replication stress (Buisson et al., 2015).

We next investigated whether the replication stress induced by the combination of CHK1 inhibition and IGF blockade is catastrophic, causing cell death. We performed a cell death assay using Hoechst 33342 and propidium iodide (PI) double staining method. Hoechst 33342 is cell membrane permeable DNA dye and can stain both live and dead cells, but PI is not membrane permeable and can only bind DNA in dead cells (Ellwart and Dormer, 1990). The cell death assay in MCF7 cells revealed that IGF-1R depletion by siRNA or IGF inhibition by 1 μM BI-836845 had no substantial effect on cell death (<10%), whereas 1 μM BI-885578 caused 27 ± 1.22 % cell death (Figure 4.14 A-D), which might be due to its more potent inhibition of IGF signalling (as detected in Figure 3.1) and/or additional inhibition of INSR signalling. These results supported our concept that the replication stress induced by IGF blockade alone was largely tolerable. Importantly, MK-8776 selectively killed more IGF-1R depleted cells than siControl cells (Figure 4.14 A, B). Consistently, combination treatment of MK-8776 and BI-836845 or BI-885578 led to a significant increase of cell death, compared to the effect of either drug alone (Figure 4.14 C, D). Together, these data strongly suggested CHK1 inhibition enhanced the replication stress induced by IGF blockade to intolerable replication catastrophe, causing significant increase in cell death.

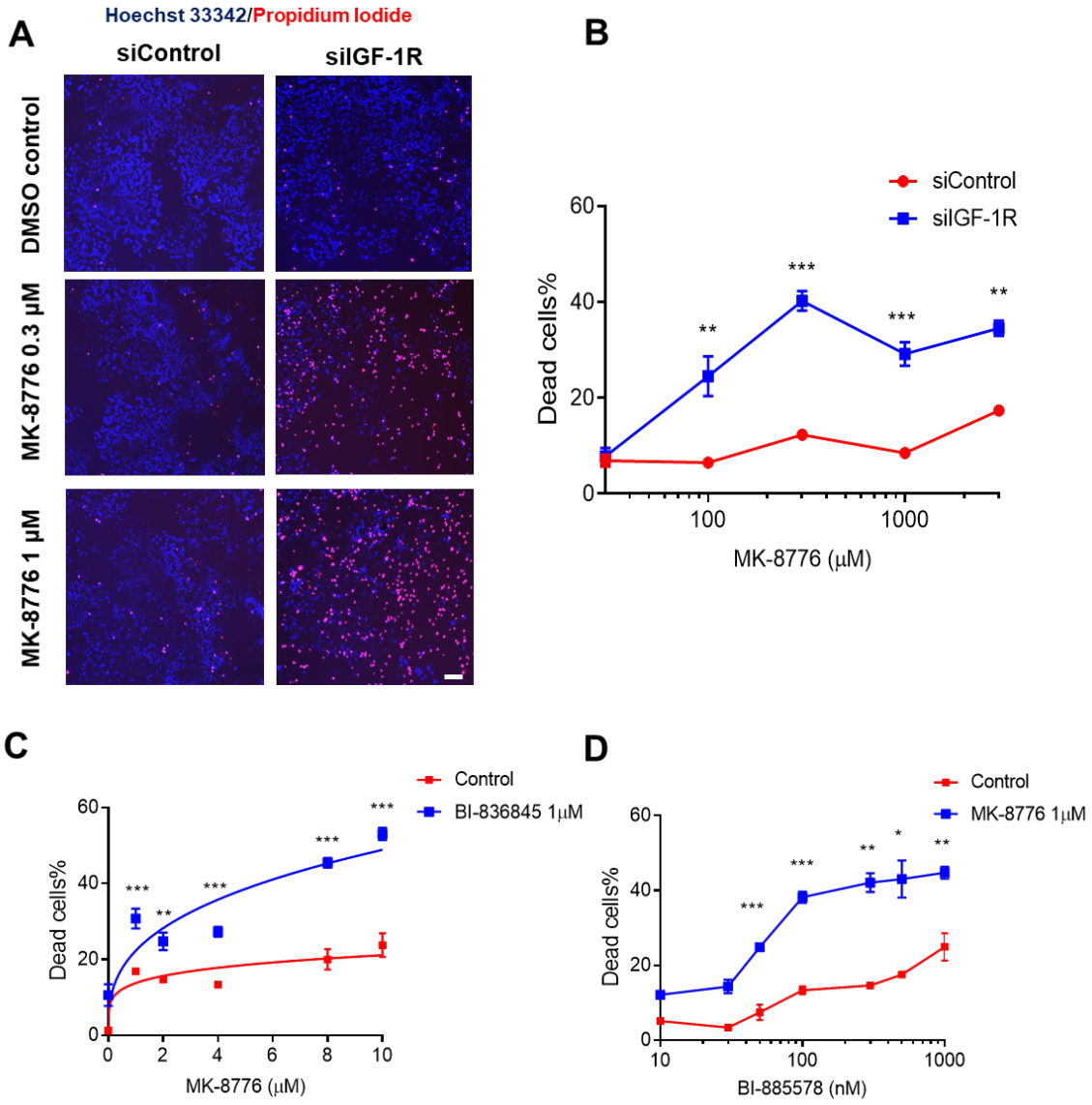

Figure 4.14 CHK1 inhibition induces cell death in IGF-1R depleted or inhibited cells

(A) Representative images of Propidium iodide/Hoechst 33342 staining in MCF7 cells transfected with siControl or siIGF-1R for 24 hours and then exposed to solvent control or MK-8776 for 5 days. Scale bar: 200 µm. (B) Dead cells% expressed as % PI positive cells/ Hoechst positive cells was determined by Celigo Imaging Cytometer. (C, D) MCF7 cells were exposed to BI-836845 (C) or BI-885578 (D) in combination of solvent control or MK-8776 for 5 days. Dead cells% expressed as % PI positive cells/ Hoechst positive cells was determined by Celigo Imaging Cytometer. Data are represented as mean ± SEM, pooled from (A-C: n=3 independent experiments; D: one experiment). Unpaired and two-tailed t test was used. ***P < 0.001, **P < 0.01, *P < 0.05.

4.2.4 Co-inhibition of IGF and CHK1 suppresses spheroid growth in 3D culture

To further assess the combination effect of IGF and CHK1 co-inhibition, and to find a model suitable for *in vivo* testing, we assessed CHK1 inhibitors in combination with IGF inhibitors in 3D spheroids. Cancer cell lines cultured in 3D spheroids have been widely used in preclinical research, as 3D spheroids recapitulate more features of tumour growth *in vivo*, such as increased cell-cell interactions and the coexistence of normoxic, hypoxic and necrotic zones, reflecting the complexity in tumours (Hirschhaeuser et al., 2010; Nath and Devi, 2016; Sant and Johnston, 2017). Compared to conventional 2D monolayer cell culture, cells grown as spheroids show different morphology, cell signalling, cell cycle duration, metabolism, drug responses, and gene and protein expressions (Desoize and Jardillier, 2000; Fischbach et al., 2009; Kumar et al., 2008; Pickl and Ries, 2009; Riedl et al., 2017). We first tested MCF7 cells in 3D culture. Cells were seeded in round bottom ultra-low attachment 96-well plates, centrifuged to induce cell aggregation and then monitored by IncuCyte live cell analysis imaging system with the help of Xiao Wan and Stephanie Hatch from Target Discovery Institute, Oxford. MCF7 cells formed single tight round spheroids 3 days after cell seeding (Figure 4.15 A). Spheroids were then treated with 1 μM BI-836845 for 6 days, but no significant suppression of spheroid growth was detected (Figure 4.15 A, B). MK-8776 inhibited spheroid growth at 3 μM and 10 μM, but not at 1 μM, and only 3 μM MK-8776 showed a significant combination effect with 1 μM BI-836845 (Figure 4.15 A, B). The growth rate of MCF7 spheroids in 3D culture was much slower than 2D culture with only ~0.5 fold increase over 6 days even without any treatment (Figure 4.15 A, B). Although 3 μM MK-8776 showed a statistically significant combination effect with 1 μM BI-836845, the lack of effect at other concentrations suggested that this might not be biologically significant. Similar

to MCF7 cells, the other ER+ breast cancer cells we used in compound screen all showed relatively slow growth rate (Figure 4.1 A). Therefore, we next examined several alternative cell lines in 3D culture to test whether the co-inhibition of IGF and CHK1 would have a larger biological effect.

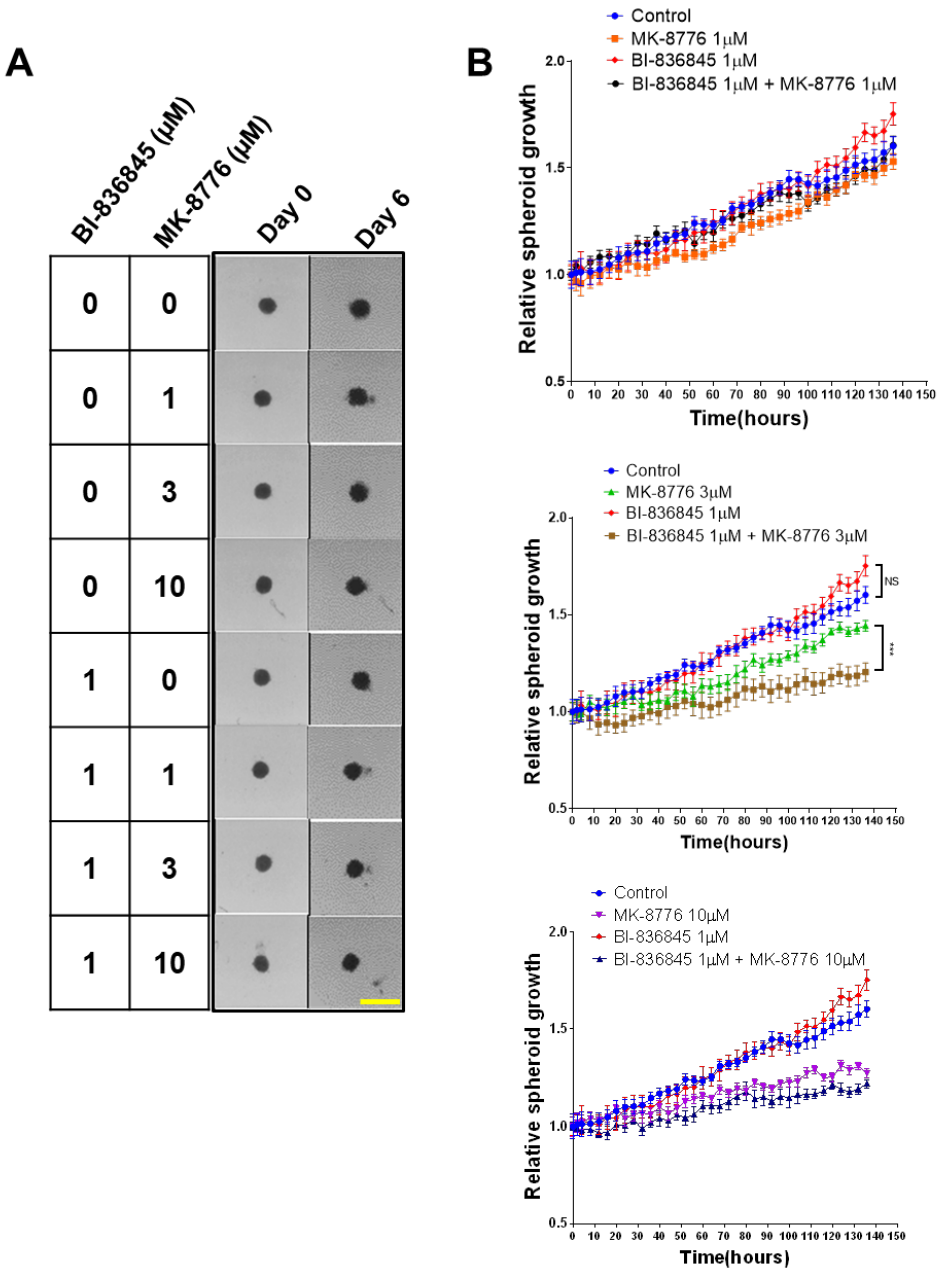

Figure 4.15 IGF and CHK1 co-inhibition shows minor combination effect in MCF7 spheroids

(A) Representative images of MCF7 spheroids treated with BI-836845 and MK-8776 for 6 days, scale bar: 2 mm; (B) Spheroid growth curves were analysed using spheroid size measured on IncuCyte Live Cell Analysis Imaging System for 6 days. Data (mean ± SEM

of 6 technical replicates) are expressed as % spheroid size on Day 0, from one representative experiment of 2 independent experiments with similar results. Two-way ANOVA was used. ***P < 0.001.

HeLa cells were sensitive to CHK1 and IGF co-inhibition in 2D culture (Figure 4.8 D). We next tested HeLa cells in 3D by culturing spheroids in round bottom ultra-low attachment 96-well plates. Since we began to see a lot of day-to-day variation in Incucyte results which possibly due to repeated opening of the incubator housing the Incucyte system at Target Discovery Institute, we switched assay platform. Hela spheroids were imaged on a Gelcount colony counter (Oxford Optronix) and the spheroid size was measured using ImageJ software (NIH). We found that HeLa cells were also able to form one compact spheroid after 3 days, and grew faster than MCF7 spheroids with ~3 fold increase of control spheroids on Day 7 compared to Day 0. Moreover, 1 μM BI-836845 and 3 μM or 10 μM MK-8776 as single treatments significantly slowed spheroid growth (~1.5 fold increase after 7 days), but the combination of BI-836845 and MK-8776 almost completely stopped spheroid growth (Figure 4.16 A, B). Similarly, IGF-1R TKI BI-885578 (300 nM) also slowed the growth of HeLa spheroids compared to solvent-treated controls, whereas the addition of 3 μM or 10 μM MK-8776 almost completely abrogated spheroid growth (Figure 4.16 C, D).

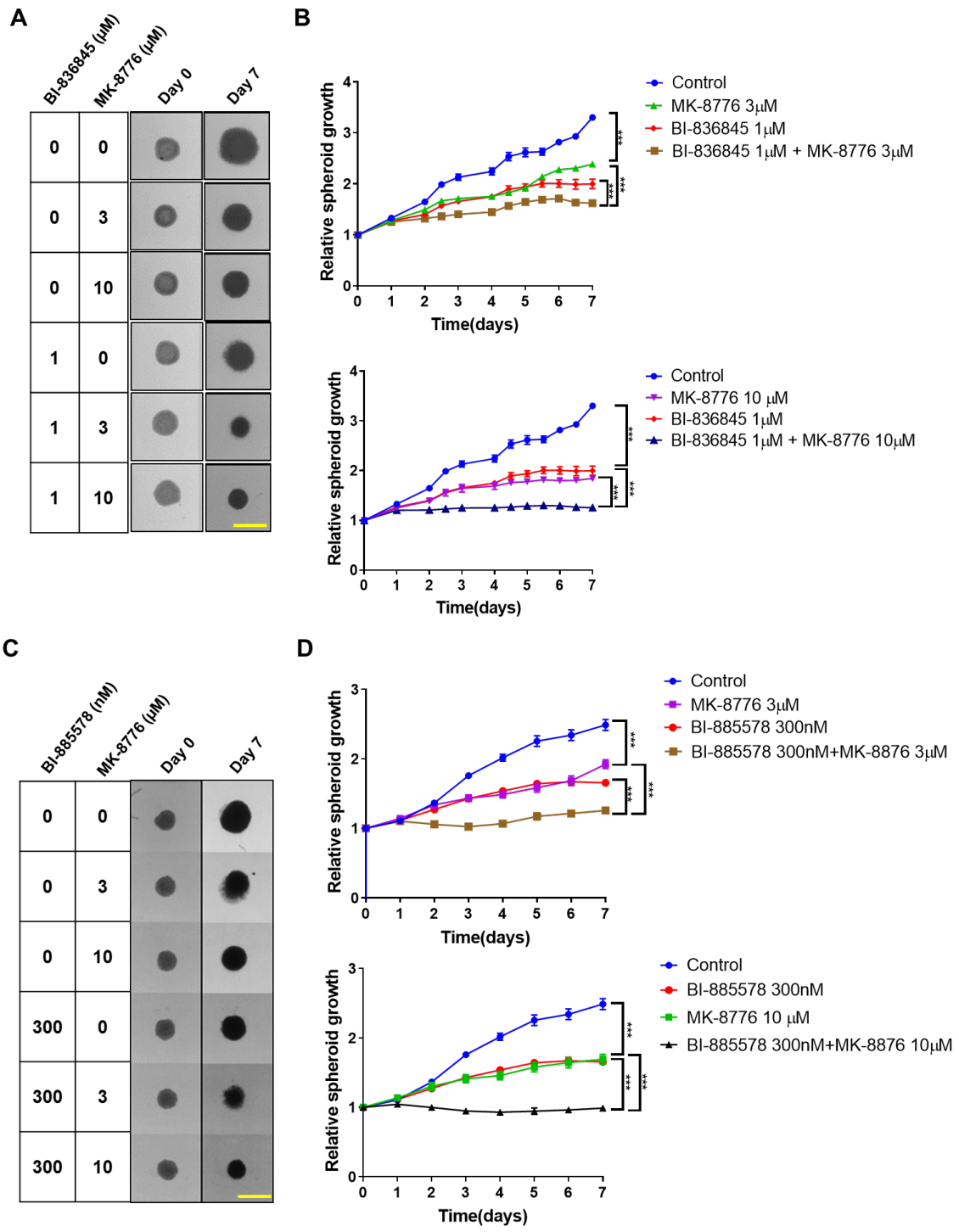

Figure 4.16 IGF and CHK1 co-inhibition shows combination effect in HeLa spheroids

(A) Representative images of HeLa spheroids treated with BI-836845 and MK-8776 for 7 days, scale bar: 2 mm; (B) Spheroid growth curves were analysed using spheroid size measured with ImageJ for 7 days. Data (mean ± SEM of 6 technical replicates) are expressed as % spheroid size on Day 0, from one representative experiment of 3 independent experiments with similar results. (C) Representative images of HeLa spheroids exposed to BI-885578 and MK-8776 for 7 days, scale bar: 2 mm; (D) Spheroid growth curves were analysed using spheroid size measured with ImageJ for 7 days. Data (mean ±

SEM of 6 technical replicates) are expressed as % spheroid size on Day 0 from one experiment. Two-way ANOVA was used. ***P < 0.001.

A previous study in our group showed that the presence of WT p53 associated with drug response to IGF-1R inhibition (Ramcharan et al., 2015). P53 plays critical roles in DNA damage, cell cycle controls and apoptosis (Brugarolas et al., 1995; Kastan et al., 1991; Kastan et al., 1992; Yonish-Rouach et al., 1991). Previous publications showed that the loss of p53 function via gene deletion or mutation was associated with drug resistance (Asada et al., 1999; Berns et al., 2000; Galmarini et al., 2001a). We next investigated whether p53 is required for the combination effect of CHK1 inhibition and IGF blockade. H1299 non-small cell lung cancer cells lack the expression of p53 tumour suppressor protein (Lin and Chang, 1996) and therefore were cultured in 3D upon the treatments BI-836845 and MK-8776 for 5 days. Under the single treatment with BI-836845 or MK-8776, H1299 spheroids grew very slowly and even regressed at 3 μM MK-8776 alone during the 7 days treatment period (Figure 4.17 A, B). The combination of 1 μM BI-836845 and 1 μM or 3 μM MK-8776 further slowed the spheroid growth, suggesting a combination effect (Figure 4.17 A, B). These data in H1299 p53 null cells suggested that the presence of WT p53 might not be essential for the combination effect of IGF and CHK1 co-inhibition.

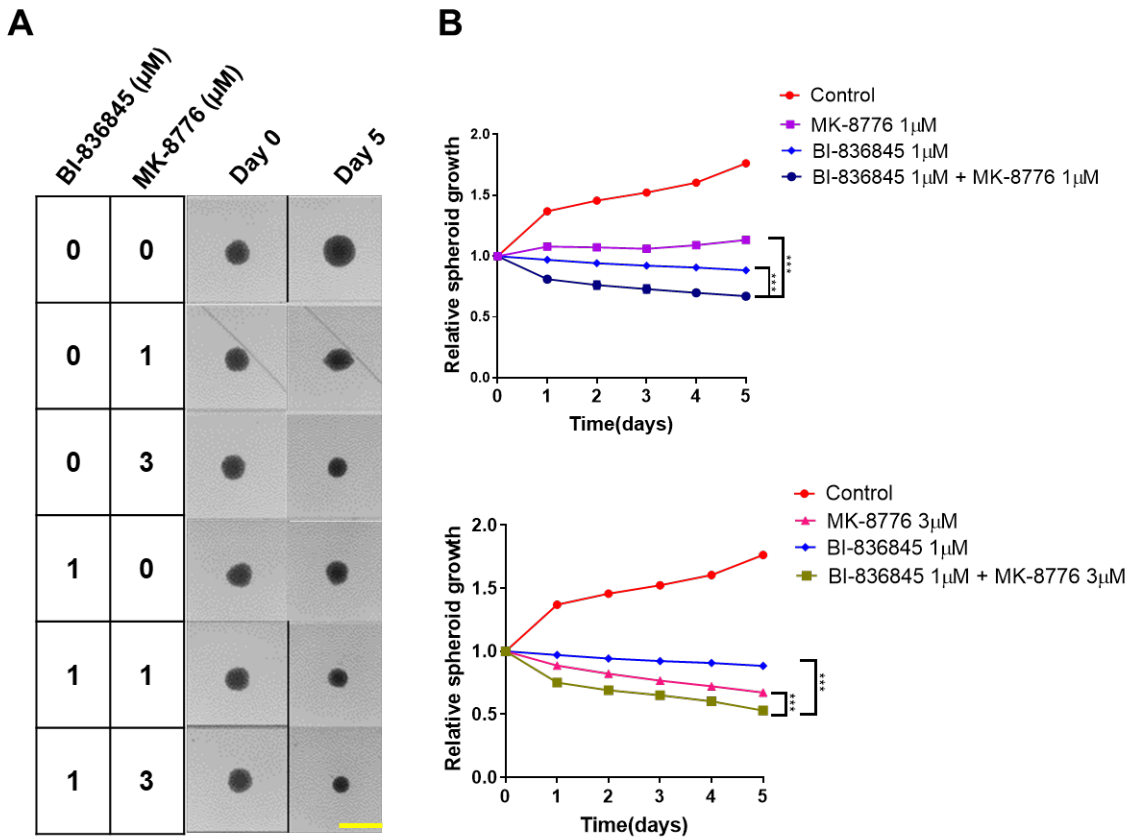

Figure 4.17 IGF and CHK1 co-inhibition shows combination effect in H1299 spheroids

(A) Representative images of H1299 spheroids exposed to BI-885578 and SRA737 for 7 days, scale bar: 2 mm; (B) Spheroid growth curves were analysed using spheroid size measured with ImageJ for 5 days. Data (mean ± SEM) are expressed as % spheroid size on Day 0 from one experiment. Two-way ANOVA was used. ***P < 0.001, **P < 0.01, *P < 0.05.

We next tested SK-CO-1 colorectal cancer cells in 3D culture. Dr Rieunier's unpublished data had shown that BI-836845 suppressed SK-CO-1 cell proliferation in 2D cell culture and *in vivo* mouse xenograft experiment. In this study, we have shown that in SK-CO-1 cells, MK-8776 dramatically suppressed replication fork progression after IGF-1R depletion (Figure 4.10 B). SK-CO-1 cells were able to form one single well-shaped spheroid after 3 days culture in round bottom ultra-low attachment 96-well plates, but they were less tightly packed than MCF7 cells and HeLa cells (Figure 4.18 A). SK-CO-1 spheroids were very sensitive to 1 μM BI-836845 alone, and almost stopped growing during the 7 days treatment period (Figure 4.18 A, B), consistent with Dr Rieunier's previous findings in 2D cell culture and *in vivo* mouse xenografts.

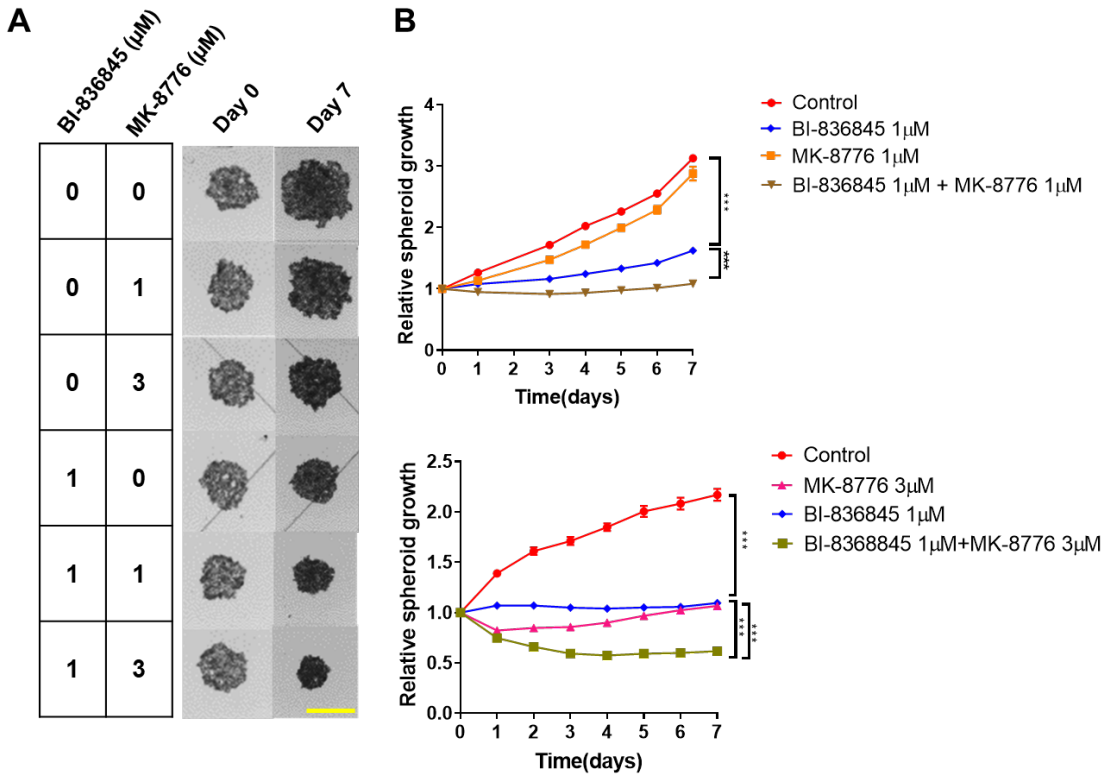

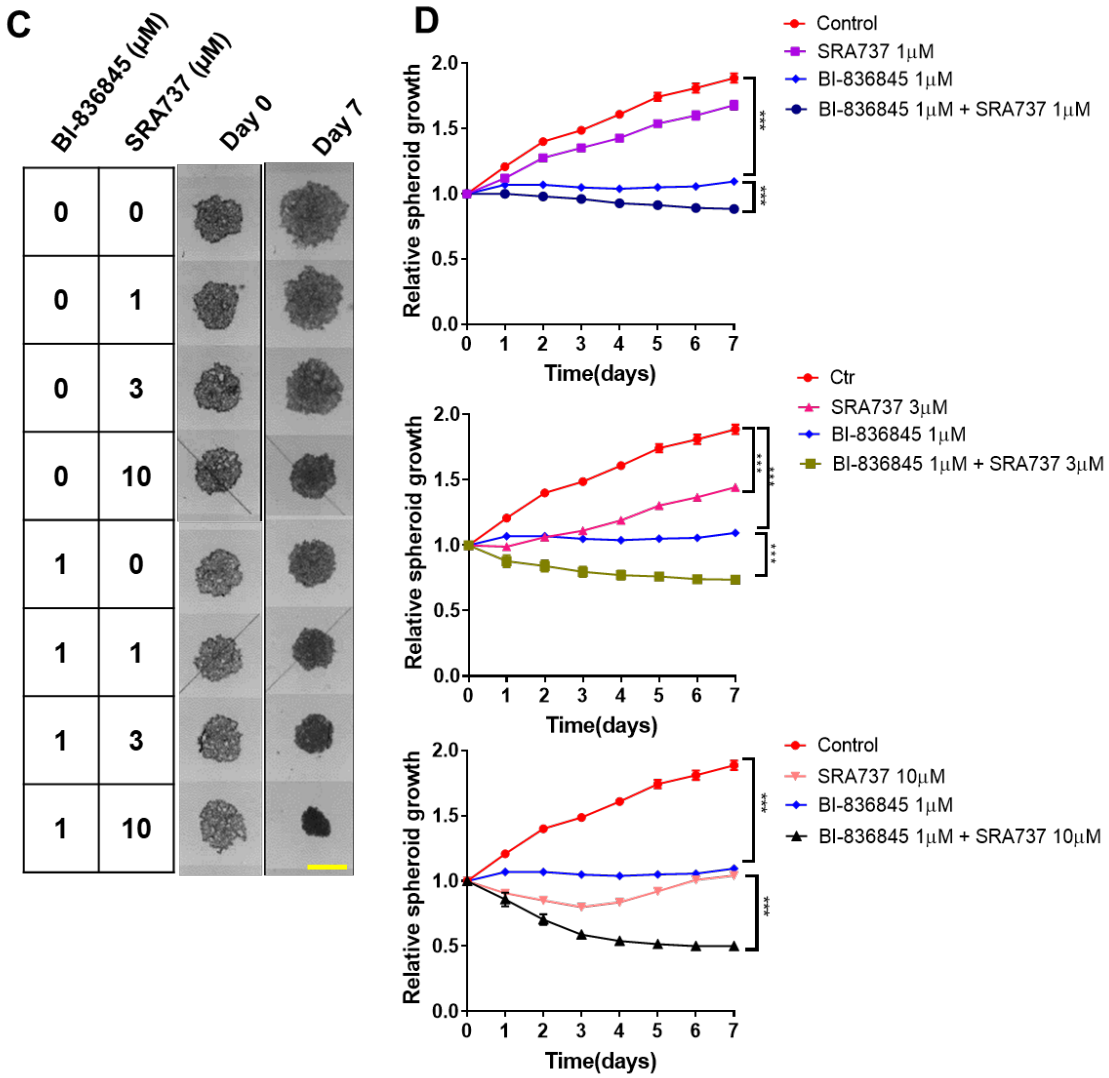

Figure 4.18 IGF and CHK1 co-inhibition shows combination effect in SK-CO-1 spheroids

(A) Representative images of SK-CO-1 spheroids exposed to BI-885578 and MK-8776 for 7 days, scale bar: 2 mm; (B) Spheroid growth curves were analysed using spheroid size measured with ImageJ for 7 days. (C) Representative images of SK-CO-1 spheroids exposed to BI-885578 and SRA737 for 7 days, scale bar: 2 mm; (D) Spheroid growth curves were analysed using spheroid size measured with ImageJ for 7 days. Data (mean ± SEM of 6 technical replicates) are expressed as % spheroid size on Day 0, from one representative of 3 independent experiments with similar results. Two-way ANOVA was used. ***P < 0.001.

SK-CO-1 spheroids were sensitive to CHK1 inhibitor MK-8776 alone at 3 μM, whereas 1 μM MK-8776 did not inhibition spheroid growth (Figure 4.18 A). The combination treatment of 1 μM BI-836845 and 1 μM or 3 μM MK-8776 further

reduced the spheroid growth, compared to treatment with either drug alone. Moreover, the combination of 1 μM BI-836845 and 3 μM MK-8776 led to significant spheroid regression over 7 days treatment that the spheroid size at Day 7 was 61.57 ± 4.76 % of the Day 0 value with p-value < 0.001 (Unpaired and two-tailed t test).

We next tested a different CHK1 inhibitor SRA737 to treat SK-CO-1 spheroids in combination with BI-836845. SRA737 is a highly selective oral CHK1 inhibitor (Booth et al., 2018), which is currently in Phase I/II clinical trials (NCT02797964, NCT02797977). The analyses of spheroid size showed that SRA737 dose-dependently suppressed SK-CO-1 growth at 1, 3, 10 μM, compared to solvent-treated controls during the 7 days treatment (Figure 4.15 A, B). The addition of BI-836845 significantly further suppressed spheroid growth (Figure 4.15 A, B). The combination of 10 μM SRA737 and 1 μM BI-836845 resulted in regression of SK-CO-1 spheroids to 50 ± 3.6% at Day 7 compared to Day 0 (Figure 4.15 A, B).

In SK-CO-1 spheroids, we observed that spheroids seemed more dense over 7 days treatment period (Figure 4.18), suggesting that comparing the spheroid sizes might not accurately reflect the drug responses in 3D. We therefore re-examined SK-CO-1 spheroids utilising CellTiter-Glo 3D assay to determine cell viability, using 3 replicate spheroids for each condition. SK-CO-1 spheroids were treated with BI-836845 and MK-8776 or SRA737 for 7 days, followed by CellTiter-Glo 3D assay as the endpoint experiment. BI-836845 or MK-8776 alone induced a moderate reduction of cell viability in SK-CO-1 spheroids, whereas the combination significantly decreased cell viability in spheroids to a significant lower level (Figure 4.19 A). SRA737 reduced cell viability in SK-CO-1 spheroids in a dose-dependent manner, and the addition of 1 μM BI-836845 led to a significantly lower cell viability in spheroids (Figure 4.19 B). Therefore, the drug responses analysed by CellTiter-

Glo 3D assay in SK-CO-1 spheroids were consistent with the data analysed from size measurements.

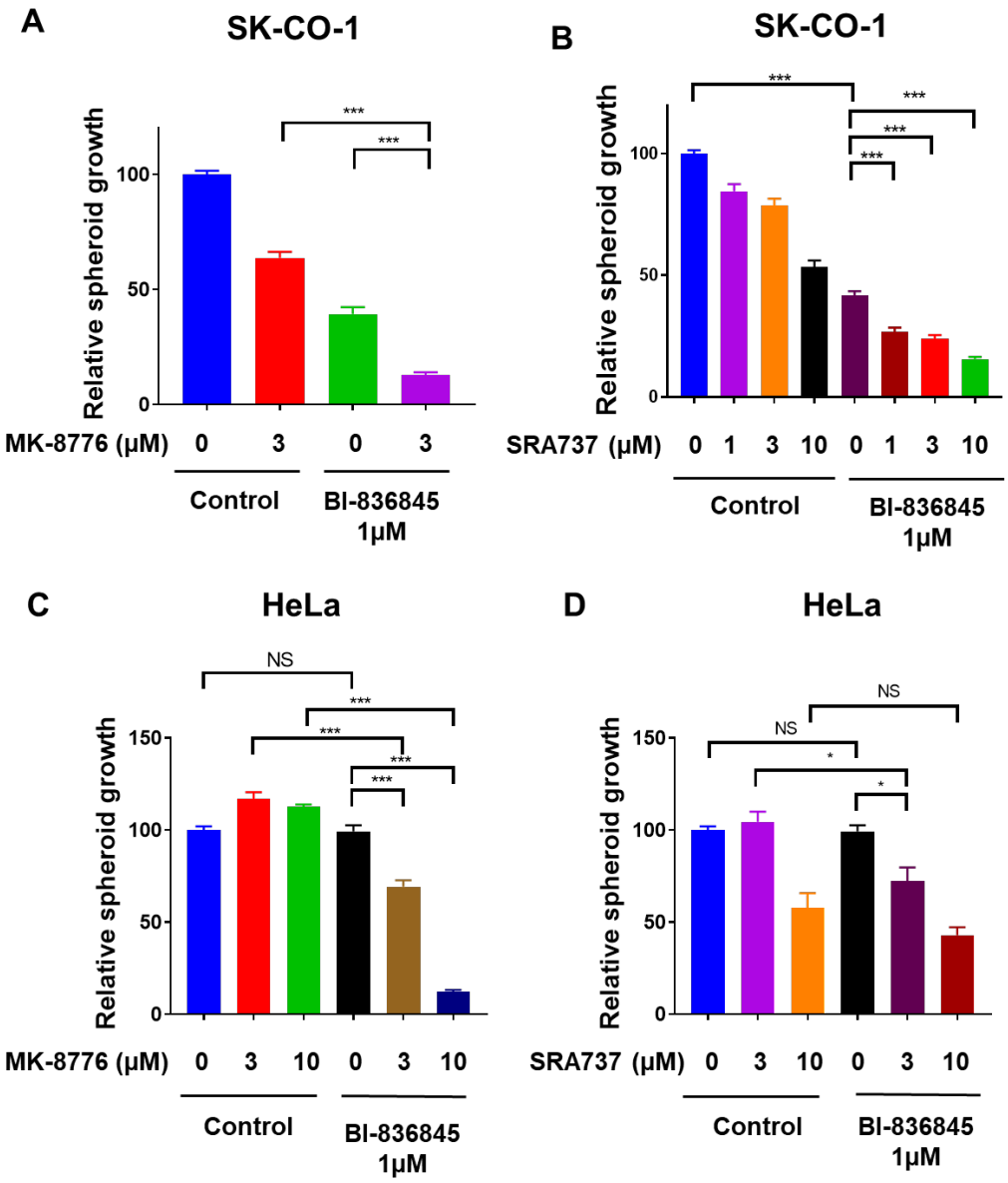

Figure 4.19 IGF and CHK1 co-inhibition shows combination effect in SK-CO-1 and HeLa spheroids in CellTiter-Glo 3D viability assay

(A) SK-CO-1 spheroids and (B) HeLa spheroids were treated with 1 μM BI-836845 and MK-8776 or SRA737 for 7 days, followed by CellTiter Glo 3D viability assay. Data are expressed as % solvent-treated controls and represented as mean ± SEM, pooled from (A: n=3 independent experiments, B: n=2 independent experiments, C, D: one experiment, each with 3 technical replicate spheroids). One-way ANOVA analysis was applied. ***P < 0.001, **P < 0.01, *P < 0.05.

A different drug response was observed in HeLa spheroids in CellTiter-Glo 3D assay. Viability of HeLa spheroids was largely unaffected by the treatment of 1 µM BI-836845 and 3 µM or 10 µM MK-8776 alone in CellTiter-Glo 3D assay (Figure 4.19 C), even though a clear reduction of spheroid size was observed after the treatment (Figure 4.16 A). However, the co-treatment of 1 µM BI-836845 with 3 µM or 10 µM MK-8776 still showed a significant combination effect on cell viability in spheroids (Figure 4.19 C). HeLa spheroids were also tested with SRA737 in combination with 1 µM BI-836845 in CellTiter Glo 3D assay. A combination effect was only detected when SRA737 was treated at 10 µM, but not at 3 µM (Figure 4.19 D).

Combination Index

		MK-8776 (µM)			
		0.3	1	3	10
BI-836845 (nM)	100	≫1	0.19 ±0.01	0.42 ±0.01	0.70 ±0.09
	300	0.12 ±0.09	0.18 ±0.02	0.39 ±0.04	0.49 ±0.04
	1000	0.06 ±0.01	0.13 ±0.01	0.33 ±0.03	0.31 ±0.22

Figure 4.20 BI-836845 and MK-8776 are synergistic in SK-CO-1 spheroids
SK-CO-1 spheroids were treated with BI-836845 and MK-8776 for 7 days, followed by CellTiter Glo 3D viability assay. The cell viability results were imported into CalcuSyn Software for CI value calculation. CI<0.8 indicates synergism, CI<0.3 strong synergism (Chou, 2006). Data are represented as mean ± SD, pooled from 3 independent experiments.

Combination index (CI) has been widely used to evaluate synergistic interaction of drug combinations (Chou, 2010). CI values were calculated based on the cell viability data from CellTiter Glo 3D assay performed in SK-CO-1 spheroids, in which MK-8776 was applied at 0.3 µM, 1 µM, 3 µM and 10 µM in combination with BI-836845 at 100 nM, 300 nM and 1000 nM for 7 days. The CI calculation showed that the lower concentration combination (100 nM BI-836845 and 0.3 µM MK-8776) was not synergistic (CI > 1), but all other combinations had CI value < 0.8, indicating

synergy, with some values of 0.1 ~ 0.3, indicating strong synergy (Chou, 2006) (Figure 4.20). Together, these results suggested that co-inhibition of IGF and CHK1 has synergistic effects on suppression of spheroid growth.

4.3 Discussion

In this chapter, aiming to exploit the replication stress induced by IGF blockade in cancer treatment, we first performed a compound screen with the drugs targeting DNA replication, cell cycle control and DNA repair that could potentially exacerbate replication stress. We identified two positive hits: ATM inhibitor KU-55933 and CHK1 inhibitor MK-8776 in this screen, which sensitised cells to IGF ligand antibody drug BI-836845. Targeting ATM or CHK1 has not been reported as a sensitiser to IGF inhibition in previous studies. Given the critical role of ATM in coordinating SSB repair (Khoronenkova and Dianov, 2015), the unpublished data generated by Dr Rieunier showed that IGF inhibition induced accumulation of SSB, while the addition of ATM inhibitors converted the SSBs to deleterious DSBs, resulting in cell death. The results in this Chapter also demonstrated that SK-CO-1 cells, which lack ATM expression, were hypersensitive to BI-836845 in 3D spheroid model. The addition of CHK1 inhibitors significantly increased the sensitivity of SK-CO-1 spheroids to IGF inhibition, resulting in spheroid regression.

The results presented here validated the combination effect of CHK1 and IGF co-inhibition in both 2D and 3D culture in different cell lines (Figure 4.8-4.9, 4.15-4.20). CHK1 had not been identified a screen hit in MCF7 cells (Figure 4.2) but this seems to have been a false negative since low throughput assays were positive (Figure 4.8A). Importantly, we showed that CHK1 inhibition markedly exacerbates the

replication stress phenotype in IGF-1R depleted cells, resulting in replication catastrophe and cell death. Of note, BI-885578 had more potent effects than BI-836845 in several assays (Figure 4.11, 4.14, 4.16), consistent with its more profound inhibition of IGF signalling (Figure 3.1).

The identification of CHK1 as an effective target whose inhibition worsens replication stress induced by IGF blockade might suggest that IGF-1R depleted or inhibited cells are more dependent on ATR/CHK1-mediated replication stress responses to maintain replication fork progression and proliferation, albeit at a lower rate than in controls. Indeed, unpublished work by Dr Rieunier showed that IGF-1R inhibition or depletion led to ATR-activated CHK1 phosphorylation at serine 345. In support of this, a previous study reported that ATR and IGF-1R co-inhibition led to a synergistic inhibition on the survival of breast cancer cells (O'Flanagan et al., 2016). However, ATR was not a hit in the compound screen (Figure 4.2 - 4.6) and Dr Rieunier has confirmed that BI-836845 does not sensitise cells to ATR inhibition. The presence of DNA-PK/CHK1-mediated backup pathway in response to ATR inhibition suggests that inhibiting CHK1 might be more effective than ATR inhibition to induce replication stress (Buisson et al., 2015).

Our findings demonstrate that co-inhibition of IGF and CHK1 induced replication catastrophe, suggesting a potential drug combination for cancer treatment. Previous unpublished work in our group by Dr Rieunier indicated that IGF blockade induced replication stress by disturbing dNTP pool via downregulating RRM2 expression. This prompted us to consider whether targeting CHK1 was also involved in regulating dNTP availability, contributing the enhanced replication stress after IGF blockade.

Chapter 5

CHK1 inhibition exacerbates replication stress induced by IGF blockade via RRM2 downregulation

5.1 Introduction

As discussed in Chapter 1, maintaining a balanced dNTP supply via regulating RNR complex is crucial for DNA replication. RNR subunit RRM2 is frequently overexpressed in cancers, suggesting that tumour cells might be more dependent on RNR-mediated dNTP biosynthesis to support sustained proliferation (Aye et al., 2015). RRM2 reduction and insufficient dNTP pools have been shown to cause replication fork stalling and replication stress (Bester et al., 2011; D'Angiolella et al., 2012). Unpublished data generated by Dr Rieunier in our group suggested that IGF-1R signalling regulated RRM2 expression at the transcription level, protecting breast cancer cells from endogenous replication stress. Dr Rieunier further showed that IGF-1R depletion or inhibition downregulates RRM2 expression, resulting in dATP reduction. Notably, RRM2 regulation was reported to be tightly coordinated during cell cycle progression through E2F-mediated transcription, mTORC1-mediated translation, and CDK-SCF(Cyclin F)-mediated degradation (D'Angiolella et al., 2012; He et al., 2017; Zhang et al., 2009). Previous studies demonstrated that cell cycle

checkpoint abrogation by CHK1 or WEE1 inhibition reduces RRM2 through activating CDK1/2-mediated degradation (Buisson et al., 2015; Koppenhafer et al., 2020; Pfister et al., 2015). In Chapter 4, we showed that combining IGF blockade and CHK1 inhibition induced severe replication stress, resulting in cell death. We hypothesised that IGF blockade partially reduces RRM2 and dNTP pool to a tolerable level, and combining with CHK1 inhibition leads to further critical RRM2 and dNTP reduction, causing cell death via replication catastrophe. Investigating this hypothesis was the focus of work in this chapter.

5.2 Results

5.2.1 Co-inhibition of IGF and CHK1 downregulates RRM2 expression

We first used western blot analysis to assess RRM2 protein levels in MCF7 cells after IGF signalling inhibition or IGF-1R depletion. Consistent with Dr Rieunier's results, IGF stimulation for 24 hours upregulated RRM2 at protein level in MCF7 cells (Figure 5.1 A, B). IGF signalling blockade by either IGF ligand antibody drug BI-836845 or IGF-1R TKI BI-885578 led to the reduction of IGF-1-induced pAKT, pERK and RRM2 (Figure 5.1 A, B). These results were in line with Dr Rieunier's findings that IGF signalling mediated RRM2 expression through both MEK/ERK and PI3K/AKT pathways. BI-885578 caused more downregulation of RRM2 than BI-836845, but the differences in pAKT and pERK between these two inhibitors were not statistically significant (Figure 5.1 A, B). Consistently, a reduction of RRM2 was observed in cells after IGF-1R depletion by two different siRNAs (Figure 5.1 C, D). We also observed a minor increase of ATR-induced CHK1 phosphorylation at serine 345 after IGF-1R depletion for 48 hours compared with controls, but the differences were not significant when one-way ANOVA was used for analysis (Figure 5.1 C, D). Dr Rieunier's unpublished results showed that IGF-1R depletion or IGF inhibition by

BI-836845 significantly induced more ATR-mediated CHK1 phosphorylation at serine 345 after 72 and 96 hours, suggesting the activation of ATR/CHK1 pathway by IGF blockade.

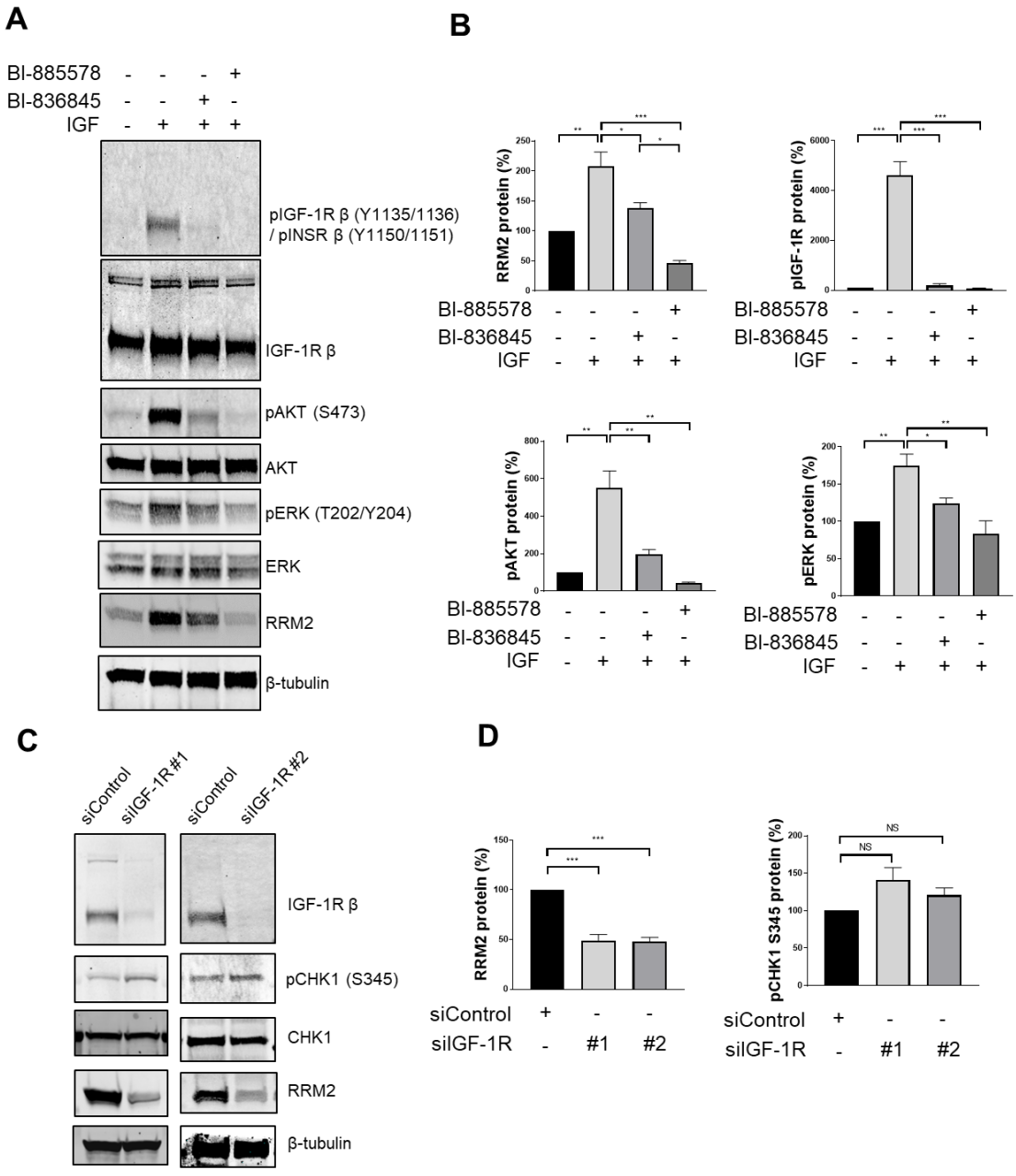

Figure 5.1 IGF blockade leads to the reduction of RRM2

(A) Western blot analysis of MCF7 cells serum starved for 24 hours, and then stimulated with 50 nM IGF-1 for 24 hours in the presence of solvent control, 1 μM BI-836845 or 300 nM BI-885578. (B) RRM2 and β-tubulin protein levels were quantified using ImageJ software. Results were expressed as % RRM2 protein of solvent control (left) after normalisation with β-tubulin. Same method was used for quantification of pIGF-1R (Y1135/1136), pAKT (S473), pERK (T202/Y204). Data are represented as mean ± SEM

from 3 independent experiments. (C) Western blot analysis of MCF7 cells transfected with siControl or siIGF-1R for 48 hours. Experiment was performed 3 times with independently prepared lysates and results were similar. (D) RRM2 and β-tubulin protein levels were quantified using ImageJ software. Results were expressed as % RRM2 protein of solvent control (left) after normalisation with β-tubulin. Same method was used for quantification of pCHK1 (S345). Data are represented as mean ± SEM from 3 independent experiments. One-way ANOVA analysis was used. ***P < 0.001, **P < 0.01, *P < 0.05.

Inactivating ATR/CHK1 pathway was previously reported to downregulate RRM2 (Buisson et al., 2015; Koppenhafer et al., 2020). We next assessed whether the addition of CHK1 inhibitor MK-8776 affected RRM2 protein levels. Western blot was performed in MCF7 cells transfected with siControl or siIGF-1R and then exposed to MK-8776 for 24 hours. Confirming compound bioactivity, we found that MK-8776 strongly suppressed CHK1 autophosphorylation at serine 296 (Figure 5.2 A), which is essential for targeting its substrates CDC25 phosphatases to arrest cell cycle (Kasahara et al., 2010). We also detected an increase of CHK1 phosphorylation at serine 345 upon MK-8776 treatment (Figure 5.2 A). This was in concordance with the previous findings that CHK1 inhibition enhanced ATR-mediated CHK1 phosphorylation at serine 345 by reducing protein phosphatase 2A (PP2A) (Leung-Pineda et al., 2006). The quantification of RRM2 protein levels showed that MK-8776 treatment or IGF-1R depletion alone led to a moderate reduction of RRM2, whereas combining MK-8776 with IGF-1R depletion further reduced RRM2 protein levels (Figure 5.2 A, B). RRM2 protein levels were also analysed in cells treated with MK-8776 after IGF signalling blockade by BI-886845 or BI-885578. We found that BI-886845 or BI-885578 alone reduced IGF-1-induced RRM2, whereas the addition of MK-8776 further reduced RRM2 protein levels (Figure 5.2 C).

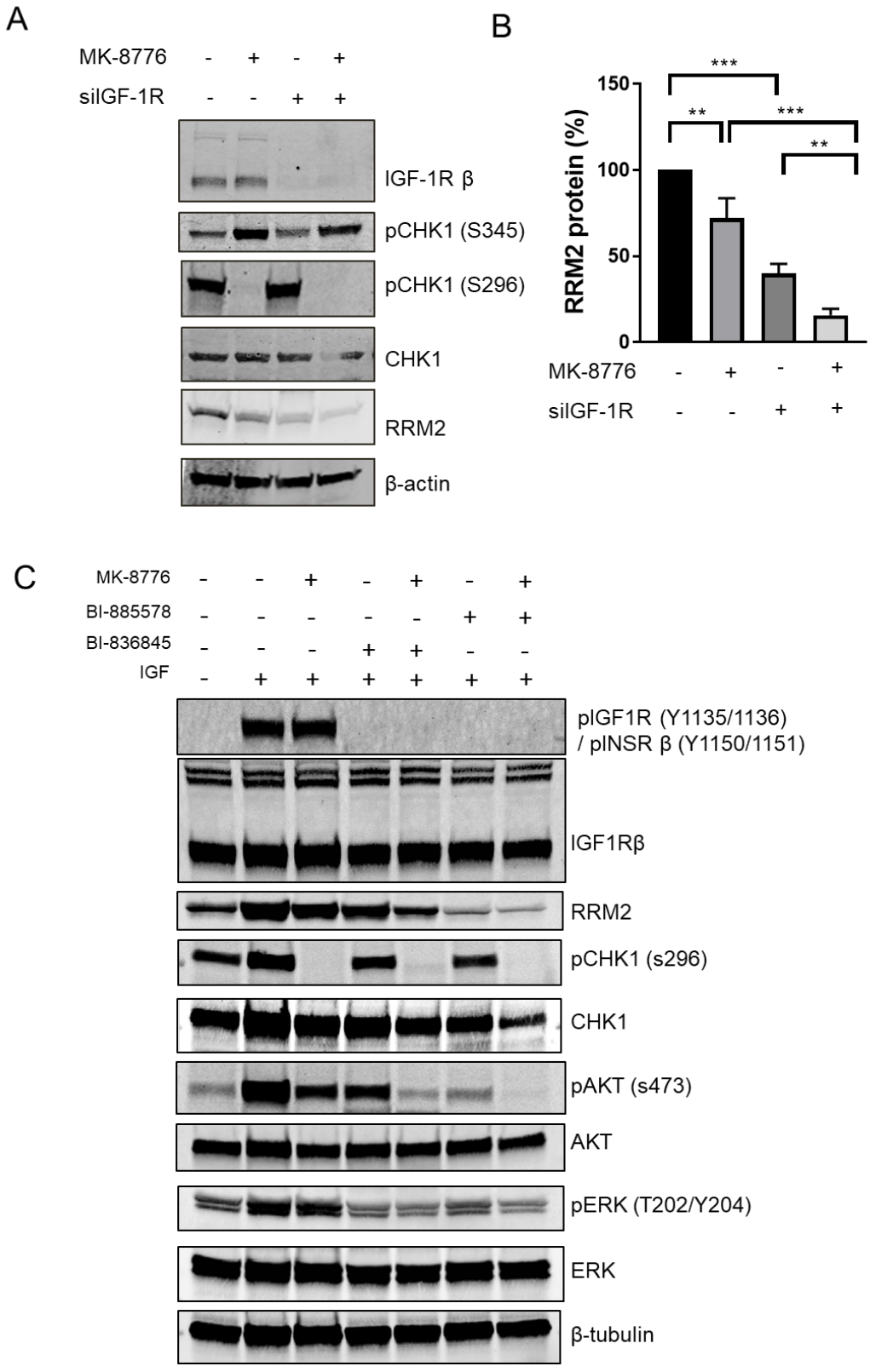

Figure 5.2 CHK1 inhibition further reduces RRM2 protein after IGF blockade
(A) Western blot analysis of MCF7 cells transfected with siControl or siIGF-1R for 24 hours, and then exposed to solvent control or 300 nM MK-8776 for 24 hours. (B) RRM2 protein levels were quantified as described in legend to Figure 5.1. Data are represented as mean

± SEM from 3 independent experiments. One-way ANOVA analysis was used. ***P < 0.001, **P < 0.01. (C) Western blot analysis of MCF7 cells serum starved for 24 hours, and then stimulated with 50 nM IGF-1 for 24 hours in the presence of solvent control, 1 μM BI-836845, 300 nM BI-885578 or 10 μM MK-8776. This experiment was only performed once.

To further assess the effect of co-inhibiting IGF and CHK1 on RRM2, we next assessed RRM2 protein levels in SK-CO-1 spheroids after 7 days treatment with BI-836845 and MK-8776, as shown in Figure 4.18 A. Western blot analysis of the protein extracted from spheroids using RIPA lysis buffer showed that BI-836845 or MK-8776 alone did not lead to a substantial decrease of RRM2, whereas the combination treatment significantly reduced RRM2 protein levels (Figure 5.3 A, B). In order to detect chromatin bound γH2AX protein, we used UTB lysis butter for protein extraction as described by Olcina *et al.* (Olcina et al., 2013). In these lysates, progressive reduction in RRM2 protein was confirmed, with a suggestion that combining BI-836845 and MK-8776 induced more γH2AX than either drug treatment alone (Figure 5.3 A), suggesting the increased replication stress after co-inhibiting IGF and CHK1. Of note, as shown in Figure 5.3 A, we observed unexpected bands below pIGF-1R (Y1135/1136), identity unknown, which were only present in samples extracted from BI-836845-treated cells. As this pIGF-1R (Y1135/1136) antibody (CST #3024) was also able to recognise Insulin Receptor phosphorylation at Tyr1150/1151, this might suggest the activation of Insulin signalling after 7 days treatment of BI-836845.

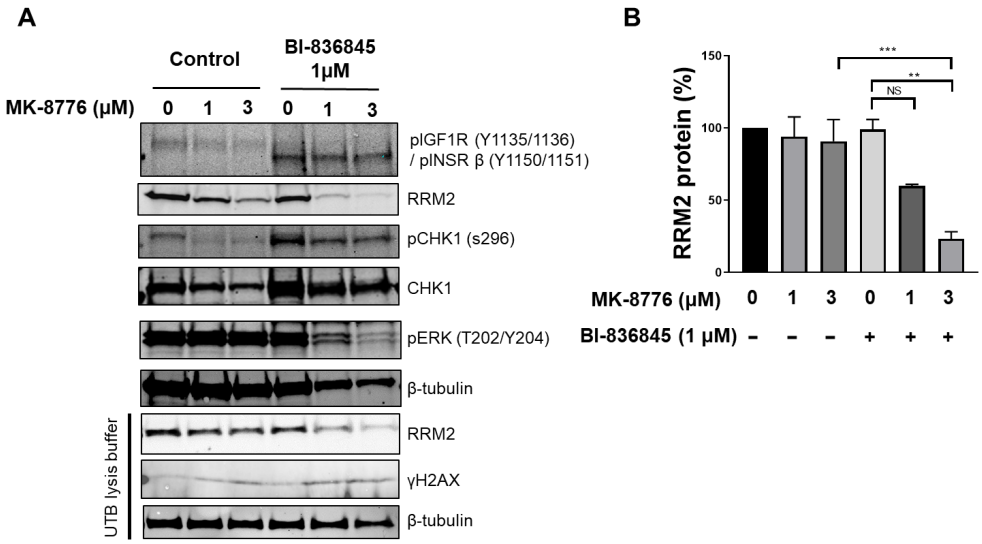

Figure 5.3 Co-inhibition of IGF and CHK1 reduces RRM2 protein in SK-CO-1 spheroids

(A) Western blot analysis of SK-CO-1 spheroids (6 spheroids per condition) exposed to solvent control or MK-8776 in the presence or absence of 1 μM BI-836845 for 7 days, as shown in Figure 4.14 and lysed in RIPA lysis buffer or UTB lysis buffer. (B) RRM2 protein levels were quantified as described in legend to Figure 5.1. Data are represented as mean ± SEM from 3 independent experiments. One-way ANOVA analysis was used. ***P < 0.001, **P < 0.01.

Together, these data supported our hypothesis that IGF blockade downregulated RRM2 expression, and combining with CHK1 inhibition led to a further reduction of RRM2 protein levels.

5.2.2 Co-inhibition of IGF and CHK1 reduces dNTP availability

RRM2 is a key component of RNR complex, which is required for the conversion of NDPs into dNDPs, the rate-limiting step for dNTP production (Stubbe and van der Donk, 1995). We next investigated whether RRM2 protein reduction after co-inhibiting IGF and CHK1 affected cellular dNTP levels. Unpublished results of HPLC assay performed by Dr Rieunier showed that IGF-1R depletion induced a significant reduction in only dATP level with no change in dTTP, and dCTP and dGTP were not

detectable in MCF7 cells using HPLC assay. Here, we modified an alternative dNTP measurement assay (Landoni et al., 2018) as described in Chapter 2.12 that was based on *in vitro* polymerase reaction for incorporation of tritium-labelled dNTPs into a template DNA. Exogenous dNTPs with known concentrations were used to determine the optimal measurement range to be between 10 nM to 100 nM in which radioactivity showed good linear correlation with concentrations of all four dNTPs with R square values of 0.66 – 0.97(Figure 5.4 A).

A

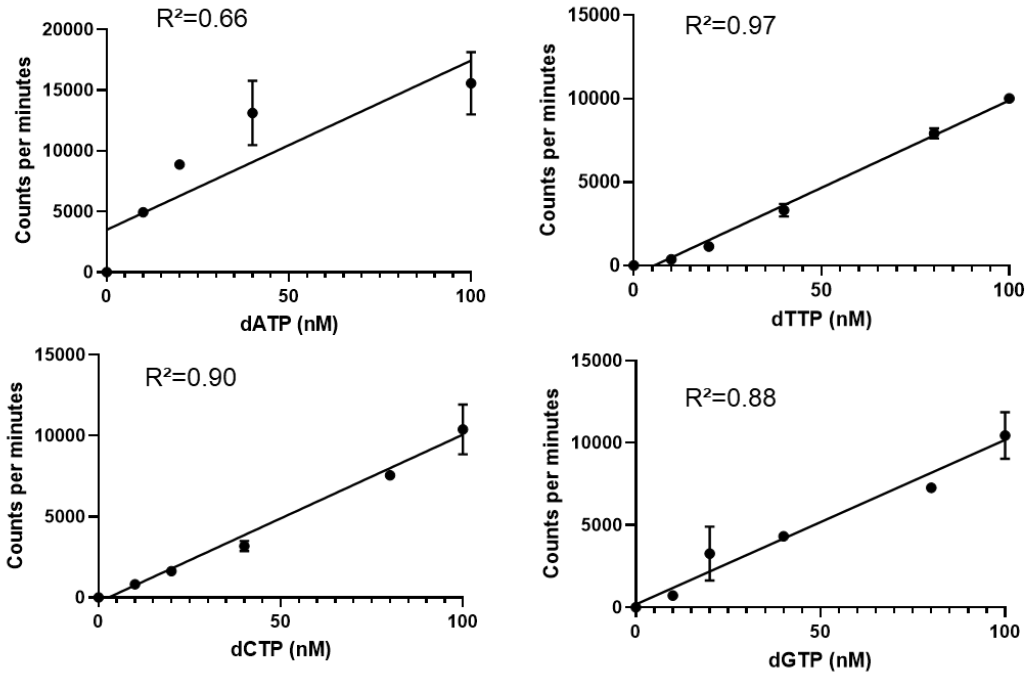

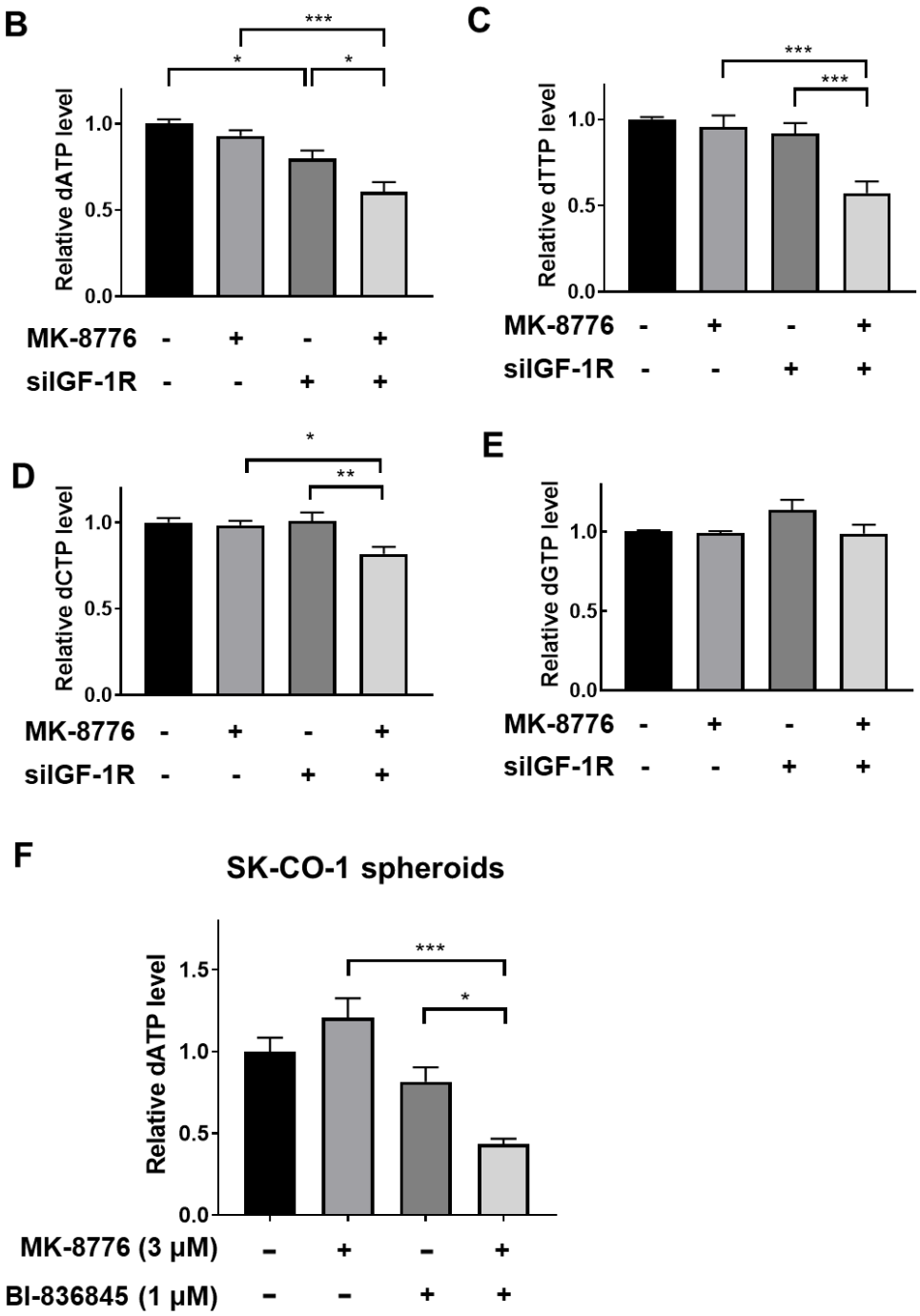

Figure 5.4 Co-inhibition of IGF and CHK1 reduces dNTP availability

(A) H^3 radioactivity (counts per minutes) showed good linear correlations with the concentrations of exogenous dATP, dTTP, dCTP and dGTP within the range of 10 nM ~ 100 nM. Data are represented as mean ± SEM, pooled from 2 independent experiments and each experiment has duplicate datapoints. R square values for linear regression were determined in Graphpad Prim 8. (B-E) MCF7 cells transfected with siControl or siIGF-1R for 24 hours and then exposed to solvent-treated control or 300 nM MK-8776 for 24 hours. dATP (B), dTTP (C), dCTP (D) and dGTP (E) were measured. (F) dATP levels in SK-CO-1 spheroids exposed to solvent control or MK-8776 in the presence or absence of 1 μM BI-836845 for 7 days. Results were normalised to solvent controls (left bar) and represented

as mean ± SEM, pooled from 3 independent experiments. One-way ANOVA analysis was used. ***P < 0.001, **P < 0.01, *P < 0.05.

MCF7 cells were transfected with siControl or siIGF-1R and then exposed to MK-8776 for 24 hours. We extracted the cellular dNTPs and diluted to concentrations within optimal measurement range as described in section 2.12. All four dNTPs were detectable using this assay. Consistent with Dr Rieunier's HPLC results, IGF-1R depletion reduced dATP level, but did not affect dTTP, dCTP, and dGTP levels (Figure 5.4 A-D). MK-8776 alone did not lead to reduction of any dNTPs, whereas combining MK-8776 and IGF-1R depletion significantly reduced dATP, dTTP, and dCTP levels, but not dGTP level (Figure 5.4 A-D). We also measured dATP levels in SK-CO-1 spheroids exposed to MK-8776 in the presence or absence of 1 μM BI-836845 for 7 days, following serial measurement of spheroid growth shown in Figure 4.18 A. In the small amount of material available, only dATP was detectable. The combination of MK-8776 and BI-836845 markedly reduced dATP levels, whereas either drug alone had no significant effect (Figure 5.4 E). These data suggested that combining CHK1 inhibition and IGF blockade significantly decreased cellular dNTP availability, indicating a functional consequence of the reduction in RRM2 protein levels.

5.2.3 Generation of RRM2-overexpressing cell lines

So far, we have shown that CHK1 inhibition enhanced replication stress induced by IGF blockade, accompanied by a further reduction of RRM2 protein levels. This prompted us to ask whether the reduction of RRM2 contributed to the interaction between CHK1 inhibition and IGF blockade, and whether this significant reduction in RRM2 resulted in replication catastrophe. We next generated MCF7 cells overexpressing exogenous RRM2. As described in section 2.7, MCF7 cells were transfected with pcDNA3.1 empty vector control or pcDNA3.1 RRM2. G418

selection led to the emergence of positive clones. We continued to culture the surviving colonies with medium containing G418 for 30 days to obtain the stably expressing clonal cells. Using western blot analysis, we confirmed that RRM2-overexpressing cells expressed a higher level of RRM2 than empty vector control cells (Figure 5.5). IGF-1R depletion led to a reduction of RRM2 protein levels in empty vector control cells (Figure 5.5), similar to the results in parental MCF7 cells (Figure 5.1 C). Although IGF-1R depletion detectably reduced RRM2 in RRM2-overexpressing cells, which might be due to the reduction of endogenous RRM2 after IGF-1R depletion, residual RRM2 was at the similar levels to siControl-transfected empty vector control cells (Figure 5.5). Furthermore, there was a minor increase of ATR-induced CHK1 phosphorylation in empty vector control cells upon IGF-1R depletion for 48 hours, but not in RRM2-overexpressing cells (Figure 5.5), suggesting that replication stress might be at a lower level in RRM2-overexpressing cells.

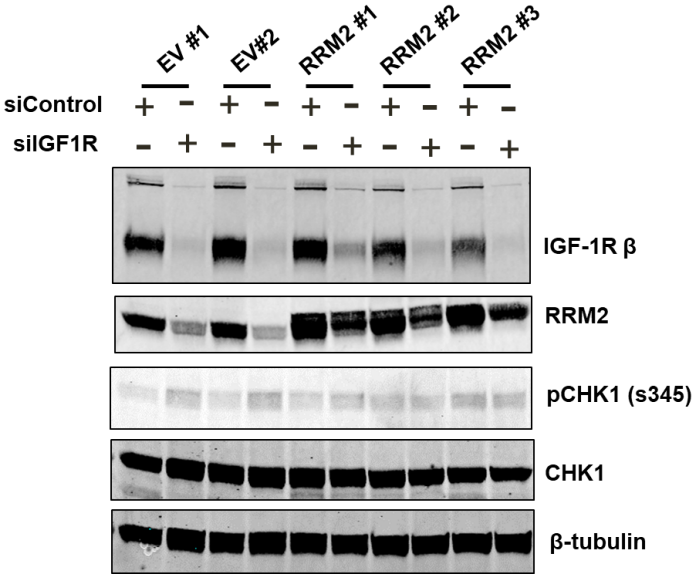

Figure 5.5 RRM2 protein expression in empty vector control cells and RRM2-overexpressing cells after IGF-1R depletion

MCF7 cells were transfected with pcDNA3.1 RRM2 or pcDNA3.1 empty vector control for 48 hours, and then cultured in medium containing 800 μg/mL G418 for selection. The

surviving colonies were expanded in medium containing 800 μg/mL G418 for 30 day to obtain the stably expressing cells. Two empty vector clones and three RRM2-overexpressing clones were transfected with siControl or siIGF-1R for 24 hours, followed by protein extraction and western blot analysis. Western blot was performed with lysates prepared in 3 independent experiments and results in the other two experiments were similar to this result.

We next assessed the effect of CHK1 inhibition on RRM2 expression in empty vector control cells and RRM2-overexpressing cells. In empty vector controls, MK-8776 alone did not affect RRM2 protein levels and IGF-1R depletion partially reduced RRM2, whereas combining MK-8776 with IGF-1R depletion led to a further reduction of RRM2 (Figure 5.6), comparable to results in parental MCF7 cells (Figure 5.2). In contrast, RRM2-overexpressing cells maintained RRM2 protein levels after CHK1 inhibition and IGF-1R depletion, compared to empty vector control cells (Figure 5.6). MK-8776 reduced pCHK1 at serine 296 in both empty vector controls and RRM2-overexpressing cells, confirming the drug bioactivity of MK-8776 (Figure 5.6). MK-8776 increased ATR-activated pCHK1 at serine 345 in not only empty vector controls, but also RRM2-overexpressing cells (Figure 5.6). As previously discussed, this might due to the reduced phosphatase activity of PP2A upon CHK1 inhibition (Leung-Pineda et al., 2006), leading to the increase of pCHK1 at serine 345 in both empty vector controls and RRM2-overexpressing cells. Together, these data validated the RRM2-overexpressing cells that restored RRM2 upon CHK1 inhibition and IGF-1R depletion.

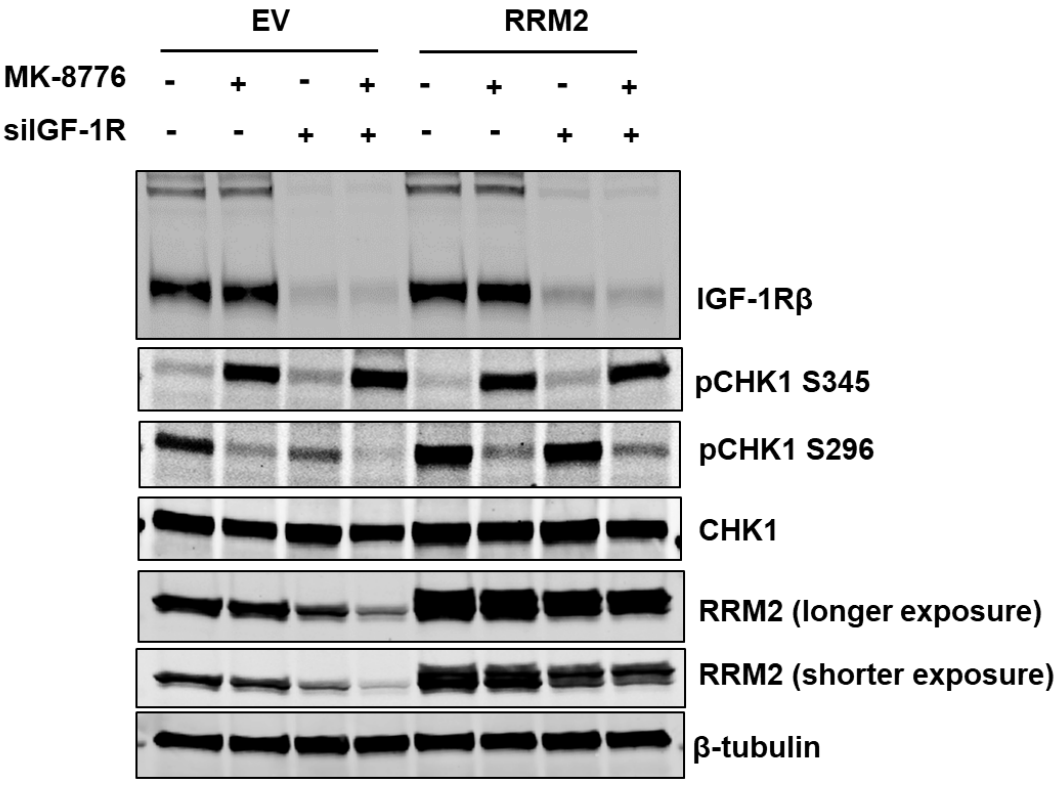

Figure 5.6 RRM2 protein expression in empty vector control cells and RRM2-overexpressing cells upon CHK1 inhibition and IGF-1R depletion

Empty vector control cells and RRM2-overexpressing cells were transfected with siControl or siIGF-1R for 24 hours and then exposed to solvent control or 300nM MK-8776 for 24 hours, followed by protein extraction and western blot analysis. This experiment was only performed once.

5.2.4 RRM2 overexpression alleviates severe replication stress induced by co-inhibition of IGF and CHK1

To investigate whether RRM2 was an important target of the interaction between CHK1 inhibition and IGF blockade, we next performed cell viability assay in empty vector control cells and RRM2-overexpressing cells. Cells were transfected with siControl or siIGF-1R for 24 hours and then exposed to MK-8776 for 5 days. Dose-response curves against MK-8776 were generated using cell viability data (Figure 5.7 A). We found that IGF-1R depletion shifted the dose-response curves to the left in empty vector control cells (Figure 5.7 A), consistent with the results in parental MCF7 cells (Figure 4.9 A). However, RRM2 overexpression shifted the dose-

response curves to the right (Figure 5.7 A), suggesting a decreased sensitivity. We calculated the GI50s for MK-8776 based on the dose-response curves. The GI50s for MK-8776 in controls were higher than 10 μM, which was the highest concentration we used in this experiment (Figure 5.7 A, B). In empty vector control cells, IGF-1R depletion decreased the GI50 for MK-8776 from >10 μM to 2.7 μM (Figure 5.7 A, B). However, in RRM2-overexpressing cells, the GI50 for MK-8776 after IGF-1R depletion remained >10 μM after IGF-1R depletion (Figure 5.7 A, B). These results suggested a reduced sensitivity to the combination of MK-8776 and IGF-1R depletion in RRM2-overexpressing cells.

We next tested the drug combination of BI-836845 and MK-8776 in empty vector control cells and RRM2-overexpressing cells. Consistently, RRM2-overexpression shifted the dose-response curves to the right (Figure 5.7 C), suggesting a reduced sensitivity to combination of BI-836845 and MK-8776. Addition of BI-836845 reduced the GI50 for MK-8776 from >10 μM to 3.8 μM in empty vector control cells, similar to the effect of IGF-1R depletion (Figure 5.7 D). In RRM2-overexpressing cells, the GI50 for MK-8776 after BI-836845 treatment was 9.6 μM, which was higher than the GI50 (3.8 μM) in empty vector control cells (Figure 5.7 D). Thus, these data suggested that RRM2 overexpression had a rescue effect on cell proliferation upon CHK1 inhibition and IGF blockade.

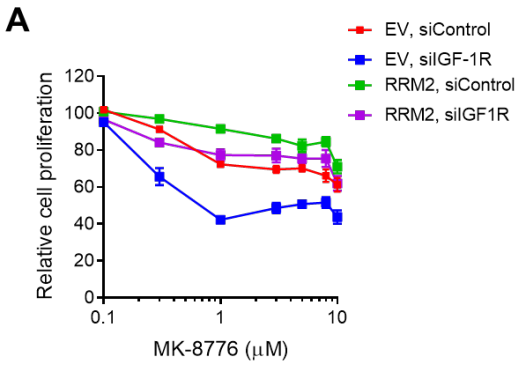

B

GI50 (95%CI, μM) for MK-8776

	EV	RRM2
siControl	>10	>10
siIGF-1R	0.52 (0.35-0.9)	>10

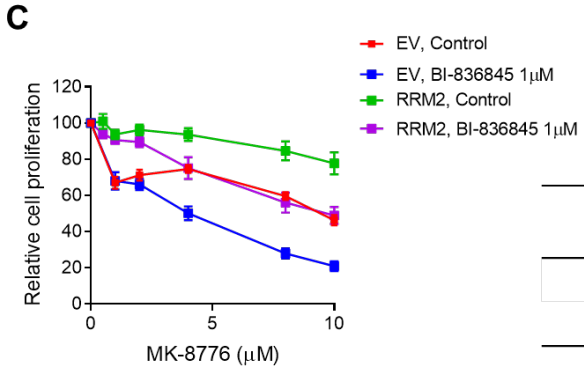

D

GI50 (95%CI, μM) for MK-8776

	EV	RRM2
Control	>10	>10
BI-836845	3.8 (3.14-4.67)	9.6 (>8.18)

Figure 5.7 RRM2 overexpression rescues cell proliferation upon CHK1 inhibition and IGF blockade

(A) Empty vector control cells and RRM2-overexpressing cells were transfected with siControl or siIGF-1R for 24 hours and then exposed to solvent control or MK-8776 for 5 days, followed by cell viability assay. Results were expressed as % viability of solvent-treated control. Data are represented as mean ± SEM, pooled from n=3 independent experiments; (B) GI50 values and 95% confidence intervals were calculated based on the drug response curves in A; (C) Empty vector control cells and RRM2-overexpressing cells were exposed to solvent control or MK-8776 in the presence or absence of 1 μM BI-836845 for 5 days, followed by cell viability assay. Results were expressed as % viability of solvent-treated control. Data are represented as mean ± SEM, pooled from n=3 independent experiments; (D) GI50 values 95% confidence intervals were calculated based on the drug-response curves in C.

We next investigated whether RRM2 overexpression rescued replication stress induced by CHK1 inhibition and IGF-1R depletion. DNA fiber assay was performed

in empty vector control cells and RRM2-overexpressing cells. Cells were transfected with siControl or siIGF-1R for 24 hours and then exposed to MK-8776 or solvent control for 24 hours. In empty vector control cells, MK-8776 or IGF-1R depletion alone led to a moderate reduction of DNA fiber length, whereas combining MK-8776 and IGF-1R depletion further shortened DNA fibers, consistent with the observation in parental MCF7 cells (Figure 5.8). In RRM2-overexpressing cells, DNA fiber tracts were found significantly longer than empty vector control cells upon IGF-1R depletion and MK-8776 treatment alone or in combination (Figure 5.8), suggesting a rescue effect of RRM2 overexpression on suppressed replication fork progression by CHK1 inhibition and IGF-1R depletion. However, this rescue effect was partial since the mean fiber length upon the combination treat was still significantly shorter compared with the untreated controls in RRM2-overexpressing cells (Figure 5.8). Notably, RRM2 overexpression did not appear to affect the aberrant origin firing induced by CHK1 inhibition since we observed that MK-8776 increased newly fired origins to similar levels in empty vector control cells and RRM2-overexpressing cells (Figure 5.8).

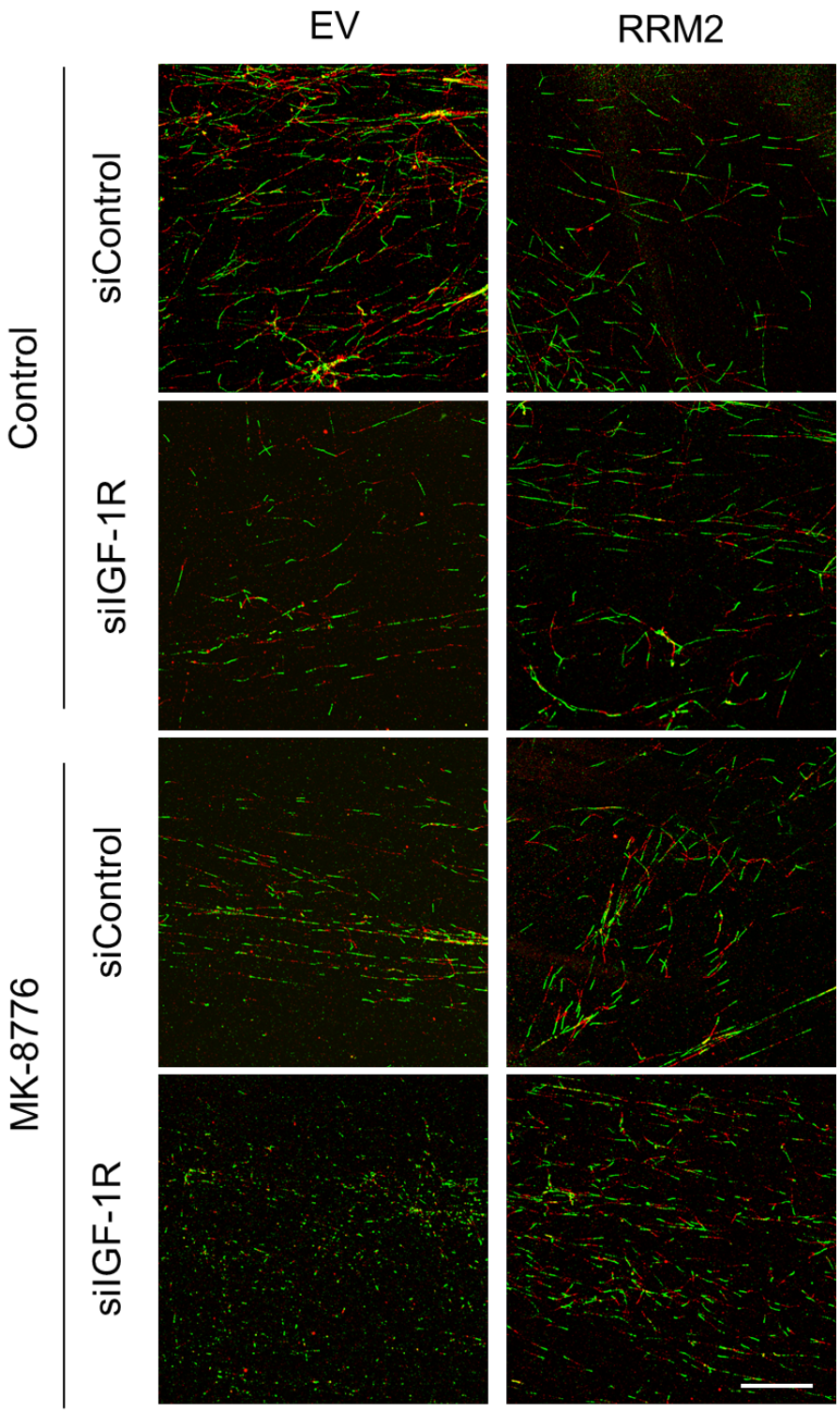
EV
RRM2
Control
siControl
siIGF-1R
MK-8776
siControl
siIGF-1R

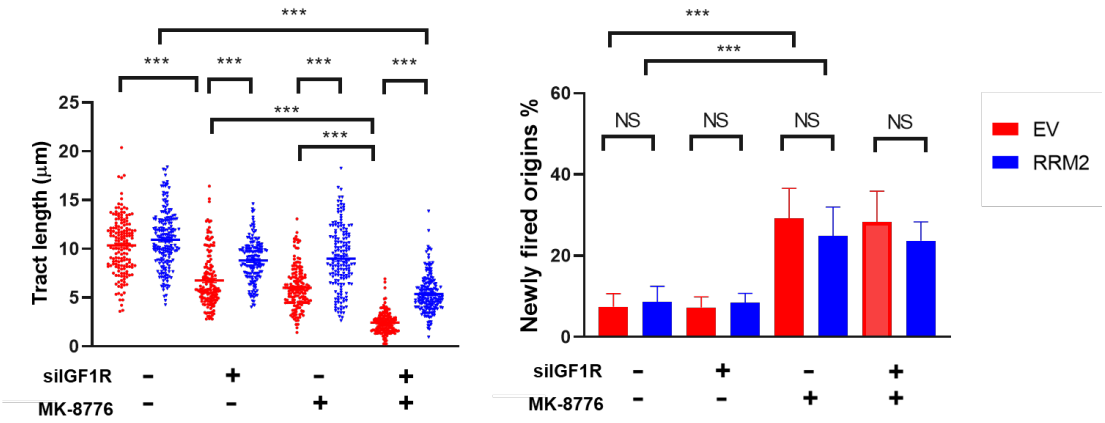

Figure 5.8 RRM2 overexpression rescues DNA replication fork progression upon CHK1 inhibition in IGF-1R depleted cells

Representative images of DNA fiber tracts (CIdU (Red), IdU (Green)) in empty vector control cells and RRM2-overexpressing cells transfected with siControl or siIGF-1R for 24 hours and then exposed to solvent control or 1 μM MK-8776 for 24 hours. Scale bar: 20 μm. Quantification of fiber tract length (>150 tracts) and newly fired origins (IdU (green)-only tracts as percentages of the total number of tracts (⩾ 5 images)) was shown below. Data (mean ± SEM) are one representative experiment of 2 independent experiments with similar results. One-way ANOVA was used. ***P < 0.001.

To further assess the rescue effect of RRM2 overexpression on DNA replication, we next assessed S phase distribution by cell cycle analysis in empty vector control cells and RRM2-overexpressing cells upon MK-8776 treatment and IGF-1R depletion. Combining MK-8776 and IGF-1R depletion induced a significant accumulation of non-replicating S-phase population in empty vector control cells (Figure 5.9), similar to parental MCF7 cells (Figure 4.12). In contrast, we didn't detect a significant accumulation of non-replicating S-phase population in RRM2 overexpressing cells (Figure 5.9). These results suggested a rescue effect of RRM2 overexpression on suppressed DNA replication upon CHK1 inhibition and IGF-1R depletion.

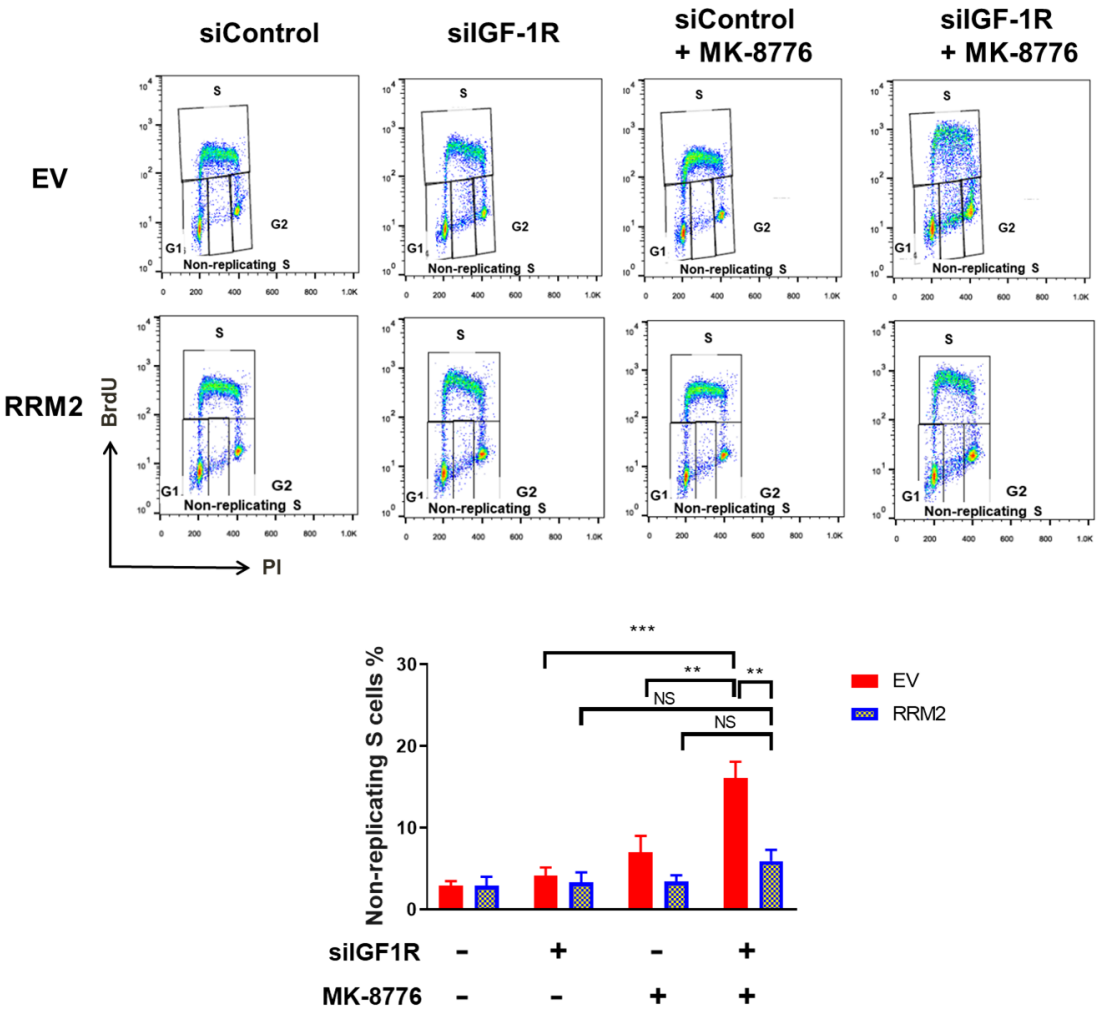

Figure 5.9 RRM2 overexpression rescues non-replicating S phase cells upon CHK1 inhibition in IGF-1R depleted cells

BrdU FACS analysis of cell cycle distribution of empty vector control cells and RRM2-overexpressing cells transfected with siControl or siIGF-1R for 24 hours and then exposed to solvent control or 1 μM MK-8776 for 24 hours. Quantification of non-replicating S phase cells was shown below. Data are represented as mean ± SD, pooled from 3 independent experiments. One-way ANOVA analysis was used. ***P < 0.001, **P < 0.01.

To further investigate whether RRM2 overexpression rescued replication stress induced by CHK1 inhibition and IGF-1R depletion, we next performed double immunostaining assay to assess γH2AX and ssDNA in empty vector control cells and RRM2-overexpressing cells. Cells were transfected with siControl or siIGF-1R for 24 hours and then exposed to MK-8776 for 24 hours. Combining MK-8776 and IGF-1R led to a significant accumulation of both γH2AX positive cells and BrdU positive cells in empty vector control cells, suggesting replication stress (Figure 5.10 A, C). This was consistent with the results in parental MCF7 cells (Figure 4.13). In RRM2-overexpressing cells, we detected significantly fewer γH2AX positive cells and BrdU positive cells upon the combination treatment of MK-8776 and IGF-1R depletion, compared to empty vector control cells (Figure 5.10 A-C). Moreover, combining MK-8776 and IGF-1R depletion caused accumulation of 34.35 ± 4.77 % double positive cells in empty vector control cells, whereas 15.6 ± 4.82 % double positive cells were detected in RRM2-overexpressing cells (Figure 5.10 A-C), suggesting that RRM2 overexpression caused partial rescue from replication stress induced by CHK1 inhibition and IGF-1R depletion.

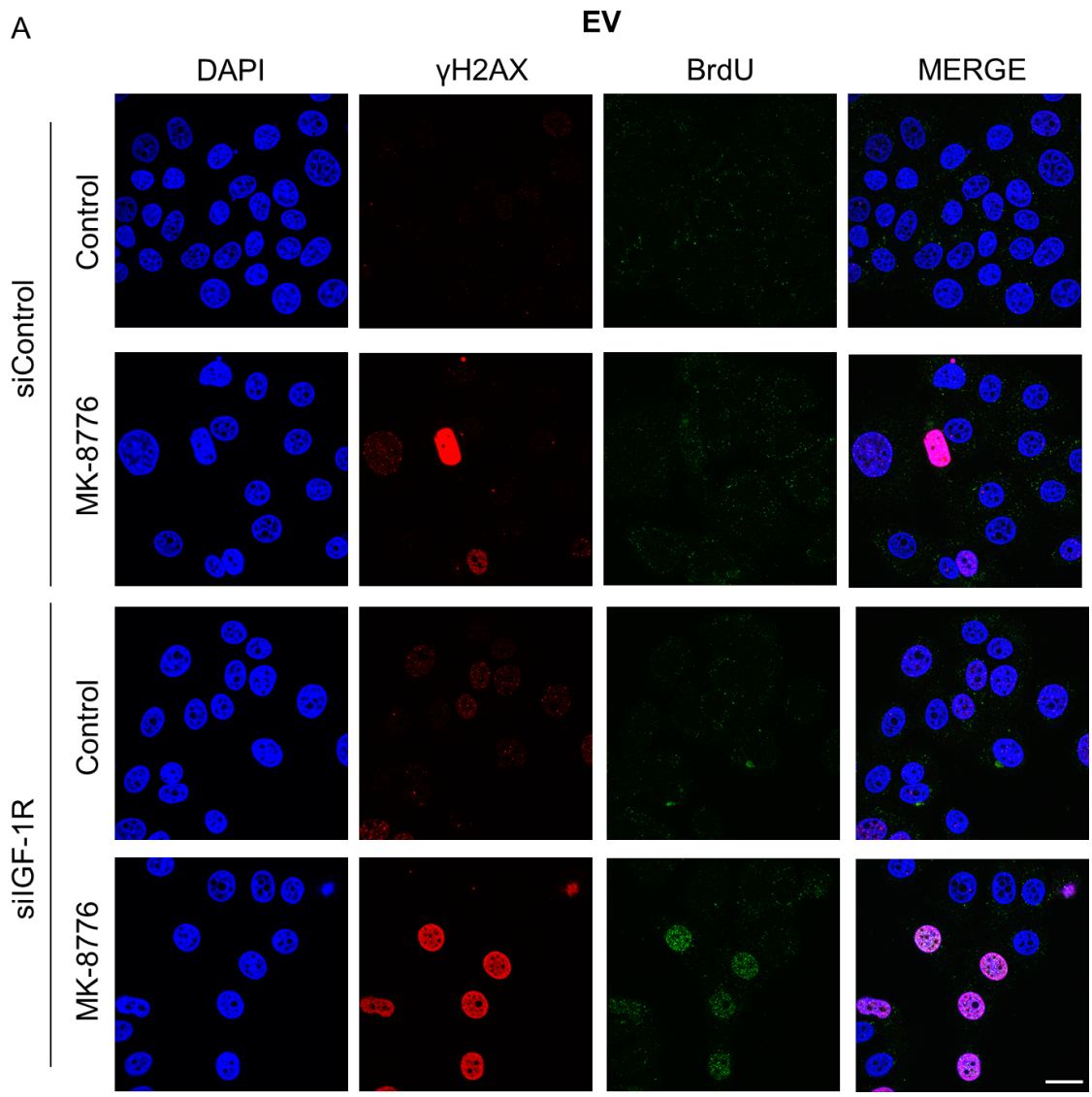
A
EV
DAPI
γH2AX
BrdU
MERGE
siControl
Control
MK-8776
siIGF-1R
Control
MK-8776

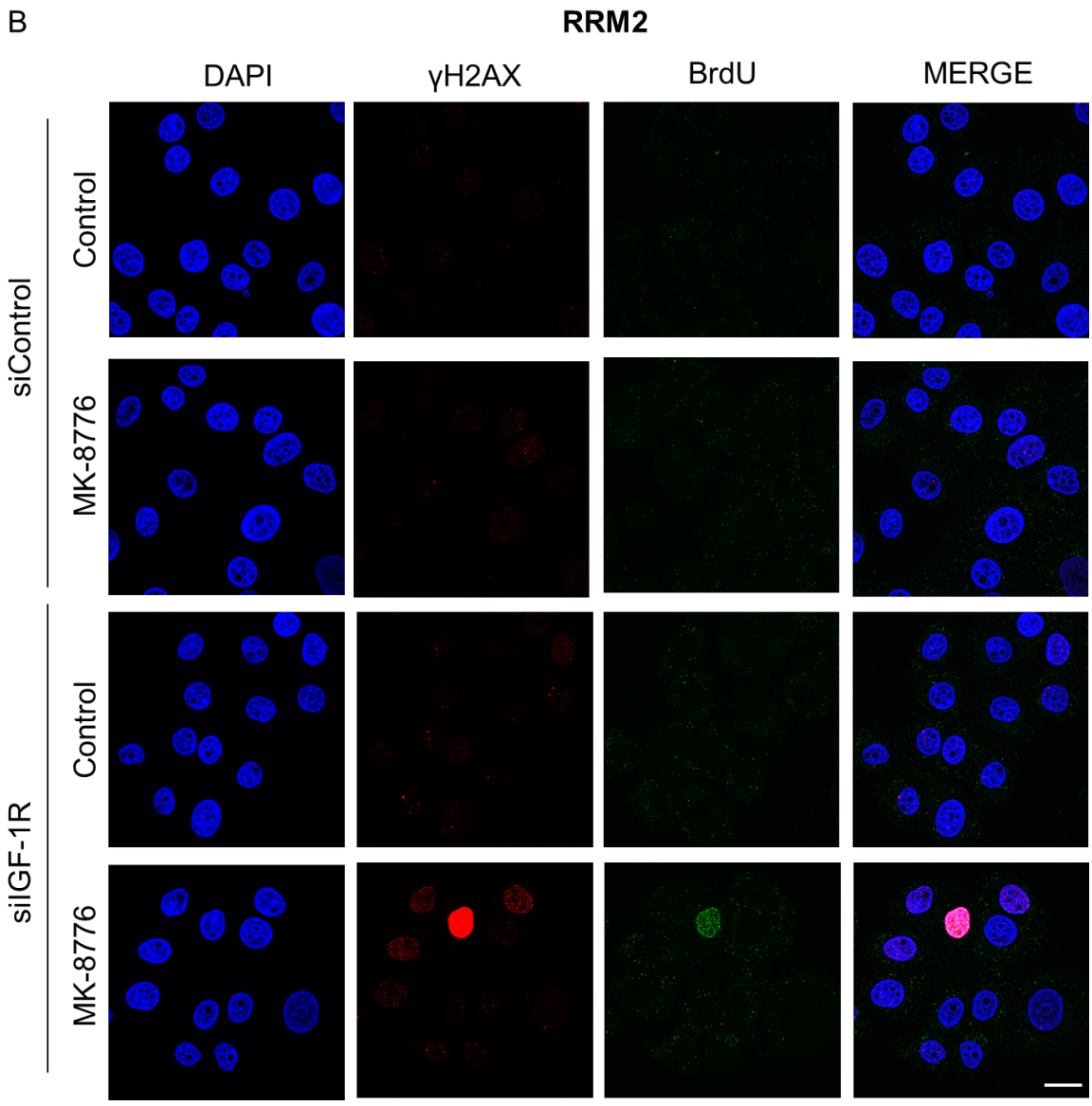
B
RRM2
DAPI
γH2AX
BrdU
MERGE
siControl
siIGF-1R
Control
MK-8776
Control
MK-8776

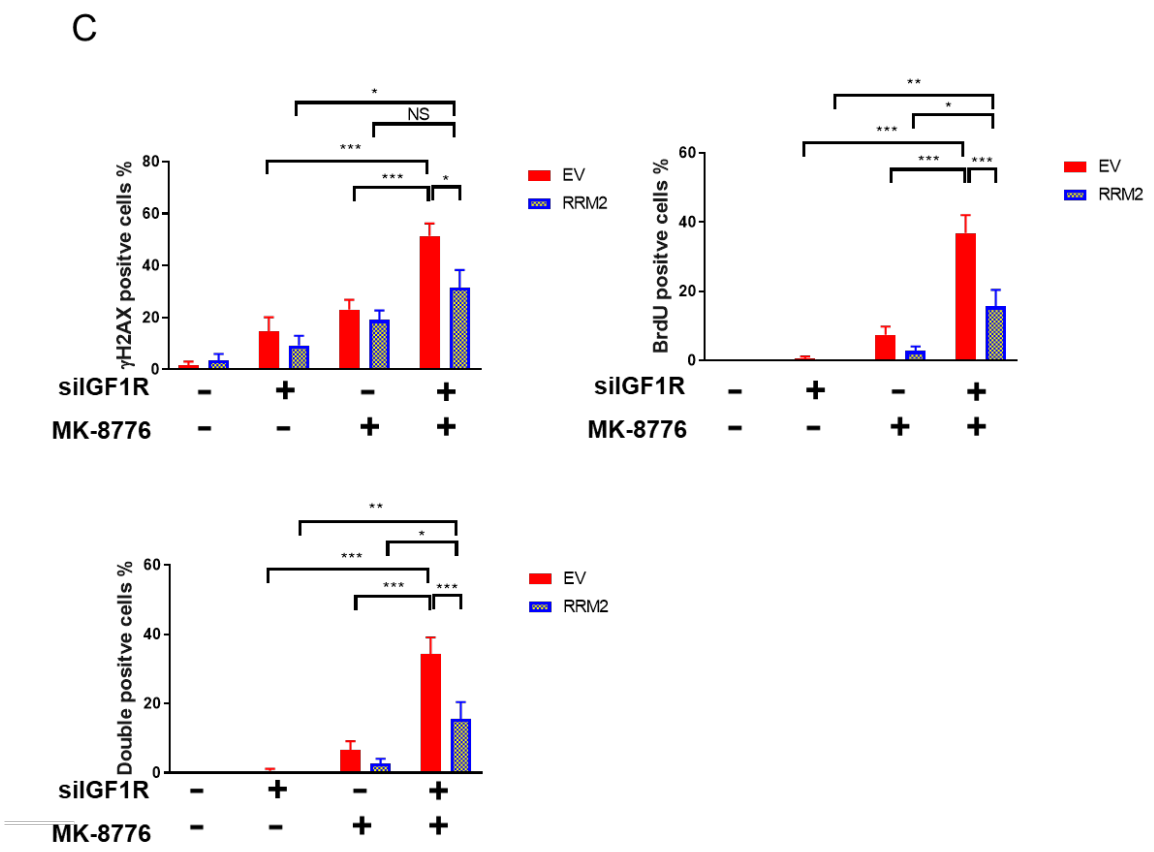

Figure 5.10 RRM2 overexpression alleviates replication stress induced by CHK1 inhibition and IGF-1R depletion

(A-B) Representative images of BrdU and γH2AX immunostaining in empty vector control cells (A) and RRM2-overexpressing cells (B) transfected with siControl or siIGF-1R for 24 hours and then exposed to solvent control or 1 μM MK-8776 for 24 hours. Cells were cultured with 10 μM BrdU for 36 hours before fixation and analysed in non-denaturing condition to detect ssDNA. Nucleus was stained by DAPI. Scale bar: 20 μm. (C) Quantification of γH2AX positive (>10 foci + pan-nuclear staining) and BrdU positive (>5 foci + pan-nuclear staining) cells (≥10 images) shown on the right. Data are represented as mean ± SEM, pooled from 3 independent experiments. One-way ANOVA analysis was applied. ***P < 0.001, **P < 0.01, *P < 0.05.

We have shown that CHK1 inhibition induced cell death in IGF-1R depleted cells (Figure 4.13), associated with exacerbated replication stress. As we found that RRM2 overexpression alleviated replication stress induced by CHK1 inhibition and IGF-1R depletion, we next investigated whether RRM2 overexpression rescued from cell death. Empty vector control cells and RRM2-overexpressing cells were

transfected with siControl or siIGF-1R for 24 hours and then exposed to MK-8776 for 5 days, followed by cell death assay. In empty vector control cells, we found that combining MK-8776 and IGF-1R depletion caused significant increase in cell death, compared with the effect of either treatment alone (Figure 5.11). This is consistent with the observation in parental MCF7 cells (Figure 4.14). In concordance with the rescue effect on replication stress, RRM2 overexpression significantly rescued from cell death caused by MK-8776 and IGF-1R depletion. (Figure 5.11)

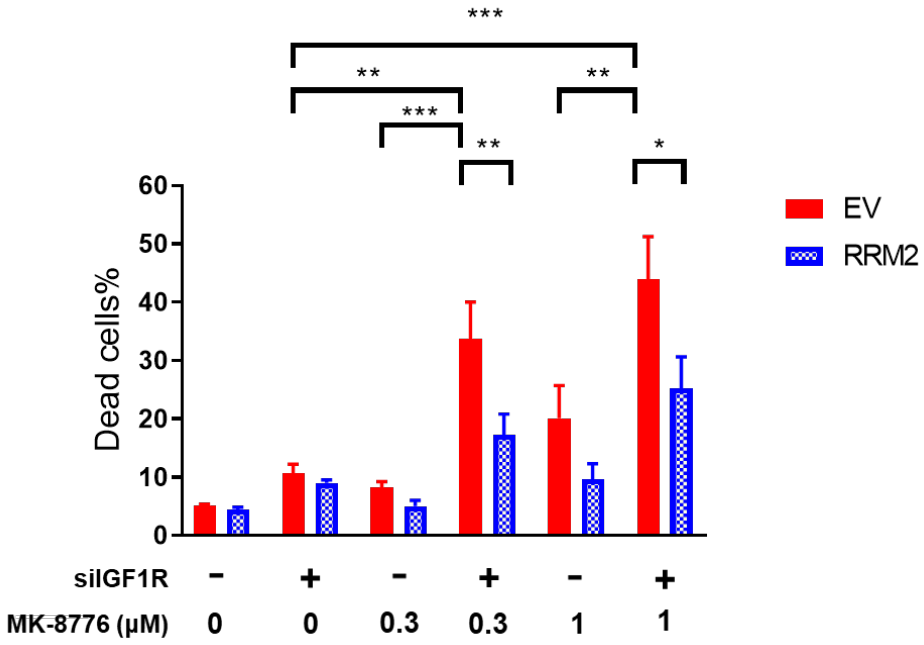

Figure 5.11 RRM2 overexpression rescues from cell death caused by CHK1 inhibition in IGF-1R depleted cells

Empty vector control cells and RRM2-overexpressing cells were transfected with siControl or siIGF-1R for 24 hours and then exposed to solvent control or MK-8776 for 5 days, followed by Propidium iodide/Hoechst 33342 staining. Dead cells% expressed as % PI positive cells/ Hoechst positive cells was determined by Celigo Imaging Cytometer. Data are represented as mean ± SEM, pooled from 3 independent experiments each with 3 technical replicates. One-way ANOVA analysis was used. ***P < 0.001, **P < 0.01.

Together, we showed that CHK1 inhibition markedly reduced RRM2 protein level and induced replication catastrophe after IGF-1R depletion, while RRM2 overexpression restored RRM2 protein, alleviated replication stress, and rescued cell death. These results suggested RRM2 as an important target of the interaction between CHK1 inhibition and IGF blockade.

5.2.5 WEE1 inhibition induces replication catastrophe in IGF-1R depleted cells through downregulating RRM2

So far, we have shown results to support a model that simultaneous inhibition of CHK1 and IGF signalling through downregulating RRM2 induced severe replication stress, causing cell death. This prompted us to consider whether a similar impact on DNA replication and response to IGF blockade could be achieved by any other compounds that are reported to influence RRM2 protein levels. WEE1 is another cell cycle checkpoint kinase whose inhibition has been shown to promote CDK-mediated degradation of RRM2 in S-phase (Pfister et al., 2015). In our compound screen, selective WEE1 inhibitor MK-1775 was identified as a positive hit in KPL1 cells that sensitises cells to BI-836845 (Figure 4.5), although it was not a hit in other 4 cell lines. We first used western blot analysis to assess RRM2 protein level after WEE1 inhibition. MCF7 cells were transfected with siControl or siIGF-1R for 24 hours and then exposed to MK-1775. As expected, MK-1775 decreased the inhibitory phosphorylation of CDK1 at Tyrosine 15 and reduced RRM2 (Figure 5.12 A), consistent with previous findings (Pfister et al., 2015). Importantly, combining IGF-1R depletion with MK-1775 resulted in a further reduction of RRM2 protein levels (Figure 5.12 A, B). We also observed an increase of ATR-induced CHK1 phosphorylation at Serine 345 upon MK-1775 treatment, suggesting the activation of replication stress responses (Figure 5.12 A). Notably, IGF depletion led to an

increase of pCDK1 at tyrosine 15 (Figure 5.12 A), which has not been reported before, but could indicate the increased WEE1 activity after IGF blockade.

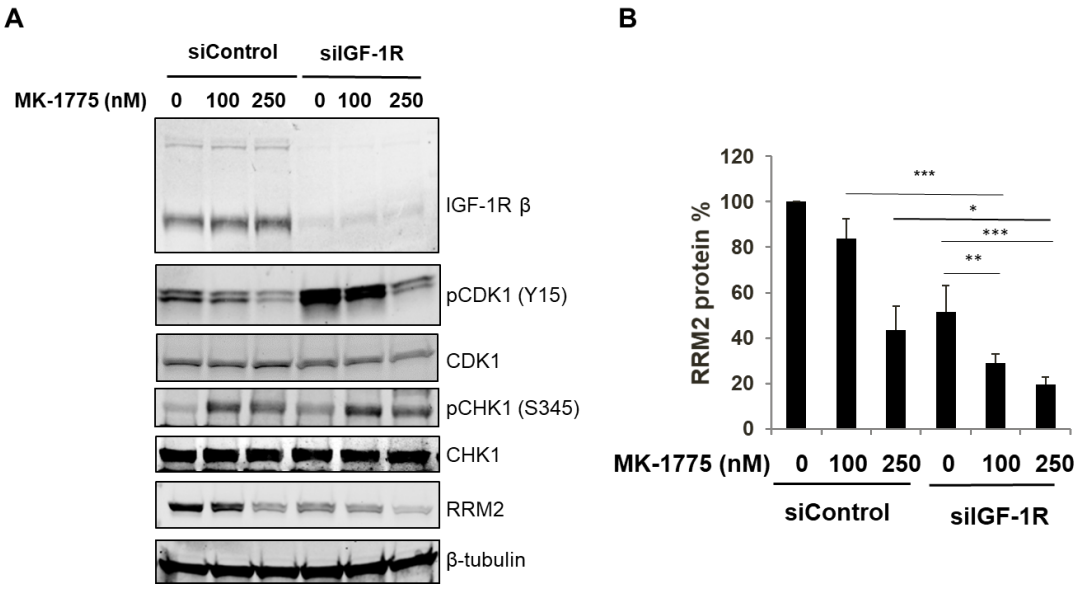

Figure 5.12 WEE1 inhibition further reduces RRM2 protein after IGF-1R depletion

(A) Western blot analysis of MCF7 cells transfected with siControl or siIGF-1R for 24 hours, and then exposed to solvent control or MK-1775 for 24 hours. (B) RRM2 and β-tubulin protein levels were quantified by ImageJ software. RRM2 protein levels were quantified as described in legend to Figure 5.1. Data are represented as mean ± SEM from 3 independent experiments. One-way ANOVA analysis was used. ***P < 0.001, **P < 0.01, **P < 0.05.

We next examined whether WEE1 inhibition sensitised cells to IGF-1R depletion. Cell viability assay and cell death assay were performed in MCF7 cells transfected with siControl or siIGF-1R and then exposed to different concentrations of MK-1775. WEE1 inhibition by MK-1775 reduced cell viability and induced cell death in a dose-dependent manner (Figure 5.13 A, B). We found that IGF-1R depleted cells were more sensitive to MK-1775 in both cell viability assay and cell death assay, compared to siControl cells (Figure 5.13 A, B). We next found that IGF-1R inhibition by BI-346845 or BI885578 also significantly sensitised cells to MK-1775 in cell viability assay, although the combination effect was less than combining MK-1775 with IGF-1R depletion (Figure 5.13 C, D). The drug combination of BI-836845 and MK-1775 was tested in 3D culture using SK-CO-1 spheroids. As shown in Figure 4.18, SK-CO-1 spheroids were sensitive to CHK1 inhibition and IGF blockade. Consistently, BI-836845 alone markedly suppressed SK-CO-1 spheroid growth (Figure 5.13 E). Addition of 300nM or 1 μM MK-1775 led to a further significant reduction of spheroid growth rate (Figure 5.13 E), suggesting a combination effect of co-inhibiting IGF and WEE1 in 3D.

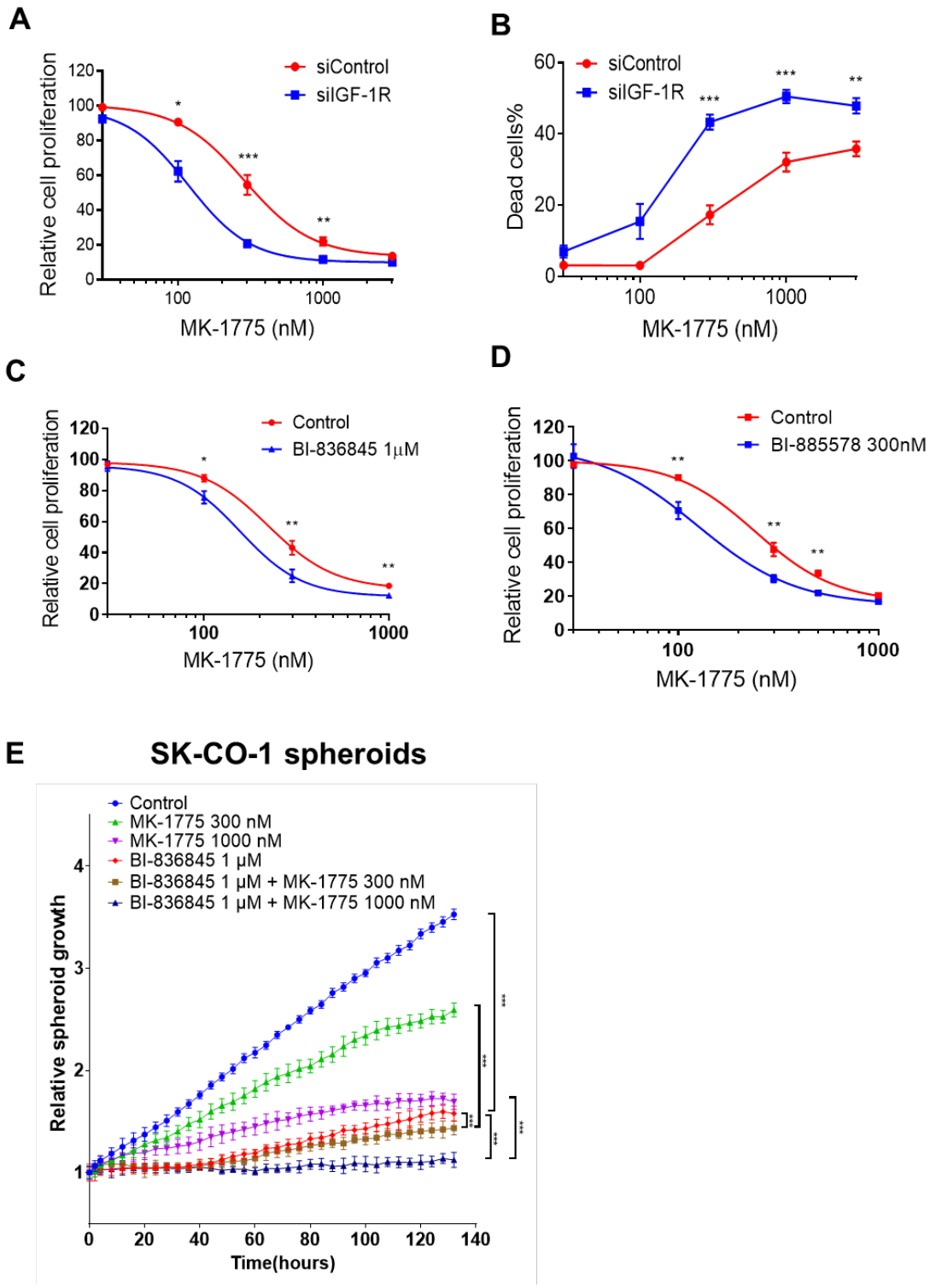

Figure 5.13 IGF-1R depleted or inhibited cells are more sensitive to WEE1 inhibition

(A-B) MCF7 cells were transfected with siControl or siIGF-1R for 24 hours, and then exposed to solvent control or MK-1775 for 5 days, followed by cell viability assay (A) or cell death assay (B). Cell viability was expressed as % viability of siControl cells. Dead cells% was expressed as % PI positive cells/ Hoechst positive cells. (C-D) MCF7 cells were exposed to MK-1775 in the presence or absence of 1 μM BI-836845 (C) or 300 nM BI-

885578 (D) for 5 days, followed by cell viability assay. Data in A, B, C are represented as mean ± SEM, pooled from n=3 independent experiments. Data in D are represented as mean ± SEM, pooled from n=2 independent experiments. Unpaired and two-tailed t test was used. ***P < 0.001, **P < 0.01, *P < 0.05. (E) SK-CO-1 spheroids were exposed to solvent control or MK-1775 in the presence or absence of 1 μM BI-836845 for 6 days. Spheroid growth curves were analysed using spheroid size measured on IncuCyte Live Cell Analysis Imaging System. Results were expressed as % spheroid size on Day 0. Data are represented as mean ± SEM from one experiment with 6 technical replicates. Two-way ANOVA was used. ***P < 0.001.

We next tested whether WEE1 inhibition worsens replication stress induced by IGF-1R depletion. To assess replication fork progression, DNA fiber assay was performed in MCF7 cells transfected with siControl or siIGF-1R for 24 hours and then exposed to MK-1775 for 24 hours. MK-1775 alone led to a significant reduction of DNA fiber length (Figure 5.14 A, B), supporting the important role of WEE1 in maintaining DNA replication. WEE1 inhibition has also been shown to promote CDK1/2-mediated aberrant origin firing (Beck et al., 2012). Our DNA fiber analysis showed that MK-1775 significantly increased newly fired origins (Figure 5.14 A, B). Combining MK-1775 with IGF-1R depletion further suppressed replication fork progression, resulting in much shorter DNA fibers, but not further affected origin firing (Figure 5.14 A, B). In addition, cell cycle analysis in MCF7 cells showed that combining MK-1775 with IGF-1R depletion caused the accumulation of cells in non-replicating S-phase, whereas MK-1775 or IGF-1R depletion alone had no effect (Figure 5.14 C, D). These data suggested that combining WEE1 inhibition and IGF-1R depletion suppressed DNA replication in S phase.

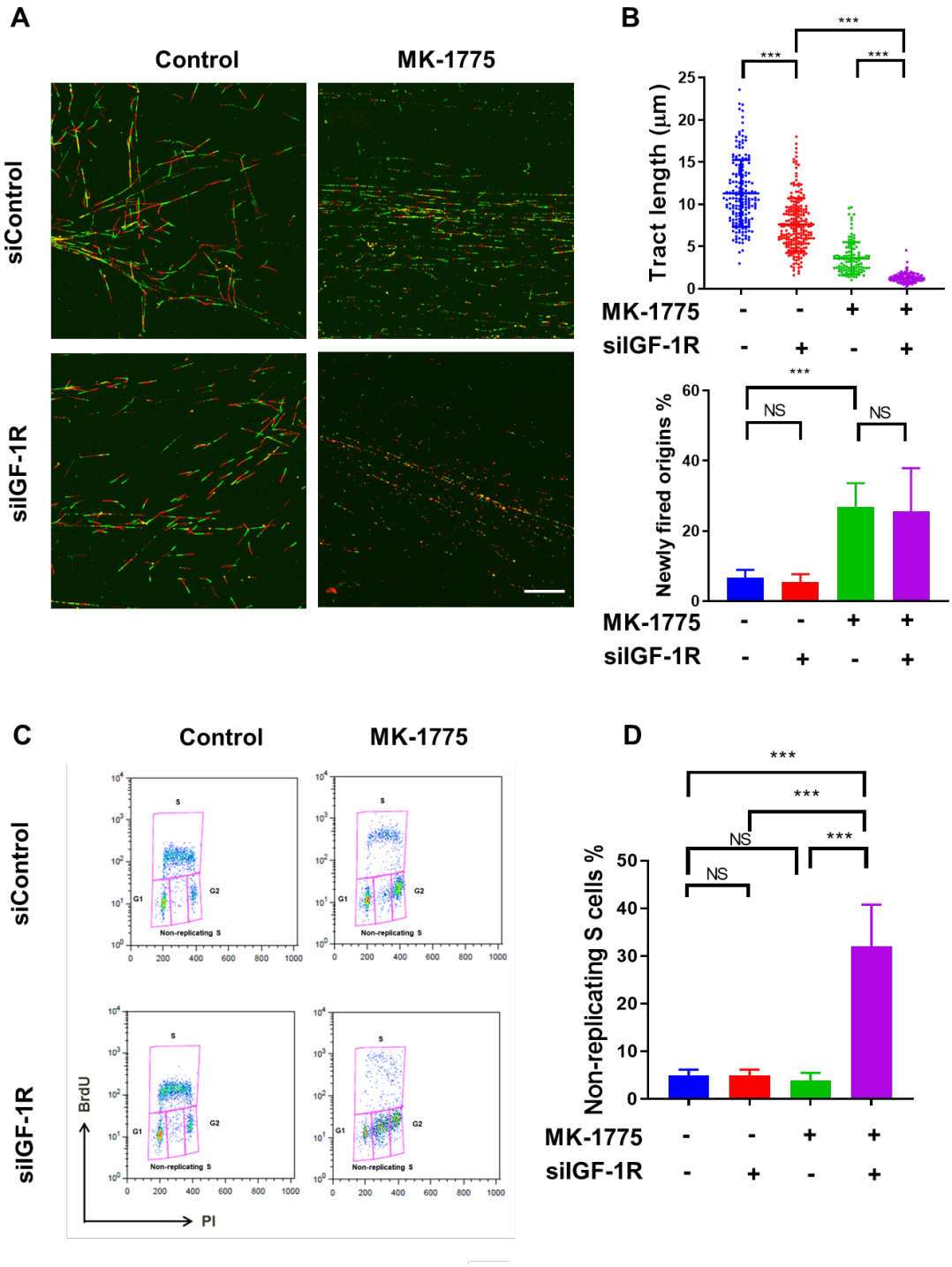

Figure 5.14 WEE1 inhibition suppresses DNA replication in IGF-1R depleted cells

(A) Representative images of DNA fiber tract (CIdU (Red), IdU (Green)) in MCF7 cells transfected with siControl or siIGF-1R for 24 hours and then exposed to solvent control or 300 nM MK-1775 for 24 hours. Scale bar: 20 µm. (B) Quantification of fiber tract length (>150 tracts) and newly fired origins (IdU (green)-only tracts as percentages of the total number of tracts (⩾ 5 images in A)) was shown on the right. Data are represented as mean ± SEM. This experiment was performed only once. One-way ANOVA was applied. ***P < 0.001. (C) BrdU FACS analysis of cell cycle distribution of MCF7 cells transfected with

siControl or siIGF-1R for 24 hours and then exposed to solvent control or 300 nM MK-1775 for 24 hours. (D) Quantification of non-replicating S phase cells in C. Data are represented as mean ± SD, pooled from 3 independent experiments. One-way ANOVA analysis was used. ***P < 0.001, **P < 0.01.

To further investigate replication stress upon WEE1 inhibition, we next performed double immunostaining assay to assess the cellular levels of γH2AX and ssDNA. MCF7 cells were transfected with siControl or siIGF-1R for 24 hours and then exposed to MK-1775 for 24 hours. Similar to the observation in CHK1-inhibited cells, WEE1 inhibition by MK-1775 also promoted γH2AX foci formation and accumulated cells with γH2AX pan-nuclear staining (Figure 5.15). The quantification results showed that combining MK-1775 with IGF-1R depletion led to a significant accumulation of γH2AX positive cells, compared to effect of either treatment alone (Figure 5.15). We also detected more BrdU positive cells upon MK-1775 treatment and IGF-1R depletion, indicating a higher level of ssDNA (Figure 5.15). Moreover, MK-1775 caused accumulation of 8.57 ± 2.23 % double positive cells after siControl transfection, whereas 25.07 ± 3.56 % double positive cells were detected upon MK-1775 treatment after IGF-1R depletion (Figure 5.15), suggesting that the combination of MK-1775 and IGF-1R depletion had an additive effect to induce replication stress. Collectively, these results suggested that WEE1 inhibition exacerbated replication stress induced by IGF blockade to intolerable levels, suggesting replication catastrophe.

A

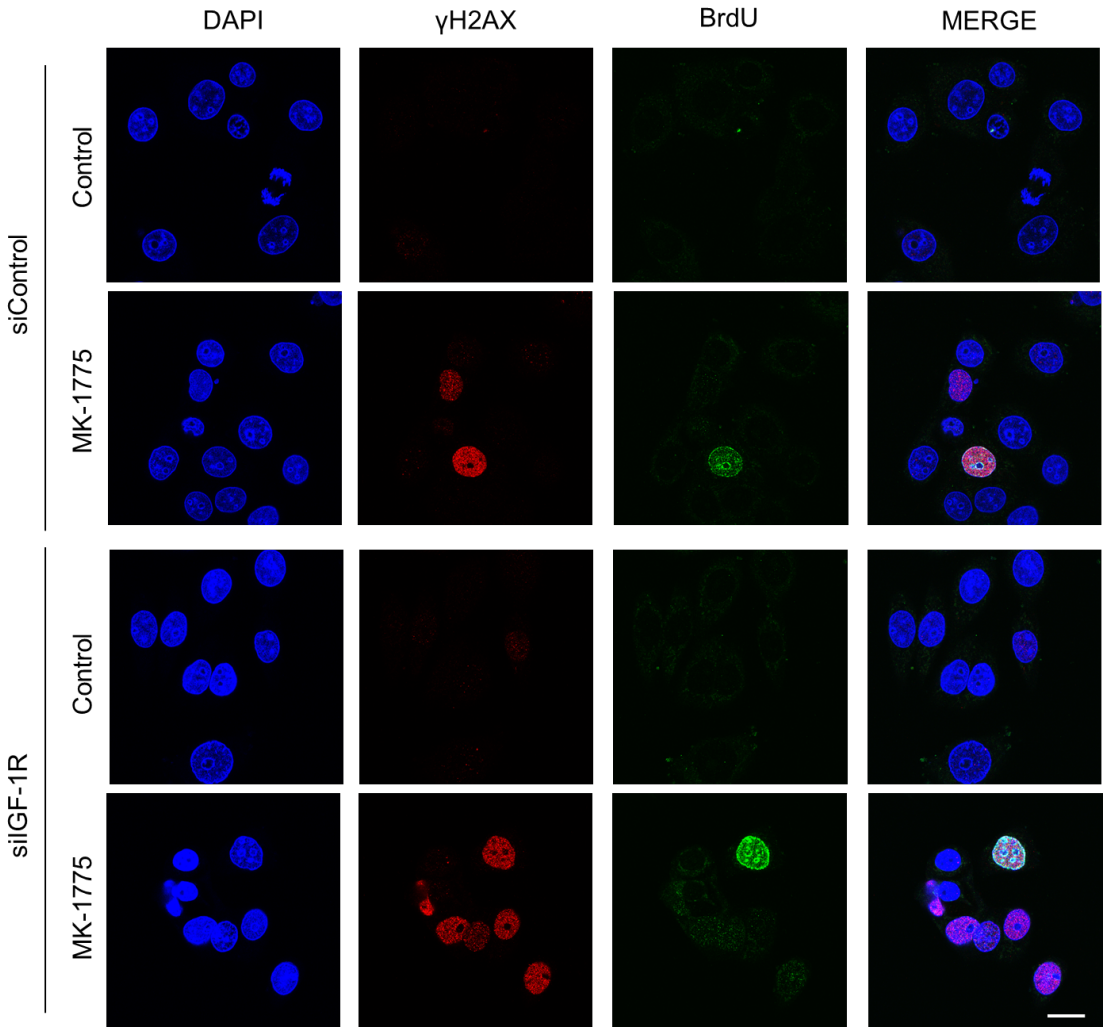

B

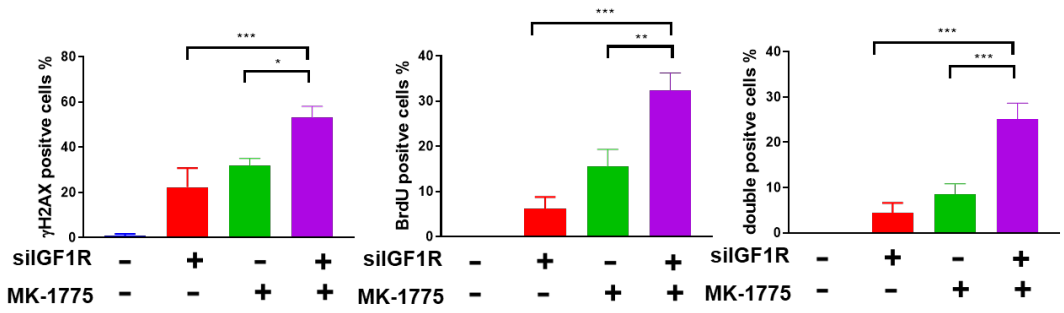

Figure 5.15 WEE1 inhibition induces the accumulation of ssDNA and DNA damage in IGF-1R depleted cells

(A) Representative images of BrdU and γH2AX immunostaining in MCF7 cells transfected with siControl or siIGF-1R for 24 hours and then exposed to solvent control or 300 nM MK-

1775 for 24 hours. Cells were cultured with 10 μM BrdU for 36 hours before fixation and analysed in non-denaturing condition to detect ssDNA. Nucleus was stained by DAPI. Scale bar: 20 μm. (B) Quantification of γH2AX positive (>10 foci + pan-nuclear staining) and BrdU positive (>5 foci + pan-nuclear staining) cells (≥10 images) shown on the right. Data are represented as mean ± SEM, pooled from 3 independent experiments. One-way ANOVA analysis was applied. ***P < 0.001, **P < 0.01, *P < 0.05.

We next investigated whether WEE1 inhibition sensitised cells to IGF blockade via targeting RRM2 by using Empty vector control cells and RRM2 overexpressing cells. These cells were transfected with siControl or siIGF-1R for 24 hours and then exposed to MK-1775 for 5 days. The viability assay results in empty vector control cells were consistent with data in parental MCF7 cells (Figure 5.13 A) that IGF-1R depletion sensitised cells to MK-1775, with a >2-fold decrease of GI50 (Figure 5.16 A, B). IGF inhibition by BI-836845 reduced the GI50 for MK-1775 from 690 nM to 392 nM, suggesting a combination effect of WEE1 inhibition and IGF blockade (Figure 5.15 C, D). RRM2 overexpression shifted the MK-1775 dose-response curves to the right (Figure 5.16 A, C). This resulted in the increased GI50s for MK-1775 with GI50 values >1000 nM in control-treated or control-transfected cells (Figure 5.16 B, D). In RRM2-overexpressing cells in which IGF signalling was compromised, the growth response curves were lower, with GI50 values of 882 nM upon IGF-1R depletion and 957 nM upon 1 μM BI-836845 treatment. This inhibitory response to MK-1775 was comparable to viability in control-treated/transfected EV cells but was less growth inhibitory than was induced by MK-1775 in IGF-1R-depleted or BI-836845-treated EV cells (Figure 5.16 B, D). These results suggested at least a partial rescue effect of RRM2 overexpression on cell proliferation upon WEE1 inhibition and IGF blockade. Together, these data supported our hypothesis that WEE1 inhibition induced replication catastrophe in IGF-1R depleted cells via downregulating RRM2.

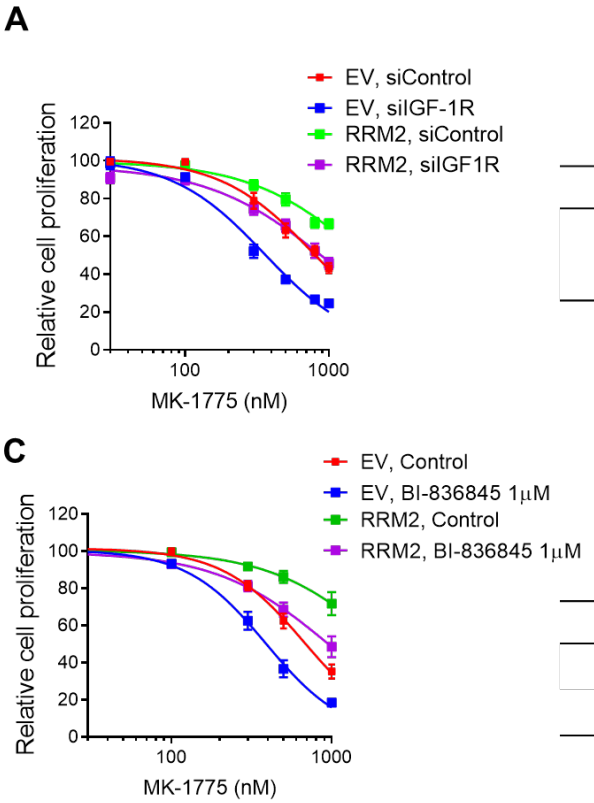

B

GI50 (95%CI, nM) for MK-1775

	EV	RRM2
siControl	806 (737-895)	>1000
siIGF-1R	364 (334-395)	883 (>778)

D

GI50 (95%CI, nM) for MK-1775

	EV	RRM2
Control	691 (631-764)	>1000
BI-836845	392 (353-433)	958 (>811)

Figure 5.16 RRM2 overexpression rescues cell proliferation upon WEE1 inhibition and IGF blockade

(A) Empty vector control cells and RRM2-overexpressing cells were transfected with siControl or siIGF-1R for 24 hours and then exposed to solvent control or MK-1775 for 5 days, followed by cell viability assay. Results were expressed as % viability of solvent-treated control. Data are represented as mean ± SEM, pooled from n=3 independent experiments; (B) GI50 values and 95% confidence intervals were calculated based on the drug response curves in A; (C) Empty vector control cells and RRM2-overexpressing cells were exposed to solvent control or MK-1775 in the presence or absence of 1 μM BI-836845 for 5 days, followed by cell viability assay. Results were expressed as % viability of solvent-treated control. Data are represented as mean ± SEM, pooled from n=3 independent experiments; (D) GI50 values and 95% confidence intervals were calculated based on the drug response curves in C.

5.3 Discussion

In this chapter, we demonstrated that combining CHK1 inhibition with IGF blockade downregulated RRM2 and reduced dNTP availability. We further showed that overexpressing exogenous RRM2 rescued replication stress phenotype in cells upon CHK1 inhibition and IGF-1R depletion, suggesting RRM2 as an important target of the interaction between CHK1 inhibition and IGF blockade. Notably, the rescue by RRM2 overexpression was partial in most experiments. This could be due to the reduction in endogenous RRM2 in RRM2 overexpressing cells. The residual RRM2 levels in RRM2-overexpressing cells after IGF depletion was comparable to levels in untreated control cells (Figure 5.4), and thus showed similar dose-response curves to MK-8776 (Figure 5.7).

Because of the critical role of RRM2 in maintaining dNTP homeostasis, RRM2 has been recognised as a promising prognostic biomarker and therapeutic target in cancers (Aye et al., 2015; Fisher et al., 2013; Tang et al., 2013). Our data suggested that IGF blockade caused the reduction of RRM2 protein levels. Dr Rieunier in our group found that RRM2 mRNA levels paralleled the decrease in protein expression after IGF-1R depletion or inhibition, suggesting that IGFs regulate RRM2 mainly at the transcription level. It is possible that IGF-1R depleted or inhibited cells depend on residual RRM2 to limit replication stress within a tolerable level and maintain cell survival. Thus, targeting the residual RRM2 in IGF-inhibited cells might be a potential therapeutic strategy to sensitise cancer cells to IGF-targeted therapy. Here we demonstrated that targeting CHK1 was an effective approach to further deplete RRM2 protein after IGF blockade, leading to cell death.

We further showed that targeting WEE1 also sensitised cells to IGF blockade through downregulating RRM2. Abrogating cell cycle checkpoints by CHK1 or

WEE1 inhibition has been reported as an effective approach to reduce RRM2 protein, deplete dNTP pools and suppress DNA replication in S phase that may have implications for cancer treatment (Buisson et al., 2015; Koppenhafer et al., 2020; Pfister et al., 2015). Our data in this chapter demonstrated that IGF-1R depleted or inhibited cells had low levels of RRM2 protein and thus were more sensitive to CHK1 or WEE1 inhibition, suggesting a rationale for drug combinations of CHK1 or WEE1 inhibitors and IGF-targeted drugs for cancer treatment.

Chapter 6

General summary and discussion

6.1 IGF blockade reduces RRM2 protein expression

In this study, we first confirmed the previous findings by Dr Rieunier in our group that IGF blockade induces replication stress in breast cancer cells. We showed that either genetic depletion of IGF-1R or pharmacological inhibition of IGF signalling slowed replication fork progression and accumulated endogenous DNA lesions (Figure 3.3- 3.5). A previous study suggested that RRM2, the regulatory subunit of RNR, a key enzyme in mediating cellular dNTP pools for DNA replication, is regulated by mTORC1 signalling at both transcriptional and translational levels (He et al., 2017). In agreement with this report, recent unpublished work in our group by Dr Rieunier suggested that IGF-1R signalling through both PI3K/ATK/mTOR and MAPK pathways regulates RRM2 expression (Figure 6.1 left), in concordance with a previous report that RRM2 is a component of IGF-induced transcriptional signature in breast cancer cells (Creighton et al., 2008). Consistently, in this study we showed that IGF-1 activated downstream signalling and elevated RRM2 expression, while IGF signalling blockade reduced RRM2 protein levels (Figure 5.1).

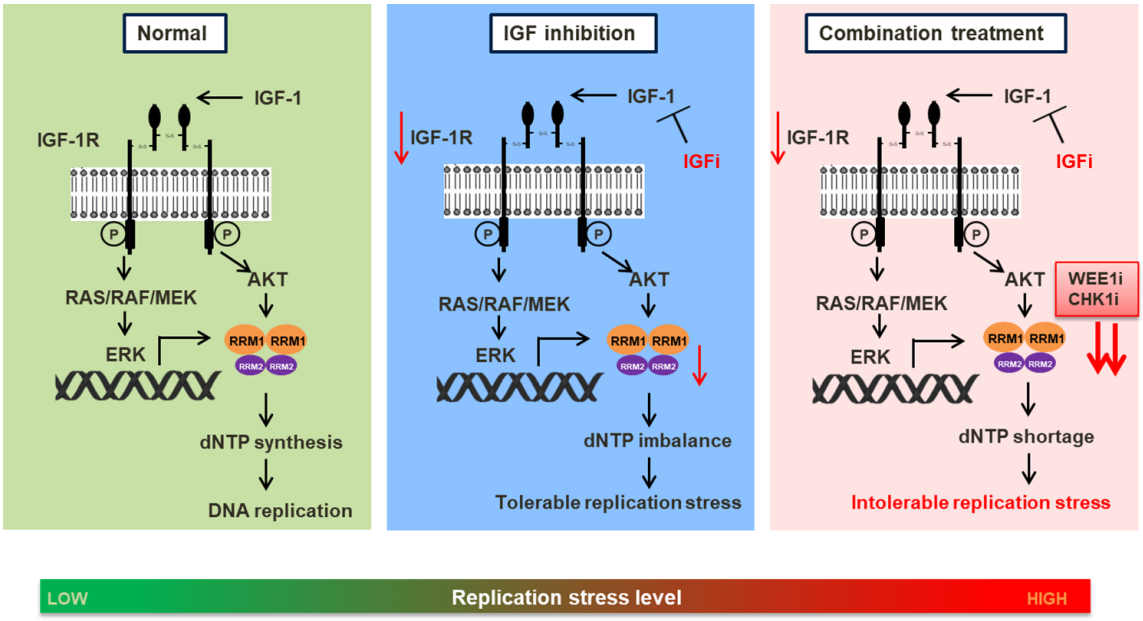

Figure 6.1 CHK1 or WEE1 inhibition exacerbates replication stress induced by IGF blockade via downregulating RRM2

Left: IGF signalling regulates RRM2 protein expression through both PI3K/AKT and MEK/ERK pathways to maintain dNTP de novo biosynthesis, supporting DNA replication. **Middle:** IGF signalling blockade by either IGF-1R depletion or IGF inhibition downregulates RRM2 protein expression via reduced PI3K/AKT and MEK/ERK signalling, resulting in dNTP imbalance and tolerable replication stress. **Right:** Upon IGF signalling blockade, the addition of CHK1 inhibitor or WEE1 inhibitor further reduces RRM2 protein levels and dNTP supplies, thus exacerbating replication stress to intolerable replication catastrophe.

The link between RRM2 downregulation and replication stress has been described in a number of studies. For example, BCL2, an anti-apoptotic and oncogenic protein, directly interacts with RRM2 via its BH4 domain activity, resulting in the reduction of RNR activity and replication stress (Xie et al., 2014a). Oncogenic RAS activation and tumour suppressor BRCA1 loss in cancers have been reported to suppress RRM2 expression, leading to replication stress and genomic instability (Aird et al., 2013; Rasmussen et al., 2016). Unpublished data generated by Dr Rieunier in our group suggested that BRCA1 deficient breast cancer cells are more sensitive to IGF-1R depletion compared with BRCA1 wild-type cells when assessed in cell proliferation and DNA fiber assays. These results are in line with the synergistic

interaction of targeting IGF-1R and BRCA1 loss shown in studies by other groups (Amin et al., 2015; Kang et al., 2012). Whether BRCA1-mediated RRM2 expression plays a role in protecting IGF-1R depleted or inhibited cells from replication stress may be worthy of future investigation.

6.2 CHK1 or WEE1 inhibition exacerbates replication stress induced by IGF blockade

The replication stress phenotype was striking in cells upon IGF-1R depletion or IGF inhibition, but the effect on cell proliferation was moderate and no substantial cell death was observed (Figure 3.1, 3.2, 4.14). IGF-1R depleted or IGF inhibited cells were still able to undergo DNA replication and cell proliferation, albeit at a slower rate, suggesting that replication stress induced by IGF blockade was tolerable. We hypothesised that cancer cells after IGF blockade might activate replication stress and DNA damage response cascades to resolve toxic replication intermediates, thus limiting the replication stress to within a tolerable threshold. Indeed, Dr Rieunier's unpublished results showed that replication stress induced by IGF-1R blockade was accompanied by ATR-induced CHK1 phosphorylation at Serine 345 and accumulation of cells in S phase. We reasoned that although replication stress induced by IGF blockade was tolerable for tumour cells, this might be an exploitable vulnerability for cancer treatment. My project aimed to develop approaches to exacerbate IGF blockade-induced replication stress to intolerable level, causing cell death. Therefore, we performed a compound screen in breast cancer cells to test drug combinations with IGF ligand neutralising antibody drug BI-836845, which is also known as xentuzumab and currently under evaluation in several ongoing clinical trials (discussed in section 1.1.4). We identified several positive hits whose inhibition sensitised breast cancer cells to IGF inhibition, including CHK1 and ATM

(Figure 4.7), which haven't been shown as effective treatment partners for combining IGF-1R inhibitors in any published studies. Validation experiments in multiple cancer cell lines in this study (Figure 4.8, 4.15-4.18) and unpublished work by Dr Rieunier substantiated the combinational or synergistic effect of co-targeting CHK1 or ATM and IGF signalling in both conventional 2D cell culture and 3D spheroid culture models.

Given that activating CHK1 by ATR signalling is one of the major replication stress response events (Cimprich and Cortez, 2008), targeting ATR/CHK1 pathway is a potential approach to induce replication stress. We showed that CHK1 inhibitor suppressed CHK1 autophosphorylation at Serine 296, while surprisingly enhanced ATR-induced phosphorylation at Serine 345 (Figure 5.2). This could be the feedback activation by suppressing PP2A phosphatase (Leung-Pineda et al., 2006), but might also indicate the enhanced replication stress after CHK1 inhibition. Indeed, inhibiting ATR/CHK1 signalling has been shown to increase replication stress by accumulating ssDNA and exhausting RPA (Buisson et al., 2015; Toledo et al., 2013). Consistently, we detected the increase of ssDNA and γH2AX foci in cells upon CHK1 inhibitor treatment (Figure 4.13). We further showed that CHK1 inhibition slowed replication fork progression in DNA fiber assay (Figure 4.10, 4.11). These data supported the concept that targeting CHK1 induces replication stress, which prompted us to investigate whether CHK1 inhibition can exacerbate replication stress induced by IGF blockade to intolerable levels, causing cell death. Our hypothesis was supported by our data that addition of CHK1 inhibitor upon IGF-1R depletion led to a further suppression of DNA replication and dramatic accumulation of ssDNA and DNA damage (Figure 4.13). It would have been interesting to check whether the accumulation of ssDNA leads to the increase of RPA protein on

chromatin, which can be detected by immunostaining, and immunoblot after chromatin fractionation (Buisson et al., 2015; Toledo et al., 2013). We further showed that combining CHK1 inhibition and IGF blockade markedly increased cell death, compared to the effect of either treatment alone (Figure 4.14). These results collectively suggested that combining CHK1 inhibition and IGF blockade induced replication catastrophe. Notably, we found that inhibiting ATR did not sensitise breast cancer cells to IGF inhibition in our compound screen (Figure 4.2 - 4.6) and the validation experiments performed by Dr Rieunier. We reasoned that ATR inhibition could activate DNA-PK/CHK1-mediated backup pathway as reported by Buisson *et al.* (Buisson et al., 2015), and therefore might be less effective than CHK1 inhibition to exacerbate replication stress induced by IGF blockade.

We next demonstrated that CHK1 inhibition exacerbated replication stress induced by IGF blockade via further downregulating RRM2 protein (Figure 6.1 middle and right). It has been reported that cell cycle checkpoint abrogation via ATR/CHK1 or WEE1 inhibition activates CDKs-mediated RRM2 degradation, inducing replication stress (Buisson et al., 2015; Koppenhafer et al., 2020; Pfister et al., 2015). In this study, we showed that the addition of CHK1 inhibitor further reduced RRM2 levels after IGF blockade (Figure 5.2, 5.3). In support of the critical role of RRM2 in mediating dNTP synthesis (Mathews, 2015), the reduction in RRM2 protein levels upon CHK1 inhibition and IGF blockade was reflected in the reduction of cellular dNTPs (Figure 5.4). We utilised the method using radiolabelled polymerase reactions *in vitro* (described in section 2.12), which appeared to be more sensitive than the HPLC assay previously used in our group and allowed detection of all dNTPs. By investigating the cells exogenously overexpressing RRM2 generated in this study, we showed that RRM2 overexpression significantly rescued the

replication catastrophe phenotype in cells upon CHK1 inhibition and IGF blockade (Figure 5.6-5.11). Of note, a previous study in a transgenic mouse model showed that constitutive RRM2-overexpression reduced chromosomal breakage at fragile sites in response to ATR inhibition and extended the life span of ATR mutant mice (Lopez-Contreras et al., 2015). It has been reported that WEE1 inhibition is also capable of reducing RRM2 protein in a similar mechanism involving CDK-mediated degradation (Pfister et al., 2015). Our data demonstrated that WEE1 inhibition also sensitised cells to IGF depletion by exacerbating replication stress via RRM2 downregulation, similar to the effect of CHK1 inhibition (Figure 5.12-5.16). Notably, we observed that RRM2 overexpression completely restored RRM2 protein levels, but only partially rescued cell proliferation suppression and cell death upon CHK1 or WEE1 inhibition and IGF blockade (Figure 5.7, 5.11, 5.15). This could be due to the endogenous RRM2 downregulation induced by IGF-1R depletion in RRM2 overexpressing cells (Figure 5.4). It has been previously shown that targeting ATR/CHK1 signalling activates CDC7 and CDK2-mediated origin firing through reducing the interaction between Replication Timing Regulatory Factor 1 (RIF1) and Protein phosphatase 1 (PP1) via CDK1-dependent phosphorylation (Moiseeva et al., 2019). Thus, it could be possible that CHK1 or WEE1 inhibition reduces dNTP pool through downregulating RRM2 protein levels and elevating origin firing in parallel, which might explain the partial rescue effect of RRM2 overexpression. It is tempting to speculate that restoring dNTP pool might lead to a better rescue effect. Unfortunately, we failed to obtain significant biological results of rescuing from viability inhibition when we tried to supplement cells with exogenous dNTPs upon CHK1 inhibition and IGF blockade. This might be due to fact that we were unable to precisely manipulate the levels of four individual dNTPs, suggesting the necessity

of determining the uptake efficiency of exogenous dNTPs, and a more accurate and quantitative method to measure cellular dNTP concentrations. Moreover, nucleoside mixtures are more commonly used to restore cellular dNTP pool since nucleosides are easier for cells to uptake than nucleotides (Bester et al., 2011). It might be beneficial to supplement cells with nucleoside mixtures in future rescue experiments. Moreover, previous studies targeting cell cycle checkpoints suggested that CHK1 or WEE1 inhibition promotes mitotic catastrophe in cancer cells exposed to DNA damaging agents, such as cisplatin, gemcitabine, PARP inhibitors (Gadhikar et al., 2013; Kim et al., 2017; Rajeshkumar et al., 2011). It would be interesting to investigate whether CHK1 or WEE1 inhibition can facilitate premature mitotic entry in IGF-1R depleted or inhibited cells.

6.3 Potential implications for design of future clinical trials

In this study, we identified the effective drug combinations of IGF neutralising antibody drug BI-836845 with CHK1 inhibitor MK-8776 or WEE1 inhibitor MK-1775, and validated their efficacies in 2D and 3D culture models *in vitro* (Figure 4.8, 4.15, 4.17, 4.18, 4.19, 5.13). All three drugs are currently under evaluation in clinical trials at different stages (discussed in Chapter 1). Although IGF-1R TKI BI-885578 appeared to be more potent than BI-836845, BI-885578 is not being tested clinically. Aiming to test the potential of the drug combinations as clinical therapies, current ongoing work in our lab is assessing the efficacies of MK-8776 and BI-836845 combination *in vivo*. Our *in vitro* data suggested that the drug combination of MK-8776 and BI-836845 was synergistic in SK-CO-1 spheroids in 3D culture (Figure 4.17). Unfortunately, the preliminary data from our current mouse experiment showed a slow growth rate of SK-CO-1 xenografts, even in mice treated with solvent control. This could reflect growth inhibitory effects of the solvent (2-Hydroxypropyl)-

beta-cyclodextrin as reported by Yamaguchi *et al.* (Yamaguchi et al., 2015). It may be worthwhile testing the drug combination of BI-836845 and SRA737, another CHK1 inhibitor that uses castor oil as solvent (Booth et al., 2018) since we have shown that SRA737 significantly sensitised SK-CO-1 and HeLa spheroids to BI-836845 *in vitro* (Figure 4.18, 4.19). We could also test the drug combinations of MK-8776 or SRA737 and BI-836845 in HeLa xenografts as we also demonstrated a combination effect in HeLa spheroids in 3D (Figure 4.16, 4.19). If the *in vitro* test of the combinations of CHK1 inhibitors and BI-836845 can translate to *in vivo* efficacy, these results will have potential to inform future clinical trials.

Our analysis of the compound screen of drug combinations highlighted ATM as another novel target that sensitised cells to IGF inhibition. ATM is a master regulator in mediating DNA damage responses (Shiloh, 2003). ATM signalling also responds to replication stress particularly under hypoxic conditions (Olcina et al., 2013). Moreover, ATM is involved in dNTP pool regulation by reprogramming glucose and glutamine metabolic pathways during replication stress-induced senescence (Aird et al., 2015). Current work in our lab by Dr Rieunier demonstrated ATM inhibition can convert SSBs that resulted from IGF blockade-induced replication stress to toxic DSBs, causing synergistic cell death. These results reflected the critical role of ATM in coordinating SSB repair and cell cycle progression during replication stress (Khoronenkova and Dianov, 2015). The synergistic interaction between ATM inhibition and IGF blockade has important therapeutic implications. First, this provides a molecular rationale to combine clinical ATM inhibitors with IGF-targeted drugs for cancer treatment. Secondly, unlike CHK1 in which so far homozygous mutations in human cancers haven't been reported (Zhang and Hunter, 2014), ATM mutation or deletion was observed in human breast, prostate and endometrial

cancers (Rafiei et al., 2020). ATM status in patients might serve as a predictive biomarker for sensitivity to IGF inhibitors, which provides guidance to select patients for clinical trials of IGF-targeted therapy.

6.4 Potential implications for anti-cancer immune response

In this study, we demonstrated a strong replication stress phenotype in cells upon IGF blockade and CHK1 inhibition. Using the established native BrdU labelling method, we evaluated the levels of ssDNA in nucleus, which is highly correlated to the levels of replication stress (Figure 4.13, 5.9, 5.14). Interestingly, we also observed BrdU staining in cytoplasm especially in cells after combination inhibition of CHK1 and IGF-1R, which might indicate the presence of cytoplasmic ssDNA fragments. It has been well-established that cytoplasmic self-DNA triggers innate immune responses through activating cGAS-STING pathway (Kwon and Bakhoum, 2020). Specifically, cytoplasmic DNA is recognised by cyclic guanosine monophosphate–adenosine monophosphate (cyclic GMP–AMP) synthase (cGAS), driving the production of cyclic guanosine monophosphate–adenosine monophosphate (cGAMP) protein (Sun et al., 2013; Wu et al., 2013). The accumulation of cGAMP protein in cytoplasm actives Stimulator of interferon genes (STING) protein, which is a dimeric endoplasmic reticulum-binding protein (Ishikawa and Barber, 2008). Upon binding with cGAMP, STING undergoes oligomerisation and recruits TANK-binding kinase 1 (TBK1) that sequentially phosphorylates interferon response factor 3 (IRF3) proteins, which translocate to nucleus and promote the transcription of Type I interferon (IFN) genes (Ishikawa et al., 2009). STING also activates protein members of NF-κB pathway, which stimulate the transactivation of immune and inflammatory genes (Ishikawa et al., 2009). Type I IFN pathways stimulate cytotoxic T-cell activation, which could be tumour

suppressive in the context of some cancer treatments (Kwon and Bakhoum, 2020). For example, previous studies have reported that Type I IFN signalling is induced upon chemotherapy or radiotherapy that contributes to their anti-tumour effects (Deng et al., 2014; Sistigu et al., 2014).

It is still not very clear how these cytoplasmic-self DNA fragments are generated. It has been reported that DNA damage induced by IR or genotoxic chemicals can be released to cytoplasm, which requires the end resection by Bloom syndrome helicase (BLM) and Exonuclease 1 (EXO1), resulting in the accumulation of cytoplasmic ssDNA that triggers Type I IFN release (Erdal et al., 2017). However, the role of BLM in mediating the production of cytoplasmic DNA remains a matter of controversy since Gratia *et. al.* reported that accumulation of cytoplasmic micronuclei was increased in BLM-deficient fibroblasts, leading to the upregulation of cGAS-STING signalling (Gratia et al., 2019). Deficiencies in DSB repair machinery, such as BRCA2 loss and PARP inhibition, lead to the accumulation of cytoplasmic micronuclei that have also been shown to activate cGAS-STING signalling (Reisländer et al., 2019). The link between replication stress and the activation of innate immune response is a relatively new concept. Recently, the association between replication stress and upregulated cGAS-STING pathway was demonstrated in Hutchinson-Gilford progeria syndrome (HGPS) cells (Kreienkamp et al., 2018). Another recent study suggested that Sterile alpha motif and HD domain-containing protein 1 (SAMHD1) plays a critical role in promoting the degradation of nascent DNA at stalled forks in a MRE11-dependent manner, which can prevent the release of cytoplasmic DNA (Coquel et al., 2018). We can speculate that the protective role of SAMHD1 at replication fork might create a threshold such that DNA fragments are cleaved and released to cytoplasm under high replication

stress. To what extent the cytoplasmic DNA potentially induced by replication stress can trigger cGAS-STING pathway remains to be elucidated. It might be interesting to consider whether replication stress induced by IGF blockade can trigger innate immune response. Future experiments may seek to use different techniques to detect other forms of DNA fragments in cytoplasm, such as cytoplasmic dsDNA, which can be detected by PicoGreen DNA staining (Parkes et al., 2017). It has been reported that genotoxic stress activates innate immune responses in the context of compromised ATR/CHK1 and ATM/CHK2 functions (Dillon et al., 2019; Härtlova et al., 2015). If IGF blockade is capable of activating cGAS-STING pathway, it is very likely that targeting CHK1 or ATM in cells upon IGF blockade can potentiate Type I IFN signalling. These future investigations of the possible link between IGF blockade-induced replication stress and immune response activation would be of interest, and the results can potentially provide a rationale of combining IGF inhibitors with clinical immunotherapy for cancer treatment.

6.5 Potential implications for cancer risk

The data we showed in this study and the unpublished results by Dr Rieunier in our group strongly suggested that IGF signalling mediates RRM2 expression and cellular dNTP supplies. As discussed in section 1.4.3, imbalanced cellular dNTP pool with either decreased or elevated dNTP levels can possibly induce replication stress and genome instability. This is largely because imbalance in cellular dNTP pool impairs the proofreading capacity of replicative DNA polymerases, causing them to introduce mutations into DNA (Mertz et al., 2015; Williams et al., 2015). Here we showed that IGF stimulation upregulated RRM2 protein levels (Figure 5.1, 5.2). Dr Rieunier's unpublished data further showed that short-term (24 hours) IGF-1 stimulation elevated dATP and dTTP supplies and accelerated replication fork

speed, while long-term high IGF-1 treatment slowed replication fork progression. This prompted us to hypothesise that IGF-1 stimulation might cause significant dNTP pool imbalance to the extent that DNA polymerases lose fidelity, promoting dNTP misincorporation and mutagenic potential. Therefore, current work in our lab is assessing whether short-term or long-term high IGF-1 treatment *in vitro* and *in vivo* can cause a hypermutation phenotype, which could contribute to the association of high serum IGF-1 to risk of cancer (Ahlgren et al., 2004; Chan et al., 1998; Kaaks et al., 2014; Ma et al., 1999; Renehan et al., 2004; Travis et al., 2016). The identification of replicative DNA polymerase variants (Mertz et al., 2015; Williams et al., 2015) suggests that it may be informative to investigate whether the mutagenic potential of these variants is increased by high IGF-1 treatment. Moreover, it would have been of interest to determine whether high IGF-1 induces replication stress that can eventually trigger cGAS-STING signalling in a similar way to IGF inhibition in our previous discussion. Chronic activation of cGAS-STING signalling in cancer has been reported to promote tumorigenesis and tumour metastasis via noncanonical NF-κB pathway (Ahn et al., 2014; Bakhoum et al., 2018; Kwon and Bakhoum, 2020). It may be possible that long-term treatment of high IGF-1 can contribute to the formation of an immunosuppressive microenvironment via chronically activating cGAS-STING signalling. These future investigations may provide important evidences to explain the link between high circulating IGF-1 and high cancer risk.

In summary, the IGF axis is a well-established therapeutic target in various types of cancers. Although many inhibitors have been developed and have shown strong preclinical activities, almost all IGF-targeted drugs were not successful as monotherapies in clinical trials, with the possible exception of Ewing sarcoma (van

Maldegem et al., 2016). The lack of insufficient efficacies in unselected patients is mainly due to the dose-limiting hyperglycaemia and activation of compensating pathways, leading to the intense research efforts to characterise sensitive tumours and design rational drug combinations. In this study, we demonstrated that targeting cell cycle checkpoints by CHK1 or WEE1 inhibition exacerbates replication stress induced by IGF blockade via downregulating RRM2, suggesting a potential drug combination to improve IGF-targeted therapy. Our work sheds light on a novel role of IGF signalling in mediating DNA replication, which has important therapeutic implications in cancer treatment and prognosis.

References

Aarts, M., Sharpe, R., Garcia-Murillas, I., Gevensleben, H., Hurd, M.S., Shumway, S.D., Toniatti, C., Ashworth, A., and Turner, N.C. (2012). Forced mitotic entry of S-phase cells as a therapeutic strategy induced by inhibition of WEE1. Cancer discovery *2*, 524-539.

Adam, K., Cartel, M., Lambert, M., David, L., Yuan, L., Besson, A., Mayeux, P., Manenti, S., and Didier, C. (2018). A PIM-CHK1 signaling pathway regulates PLK1 phosphorylation and function during mitosis. Journal of cell science *131*.

Ahlgren, M., Melbye, M., Wohlfahrt, J., and Sorensen, T.I. (2004). Growth patterns and the risk of breast cancer in women. The New England journal of medicine *351*, 1619-1626.

Ahn, J., Xia, T., Konno, H., Konno, K., Ruiz, P., and Barber, G.N. (2014). Inflammation-driven carcinogenesis is mediated through STING. Nature communications *5*, 5166.

Aird, K.M., Worth, A.J., Snyder, N.W., Lee, J.V., Sivanand, S., Liu, Q., Blair, I.A., Wellen, K.E., and Zhang, R. (2015). ATM couples replication stress and metabolic reprogramming during cellular senescence. Cell reports *11*, 893-901.

Aird, K.M., Zhang, G., Li, H., Tu, Z., Bitler, B.G., Garipov, A., Wu, H., Wei, Z., Wagner, S.N., Herlyn, M.*, et al.* (2013). Suppression of nucleotide metabolism underlies the establishment and maintenance of oncogene-induced senescence. Cell reports *3*, 1252-1265.

Akiyama, T., Ohuchi, T., Sumida, S., Matsumoto, K., and Toyoshima, K. (1992). Phosphorylation of the retinoblastoma protein by cdk2. Proceedings of the National Academy of Sciences of the United States of America *89*, 7900-7904.

Aleksic, T., Chitnis, M.M., Perestenko, O.V., Gao, S., Thomas, P.H., Turner, G.D., Protheroe, A.S., Howarth, M., and Macaulay, V.M. (2010). Type 1 insulin-like growth factor receptor translocates to the nucleus of human tumor cells. Cancer research *70*, 6412-6419.

Aleksic, T., Gray, N., Wu, X., Rieunier, G., Osher, E., Mills, J., Verrill, C., Bryant, R.J., Han, C., Hutchinson, K.*, et al.* (2018). Nuclear IGF1R Interacts with Regulatory Regions of Chromatin to Promote RNA Polymerase II Recruitment and Gene Expression Associated with Advanced Tumor Stage. Cancer research *78*, 3497-3509.

Aleksic, T., Verrill, C., Bryant, R.J., Han, C., Worrall, A.R., Brureau, L., Larre, S., Higgins, G.S., Fazal, F., Sabbagh, A.*, et al.* (2017). IGF-1R associates with adverse outcomes after radical radiotherapy for prostate cancer. Br J Cancer *117*, 1600-1606.

Alessi, D.R., Andjelkovic, M., Caudwell, B., Cron, P., Morrice, N., Cohen, P., and Hemmings, B.A. (1996). Mechanism of activation of protein kinase B by insulin and IGF-1. The EMBO journal *15*, 6541-6551.

Alzu, A., Bermejo, R., Begnis, M., Lucca, C., Piccini, D., Carotenuto, W., Saponaro, M., Brambati, A., Cocito, A., Foiani, M.*, et al.* (2012). Senataxin associates with replication forks to protect fork integrity across RNA-polymerase-II-transcribed genes. Cell *151*, 835-846.

Amin, O., Beauchamp, M.C., Nader, P.A., Laskov, I., Iqbal, S., Philip, C.A., Yasmeen, A., and Gotlieb, W.H. (2015). Suppression of Homologous Recombination by insulin-like growth factor-1 inhibition sensitizes cancer cells to PARP inhibitors. BMC cancer *15*, 817.

Anglana, M., Apiou, F., Bensimon, A., and Debatisse, M. (2003). Dynamics of DNA replication in mammalian somatic cells: nucleotide pool modulates origin choice and interorigin spacing. Cell *114*, 385-394.

Asada, N., Tsuchiya, H., and Tomita, K. (1999). De novo deletions of p53 gene and wild-type p53 correlate with acquired cisplatin-resistance in human osteosarcoma OST cell line. Anticancer Res *19*, 5131-5137.

Aye, Y., Li, M., Long, M.J., and Weiss, R.S. (2015). Ribonucleotide reductase and cancer: biological mechanisms and targeted therapies. Oncogene *34*, 2011-2021.

Baker, J., Liu, J.P., Robertson, E.J., and Efstratiadis, A. (1993). Role of insulin-like growth factors in embryonic and postnatal growth. Cell *75*, 73-82.

Bakhoum, S.F., Ngo, B., Laughney, A.M., Cavallo, J.A., Murphy, C.J., Ly, P., Shah, P., Sriram, R.K., Watkins, T.B.K., Taunk, N.K.*, et al.* (2018). Chromosomal instability drives metastasis through a cytosolic DNA response. Nature *553*, 467-472.

Barlow, J.H., Faryabi, R.B., Callen, E., Wong, N., Malhowski, A., Chen, H.T., Gutierrez-Cruz, G., Sun, H.W., McKinnon, P., Wright, G.*, et al.* (2013). Identification of early replicating fragile sites that contribute to genome instability. Cell *152*, 620-632.

Bartek, J., and Lukas, J. (2003). Chk1 and Chk2 kinases in checkpoint control and cancer. Cancer cell *3*, 421-429.

Baserga, R., Hongo, A., Rubini, M., Prisco, M., and Valentinis, B. (1997). The IGF-I receptor in cell growth, transformation and apoptosis. Biochimica et biophysica acta *1332*, F105-126.

Baxter, R.C. (1990). Circulating levels and molecular distribution of the acid-labile (alpha) subunit of the high molecular weight insulin-like growth factor-binding protein complex. J Clin Endocrinol Metab *70*, 1347-1353.

Baxter, R.C. (2000). Insulin-like growth factor (IGF)-binding proteins: interactions with IGFs and intrinsic bioactivities. Am J Physiol Endocrinol Metab *278*, E967-976.

Baxter, R.C. (2014). IGF binding proteins in cancer: mechanistic and clinical insights. Nature reviews Cancer *14*, 329-341.

Beck, H., Nahse-Kumpf, V., Larsen, M.S., O'Hanlon, K.A., Patzke, S., Holmberg, C., Mejlvang, J., Groth, A., Nielsen, O., Syljuasen, R.G.*, et al.* (2012). Cyclin-dependent kinase suppression by WEE1 kinase protects the genome through control of replication initiation and nucleotide consumption. Molecular and cellular biology *32*, 4226-4236.

Bell, S.P., and Dutta, A. (2002). DNA replication in eukaryotic cells. Annual review of biochemistry *71*, 333-374.

Beltran, P.J., Calzone, F.J., Mitchell, P., Chung, Y.A., Cajulis, E., Moody, G., Belmontes, B., Li, C.M., Vonderfecht, S., Velculescu, V.E.*, et al.* (2014). Ganitumab (AMG 479) inhibits IGF-II-dependent ovarian cancer growth and potentiates platinum-based chemotherapy. Clinical cancer research : an official journal of the American Association for Cancer Research *20*, 2947-2958.

Bepler, G., Kusmartseva, I., Sharma, S., Gautam, A., Cantor, A., Sharma, A., and Simon, G. (2006). RRM1 modulated in vitro and in vivo efficacy of gemcitabine and platinum in non-small-cell lung cancer. Journal of clinical oncology : official journal of the American Society of Clinical Oncology *24*, 4731-4737.

Bermejo, R., Capra, T., Gonzalez-Huici, V., Fachinetti, D., Cocito, A., Natoli, G., Katou, Y., Mori, H., Kurokawa, K., Shirahige, K.*, et al.* (2009). Genome-organizing factors Top2 and Hmo1 prevent chromosome fragility at sites of S phase transcription. Cell *138*, 870-884.

Bermejo, R., Lai, M.S., and Foiani, M. (2012). Preventing replication stress to maintain genome stability: resolving conflicts between replication and transcription. Mol Cell *45*, 710-718.

Berns, E.M., Foekens, J.A., Vossen, R., Look, M.P., Devilee, P., Henzen-Logmans, S.C., van Staveren, I.L., van Putten, W.L., Inganas, M., Meijer-van Gelder, M.E.*, et al.* (2000). Complete sequencing of TP53 predicts poor response to systemic therapy of advanced breast cancer. Cancer research *60*, 2155-2162.

Beroukhim, R., Mermel, C.H., Porter, D., Wei, G., Raychaudhuri, S., Donovan, J., Barretina, J., Boehm, J.S., Dobson, J., Urashima, M.*, et al.* (2010). The landscape of somatic copy-number alteration across human cancers. Nature *463*, 899-905.

Bertoli, C., Skotheim, J.M., and de Bruin, R.A. (2013). Control of cell cycle transcription during G1 and S phases. Nature reviews Molecular cell biology *14*, 518-528.

Bester, A.C., Roniger, M., Oren, Y.S., Im, M.M., Sarni, D., Chaoat, M., Bensimon, A., Zamir, G., Shewach, D.S., and Kerem, B. (2011). Nucleotide deficiency promotes genomic instability in early stages of cancer development. Cell *145*, 435-446.

Beucher, A., Birraux, J., Tchouandong, L., Barton, O., Shibata, A., Conrad, S., Goodarzi, A.A., Krempler, A., Jeggo, P.A., and Löbrich, M. (2009). ATM and Artemis promote homologous recombination of radiation-induced DNA double-strand breaks in G2. The EMBO journal *28*, 3413-3427.

Bian, X., and Lin, W. (2019). Targeting DNA Replication Stress and DNA Double-Strand Break Repair for Optimizing SCLC Treatment. Cancers *11*.

Bohula, E.A., Salisbury, A.J., Sohail, M., Playford, M.P., Riedemann, J., Southern, E.M., and Macaulay, V.M. (2003). The efficacy of small interfering RNAs targeted to the type 1 insulin-like growth factor receptor (IGF1R) is influenced by secondary structure in the IGF1R transcript. The Journal of biological chemistry *278*, 15991-15997.

Booher, R.N., Holman, P.S., and Fattaey, A. (1997). Human Myt1 is a cell cycle-regulated kinase that inhibits Cdc2 but not Cdk2 activity. The Journal of biological chemistry *272*, 22300-22306.

Booth, L., Roberts, J., Poklepovic, A., and Dent, P. (2018). The CHK1 inhibitor SRA737 synergizes with PARP1 inhibitors to kill carcinoma cells. Cancer Biol Ther *19*, 786-796.

Borowiec, A.S., Hague, F., Gouilleux-Gruart, V., Lassoued, K., and Ouadid-Ahidouch, H. (2011). Regulation of IGF-1-dependent cyclin D1 and E expression by hEag1 channels in MCF-7 cells: the critical role of hEag1 channels in G1 phase progression. Biochimica et biophysica acta *1813*, 723-730.

Branzei, D., and Foiani, M. (2010). Maintaining genome stability at the replication fork. Nature reviews Molecular cell biology *11*, 208-219.

Brideau, C., Gunter, B., Pikounis, B., and Liaw, A. (2003). Improved statistical methods for hit selection in high-throughput screening. J Biomol Screen *8*, 634-647.

Brooks, P.J., and Theruvathu, J.A. (2005). DNA adducts from acetaldehyde: implications for alcohol-related carcinogenesis. Alcohol *35*, 187-193.

Brugarolas, J., Chandrasekaran, C., Gordon, J.I., Beach, D., Jacks, T., and Hannon, G.J. (1995). Radiation-induced cell cycle arrest compromised by p21 deficiency. Nature *377*, 552-557.

Bryant, H.E., Schultz, N., Thomas, H.D., Parker, K.M., Flower, D., Lopez, E., Kyle, S., Meuth, M., Curtin, N.J., and Helleday, T. (2005). Specific killing of BRCA2-deficient tumours with inhibitors of poly(ADP-ribose) polymerase. Nature *434*, 913-917.

Buisson, R., Boisvert, J.L., Benes, C.H., and Zou, L. (2015). Distinct but Concerted Roles of ATR, DNA-PK, and Chk1 in Countering Replication Stress during S Phase. Mol Cell *59*, 1011-1024.

Burdova, K., Yang, H., Faedda, R., Hume, S., Chauhan, J., Ebner, D., Kessler, B.M., Vendrell, I., Drewry, D.H., Wells, C.I.*, et al.* (2019). E2F1 proteolysis via SCF-cyclin F underlies synthetic lethality between cyclin F loss and Chk1 inhibition. The EMBO journal *38*, e101443.

Burgering, B.M., and Coffer, P.J. (1995). Protein kinase B (c-Akt) in phosphatidylinositol-3-OH kinase signal transduction. Nature *376*, 599-602.

Cai, W., Sakaguchi, M., Kleinridders, A., Gonzalez-Del Pino, G., Dreyfuss, J.M., O'Neill, B.T., Ramirez, A.K., Pan, H., Winnay, J.N., Boucher, J.*, et al.* (2017). Domain-dependent effects of insulin and IGF-1 receptors on signalling and gene expression. Nature communications *8*, 14892.

Carboni, J.M., Wittman, M., Yang, Z., Lee, F., Greer, A., Hurlburt, W., Hillerman, S., Cao, C., Cantor, G.H., Dell-John, J.*, et al.* (2009). BMS-754807, a small molecule inhibitor of insulin-like growth factor-1R/IR. Molecular cancer therapeutics *8*, 3341-3349.

Cardone, M.H., Roy, N., Stennicke, H.R., Salvesen, G.S., Franke, T.F., Stanbridge, E., Frisch, S., and Reed, J.C. (1998). Regulation of cell death protease caspase-9 by phosphorylation. Science (New York, NY) *282*, 1318-1321.

Chabes, A.L., Pfleger, C.M., Kirschner, M.W., and Thelander, L. (2003). Mouse ribonucleotide reductase R2 protein: a new target for anaphase-promoting complex-Cdh1-mediated proteolysis. Proceedings of the National Academy of Sciences of the United States of America *100*, 3925-3929.

Chakravarthy, M.V., Abraha, T.W., Schwartz, R.J., Fiorotto, M.L., and Booth, F.W. (2000). Insulin-like growth factor-I extends in vitro replicative life span of skeletal muscle satellite cells by enhancing G1/S cell cycle progression via the activation of phosphatidylinositol 3'-kinase/Akt signaling pathway. The Journal of biological chemistry *275*, 35942-35952.

Chan, J.M., Stampfer, M.J., Giovannucci, E., Gann, P.H., Ma, J., Wilkinson, P., Hennekens, C.H., and Pollak, M. (1998). Plasma insulin-like growth factor-I and prostate cancer risk: a prospective study. Science (New York, NY) *279*, 563-566.

Chellappan, S.P., Hiebert, S., Mudryj, M., Horowitz, J.M., and Nevins, J.R. (1991). The E2F transcription factor is a cellular target for the RB protein. Cell *65*, 1053-1061.

Chitnis, M.M., Lodhia, K.A., Aleksic, T., Gao, S., Protheroe, A.S., and Macaulay, V.M. (2014). IGF-1R inhibition enhances radiosensitivity and delays double-strand break repair by both non-homologous end-joining and homologous recombination. Oncogene *33*, 5262-5273.

Chitnis, M.M., Yuen, J.S., Protheroe, A.S., Pollak, M., and Macaulay, V.M. (2008). The type 1 insulin-like growth factor receptor pathway. Clinical cancer research : an official journal of the American Association for Cancer Research *14*, 6364-6370.

Chou, T.C. (2006). Theoretical basis, experimental design, and computerized simulation of synergism and antagonism in drug combination studies. Pharmacol Rev *58*, 621-681.

Chou, T.C. (2010). Drug combination studies and their synergy quantification using the Chou-Talalay method. Cancer research *70*, 440-446.

Chow, J.P., and Poon, R.Y. (2013). The CDK1 inhibitory kinase MYT1 in DNA damage checkpoint recovery. Oncogene *32*, 4778-4788.

Chung, N., Zhang, X.D., Kreamer, A., Locco, L., Kuan, P.F., Bartz, S., Linsley, P.S., Ferrer, M., and Strulovici, B. (2008). Median absolute deviation to improve hit selection for genome-scale RNAi screens. J Biomol Screen *13*, 149-158.

Cimprich, K.A., and Cortez, D. (2008). ATR: an essential regulator of genome integrity. Nature reviews Molecular cell biology *9*, 616-627.

Cocker, J.H., Piatti, S., Santocanale, C., Nasmyth, K., and Diffley, J.F. (1996). An essential role for the Cdc6 protein in forming the pre-replicative complexes of budding yeast. Nature *379*, 180-182.

Constancia, M., Hemberger, M., Hughes, J., Dean, W., Ferguson-Smith, A., Fundele, R., Stewart, F., Kelsey, G., Fowden, A., Sibley, C.*, et al.* (2002). Placental-specific IGF-II is a major modulator of placental and fetal growth. Nature *417*, 945-948.

Conti, C., Saccà, B., Herrick, J., Lalou, C., Pommier, Y., and Bensimon, A. (2007). Replication fork velocities at adjacent replication origins are coordinately modified during DNA replication in human cells. Molecular biology of the cell *18*, 3059-3067.

Cook Sangar, M.L., Genovesi, L.A., Nakamoto, M.W., Davis, M.J., Knobluagh, S.E., Ji, P., Millar, A., Wainwright, B.J., and Olson, J.M. (2017). Inhibition of CDK4/6 by Palbociclib Significantly Extends Survival in Medulloblastoma Patient-Derived Xenograft Mouse Models. Clinical cancer research : an official journal of the American Association for Cancer Research *23*, 5802-5813.

Coquel, F., Silva, M.J., Techer, H., Zadorozhny, K., Sharma, S., Nieminuszczy, J., Mettling, C., Dardillac, E., Barthe, A., Schmitz, A.L.*, et al.* (2018). SAMHD1 acts at stalled replication forks to prevent interferon induction. Nature *557*, 57-61.

Cosaceanu, D., Budiu, R.A., Carapancea, M., Castro, J., Lewensohn, R., and Dricu, A. (2007). Ionizing radiation activates IGF-1R triggering a cytoprotective signaling by interfering with Ku-DNA binding and by modulating Ku86 expression via a p38 kinase-dependent mechanism. Oncogene *26*, 2423-2434.

Couch, F.B., Bansbach, C.E., Driscoll, R., Luzwick, J.W., Glick, G.G., Betous, R., Carroll, C.M., Jung, S.Y., Qin, J., Cimprich, K.A.*, et al.* (2013). ATR phosphorylates SMARCAL1 to prevent replication fork collapse. Genes Dev *27*, 1610-1623.

Couvert, P., Carrie, A., Paries, J., Vaysse, J., Miroglio, A., Kerjean, A., Nahon, P., Chelly, J., Trinchet, J.C., Beaugrand, M.*, et al.* (2008). Liver insulin-like growth factor 2 methylation in hepatitis C virus cirrhosis and further occurrence of hepatocellular carcinoma. World J Gastroenterol *14*, 5419-5427.

Coverley, D., Laman, H., and Laskey, R.A. (2002). Distinct roles for cyclins E and A during DNA replication complex assembly and activation. Nature cell biology *4*, 523-528.

Creighton, C.J., Casa, A., Lazard, Z., Huang, S., Tsimelzon, A., Hilsenbeck, S.G., Osborne, C.K., and Lee, A.V. (2008). Insulin-like growth factor-I activates gene transcription programs strongly associated with poor breast cancer prognosis. Journal of clinical oncology : official journal of the American Society of Clinical Oncology *26*, 4078-4085.

Crown, J., Sablin, M.-P., Cortés, J., Bergh, J., Im, S.-A., Lu, Y.-S., Martínez, N., Neven, P., Lee, K., Morales, S.*, et al.* (2019). Abstract P6-21-01: Xentuzumab (BI 836845), an insulin-like growth factor (IGF)-neutralizing antibody (Ab), combined with exemestane and everolimus in hormone receptor-positive (HR+) locally advanced/metastatic breast cancer (LA/mBC): Randomized phase 2 results. Cancer research *79*, P6-21-01-P26-21-01.

Cui, H., Cruz-Correa, M., Giardiello, F.M., Hutcheon, D.F., Kafonek, D.R., Brandenburg, S., Wu, Y., He, X., Powe, N.R., and Feinberg, A.P. (2003). Loss of IGF2 imprinting: a potential marker of colorectal cancer risk. Science (New York, NY) *299*, 1753-1755.

Czech, M.P. (2000). PIP2 and PIP3: complex roles at the cell surface. Cell *100*, 603-606.

D'Angiolella, V., Donato, V., Forrester, F.M., Jeong, Y.T., Pellacani, C., Kudo, Y., Saraf, A., Florens, L., Washburn, M.P., and Pagano, M. (2012). Cyclin F-mediated degradation of ribonucleotide reductase M2 controls genome integrity and DNA repair. Cell *149*, 1023-1034.

Dai, Y., Chen, S., Kmieciak, M., Zhou, L., Lin, H., Pei, X.Y., and Grant, S. (2013). The novel Chk1 inhibitor MK-8776 sensitizes human leukemia cells to HDAC inhibitors by targeting the intra-S checkpoint and DNA replication and repair. Molecular cancer therapeutics *12*, 878-889.

Dale, O.T., Aleksic, T., Shah, K.A., Han, C., Mehanna, H., Rapozo, D.C., Sheard, J.D., Goodyear, P., Upile, N.S., Robinson, M.*, et al.* (2015). IGF-1R expression is associated with HPV-negative status and adverse survival in head and neck squamous cell cancer. Carcinogenesis *36*, 648-655.

Dalgaard, J.Z. (2012). Causes and consequences of ribonucleotide incorporation into nuclear DNA. Trends Genet *28*, 592-597.

Datta, S.R., Dudek, H., Tao, X., Masters, S., Fu, H., Gotoh, Y., and Greenberg, M.E. (1997). Akt phosphorylation of BAD couples survival signals to the cell-intrinsic death machinery. Cell *91*, 231-241.

Dauber, A., Munoz-Calvo, M.T., Barrios, V., Domene, H.M., Kloverpris, S., Serra-Juhe, C., Desikan, V., Pozo, J., Muzumdar, R., Martos-Moreno, G.A.*, et al.* (2016). Mutations in pregnancy-associated plasma protein A2 cause short stature due to low IGF-I availability. EMBO Mol Med *8*, 363-374.

Daud, A.I., Ashworth, M.T., Strosberg, J., Goldman, J.W., Mendelson, D., Springett, G., Venook, A.P., Loechner, S., Rosen, L.S., Shanahan, F.*, et al.* (2015). Phase I dose-escalation trial of checkpoint kinase 1 inhibitor MK-8776 as monotherapy and in combination with gemcitabine in patients with advanced solid tumors. Journal of clinical oncology : official journal of the American Society of Clinical Oncology *33*, 1060-1066.

Davidson, M.B., Katou, Y., Keszthelyi, A., Sing, T.L., Xia, T., Ou, J., Vaisica, J.A., Thevakumaran, N., Marjavaara, L., Myers, C.L.*, et al.* (2012). Endogenous DNA replication stress results in expansion of dNTP pools and a mutator phenotype. The EMBO journal *31*, 895-907.

de Bono, J., Lin, C.C., Chen, L.T., Corral, J., Michalarea, V., Rihawi, K., Ong, M., Lee, J.H., Hsu, C.H., Yang, J.C.*, et al.* (2020). Two first-in-human studies of xentuzumab, a humanised insulin-like growth factor (IGF)-neutralising antibody, in patients with advanced solid tumours. Br J Cancer *122*, 1324-1332.

de Munnik, S.A., Hoefsloot, E.H., Roukema, J., Schoots, J., Knoers, N.V., Brunner, H.G., Jackson, A.P., and Bongers, E.M. (2015). Meier-Gorlin syndrome. Orphanet J Rare Dis *10*, 114.

De Souza, A.T., Hankins, G.R., Washington, M.K., Orton, T.C., and Jirtle, R.L. (1995). M6P/IGF2R gene is mutated in human hepatocellular carcinomas with loss of heterozygosity. Nature genetics *11*, 447-449.

DeGregori, J., Kowalik, T., and Nevins, J.R. (1995). Cellular targets for activation by the E2F1 transcription factor include DNA synthesis- and G1/S-regulatory genes. Molecular and cellular biology *15*, 4215-4224.

Deng, L., Liang, H., Xu, M., Yang, X., Burnette, B., Arina, A., Li, X.D., Mauceri, H., Beckett, M., Darga, T.*, et al.* (2014). STING-Dependent Cytosolic DNA Sensing Promotes Radiation-Induced Type I Interferon-Dependent Antitumor Immunity in Immunogenic Tumors. Immunity *41*, 843-852.

Denicourt, C., and Dowdy, S.F. (2004). Cip/Kip proteins: more than just CDKs inhibitors. Genes Dev *18*, 851-855.

Desoize, B., and Jardillier, J. (2000). Multicellular resistance: a paradigm for clinical resistance? Crit Rev Oncol Hematol *36*, 193-207.

Diehl, J.A., Cheng, M., Roussel, M.F., and Sherr, C.J. (1998). Glycogen synthase kinase-3beta regulates cyclin D1 proteolysis and subcellular localization. Genes Dev *12*, 3499-3511.

Dillon, M.T., Bergerhoff, K.F., Pedersen, M., Whittock, H., Crespo-Rodriguez, E., Patin, E.C., Pearson, A., Smith, H.G., Paget, J.T.E., Patel, R.R.*, et al.* (2019). ATR Inhibition Potentiates the Radiation-induced Inflammatory Tumor Microenvironment. Clinical cancer research : an official journal of the American Association for Cancer Research *25*, 3392-3403.

Domene, H.M., Bengolea, S.V., Martinez, A.S., Ropelato, M.G., Pennisi, P., Scaglia, P., Heinrich, J.J., and Jasper, H.G. (2004). Deficiency of the circulating insulin-like growth factor system associated with inactivation of the acid-labile subunit gene. The New England journal of medicine *350*, 570-577.

Duan, C., Ren, H., and Gao, S. (2010). Insulin-like growth factors (IGFs), IGF receptors, and IGF-binding proteins: roles in skeletal muscle growth and differentiation. Gen Comp Endocrinol *167*, 344-351.

Dupont, J., and Holzenberger, M. (2003). IGF type 1 receptor: a cell cycle progression factor that regulates aging. Cell cycle (Georgetown, Tex) *2*, 270-272.

Duxbury, M.S., and Whang, E.E. (2007). RRM2 induces NF-kappaB-dependent MMP-9 activation and enhances cellular invasiveness. Biochemical and biophysical research communications *354*, 190-196.

Egan, S.E., Giddings, B.W., Brooks, M.W., Buday, L., Sizeland, A.M., and Weinberg, R.A. (1993). Association of Sos Ras exchange protein with Grb2 is implicated in tyrosine kinase signal transduction and transformation. Nature *363*, 45-51.

el-Deiry, W.S., Tokino, T., Velculescu, V.E., Levy, D.B., Parsons, R., Trent, J.M., Lin, D., Mercer, W.E., Kinzler, K.W., and Vogelstein, B. (1993). WAF1, a potential mediator of p53 tumor suppression. Cell *75*, 817-825.

Ellwart, J.W., and Dormer, P. (1990). Vitality measurement using spectrum shift in Hoechst 33342 stained cells. Cytometry *11*, 239-243.

Engeland, K. (2018). Cell cycle arrest through indirect transcriptional repression by p53: I have a DREAM. Cell Death Differ *25*, 114-132.

Engstrom, Y., Eriksson, S., Jildevik, I., Skog, S., Thelander, L., and Tribukait, B. (1985). Cell cycle-dependent expression of mammalian ribonucleotide reductase. Differential regulation of the two subunits. The Journal of biological chemistry *260*, 9114-9116.

Enserink, J.M., and Kolodner, R.D. (2010). An overview of Cdk1-controlled targets and processes. Cell Div *5*, 11.

Erdal, E., Haider, S., Rehwinkel, J., Harris, A.L., and McHugh, P.J. (2017). A prosurvival DNA damage-induced cytoplasmic interferon response is mediated by end resection factors and is limited by Trex1. Genes Dev *31*, 353-369.

Faivre, L., Le Merrer, M., Lyonnet, S., Plauchu, H., Dagoneau, N., Campos-Xavier, A.B., Attia-Sobol, J., Verloes, A., Munnich, A., and Cormier-Daire, V. (2002). Clinical and genetic heterogeneity of Seckel syndrome. Am J Med Genet *112*, 379-383.

Farabaugh, S.M., Boone, D.N., and Lee, A.V. (2015). Role of IGF1R in Breast Cancer Subtypes, Stemness, and Lineage Differentiation. Front Endocrinol (Lausanne) *6*, 59.

Farmer, H., McCabe, N., Lord, C.J., Tutt, A.N., Johnson, D.A., Richardson, T.B., Santarosa, M., Dillon, K.J., Hickson, I., Knights, C.*, et al.* (2005). Targeting the DNA repair defect in BRCA mutant cells as a therapeutic strategy. Nature *434*, 917-921.

Fassnacht, M., Berruti, A., Baudin, E., Demeure, M.J., Gilbert, J., Haak, H., Kroiss, M., Quinn, D.I., Hesseltine, E., Ronchi, C.L.*, et al.* (2015). Linsitinib (OSI-906) versus placebo for patients with locally advanced or metastatic adrenocortical carcinoma: a double-blind, randomised, phase 3 study. The Lancet Oncology *16*, 426-435.

Ferrandina, G., Mey, V., Nannizzi, S., Ricciardi, S., Petrillo, M., Ferlini, C., Danesi, R., Scambia, G., and Del Tacca, M. (2010). Expression of nucleoside transporters, deoxycitidine kinase, ribonucleotide reductase regulatory subunits, and gemcitabine catabolic enzymes in primary ovarian cancer. Cancer Chemother Pharmacol *65*, 679-686.

Ferte, C., Loriot, Y., Clemenson, C., Commo, F., Gombos, A., Bibault, J.E., Fumagalli, I., Hamama, S., Auger, N., Lahon, B.*, et al.* (2013). IGF-1R targeting increases the antitumor effects of DNA-damaging agents in SCLC model: an opportunity to increase the efficacy of standard therapy. Molecular cancer therapeutics *12*, 1213-1222.

Fischbach, C., Kong, H.J., Hsiong, S.X., Evangelista, M.B., Yuen, W., and Mooney, D.J. (2009). Cancer cell angiogenic capability is regulated by 3D culture and integrin engagement. Proceedings of the National Academy of Sciences of the United States of America *106*, 399-404.

Fisher, S.B., Patel, S.H., Bagci, P., Kooby, D.A., El-Rayes, B.F., Staley, C.A., 3rd, Adsay, N.V., and Maithel, S.K. (2013). An analysis of human equilibrative nucleoside transporter-1, ribonucleoside reductase subunit M1, ribonucleoside reductase subunit M2, and excision repair cross-complementing gene-1 expression in patients with resected pancreas adenocarcinoma: implications for adjuvant treatment. Cancer *119*, 445-453.

Flanagan, M., and Cunniff, C.M. (1993). Bloom Syndrome. In GeneReviews(®), M.P. Adam, H.H. Ardinger, R.A. Pagon, S.E. Wallace, L.J.H. Bean, K. Stephens, and A. Amemiya, eds. (Seattle (WA): University of Washington, Seattle

Forbes, B.E., Hartfield, P.J., McNeil, K.A., Surinya, K.H., Milner, S.J., Cosgrove, L.J., and Wallace, J.C. (2002). Characteristics of binding of insulin-like growth factor (IGF)-I and IGF-II analogues to the type 1 IGF receptor determined by BIAcore analysis. Eur J Biochem *269*, 961-968.

Foskolou, I.P., Jorgensen, C., Leszczynska, K.B., Olcina, M.M., Tarhonskaya, H., Haisma, B., D'Angiolella, V., Myers, W.K., Domene, C., Flashman, E.*, et al.* (2017). Ribonucleotide Reductase Requires Subunit Switching in Hypoxia to Maintain DNA Replication. Mol Cell *66*, 206-220.e209.

Frame, S., and Cohen, P. (2001). GSK3 takes centre stage more than 20 years after its discovery. The Biochemical journal *359*, 1-16.

Frasca, F., Pandini, G., Scalia, P., Sciacca, L., Mineo, R., Costantino, A., Goldfine, I.D., Belfiore, A., and Vigneri, R. (1999). Insulin receptor isoform A, a newly recognized, high-affinity insulin-like growth factor II receptor in fetal and cancer cells. Molecular and cellular biology *19*, 3278-3288.

Friedbichler, K., Hofmann, M.H., Kroez, M., Ostermann, E., Lamche, H.R., Koessl, C., Borges, E., Pollak, M.N., Adolf, G., and Adam, P.J. (2014). Pharmacodynamic and antineoplastic activity of BI 836845, a fully human IGF ligand-neutralizing antibody, and mechanistic rationale for combination with rapamycin. Molecular cancer therapeutics *13*, 399-409.

Friedlander, T.W., Weinberg, V.K., Huang, Y., Mi, J.T., Formaker, C.G., Small, E.J., Harzstark, A.L., Lin, A.M., Fong, L., and Ryan, C.J. (2012). A phase II study of insulin-like growth factor receptor inhibition with nordihydroguaiaretic acid in men with non-metastatic hormone-sensitive prostate cancer. Oncology reports *27*, 3-9.

Fu, S., Wang, Y., Keyomarsi, K., Meric-Bernstam, F., and Meric-Bernstein, F. (2018). Strategic development of AZD1775, a Wee1 kinase inhibitor, for cancer therapy. Expert Opin Investig Drugs *27*, 741-751.

Fuchs, C.S., Azevedo, S., Okusaka, T., Van Laethem, J.L., Lipton, L.R., Riess, H., Szczylik, C., Moore, M.J., Peeters, M., Bodoky, G.*, et al.* (2015). A phase 3 randomized, double-blind, placebo-controlled trial of ganitumab or placebo in combination with gemcitabine as first-line therapy for metastatic adenocarcinoma of the pancreas: the GAMMA trial. Ann Oncol *26*, 921-927.

Gadhikar, M.A., Sciuto, M.R., Alves, M.V., Pickering, C.R., Osman, A.A., Neskey, D.M., Zhao, M., Fitzgerald, A.L., Myers, J.N., and Frederick, M.J. (2013). Chk1/2 inhibition overcomes the cisplatin resistance of head and neck cancer cells secondary to the loss of functional p53. Molecular cancer therapeutics *12*, 1860-1873.

Gagou, M.E., Zuazua-Villar, P., and Meuth, M. (2010). Enhanced H2AX phosphorylation, DNA replication fork arrest, and cell death in the absence of Chk1. Molecular biology of the cell *21*, 739-752.

Galmarini, C.M., Falette, N., Tabone, E., Levrat, C., Britten, R., Voorzanger-Rousselot, N., Roesch-Gateau, O., Vanier-Viornery, A., Puisieux, A., and Dumontet, C. (2001a).

Inactivation of wild-type p53 by a dominant negative mutant renders MCF-7 cells resistant to tubulin-binding agent cytotoxicity. Br J Cancer *85*, 902-908.

Galmarini, C.M., Mackey, J.R., and Dumontet, C. (2001b). Nucleoside analogues: mechanisms of drug resistance and reversal strategies. Leukemia *15*, 875-890.

Gambus, A., Jones, R.C., Sanchez-Diaz, A., Kanemaki, M., van Deursen, F., Edmondson, R.D., and Labib, K. (2006). GINS maintains association of Cdc45 with MCM in replisome progression complexes at eukaryotic DNA replication forks. Nature cell biology *8*, 358-366.

Ganem, N.J., Godinho, S.A., and Pellman, D. (2009). A mechanism linking extra centrosomes to chromosomal instability. Nature *460*, 278-282.

Gao, J., Chesebrough, J.W., Cartlidge, S.A., Ricketts, S.A., Incognito, L., Veldman-Jones, M., Blakey, D.C., Tabrizi, M., Jallal, B., Trail, P.A.*, et al.* (2011). Dual IGF-I/II-neutralizing antibody MEDI-573 potently inhibits IGF signaling and tumor growth. Cancer research *71*, 1029-1040.

Gao, S., Bajrami, I., Verrill, C., Kigozi, A., Ouaret, D., Aleksic, T., Asher, R., Han, C., Allen, P., Bailey, D.*, et al.* (2014). Dsh homolog DVL3 mediates resistance to IGFIR inhibition by regulating IGF-RAS signaling. Cancer research *74*, 5866-5877.

Garcia-Echeverria, C., Pearson, M.A., Marti, A., Meyer, T., Mestan, J., Zimmermann, J., Gao, J., Brueggen, J., Capraro, H.G., Cozens, R.*, et al.* (2004). In vivo antitumor activity of NVP-AEW541-A novel, potent, and selective inhibitor of the IGF-IR kinase. Cancer cell *5*, 231-239.

Garinis, G.A., Uittenboogaard, L.M., Stachelscheid, H., Fousteri, M., van Ijcken, W., Breit, T.M., van Steeg, H., Mullenders, L.H., van der Horst, G.T., Brüning, J.C.*, et al.* (2009). Persistent transcription-blocking DNA lesions trigger somatic growth attenuation associated with longevity. Nature cell biology *11*, 604-615.

Geley, S., Kramer, E., Gieffers, C., Gannon, J., Peters, J.M., and Hunt, T. (2001). Anaphase-promoting complex/cyclosome-dependent proteolysis of human cyclin A starts at the beginning of mitosis and is not subject to the spindle assembly checkpoint. The Journal of cell biology *153*, 137-148.

Glotzer, M., Murray, A.W., and Kirschner, M.W. (1991). Cyclin is degraded by the ubiquitin pathway. Nature *349*, 132-138.

Goktug, A.N., Chai, S.C., and Chen, T. (2013). Data analysis approaches in high throughput screening. Drug Discovery, 201-226.

Gorgoulis, V.G., Vassiliou, L.V., Karakaidos, P., Zacharatos, P., Kotsinas, A., Liloglou, T., Venere, M., Ditullio, R.A., Jr., Kastrinakis, N.G., Levy, B.*, et al.* (2005). Activation of the DNA damage checkpoint and genomic instability in human precancerous lesions. Nature *434*, 907-913.

Graña, X., Garriga, J., and Mayol, X. (1998). Role of the retinoblastoma protein family, pRB, p107 and p130 in the negative control of cell growth. Oncogene *17*, 3365-3383.

Gratia, M., Rodero, M.P., Conrad, C., Bou Samra, E., Maurin, M., Rice, G.I., Duffy, D., Revy, P., Petit, F., Dale, R.C.*, et al.* (2019). Bloom syndrome protein restrains innate immune sensing of micronuclei by cGAS. J Exp Med *216*, 1199-1213.

Gualberto, A., and Pollak, M. (2009). Emerging role of insulin-like growth factor receptor inhibitors in oncology: early clinical trial results and future directions. Oncogene *28*, 3009-3021.

Guevara-Aguirre, J., Balasubramanian, P., Guevara-Aguirre, M., Wei, M., Madia, F., Cheng, C.W., Hwang, D., Martin-Montalvo, A., Saavedra, J., Ingles, S.*, et al.* (2011). Growth hormone receptor deficiency is associated with a major reduction in pro-aging signaling, cancer, and diabetes in humans. Science translational medicine *3*, 70ra13.

Guirouilh-Barbat, J., Lambert, S., Bertrand, P., and Lopez, B.S. (2014). Is homologous recombination really an error-free process? Front Genet *5*, 175.

Gustafson, T.A., and Rutter, W.J. (1990). The cysteine-rich domains of the insulin and insulin-like growth factor I receptors are primary determinants of hormone binding specificity. Evidence from receptor chimeras. The Journal of biological chemistry *265*, 18663-18667.

Hakuno, F., and Takahashi, S.I. (2018). IGF1 receptor signaling pathways. J Mol Endocrinol *61*, T69-t86.

Haluska, P., Menefee, M., Plimack, E.R., Rosenberg, J., Northfelt, D., LaVallee, T., Shi, L., Yu, X.Q., Burke, P., Huang, J.*, et al.* (2014). Phase I dose-escalation study of MEDI-573, a bispecific, antiligand monoclonal antibody against IGFI and IGFII, in patients with advanced solid tumors. Clinical cancer research : an official journal of the American Association for Cancer Research *20*, 4747-4757.

Hamelers, I.H., van Schaik, R.F., Sipkema, J., Sussenbach, J.S., and Steenbergh, P.H. (2002). Insulin-like growth factor I triggers nuclear accumulation of cyclin D1 in MCF-7S breast cancer cells. The Journal of biological chemistry *277*, 47645-47652.

Hanada, K., Budzowska, M., Modesti, M., Maas, A., Wyman, C., Essers, J., and Kanaar, R. (2006). The structure-specific endonuclease Mus81-Eme1 promotes conversion of interstrand DNA crosslinks into double-strands breaks. The EMBO journal *25*, 4921-4932.

Hanafusa, T., Yumoto, Y., Nouso, K., Nakatsukasa, H., Onishi, T., Fujikawa, T., Taniyama, M., Nakamura, S., Uemura, M., Takuma, Y.*, et al.* (2002). Reduced expression of insulin-like growth factor binding protein-3 and its promoter hypermethylation in human hepatocellular carcinoma. Cancer Lett *176*, 149-158.

Hanahan, D., and Weinberg, R.A. (2000). The hallmarks of cancer. Cell *100*, 57-70.

Hanahan, D., and Weinberg, R.A. (2011). Hallmarks of cancer: the next generation. Cell *144*, 646-674.

Hankins, G.R., De Souza, A.T., Bentley, R.C., Patel, M.R., Marks, J.R., Iglehart, J.D., and Jirtle, R.L. (1996). M6P/IGF2 receptor: a candidate breast tumor suppressor gene. Oncogene *12*, 2003-2009.

Harrigan, J.A., Belotserkovskaya, R., Coates, J., Dimitrova, D.S., Polo, S.E., Bradshaw, C.R., Fraser, P., and Jackson, S.P. (2011). Replication stress induces 53BP1-containing OPT domains in G1 cells. The Journal of cell biology *193*, 97-108.

Härtlova, A., Erttmann, S.F., Raffi, F.A., Schmalz, A.M., Resch, U., Anugula, S., Lienenklaus, S., Nilsson, L.M., Kröger, A., Nilsson, J.A.*, et al.* (2015). DNA damage primes the type I interferon system via the cytosolic DNA sensor STING to promote anti-microbial innate immunity. Immunity *42*, 332-343.

Hartog, H., Horlings, H.M., van der Vegt, B., Kreike, B., Ajouaou, A., van de Vijver, M.J., Marike Boezen, H., de Bock, G.H., van der Graaf, W.T., and Wesseling, J. (2011). Divergent effects of insulin-like growth factor-1 receptor expression on prognosis of estrogen receptor positive versus triple negative invasive ductal breast carcinoma. Breast Cancer Res Treat *129*, 725-736.

He, Z., Hu, X., Liu, W., Dorrance, A., Garzon, R., Houghton, P.J., and Shen, C. (2017). P53 suppresses ribonucleotide reductase via inhibiting mTORC1. Oncotarget *8*, 41422-41431.

Hellawell, G.O., Turner, G.D., Davies, D.R., Poulsom, R., Brewster, S.F., and Macaulay, V.M. (2002). Expression of the type 1 insulin-like growth factor receptor is up-regulated in primary prostate cancer and commonly persists in metastatic disease. Cancer research *62*, 2942-2950.

Helmrich, A., Ballarino, M., and Tora, L. (2011). Collisions between replication and transcription complexes cause common fragile site instability at the longest human genes. Mol Cell *44*, 966-977.

Hershko, A. (1999). Mechanisms and regulation of the degradation of cyclin B. Philos Trans R Soc Lond B Biol Sci *354*, 1571-1575; discussion 1575-1576.

Hirao, A., Cheung, A., Duncan, G., Girard, P.M., Elia, A.J., Wakeham, A., Okada, H., Sarkissian, T., Wong, J.A., Sakai, T.*, et al.* (2002). Chk2 is a tumor suppressor that regulates apoptosis in both an ataxia telangiectasia mutated (ATM)-dependent and an ATM-independent manner. Molecular and cellular biology *22*, 6521-6532.

Hirschhaeuser, F., Menne, H., Dittfeld, C., West, J., Mueller-Klieser, W., and Kunz-Schughart, L.A. (2010). Multicellular tumor spheroids: an underestimated tool is catching up again. J Biotechnol *148*, 3-15.

Hochegger, H., Takeda, S., and Hunt, T. (2008). Cyclin-dependent kinases and cell-cycle transitions: does one fit all? Nature reviews Molecular cell biology *9*, 910-916.

Hu, C.K., McCall, S., Madden, J., Huang, H., Clough, R., Jirtle, R.L., and Anscher, M.S. (2006). Loss of heterozygosity of M6P/IGF2R gene is an early event in the development of prostate cancer. Prostate Cancer Prostatic Dis *9*, 62-67.

Huang, M., Parker, M.J., and Stubbe, J. (2014). Choosing the right metal: case studies of class I ribonucleotide reductases. The Journal of biological chemistry *289*, 28104-28111.

Hunt, T., Nasmyth, K., and Novák, B. (2011). The cell cycle. Philos Trans R Soc Lond B Biol Sci *366*, 3494-3497.

Iftode, C., Daniely, Y., and Borowiec, J.A. (1999). Replication protein A (RPA): the eukaryotic SSB. Crit Rev Biochem Mol Biol *34*, 141-180.

Iguchi, H., Nishina, T., Nogami, N., Kozuki, T., Yamagiwa, Y., and Yagawa, K. (2015). Phase I dose-escalation study evaluating safety, tolerability and pharmacokinetics of MEDI-573, a dual IGF-I/II neutralizing antibody, in Japanese patients with advanced solid tumours. Invest New Drugs *33*, 194-200.

Ii, M., Li, H., Adachi, Y., Yamamoto, H., Ohashi, H., Taniguchi, H., Arimura, Y., Carbone, D.P., Imai, K., and Shinomura, Y. (2011). The efficacy of IGF-I receptor monoclonal antibody against human gastrointestinal carcinomas is independent of k-ras mutation status. Clinical cancer research : an official journal of the American Association for Cancer Research *17*, 5048-5059.

Inoué, S. (1981). Cell division and the mitotic spindle. The Journal of cell biology *91*, 131s-147s.

Ishikawa, H., and Barber, G.N. (2008). STING is an endoplasmic reticulum adaptor that facilitates innate immune signalling. Nature *455*, 674-678.

Ishikawa, H., Ma, Z., and Barber, G.N. (2009). STING regulates intracellular DNA-mediated, type I interferon-dependent innate immunity. Nature *461*, 788-792.

Jeffrey, P.D., Tong, L., and Pavletich, N.P. (2000). Structural basis of inhibition of CDK-cyclin complexes by INK4 inhibitors. Genes Dev *14*, 3115-3125.

Kaaks, R., Johnson, T., Tikk, K., Sookthai, D., Tjønneland, A., Roswall, N., Overvad, K., Clavel-Chapelon, F., Boutron-Ruault, M.C., Dossus, L.*, et al.* (2014). Insulin-like growth factor I and risk of breast cancer by age and hormone receptor status-A prospective study within the EPIC cohort. International journal of cancer *134*, 2683-2690.

Kang, H.J., Yi, Y.W., Kim, H.J., Hong, Y.B., Seong, Y.S., and Bae, I. (2012). BRCA1 negatively regulates IGF-1 expression through an estrogen-responsive element-like site. Cell Death Dis *3*, e336.

Karp, J.E., Thomas, B.M., Greer, J.M., Sorge, C., Gore, S.D., Pratz, K.W., Smith, B.D., Flatten, K.S., Peterson, K., Schneider, P.*, et al.* (2012). Phase I and pharmacologic trial of cytosine arabinoside with the selective checkpoint 1 inhibitor Sch 900776 in refractory acute leukemias. Clinical cancer research : an official journal of the American Association for Cancer Research *18*, 6723-6731.

Kasahara, K., Goto, H., Enomoto, M., Tomono, Y., Kiyono, T., and Inagaki, M. (2010). 14-3-3gamma mediates Cdc25A proteolysis to block premature mitotic entry after DNA damage. The EMBO journal *29*, 2802-2812.

Kastan, M.B., and Bartek, J. (2004). Cell-cycle checkpoints and cancer. Nature *432*, 316-323.

Kastan, M.B., Onyekwere, O., Sidransky, D., Vogelstein, B., and Craig, R.W. (1991). Participation of p53 protein in the cellular response to DNA damage. Cancer research *51*, 6304-6311.

Kastan, M.B., Zhan, Q., el-Deiry, W.S., Carrier, F., Jacks, T., Walsh, W.V., Plunkett, B.S., Vogelstein, B., and Fornace, A.J., Jr. (1992). A mammalian cell cycle checkpoint pathway utilizing p53 and GADD45 is defective in ataxia-telangiectasia. Cell *71*, 587-597.

Khoronenkova, S.V., and Dianov, G.L. (2015). ATM prevents DSB formation by coordinating SSB repair and cell cycle progression. Proceedings of the National Academy of Sciences of the United States of America *112*, 3997-4002.

Kim, H., George, E., Ragland, R., Rafail, S., Zhang, R., Krepler, C., Morgan, M., Herlyn, M., Brown, E., and Simpkins, F. (2017). Targeting the ATR/CHK1 Axis with PARP Inhibition Results in Tumor Regression in BRCA-Mutant Ovarian Cancer Models. Clinical cancer research : an official journal of the American Association for Cancer Research *23*, 3097-3108.

Kim, H.J., Litzenburger, B.C., Cui, X., Delgado, D.A., Grabiner, B.C., Lin, X., Lewis, M.T., Gottardis, M.M., Wong, T.W., Attar, R.M.*, et al.* (2007). Constitutively active type I insulin-like growth factor receptor causes transformation and xenograft growth of immortalized mammary epithelial cells and is accompanied by an epithelial-to-mesenchymal transition mediated by NF-kappaB and snail. Molecular and cellular biology *27*, 3165-3175.

King, H., Aleksic, T., Haluska, P., and Macaulay, V.M. (2014). Can we unlock the potential of IGF-1R inhibition in cancer therapy? Cancer treatment reviews *40*, 1096-1105.

Koepp, D.M., Schaefer, L.K., Ye, X., Keyomarsi, K., Chu, C., Harper, J.W., and Elledge, S.J. (2001). Phosphorylation-dependent ubiquitination of cyclin E by the SCFFbw7 ubiquitin ligase. Science (New York, NY) *294*, 173-177.

Konecny, G.E., Haluska, P., Janicke, F., Sehouli, J., Beckmann, M.W., Feisel, G., Pölcher, M., Roman, L., Rody, A., Karlan, B.*, et al.* (2014). A phase II, multicenter, randomized, double-blind, placebo-controlled trial of ganitumab or placebo in combination with carboplatin/paclitaxel as front-line therapy for optimally debulked primary ovarian cancer: The TRIO14 trial. Journal of Clinical Oncology *32*, 5529-5529.

Koppenhafer, S.L., Goss, K.L., Terry, W.W., and Gordon, D.J. (2020). Inhibition of the ATR-CHK1 Pathway in Ewing Sarcoma Cells Causes DNA Damage and Apoptosis via the CDK2-Mediated Degradation of RRM2. Mol Cancer Res *18*, 91-104.

Kornfeld, S. (1992). Structure and function of the mannose 6-phosphate/insulinlike growth factor II receptors. Annual review of biochemistry *61*, 307-330.

Kreienkamp, R., Graziano, S., Coll-Bonfill, N., Bedia-Diaz, G., Cybulla, E., Vindigni, A., Dorsett, D., Kubben, N., Batista, L.F.Z., and Gonzalo, S. (2018). A Cell-Intrinsic Interferon-like Response Links Replication Stress to Cellular Aging Caused by Progerin. Cell reports *22*, 2006-2015.

Kumar, H.R., Zhong, X., Hoelz, D.J., Rescorla, F.J., Hickey, R.J., Malkas, L.H., and Sandoval, J.A. (2008). Three-dimensional neuroblastoma cell culture: proteomic analysis between monolayer and multicellular tumor spheroids. Pediatr Surg Int *24*, 1229-1234.

Kundranda, M., Gracian, A.C., Zafar, S.F., Meiri, E., Bendell, J., Algul, H., Rivera, F., Ahn, E.R., Watkins, D., Pelzer, U.*, et al.* (2020). Randomized, double-blind, placebo-controlled phase II study of istiratumab (MM-141) plus nab-paclitaxel and gemcitabine versus nab-paclitaxel and gemcitabine in front-line metastatic pancreatic cancer (CARRIE). Ann Oncol *31*, 79-87.

Kwon, J., and Bakhoum, S.F. (2020). The Cytosolic DNA-Sensing cGAS-STING Pathway in Cancer. Cancer discovery *10*, 26-39.

Kyriakis, J.M., App, H., Zhang, X.F., Banerjee, P., Brautigan, D.L., Rapp, U.R., and Avruch, J. (1992). Raf-1 activates MAP kinase-kinase. Nature *358*, 417-421.

Labib, K., Tercero, J.A., and Diffley, J.F. (2000). Uninterrupted MCM2-7 function required for DNA replication fork progression. Science (New York, NY) *288*, 1643-1647.

Landoni, J.C., Wang, L., and Suomalainen, A. (2018). Quantitative solid-phase assay to measure deoxynucleoside triphosphate pools. Biology Methods and Protocols *3*, bpy011.

Laron, Z. (2015). LESSONS FROM 50 YEARS OF STUDY OF LARON SYNDROME. Endocrine practice : official journal of the American College of Endocrinology and the American Association of Clinical Endocrinologists *21*, 1395-1402.

Laugel, V. (2013). Cockayne syndrome: the expanding clinical and mutational spectrum. Mech Ageing Dev *134*, 161-170.

Lavoie, J.N., L'Allemain, G., Brunet, A., Müller, R., and Pouysségur, J. (1996). Cyclin D1 expression is regulated positively by the p42/p44MAPK and negatively by the p38/HOGMAPK pathway. The Journal of biological chemistry *271*, 20608-20616.

Lee, J.H., Goodarzi, A.A., Jeggo, P.A., and Paull, T.T. (2010). 53BP1 promotes ATM activity through direct interactions with the MRN complex. The EMBO journal *29*, 574-585.

Lemmon, M.A., and Schlessinger, J. (2010). Cell signaling by receptor tyrosine kinases. Cell *141*, 1117-1134.

Leung-Pineda, V., Ryan, C.E., and Piwnica-Worms, H. (2006). Phosphorylation of Chk1 by ATR is antagonized by a Chk1-regulated protein phosphatase 2A circuit. Molecular and cellular biology *26*, 7529-7538.

Li, J., Choi, E., Yu, H., and Bai, X.C. (2019). Structural basis of the activation of type 1 insulin-like growth factor receptor. Nature communications *10*, 4567.

Li, P., Veldwijk, M.R., Zhang, Q., Li, Z.B., Xu, W.C., and Fu, S. (2013). Co-inhibition of epidermal growth factor receptor and insulin-like growth factor receptor 1 enhances radiosensitivity in human breast cancer cells. BMC cancer *13*, 297.

Li, X., and Manley, J.L. (2005). Inactivation of the SR protein splicing factor ASF/SF2 results in genomic instability. Cell *122*, 365-378.

Liang, J., and Slingerland, J.M. (2003). Multiple roles of the PI3K/PKB (Akt) pathway in cell cycle progression. Cell cycle (Georgetown, Tex) *2*, 339-345.

Lin, C.Y., Loven, J., Rahl, P.B., Paranal, R.M., Burge, C.B., Bradner, J.E., Lee, T.I., and Young, R.A. (2012). Transcriptional amplification in tumor cells with elevated c-Myc. Cell *151*, 56-67.

Lin, D.L., and Chang, C. (1996). p53 is a mediator for radiation-repressed human TR2 orphan receptor expression in MCF-7 cells, a new pathway from tumor suppressor to member of the steroid receptor superfamily. The Journal of biological chemistry *271*, 14649-14652.

Litzenburger, B.C., Kim, H.J., Kuiatse, I., Carboni, J.M., Attar, R.M., Gottardis, M.M., Fairchild, C.R., and Lee, A.V. (2009). BMS-536924 reverses IGF-IR-induced transformation of mammary epithelial cells and causes growth inhibition and polarization of MCF7 cells. Clinical cancer research : an official journal of the American Association for Cancer Research *15*, 226-237.

Liu, J.P., Baker, J., Perkins, A.S., Robertson, E.J., and Efstratiadis, A. (1993). Mice carrying null mutations of the genes encoding insulin-like growth factor I (Igf-1) and type 1 IGF receptor (Igf1r). Cell *75*, 59-72.

Liu, R., Tang, W., Han, X., Geng, R., Wang, C., and Zhang, Z. (2018). Hepatocyte growth factor-induced mesenchymal-epithelial transition factor activation leads to insulin-like growth factor 1 receptor inhibitor unresponsiveness in gastric cancer cells. Oncol Lett *16*, 5983-5991.

Liu, X., Zhang, H., Lai, L., Wang, X., Loera, S., Xue, L., He, H., Zhang, K., Hu, S., Huang, Y*., et al.* (2013). Ribonucleotide reductase small subunit M2 serves as a prognostic biomarker and predicts poor survival of colorectal cancers. Clin Sci (Lond) *124*, 567-578.

Lodhia, K.A., Gao, S., Aleksic, T., Esashi, F., and Macaulay, V.M. (2015). Suppression of homologous recombination sensitizes human tumor cells to IGF-1R inhibition. International journal of cancer *136*, 2961-2966.

Lopez-Contreras, A.J., Specks, J., Barlow, J.H., Ambrogio, C., Desler, C., Vikingsson, S., Rodrigo-Perez, S., Green, H., Rasmussen, L.J., Murga, M*., et al.* (2015). Increased Rrm2

gene dosage reduces fragile site breakage and prolongs survival of ATR mutant mice. Genes Dev *29*, 690-695.

Lopez, T., and Hanahan, D. (2002). Elevated levels of IGF-1 receptor convey invasive and metastatic capability in a mouse model of pancreatic islet tumorigenesis. Cancer cell *1*, 339-353.

Lou, Z., Minter-Dykhouse, K., Franco, S., Gostissa, M., Rivera, M.A., Celeste, A., Manis, J.P., van Deursen, J., Nussenzweig, A., Paull, T.T.*, et al.* (2006). MDC1 maintains genomic stability by participating in the amplification of ATM-dependent DNA damage signals. Mol Cell *21*, 187-200.

Lukas, C., Savic, V., Bekker-Jensen, S., Doil, C., Neumann, B., Pedersen, R.S., Grøfte, M., Chan, K.L., Hickson, I.D., Bartek, J.*, et al.* (2011). 53BP1 nuclear bodies form around DNA lesions generated by mitotic transmission of chromosomes under replication stress. Nature cell biology *13*, 243-253.

Lundberg, A.S., and Weinberg, R.A. (1998). Functional inactivation of the retinoblastoma protein requires sequential modification by at least two distinct cyclin-cdk complexes. Molecular and cellular biology *18*, 753-761.

Ma, J., Pollak, M.N., Giovannucci, E., Chan, J.M., Tao, Y., Hennekens, C.H., and Stampfer, M.J. (1999). Prospective study of colorectal cancer risk in men and plasma levels of insulin-like growth factor (IGF)-I and IGF-binding protein-3. J Natl Cancer Inst *91*, 620-625.

Macaulay, V.M., Middleton, M.R., Eckhardt, S.G., Rudin, C.M., Juergens, R.A., Gedrich, R., Gogov, S., McCarthy, S., Poondru, S., Stephens, A.W.*, et al.* (2016). Phase I Dose-Escalation Study of Linsitinib (OSI-906) and Erlotinib in Patients with Advanced Solid Tumors. Clinical cancer research : an official journal of the American Association for Cancer Research *22*, 2897-2907.

Macheret, M., and Halazonetis, T.D. (2015). DNA replication stress as a hallmark of cancer. Annu Rev Pathol *10*, 425-448.

Maehama, T., and Dixon, J.E. (1998). The tumor suppressor, PTEN/MMAC1, dephosphorylates the lipid second messenger, phosphatidylinositol 3,4,5-trisphosphate. The Journal of biological chemistry *273*, 13375-13378.

Magnussen, G.I., Holm, R., Emilsen, E., Rosnes, A.K., Slipicevic, A., and Flørenes, V.A. (2012). High expression of Wee1 is associated with poor disease-free survival in malignant melanoma: potential for targeted therapy. PLoS One *7*, e38254.

Mailand, N., Gibbs-Seymour, I., and Bekker-Jensen, S. (2013). Regulation of PCNA-protein interactions for genome stability. Nature reviews Molecular cell biology *14*, 269-282.

Malempati, S., Weigel, B., Ingle, A.M., Ahern, C.H., Carroll, J.M., Roberts, C.T., Reid, J.M., Schmechel, S., Voss, S.D., Cho, S.Y.*, et al.* (2012). Phase I/II trial and pharmacokinetic study of cixutumumab in pediatric patients with refractory solid tumors and Ewing sarcoma: a report from the Children's Oncology Group. Journal of clinical oncology : official journal of the American Society of Clinical Oncology *30*, 256-262.

Malumbres, M., and Barbacid, M. (2005). Mammalian cyclin-dependent kinases. Trends Biochem Sci *30*, 630-641.

Malumbres, M., and Barbacid, M. (2009). Cell cycle, CDKs and cancer: a changing paradigm. Nature reviews Cancer *9*, 153-166.

Malumbres, M., Harlow, E., Hunt, T., Hunter, T., Lahti, J.M., Manning, G., Morgan, D.O., Tsai, L.H., and Wolgemuth, D.J. (2009). Cyclin-dependent kinases: a family portrait. Nature cell biology *11*, 1275-1276.

Manders, E.M., Stap, J., Brakenhoff, G.J., van Driel, R., and Aten, J.A. (1992). Dynamics of three-dimensional replication patterns during the S-phase, analysed by double labelling of DNA and confocal microscopy. Journal of cell science *103 (Pt 3)*, 857-862.

Manning, B.D., and Cantley, L.C. (2007). AKT/PKB signaling: navigating downstream. Cell *129*, 1261-1274.

Martin-Kleiner, I., and Gall Troselj, K. (2010). Mannose-6-phosphate/insulin-like growth factor 2 receptor (M6P/IGF2R) in carcinogenesis. Cancer Lett *289*, 11-22.

Masaki, T., Shiratori, Y., Rengifo, W., Igarashi, K., Yamagata, M., Kurokohchi, K., Uchida, N., Miyauchi, Y., Yoshiji, H., Watanabe, S.*, et al.* (2003). Cyclins and cyclin-dependent kinases: comparative study of hepatocellular carcinoma versus cirrhosis. Hepatology *37*, 534-543.

Mathews, C.K. (2015). Deoxyribonucleotide metabolism, mutagenesis and cancer. Nature reviews Cancer *15*, 528-539.

Matsuoka, S., Rotman, G., Ogawa, A., Shiloh, Y., Tamai, K., and Elledge, S.J. (2000). Ataxia telangiectasia-mutated phosphorylates Chk2 in vivo and in vitro. Proceedings of the National Academy of Sciences of the United States of America *97*, 10389-10394.

Maya-Mendoza, A., Moudry, P., Merchut-Maya, J.M., Lee, M., Strauss, R., and Bartek, J. (2018). High speed of fork progression induces DNA replication stress and genomic instability. Nature *559*, 279-284.

McClue, S.J., Blake, D., Clarke, R., Cowan, A., Cummings, L., Fischer, P.M., MacKenzie, M., Melville, J., Stewart, K., Wang, S.*, et al.* (2002). In vitro and in vivo antitumor properties of the cyclin dependent kinase inhibitor CYC202 (R-roscovitine). International journal of cancer *102*, 463-468.

McIntosh, D., and Blow, J.J. (2012). Dormant origins, the licensing checkpoint, and the response to replicative stresses. Cold Spring Harb Perspect Biol *4*.

Menoyo, A., Alazzouzi, H., Espín, E., Armengol, M., Yamamoto, H., and Schwartz, S., Jr. (2001). Somatic mutations in the DNA damage-response genes ATR and CHK1 in sporadic stomach tumors with microsatellite instability. Cancer research *61*, 7727-7730.

Merrick, C.J., Jackson, D., and Diffley, J.F. (2004). Visualization of altered replication dynamics after DNA damage in human cells. The Journal of biological chemistry *279*, 20067-20075.

Mertz, T.M., Sharma, S., Chabes, A., and Shcherbakova, P.V. (2015). Colon cancer-associated mutator DNA polymerase delta variant causes expansion of dNTP pools increasing its own infidelity. Proceedings of the National Academy of Sciences of the United States of America *112*, E2467-2476.

Mir, S.E., De Witt Hamer, P.C., Krawczyk, P.M., Balaj, L., Claes, A., Niers, J.M., Van Tilborg, A.A., Zwinderman, A.H., Geerts, D., Kaspers, G.J.*, et al.* (2010). In silico analysis of kinase expression identifies WEE1 as a gatekeeper against mitotic catastrophe in glioblastoma. Cancer cell *18*, 244-257.

Mireuta, M., Birman, E., Barmash, M., and Pollak, M. (2014). Quantification of binding of IGF-1 to BI 836845, a candidate therapeutic antibody against IGF-1 and IGF-2, and effects of this antibody on IGF-1:IGFBP-3 complexes in vitro and in male C57BL/6 mice. Endocrinology *155*, 703-715.

Mirkin, E.V., and Mirkin, S.M. (2007). Replication fork stalling at natural impediments. Microbiol Mol Biol Rev *71*, 13-35.

Moeglin, E., Desplancq, D., Conic, S., Oulad-Abdelghani, M., Stoessel, A., Chiper, M., Vigneron, M., Didier, P., Tora, L., and Weiss, E. (2019). Uniform Widespread Nuclear Phosphorylation of Histone H2AX Is an Indicator of Lethal DNA Replication Stress. Cancers *11*.

Moiseeva, T., Hood, B., Schamus, S., O'Connor, M.J., Conrads, T.P., and Bakkenist, C.J. (2017). ATR kinase inhibition induces unscheduled origin firing through a Cdc7-dependent association between GINS and And-1. Nature communications *8*, 1392.

Moiseeva, T.N., Yin, Y., Calderon, M.J., Qian, C., Schamus-Haynes, S., Sugitani, N., Osmanbeyoglu, H.U., Rothenberg, E., Watkins, S.C., and Bakkenist, C.J. (2019). An ATR and CHK1 kinase signaling mechanism that limits origin firing during unperturbed DNA replication. Proceedings of the National Academy of Sciences of the United States of America *116*, 13374-13383.

Moller, D.E., Yokota, A., Caro, J.F., and Flier, J.S. (1989). Tissue-specific expression of two alternatively spliced insulin receptor mRNAs in man. Mol Endocrinol *3*, 1263-1269.

Monnat, R.J., Jr. (2007). From broken to old: DNA damage, IGF1 endocrine suppression and aging. DNA Repair (Amst) *6*, 1386-1390.

Morgan, D.O., Edman, J.C., Standring, D.N., Fried, V.A., Smith, M.C., Roth, R.A., and Rutter, W.J. (1987). Insulin-like growth factor II receptor as a multifunctional binding protein. Nature *329*, 301-307.

Morikawa, T., Maeda, D., Kume, H., Homma, Y., and Fukayama, M. (2010). Ribonucleotide reductase M2 subunit is a novel diagnostic marker and a potential therapeutic target in bladder cancer. Histopathology *57*, 885-892.

Mu, K., Li, L., Yang, Q., Zhang, T., Gao, P., Meng, B., Liu, Z., Wang, Y., and Zhou, G. (2011). Detection of CHK1 and CCND1 gene copy number changes in breast cancer with dual-colour fluorescence in-situ hybridization. Histopathology *58*, 601-607.

Muise-Helmericks, R.C., Grimes, H.L., Bellacosa, A., Malstrom, S.E., Tsichlis, P.N., and Rosen, N. (1998). Cyclin D expression is controlled post-transcriptionally via a phosphatidylinositol 3-kinase/Akt-dependent pathway. The Journal of biological chemistry *273*, 29864-29872.

Mulvihill, M.J., Cooke, A., Rosenfeld-Franklin, M., Buck, E., Foreman, K., Landfair, D., O'Connor, M., Pirritt, C., Sun, Y., Yao, Y.*, et al.* (2009). Discovery of OSI-906: a selective and orally efficacious dual inhibitor of the IGF-1 receptor and insulin receptor. Future Med Chem *1*, 1153-1171.

Myers, M.G., Jr., Backer, J.M., Sun, X.J., Shoelson, S., Hu, P., Schlessinger, J., Yoakim, M., Schaffhausen, B., and White, M.F. (1992). IRS-1 activates phosphatidylinositol 3'-kinase by associating with src homology 2 domains of p85. Proceedings of the National Academy of Sciences of the United States of America *89*, 10350-10354.

Nai, S., Shi, Y., Ru, H., Ding, Y., Geng, Q., Li, Z., Dong, M.Q., Xu, X., and Li, J. (2019). Chk2-dependent phosphorylation of myosin phosphatase targeting subunit 1 (MYPT1) regulates centrosome maturation. Cell cycle (Georgetown, Tex) *18*, 2651-2659.

Nakae, J., Kido, Y., and Accili, D. (2001). Distinct and overlapping functions of insulin and IGF-I receptors. Endocr Rev *22*, 818-835.

Nath, S., and Devi, G.R. (2016). Three-dimensional culture systems in cancer research: Focus on tumor spheroid model. Pharmacol Ther *163*, 94-108.

Niida, H., Katsuno, Y., Sengoku, M., Shimada, M., Yukawa, M., Ikura, M., Ikura, T., Kohno, K., Shima, H., Suzuki, H.*, et al.* (2010). Essential role of Tip60-dependent recruitment of ribonucleotide reductase at DNA damage sites in DNA repair during G1 phase. Genes Dev *24*, 333-338.

Nilsson, A., Isgaard, J., Lindahl, A., Dahlstrom, A., Skottner, A., and Isaksson, O.G. (1986). Regulation by growth hormone of number of chondrocytes containing IGF-I in rat growth plate. Science (New York, NY) *233*, 571-574.

Nishitani, H., Lygerou, Z., Nishimoto, T., and Nurse, P. (2000). The Cdt1 protein is required to license DNA for replication in fission yeast. Nature *404*, 625-628.

O'Brien, N., Conklin, D., Beckmann, R., Luo, T., Chau, K., Thomas, J., Mc Nulty, A., Marchal, C., Kalous, O., von Euw, E.*, et al.* (2018). Preclinical Activity of Abemaciclib Alone or in Combination with Antimitotic and Targeted Therapies in Breast Cancer. Molecular cancer therapeutics *17*, 897-907.

O'Farrell, P.H. (2011). Quiescence: early evolutionary origins and universality do not imply uniformity. Philos Trans R Soc Lond B Biol Sci *366*, 3498-3507.

O'Flanagan, C.H., O'Shea, S., Lyons, A., Fogarty, F.M., McCabe, N., Kennedy, R.D., and O'Connor, R. (2016). IGF-1R inhibition sensitizes breast cancer cells to ATM-related kinase (ATR) inhibitor and cisplatin. Oncotarget *7*, 56826-56841.

Okuda, M., Horn, H.F., Tarapore, P., Tokuyama, Y., Smulian, A.G., Chan, P.K., Knudsen, E.S., Hofmann, I.A., Snyder, J.D., Bove, K.E.*, et al.* (2000). Nucleophosmin/B23 is a target of CDK2/cyclin E in centrosome duplication. Cell *103*, 127-140.

Olcina, M.M., Foskolou, I.P., Anbalagan, S., Senra, J.M., Pires, I.M., Jiang, Y., Ryan, A.J., and Hammond, E.M. (2013). Replication stress and chromatin context link ATM activation to a role in DNA replication. Mol Cell *52*, 758-766.

Olivier, M., Hollstein, M., and Hainaut, P. (2010). TP53 mutations in human cancers: origins, consequences, and clinical use. Cold Spring Harb Perspect Biol *2*, a001008.

Osher, E., and Macaulay, V.M. (2019). Therapeutic Targeting of the IGF Axis. Cells *8*.

Otto, T., and Sicinski, P. (2017). Cell cycle proteins as promising targets in cancer therapy. Nature reviews Cancer *17*, 93-115.

Ou, D.L., Lee, B.S., Lin, L.I., Liou, J.Y., Liao, S.C., Hsu, C., and Cheng, A.L. (2014). Vertical blockade of the IGFR- PI3K/Akt/mTOR pathway for the treatment of hepatocellular carcinoma: the role of survivin. Molecular cancer *13*, 2.

Overgaard, M.T., Boldt, H.B., Laursen, L.S., Sottrup-Jensen, L., Conover, C.A., and Oxvig, C. (2001). Pregnancy-associated plasma protein-A2 (PAPP-A2), a novel insulin-like growth factor-binding protein-5 proteinase. The Journal of biological chemistry *276*, 21849-21853.

Packham, S., Warsito, D., Lin, Y., Sadi, S., Karlsson, R., Sehat, B., and Larsson, O. (2015). Nuclear translocation of IGF-1R via p150(Glued) and an importin-beta/RanBP2-dependent pathway in cancer cells. Oncogene *34*, 2227-2238.

Palumbo, A., Lau, G., and Saraceni, M. (2019). Abemaciclib: The Newest CDK4/6 Inhibitor for the Treatment of Breast Cancer. Ann Pharmacother *53*, 178-185.

Parker, L.L., and Piwnica-Worms, H. (1992). Inactivation of the p34cdc2-cyclin B complex by the human WEE1 tyrosine kinase. Science (New York, NY) *257*, 1955-1957.

Parkes, E.E., Walker, S.M., Taggart, L.E., McCabe, N., Knight, L.A., Wilkinson, R., McCloskey, K.D., Buckley, N.E., Savage, K.I., Salto-Tellez, M.*, et al.* (2017). Activation of STING-Dependent Innate Immune Signaling By S-Phase-Specific DNA Damage in Breast Cancer. J Natl Cancer Inst *109*.

Parsels, L.A., Parsels, J.D., Tanska, D.M., Maybaum, J., Lawrence, T.S., and Morgan, M.A. (2018). The contribution of DNA replication stress marked by high-intensity, pan-nuclear gammaH2AX staining to chemosensitization by CHK1 and WEE1 inhibitors. Cell cycle (Georgetown, Tex) *17*, 1076-1086.

Pfister, S.X., Markkanen, E., Jiang, Y., Sarkar, S., Woodcock, M., Orlando, G., Mavrommati, I., Pai, C.C., Zalmas, L.P., Drobnitzky, N.*, et al.* (2015). Inhibiting WEE1 Selectively Kills Histone H3K36me3-Deficient Cancers by dNTP Starvation. Cancer cell *28*, 557-568.

Pickl, M., and Ries, C.H. (2009). Comparison of 3D and 2D tumor models reveals enhanced HER2 activation in 3D associated with an increased response to trastuzumab. Oncogene *28*, 461-468.

Plyte, S., and Musacchio, A. (2007). PLK1 inhibitors: setting the mitotic death trap. Current biology : CB *17*, R280-283.

Puche, J.E., and Castilla-Cortázar, I. (2012). Human conditions of insulin-like growth factor-I (IGF-I) deficiency. J Transl Med *10*, 224.

Rafiei, S., Fitzpatrick, K., Liu, D., Cai, M.Y., Elmarakeby, H.A., Park, J., Ricker, C., Kochupurakkal, B.S., Choudhury, A.D., Hahn, W.C.*, et al.* (2020). ATM Loss Confers Greater Sensitivity to ATR Inhibition than PARP Inhibition in Prostate Cancer. Cancer research.

Rajeshkumar, N.V., De Oliveira, E., Ottenhof, N., Watters, J., Brooks, D., Demuth, T., Shumway, S.D., Mizuarai, S., Hirai, H., Maitra, A.*, et al.* (2011). MK-1775, a potent Wee1 inhibitor, synergizes with gemcitabine to achieve tumor regressions, selectively in p53-deficient pancreatic cancer xenografts. Clinical cancer research : an official journal of the American Association for Cancer Research *17*, 2799-2806.

Ramcharan, R., Aleksic, T., Kamdoum, W.P., Gao, S., Pfister, S.X., Tanner, J., Bridges, E., Asher, R., Watson, A.J., Margison, G.P.*, et al.* (2015). IGF-1R inhibition induces schedule-dependent sensitization of human melanoma to temozolomide. Oncotarget *6*, 39877-39890.

Rasmussen, R.D., Gajjar, M.K., Tuckova, L., Jensen, K.E., Maya-Mendoza, A., Holst, C.B., Møllgaard, K., Rasmussen, J.S., Brennum, J., Bartek, J., Jr.*, et al.* (2016). BRCA1-regulated RRM2 expression protects glioblastoma cells from endogenous replication stress and promotes tumorigenicity. Nature communications *7*, 13398.

Ravichandran, K.S., Lorenz, U., Shoelson, S.E., and Burakoff, S.J. (1995). Interaction of Shc with Grb2 regulates association of Grb2 with mSOS. Molecular and cellular biology *15*, 593-600.

Reck, M., Horn, L., Novello, S., Barlesi, F., Albert, I., Juhasz, E., Kowalski, D., Robinet, G., Cadranel, J., Bidoli, P.*, et al.* (2019). Phase II Study of Roniciclib in Combination with Cisplatin/Etoposide or Carboplatin/Etoposide as First-Line Therapy in Patients with Extensive-Disease Small Cell Lung Cancer. J Thorac Oncol *14*, 701-711.

Reisländer, T., Lombardi, E.P., Groelly, F.J., Miar, A., Porru, M., Di Vito, S., Wright, B., Lockstone, H., Biroccio, A., Harris, A.*, et al.* (2019). BRCA2 abrogation triggers innate immune responses potentiated by treatment with PARP inhibitors. Nature communications *10*, 3143.

Renehan, A.G., Zwahlen, M., Minder, C., O'Dwyer, S.T., Shalet, S.M., and Egger, M. (2004). Insulin-like growth factor (IGF)-I, IGF binding protein-3, and cancer risk: systematic review and meta-regression analysis. Lancet *363*, 1346-1353.

Resnicoff, M., Abraham, D., Yutanawiboonchai, W., Rotman, H.L., Kajstura, J., Rubin, R., Zoltick, P., and Baserga, R. (1995). The insulin-like growth factor I receptor protects tumor cells from apoptosis in vivo. Cancer research *55*, 2463-2469.

Riballo, E., Kühne, M., Rief, N., Doherty, A., Smith, G.C., Recio, M.J., Reis, C., Dahm, K., Fricke, A., Krempler, A.*, et al.* (2004). A pathway of double-strand break rejoining dependent upon ATM, Artemis, and proteins locating to gamma-H2AX foci. Mol Cell *16*, 715-724.

Rieder, C.L., and Salmon, E.D. (1994). Motile kinetochores and polar ejection forces dictate chromosome position on the vertebrate mitotic spindle. The Journal of cell biology *124*, 223-233.

Riedl, A., Schlederer, M., Pudelko, K., Stadler, M., Walter, S., Unterleuthner, D., Unger, C., Kramer, N., Hengstschlager, M., Kenner, L.*, et al.* (2017). Comparison of cancer cells in 2D vs 3D culture reveals differences in AKT-mTOR-S6K signaling and drug responses. Journal of cell science *130*, 203-218.

Riesterer, O., Yang, Q., Raju, U., Torres, M., Molkentine, D., Patel, N., Valdecanas, D., Milas, L., and Ang, K.K. (2011). Combination of anti-IGF-1R antibody A12 and ionizing radiation in upper respiratory tract cancers. Int J Radiat Oncol Biol Phys *79*, 1179-1187.

Rinderknecht, E., and Humbel, R.E. (1978). The amino acid sequence of human insulin-like growth factor I and its structural homology with proinsulin. The Journal of biological chemistry *253*, 2769-2776.

Roberts, B.T., Ying, C.Y., Gautier, J., and Maller, J.L. (1999). DNA replication in vertebrates requires a homolog of the Cdc7 protein kinase. Proceedings of the National Academy of Sciences of the United States of America *96*, 2800-2804.

Rocha, R.L., Hilsenbeck, S.G., Jackson, J.G., Lee, A.V., Figueroa, J.A., and Yee, D. (1996). Correlation of insulin-like growth factor-binding protein-3 messenger RNA with protein expression in primary breast cancer tissues: detection of higher levels in tumors with poor prognostic features. J Natl Cancer Inst *88*, 601-606.

Rochester, M.A., Patel, N., Turney, B.W., Davies, D.R., Roberts, I.S., Crew, J., Protheroe, A., and Macaulay, V.M. (2007). The type 1 insulin-like growth factor receptor is over-expressed in bladder cancer. BJU international *100*, 1396-1401.

Rochester, M.A., Riedemann, J., Hellawell, G.O., Brewster, S.F., and Macaulay, V.M. (2005). Silencing of the IGF1R gene enhances sensitivity to DNA-damaging agents in both PTEN wild-type and mutant human prostate cancer. Cancer Gene Ther *12*, 90-100.

Rogakou, E.P., Pilch, D.R., Orr, A.H., Ivanova, V.S., and Bonner, W.M. (1998). DNA double-stranded breaks induce histone H2AX phosphorylation on serine 139. The Journal of biological chemistry *273*, 5858-5868.

Rowzee, A.M., Lazzarino, D.A., Rota, L., Sun, Z., and Wood, T.L. (2008). IGF ligand and receptor regulation of mammary development. J Mammary Gland Biol Neoplasia *13*, 361-370.

Saldivar, J.C., Cortez, D., and Cimprich, K.A. (2017). The essential kinase ATR: ensuring faithful duplication of a challenging genome. Nature reviews Molecular cell biology *18*, 622-636.

Saltiel, A.R., and Kahn, C.R. (2001). Insulin signalling and the regulation of glucose and lipid metabolism. Nature *414*, 799-806.

Sanderson, M.P., Apgar, J., Garin-Chesa, P., Hofmann, M.H., Kessler, D., Quant, J., Savchenko, A., Schaaf, O., Treu, M., Tye, H.*, et al.* (2015). BI 885578, a Novel IGF1R/INSR Tyrosine Kinase Inhibitor with Pharmacokinetic Properties That Dissociate Antitumor Efficacy and Perturbation of Glucose Homeostasis. Molecular cancer therapeutics *14*, 2762-2772.

Sanderson, M.P., Hofmann, M.H., Garin-Chesa, P., Schweifer, N., Wernitznig, A., Fischer, S., Jeschko, A., Meyer, R., Moll, J., Pecina, T.*, et al.* (2017). The IGF1R/INSR Inhibitor BI 885578 Selectively Inhibits Growth of IGF2-Overexpressing Colorectal Cancer Tumors and Potentiates the Efficacy of Anti-VEGF Therapy. Molecular cancer therapeutics *16*, 2223-2233.

Sant, S., and Johnston, P.A. (2017). The production of 3D tumor spheroids for cancer drug discovery. Drug Discov Today Technol *23*, 27-36.

Sasaoka, T., Rose, D.W., Jhun, B.H., Saltiel, A.R., Draznin, B., and Olefsky, J.M. (1994). Evidence for a functional role of Shc proteins in mitogenic signaling induced by insulin, insulin-like growth factor-1, and epidermal growth factor. The Journal of biological chemistry *269*, 13689-13694.

Scagliotti, G.V., Bondarenko, I., Blackhall, F., Barlesi, F., Hsia, T.C., Jassem, J., Milanowski, J., Popat, S., Sanchez-Torres, J.M., Novello, S.*, et al.* (2015). Randomized, phase III trial of figitumumab in combination with erlotinib versus erlotinib alone in patients with nonadenocarcinoma nonsmall-cell lung cancer. Ann Oncol *26*, 497-504.

Schlacher, K., Christ, N., Siaud, N., Egashira, A., Wu, H., and Jasin, M. (2011). Double-strand break repair-independent role for BRCA2 in blocking stalled replication fork degradation by MRE11. Cell *145*, 529-542.

Schlacher, K., Wu, H., and Jasin, M. (2012). A distinct replication fork protection pathway connects Fanconi anemia tumor suppressors to RAD51-BRCA1/2. Cancer cell *22*, 106-116.

Schwartz, G.K., Dickson, M.A., LoRusso, P.M., Sausville, E.A., Maekawa, Y., Watanabe, Y., Kashima, N., Nakashima, D., and Akinaga, S. (2016). Preclinical and first-in-human phase I studies of KW-2450, an oral tyrosine kinase inhibitor with insulin-like growth factor receptor-1/insulin receptor selectivity. Cancer Sci *107*, 499-506.

Scully, R., Panday, A., Elango, R., and Willis, N.A. (2019). DNA double-strand break repair-pathway choice in somatic mammalian cells. Nature reviews Molecular cell biology *20*, 698-714.

Sehat, B., Tofigh, A., Lin, Y., Trocme, E., Liljedahl, U., Lagergren, J., and Larsson, O. (2010). SUMOylation mediates the nuclear translocation and signaling of the IGF-1 receptor. Science signaling *3*, ra10.

Shechter, D., Costanzo, V., and Gautier, J. (2004). ATR and ATM regulate the timing of DNA replication origin firing. Nature cell biology *6*, 648-655.

Sherman, P.A., and Fyfe, J.A. (1989). Enzymatic assay for deoxyribonucleoside triphosphates using synthetic oligonucleotides as template primers. Anal Biochem *180*, 222-226.

Shevah, O., and Laron, Z. (2007). Patients with congenital deficiency of IGF-I seem protected from the development of malignancies: a preliminary report. Growth Horm IGF Res *17*, 54-57.

Shieh, S.Y., Ahn, J., Tamai, K., Taya, Y., and Prives, C. (2000). The human homologs of checkpoint kinases Chk1 and Cds1 (Chk2) phosphorylate p53 at multiple DNA damage-inducible sites. Genes Dev *14*, 289-300.

Shiloh, Y. (2003). ATM and related protein kinases: safeguarding genome integrity. Nature reviews Cancer *3*, 155-168.

Simpson, A.D., Soo, Y.W.J., Rieunier, G., Aleksic, T., Ansorge, O., Jones, C., and Macaulay, V.M. (2020). Type 1 IGF receptor associates with adverse outcome and cellular radioresistance in paediatric high-grade glioma. Br J Cancer *122*, 624-629.

Sistigu, A., Yamazaki, T., Vacchelli, E., Chaba, K., Enot, D.P., Adam, J., Vitale, I., Goubar, A., Baracco, E.E., Remédios, C.*, et al.* (2014). Cancer cell-autonomous contribution of type I interferon signaling to the efficacy of chemotherapy. Nature medicine *20*, 1301-1309.

Smith, M.E., Cimica, V., Chinni, S., Challagulla, K., Mani, S., and Kalpana, G.V. (2008). Rhabdoid tumor growth is inhibited by flavopiridol. Clinical cancer research : an official journal of the American Association for Cancer Research *14*, 523-532.

Solier, S., Sordet, O., Kohn, K.W., and Pommier, Y. (2009). Death receptor-induced activation of the Chk2- and histone H2AX-associated DNA damage response pathways. Molecular and cellular biology *29*, 68-82.

Soos, M.A., Whittaker, J., Lammers, R., Ullrich, A., and Siddle, K. (1990). Receptors for insulin and insulin-like growth factor-I can form hybrid dimers. Characterisation of hybrid receptors in transfected cells. The Biochemical journal *270*, 383-390.

Srinivasan, S.V., Dominguez-Sola, D., Wang, L.C., Hyrien, O., and Gautier, J. (2013). Cdc45 is a critical effector of myc-dependent DNA replication stress. Cell reports *3*, 1629-1639.

Steigen, S.E., Schaeffer, D.F., West, R.B., and Nielsen, T.O. (2009). Expression of insulin-like growth factor 2 in mesenchymal neoplasms. Mod Pathol *22*, 914-921.

Stubbe, J., and van der Donk, W.A. (1995). Ribonucleotide reductases: radical enzymes with suicidal tendencies. Chem Biol *2*, 793-801.

Suckale, J., and Solimena, M. (2008). Pancreas islets in metabolic signaling--focus on the beta-cell. Front Biosci *13*, 7156-7171.

Suleymanova, N., Crudden, C., Worrall, C., Dricu, A., Girnita, A., and Girnita, L. (2017). Enhanced response of melanoma cells to MEK inhibitors following unbiased IGF-1R down-regulation. Oncotarget *8*, 82256-82267.

Sun, L., Wu, J., Du, F., Chen, X., and Chen, Z.J. (2013). Cyclic GMP-AMP synthase is a cytosolic DNA sensor that activates the type I interferon pathway. Science (New York, NY) *339*, 786-791.

Syljuasen, R.G., Sorensen, C.S., Hansen, L.T., Fugger, K., Lundin, C., Johansson, F., Helleday, T., Sehested, M., Lukas, J., and Bartek, J. (2005). Inhibition of human Chk1 causes increased initiation of DNA replication, phosphorylation of ATR targets, and DNA breakage. Molecular and cellular biology *25*, 3553-3562.

Tanaka, H., Arakawa, H., Yamaguchi, T., Shiraishi, K., Fukuda, S., Matsui, K., Takei, Y., and Nakamura, Y. (2000). A ribonucleotide reductase gene involved in a p53-dependent cell-cycle checkpoint for DNA damage. Nature *404*, 42-49.

Tang, H., Xiao, G., Behrens, C., Schiller, J., Allen, J., Chow, C.W., Suraokar, M., Corvalan, A., Mao, J., White, M.A*., et al.* (2013). A 12-gene set predicts survival benefits from adjuvant chemotherapy in non-small cell lung cancer patients. Clinical cancer research : an official journal of the American Association for Cancer Research *19*, 1577-1586.

Tang, L., Yang, J., Chen, J., Yu, J., Zhou, Q., Lu, X., and Wang, Y. (2017). IGF-1R promotes the expression of cyclin D1 protein and accelerates the G1/S transition by activating Ras/Raf/MEK/ERK signaling pathway. Int J Clin Exp Pathol *10*, 11652-11658.

Terzi, M.Y., Izmirli, M., and Gogebakan, B. (2016). The cell fate: senescence or quiescence. Mol Biol Rep *43*, 1213-1220.

Tin Su, T. (2001). Cell cycle: how, when and why cells get rid of cyclin A. Current biology : CB *11*, R467-469.

Tolcher, A.W., Sarantopoulos, J., Patnaik, A., Papadopoulos, K., Lin, C.C., Rodon, J., Murphy, B., Roth, B., McCaffery, I., Gorski, K.S*., et al.* (2009). Phase I, pharmacokinetic, and pharmacodynamic study of AMG 479, a fully human monoclonal antibody to insulin-like growth factor receptor 1. Journal of clinical oncology : official journal of the American Society of Clinical Oncology *27*, 5800-5807.

Toledo, L., Neelsen, K.J., and Lukas, J. (2017). Replication Catastrophe: When a Checkpoint Fails because of Exhaustion. Mol Cell *66*, 735-749.

Toledo, L.I., Altmeyer, M., Rask, M.B., Lukas, C., Larsen, D.H., Povlsen, L.K., Bekker-Jensen, S., Mailand, N., Bartek, J., and Lukas, J. (2013). ATR prohibits replication catastrophe by preventing global exhaustion of RPA. Cell *155*, 1088-1103.

Travis, R.C., Appleby, P.N., Martin, R.M., Holly, J.M.P., Albanes, D., Black, A., Bueno-de-Mesquita, H.B.A., Chan, J.M., Chen, C., Chirlaque, M.D*., et al.* (2016). A Meta-analysis of Individual Participant Data Reveals an Association between Circulating Levels of IGF-I and Prostate Cancer Risk. Cancer research *76*, 2288-2300.

Turner, B.C., Haffty, B.G., Narayanan, L., Yuan, J., Havre, P.A., Gumbs, A.A., Kaplan, L., Burgaud, J.L., Carter, D., Baserga, R*., et al.* (1997). Insulin-like growth factor-I receptor

overexpression mediates cellular radioresistance and local breast cancer recurrence after lumpectomy and radiation. Cancer research *57*, 3079-3083.

Turney, B.W., Kerr, M., Chitnis, M.M., Lodhia, K., Wang, Y., Riedemann, J., Rochester, M., Protheroe, A.S., Brewster, S.F., and Macaulay, V.M. (2012). Depletion of the type 1 IGF receptor delays repair of radiation-induced DNA double strand breaks. Radiotherapy and oncology : journal of the European Society for Therapeutic Radiology and Oncology *103*, 402-409.

Tye, B.K. (1999). MCM proteins in DNA replication. Annual review of biochemistry *68*, 649-686.

Ubhi, T., and Brown, G.W. (2019). Exploiting DNA Replication Stress for Cancer Treatment. Cancer research *79*, 1730-1739.

Uhlmann, F., Wernic, D., Poupart, M.A., Koonin, E.V., and Nasmyth, K. (2000). Cleavage of cohesin by the CD clan protease separin triggers anaphase in yeast. Cell *103*, 375-386.

Ullrich, A., Gray, A., Tam, A.W., Yang-Feng, T., Tsubokawa, M., Collins, C., Henzel, W., Le Bon, T., Kathuria, S., Chen, E.*, et al.* (1986). Insulin-like growth factor I receptor primary structure: comparison with insulin receptor suggests structural determinants that define functional specificity. The EMBO journal *5*, 2503-2512.

Uziel, T., Lerenthal, Y., Moyal, L., Andegeko, Y., Mittelman, L., and Shiloh, Y. (2003). Requirement of the MRN complex for ATM activation by DNA damage. The EMBO journal *22*, 5612-5621.

Valverde, A.M., Lorenzo, M., Pons, S., White, M.F., and Benito, M. (1998). Insulin receptor substrate (IRS) proteins IRS-1 and IRS-2 differential signaling in the insulin/insulin-like growth factor-I pathways in fetal brown adipocytes. Mol Endocrinol *12*, 688-697.

van der Pluijm, I., Garinis, G.A., Brandt, R.M., Gorgels, T.G., Wijnhoven, S.W., Diderich, K.E., de Wit, J., Mitchell, J.R., van Oostrom, C., Beems, R.*, et al.* (2007). Impaired genome maintenance suppresses the growth hormone--insulin-like growth factor 1 axis in mice with Cockayne syndrome. PLoS Biol *5*, e2.

van der Veeken, J., Oliveira, S., Schiffelers, R.M., Storm, G., van Bergen En Henegouwen, P.M., and Roovers, R.C. (2009). Crosstalk between epidermal growth factor receptor- and insulin-like growth factor-1 receptor signaling: implications for cancer therapy. Curr Cancer Drug Targets *9*, 748-760.

van Maldegem, A.M., Bovee, J.V., Peterse, E.F., Hogendoorn, P.C., and Gelderblom, H. (2016). Ewing sarcoma: The clinical relevance of the insulin-like growth factor 1 and the poly-ADP-ribose-polymerase pathway. European journal of cancer (Oxford, England : 1990) *53*, 171-180.

Verlinden, L., Vanden Bempt, I., Eelen, G., Drijkoningen, M., Verlinden, I., Marchal, K., De Wolf-Peeters, C., Christiaens, M.R., Michiels, L., Bouillon, R.*, et al.* (2007). The E2F-regulated gene Chk1 is highly expressed in triple-negative estrogen receptor /progesterone receptor /HER-2 breast carcinomas. Cancer research *67*, 6574-6581.

Verloes, A., Drunat, S., Gressens, P., and Passemard, S. (1993). Primary Autosomal Recessive Microcephalies and Seckel Syndrome Spectrum Disorders – RETIRED CHAPTER, FOR HISTORICAL REFERENCE ONLY. In GeneReviews(®), M.P. Adam, H.H. Ardinger, R.A. Pagon, S.E. Wallace, L.J.H. Bean, K. Stephens, and A. Amemiya, eds. (Seattle (WA): University of Washington, Seattle

Vojtek, A.B., Hollenberg, S.M., and Cooper, J.A. (1993). Mammalian Ras interacts directly with the serine/threonine kinase Raf. Cell *74*, 205-214.

Waga, S., Hannon, G.J., Beach, D., and Stillman, B. (1994). The p21 inhibitor of cyclin-dependent kinases controls DNA replication by interaction with PCNA. Nature *369*, 574-578.

Walczak, C.E., Cai, S., and Khodjakov, A. (2010). Mechanisms of chromosome behaviour during mitosis. Nature reviews Molecular cell biology *11*, 91-102.

Wang, C., Jette, N., Moussienko, D., Bebb, D.G., and Lees-Miller, S.P. (2017). ATM-Deficient Colorectal Cancer Cells Are Sensitive to the PARP Inhibitor Olaparib. Transl Oncol *10*, 190-196.

Wang, D., and Lippard, S.J. (2005). Cellular processing of platinum anticancer drugs. Nat Rev Drug Discov *4*, 307-320.

Wang, H., Rosen, D.G., Wang, H., Fuller, G.N., Zhang, W., and Liu, J. (2006). Insulin-like growth factor-binding protein 2 and 5 are differentially regulated in ovarian cancer of different histologic types. Mod Pathol *19*, 1149-1156.

Wang, J.C. (2002). Cellular roles of DNA topoisomerases: a molecular perspective. Nature reviews Molecular cell biology *3*, 430-440.

Wang, L.L., and Plon, S.E. (1993). Rothmund-Thomson Syndrome. In GeneReviews(®), M.P. Adam, H.H. Ardinger, R.A. Pagon, S.E. Wallace, L.J.H. Bean, K. Stephens, and A. Amemiya, eds. (Seattle (WA): University of Washington, Seattle

Copyright © 1993-2020, University of Washington, Seattle. GeneReviews is a registered trademark of the University of Washington, Seattle. All rights reserved.).

Wang, Y., Yuan, J.L., Zhang, Y.T., Ma, J.J., Xu, P., Shi, C.H., Zhang, W., Li, Y.M., Fu, Q., Zhu, G.F.*, et al.* (2013). Inhibition of both EGFR and IGF1R sensitized prostate cancer cells to radiation by synergistic suppression of DNA homologous recombination repair. PLoS One *8*, e68784.

Weber, M.M., Fottner, C., Liu, S.B., Jung, M.C., Engelhardt, D., and Baretton, G.B. (2002). Overexpression of the insulin-like growth factor I receptor in human colon carcinomas. Cancer *95*, 2086-2095.

Webster, J.A., Tibes, R., Morris, L., Blackford, A.L., Litzow, M., Patnaik, M., Rosner, G.L., Gojo, I., Kinders, R., Wang, L.*, et al.* (2017). Randomized phase II trial of cytosine arabinoside with and without the CHK1 inhibitor MK-8776 in relapsed and refractory acute myeloid leukemia. Leuk Res *61*, 108-116.

Weinberg, R.A. (1995). The retinoblastoma protein and cell cycle control. Cell *81*, 323-330.

Weyer-Czernilofsky, U., Baumgartinger, R., Schmittner, S., Gong, X., Buchanan, S., Beckmann, R.P., Marugan, C., Torres, R., Boehnke, K., Lallena, M.J.*, et al.* (2018). Abstract 1852: Combination of the CDK4/6 inhibitor abemaciclib with xentuzumab, a humanized IGF-1 and IGF-2 ligand co-neutralizing monoclonal antibody, results in synergistic antineoplastic effects in human breast cancer cell lines. Cancer research *78*, 1852-1852.

Williams, L.N., Marjavaara, L., Knowels, G.M., Schultz, E.M., Fox, E.J., Chabes, A., and Herr, A.J. (2015). dNTP pool levels modulate mutator phenotypes of error-prone DNA polymerase epsilon variants. Proceedings of the National Academy of Sciences of the United States of America *112*, E2457-2466.

Wolfel, T., Hauer, M., Schneider, J., Serrano, M., Wolfel, C., Klehmann-Hieb, E., De Plaen, E., Hankeln, T., Meyer zum Buschenfelde, K.H., and Beach, D. (1995). A p16INK4a-insensitive CDK4 mutant targeted by cytolytic T lymphocytes in a human melanoma. Science (New York, NY) *269*, 1281-1284.

Wood, D.J., and Endicott, J.A. (2018). Structural insights into the functional diversity of the CDK-cyclin family. Open Biol *8*.

Wood, K.W., Sakowicz, R., Goldstein, L.S., and Cleveland, D.W. (1997). CENP-E is a plus end-directed kinetochore motor required for metaphase chromosome alignment. Cell *91*, 357-366.

Woods, K.A., Camacho-Hubner, C., Savage, M.O., and Clark, A.J. (1996). Intrauterine growth retardation and postnatal growth failure associated with deletion of the insulin-like growth factor I gene. The New England journal of medicine *335*, 1363-1367.

Wu, J., Sun, L., Chen, X., Du, F., Shi, H., Chen, C., and Chen, Z.J. (2013). Cyclic GMP-AMP is an endogenous second messenger in innate immune signaling by cytosolic DNA. Science (New York, NY) *339*, 826-830.

Wu, J.D., Haugk, K., Coleman, I., Woodke, L., Vessella, R., Nelson, P., Montgomery, R.B., Ludwig, D.L., and Plymate, S.R. (2006). Combined in vivo effect of A12, a type 1 insulin-like growth factor receptor antibody, and docetaxel against prostate cancer tumors. Clinical cancer research : an official journal of the American Association for Cancer Research *12*, 6153-6160.

Xian, L., Wu, X., Pang, L., Lou, M., Rosen, C.J., Qiu, T., Crane, J., Frassica, F., Zhang, L., Rodriguez, J.P*., et al.* (2012). Matrix IGF-1 maintains bone mass by activation of mTOR in mesenchymal stem cells. Nature medicine *18*, 1095-1101.

Xiao, Z., Chen, Z., Gunasekera, A.H., Sowin, T.J., Rosenberg, S.H., Fesik, S., and Zhang, H. (2003). Chk1 mediates S and G2 arrests through Cdc25A degradation in response to DNA-damaging agents. The Journal of biological chemistry *278*, 21767-21773.

Xie, M., Yen, Y., Owonikoko, T.K., Ramalingam, S.S., Khuri, F.R., Curran, W.J., Doetsch, P.W., and Deng, X. (2014a). Bcl2 induces DNA replication stress by inhibiting ribonucleotide reductase. Cancer research *74*, 212-223.

Xie, Y., Wei, R.R., Huang, G.L., Zhang, M.Y., Yuan, Y.F., and Wang, H.Y. (2014b). Checkpoint kinase 1 is negatively regulated by miR-497 in hepatocellular carcinoma. Med Oncol *31*, 844.

Xiong, Y., Hannon, G.J., Zhang, H., Casso, D., Kobayashi, R., and Beach, D. (1993). p21 is a universal inhibitor of cyclin kinases. Nature *366*, 701-704.

Xu, J., Li, Y., Wang, F., Wang, X., Cheng, B., Ye, F., Xie, X., Zhou, C., and Lu, W. (2013). Suppressed miR-424 expression via upregulation of target gene Chk1 contributes to the progression of cervical cancer. Oncogene *32*, 976-987.

Xu, Y., Kong, G.K., Menting, J.G., Margetts, M.B., Delaine, C.A., Jenkin, L.M., Kiselyov, V.V., De Meyts, P., Forbes, B.E., and Lawrence, M.C. (2018). How ligand binds to the type 1 insulin-like growth factor receptor. Nature communications *9*, 821.

Yamaguchi, R., Perkins, G., and Hirota, K. (2015). Targeting cholesterol with β-cyclodextrin sensitizes cancer cells for apoptosis. FEBS Lett *589*, 4097-4105.

Yekezare, M., Gómez-González, B., and Diffley, J.F. (2013). Controlling DNA replication origins in response to DNA damage - inhibit globally, activate locally. Journal of cell science *126*, 1297-1306.

Yerushalmi, R., Gelmon, K.A., Leung, S., Gao, D., Cheang, M., Pollak, M., Turashvili, G., Gilks, B.C., and Kennecke, H. (2012). Insulin-like growth factor receptor (IGF-1R) in breast cancer subtypes. Breast Cancer Res Treat *132*, 131-142.

Yonish-Rouach, E., Resnitzky, D., Lotem, J., Sachs, L., Kimchi, A., and Oren, M. (1991). Wild-type p53 induces apoptosis of myeloid leukaemic cells that is inhibited by interleukin-6. Nature *352*, 345-347.

Yoon, S., and Seger, R. (2006). The extracellular signal-regulated kinase: multiple substrates regulate diverse cellular functions. Growth Factors *24*, 21-44.

Yu, J., Zhang, Y., McIlroy, J., Rordorf-Nikolic, T., Orr, G.A., and Backer, J.M. (1998). Regulation of the p85/p110 phosphatidylinositol 3'-kinase: stabilization and inhibition of the p110alpha catalytic subunit by the p85 regulatory subunit. Molecular and cellular biology *18*, 1379-1387.

Zapf, J., and Froesch, E.R. (1986). Insulin-like growth factors/somatomedins: structure, secretion, biological actions and physiological role. Horm Res *24*, 121-130.

Zeman, M.K., and Cimprich, K.A. (2014). Causes and consequences of replication stress. Nature cell biology *16*, 2-9.

Zhang, H., Liu, X., Warden, C.D., Huang, Y., Loera, S., Xue, L., Zhang, S., Chu, P., Zheng, S., and Yen, Y. (2014). Prognostic and therapeutic significance of ribonucleotide reductase small subunit M2 in estrogen-negative breast cancers. BMC cancer *14*, 664.

Zhang, H., Pelzer, A.M., Kiang, D.T., and Yee, D. (2007). Down-regulation of type I insulin-like growth factor receptor increases sensitivity of breast cancer cells to insulin. Cancer research *67*, 391-397.

Zhang, J.H., Chung, T.D., and Oldenburg, K.R. (1999). A Simple Statistical Parameter for Use in Evaluation and Validation of High Throughput Screening Assays. J Biomol Screen *4*, 67-73.

Zhang, W., and Liu, H.T. (2002). MAPK signal pathways in the regulation of cell proliferation in mammalian cells. Cell Res *12*, 9-18.

Zhang, Y., and Hunter, T. (2014). Roles of Chk1 in cell biology and cancer therapy. International journal of cancer *134*, 1013-1023.

Zhang, Y.W., Jones, T.L., Martin, S.E., Caplen, N.J., and Pommier, Y. (2009). Implication of checkpoint kinase-dependent up-regulation of ribonucleotide reductase R2 in DNA damage response. The Journal of biological chemistry *284*, 18085-18095.

Zhao, H., and Piwnica-Worms, H. (2001). ATR-mediated checkpoint pathways regulate phosphorylation and activation of human Chk1. Molecular and cellular biology *21*, 4129-4139.

Zoncu, R., Efeyan, A., and Sabatini, D.M. (2011). mTOR: from growth signal integration to cancer, diabetes and ageing. Nature reviews Molecular cell biology *12*, 21-35.